TRANSPORTATION RESEARCH

RECORD

No. 1353

Materials and Construction

Asphalt Mixture Design

A peer-reviewed publication of the Transportation Research Board

TRANSPORTATION RESEARCH BOARD
NATIONAL RESEARCH COUNCIL

NATIONAL ACADEMY PRESS
WASHINGTON, D.C. 1992

Transportation Research Record 1353
Price: $22.00

Subscriber Category
IIIB materials and construction

TRB Publications Staff
Director of Publications: Nancy A. Ackerman
Senior Editor: Naomi C. Kassabian
Associate Editor: Alison G. Tobias
Assistant Editors: Luanne Crayton, Norman Solomon, Susan E. Gober
Office Manager: Phyllis D. Barber
Production Assistant: Betty L. Hawkins

Printed in the United States of America

Library of Congress Cataloging-in-Publication Data
National Research Council (U.S.). Transportation Research Board.
Meeting (71st : 1992 : Washington, D.C.)
Asphalt mixture design.
p. cm. — (Transportation research record, ISSN 0361-1981; no. 1353)
ISBN 0-309-05217-3
1. Pavements, Asphalt—Testing. 2. Pavements, Asphalt concrete—Testing. 3. Asphalt—Testing. I. Title. II. Series.
TE7.H5 no. 1353
[TE275]
388 s—dc20 92-30101
[625.8'5] CIP

Sponsorship of Transportation Research Record 1353

GROUP 2—DESIGN AND CONSTRUCTION OF TRANSPORTATION FACILITIES
Chairman: Raymond A. Forsyth, Sacramento, California

Bituminous Section
Chairman: Leonard E. Wood, Purdue University

Committee on Characteristics of Bituminous Mixtures to Meet Structural Requirements
Chairman: Dallas N. Little, Texas A&M University
Secretary: Robert N. Jester, Federal Highway Administration, U.S. Department of Transportation
Benjamin Colucci, Dale S. Decker, Jim Gee, R. G. Hicks, R. J. Holmgreen, Jr., Darrell V. Holmquist, Vincent C. Janoo, Rudolf A. Jimenez, Y. Richard Kim, Kang-Won Wayne Lee, J-M Machet, Kamyar Mahboub, Michael S. Mamlouk, Harold R. Paul, R. D. Pavlovich, Reynaldo Roque, A. F. Stock, Walter Tappeiner, Ronald Terrel, Bernard A. Vallerga, Harold L. Von Quintus, James P. Walter, Gary C. Whited, John S. Youtcheff

Frederick D. Hejl, Transportation Research Board staff

The organizational units, officers, and members are as of December 31, 1991.

Transportation Research Record 1353

Contents

Foreword

The papers in this Record deal with various facets of asphalt mixture design; they should be of interest to state and local construction, design, materials, and research engineers as well as contractors and material producers.

Fwa and Tan describe a study that evaluated the feasibility of using a twin-probe gamma-ray gauge to measure the density of laboratory cylindrical bituminous paving mixture specimens. Kandhal and Khatri report on a study to improve the reproducibility of the Rice method in determining the theoretical maximum specific gravity of asphalt paving mixtures, particularly those mixtures using highly absorptive aggregates. On the basis of their test data, they recommend optimum levels for temperature, residual pressure, and vacuuming time to improve the reproducibility of the Rice method. Stroup-Gardiner and Epps describe laboratory tests involving various methods of adding lime for assessing moisture damage to asphalt concrete mixtures.

Aglan et al. report on the development of a methodology to characterize the resistance of asphalt concrete mixtures to fatigue crack propagation in an effort to construct fundamental structure-fracture toughness relationships. Svec and Eldred describe the concept and the first prototype of new laboratory equipment for testing mechanical properties of asphalt concrete. Al-Swailmi et al. report on a computer-controlled loading and data acquisition subsystem that is part of a state-of-the-art test system for determining the susceptibility of an asphalt-aggregate mixture to moisture-induced damage. Boudreau et al. describe a study to select one combination of resilient modulus test parameters that would yield repeatable modulus results on laboratory-compacted asphalt concrete specimens. Hadley and Groeger describe the comprehensive test procedure that has evolved from the Strategic Highway Research Program's (SHRP) Long-Term Pavement Performance asphalt concrete resilient modulus testing program. Mohammad and Paul present the results of a study to evaluate the repeatability and performance of a new indirect tension test device that was developed by Baladi and further modified by the Louisiana Transportation Research Center.

El Hussein et al., as a result of their study, report that construction compaction techniques have a significant influence on asphalt concrete resistance to moisture damage. Fernando and Lytton demonstrate the potential benefits of performance-oriented specifications. They conducted hypothetical case studies to evaluate the expected performance of asphalt concrete pavements constructed using existing specifications. Kim et al. present the results of resilient modulus testing at North Carolina State University performed as a part of the SHRP asphalt concrete core proficiency testing program.

Von Quintus et al. summarize the procedures for an Asphalt-Aggregate Mixture Analysis System (AAMAS) that was developed under NCHRP Project 9-6(1). They also review the implementation process of the procedure and discuss some of the potential problems with field control of mixtures designed by this procedure. Mamlouk et al. describe the Arizona Department of Transportation's experience with the AAMAS procedure. They found that AAMAS seems to provide good performance predictions.

Laboratory Density Measurements of Bituminous Mixes by Gamma-Ray Probe

T. F. Fwa and S. A. Tan

An experimental study that evaluated the feasibility of applying a twin-probe gamma-ray gauge for density measurements of cylindrical bituminous specimens is described. Major considerations related to the operational features of the gauge and the characteristics of the composite structure of bituminous mixtures are highlighted. Three bituminous mix types—namely, sand asphalt, dense-graded mix, and open-graded mix—were included. The measurement precision and accuracy characteristics of the gauge with respect to the different mix types were examined. It was found that the precision and accuracy of gauge-determined densities varied with the types of mix tested. Better precision and accuracy were achieved with specimens that had more uniform density distribution within the mass and with specimens that were less porous. Recommendations concerning the use of gamma-ray probes for laboratory density measurements of bituminous paving mixtures are made. An illustration showing the ability of the twin-probe gauge to determine the density profile of a tall specimen is presented.

Measuring the density of laboratory-compacted specimens and field cores of bituminous materials is a requirement in routine laboratory testing of highway and airfield paving materials. The bulk specific gravity of bituminous paving mixtures with water-tight surfaces can be determined by weighing specimens in air and in water, as described in ASTM D2726. If the surface of a mixture is porous or if it permits the infiltration of water during the submerged weighing, specimens coated with paraffin must be used as specified by ASTM D1188. These two methods measure the overall average density of the specimen tested. For compacted specimens or field cores that contain layers of mixtures with different densities, other methods are needed if the densities of various layers are to be determined nondestructively.

This paper describes an alternative means of density measurement of bituminous mixtures in a nondestructive manner through the use of a nuclear device: a twin-probe gamma-ray gauge adapted from a direct transmission field gauge for laboratory density measurement. The precision characteristics of the twin-probe gauge with respect to different bituminous mixtures are examined. Three bituminous mixtures—a dense-graded asphaltic concrete, an open-graded mixture, and a sand asphalt mixture—are included in the study. Recommendations about the use of the gamma-ray probe for laboratory density measurement of bituminous paving mixtures are made.

Center for Transportation Research, Department of Civil Engineering, National University of Singapore, 10 Kent Ridge Crescent, Singapore 0511.

EXPERIMENTAL SETUP AND MEASUREMENT PROCEDURE

A schematic diagram of the twin-probe nuclear density gauge adopted in this study is shown in Figure 1. The gauge has a 5-milliCurie (mCi) source of cesium-137 that produces gamma photons of initial energy of 662 keV, a detector consisting of a sodium-iodide-thallium–activated crystal, NaI(Tl), and a scintillation counter capable of discriminating gamma photons according to their energy levels. The counter is designed to register only signals corresponding to photons of energy of 662 keV. The source and detector are rigidly fixed 280 mm apart. This is the recommended source-to-detector spacing for the gauge, arrived at in an earlier study by the authors (*1*); it is based on precision and accuracy considerations. The cross arm that holds the source and detector can be moved vertically on a rigid vertical guide by a drive motor. This enables density measurements to be made at different depths of a specimen. More details about the operating characteristics of the twin-probe setup are found elsewhere (*1*,*2*).

The attenuation of gamma radiation after passing through a matter can be described by the well-known gamma absorption law (*3*,*4*):

$$N = N_o F e^{-\mu t \rho} \quad (1)$$

or

$$\ln C_R = \ln(N/N_o) = \ln F - \mu t \rho \quad (2)$$

where

N_o = count rate registered by detector with no specimen between the source and detector,
N = count rate registered by detector with specimen in space,
F = a constant that is a function of the geometry of the gauge and specimen material properties,
μ = material mass absorption coefficient,
t = thickness of specimen,
ρ = density of specimen, and
C_R = count ratio, computed as the ratio of N to N_o.

Using the twin-probe gauge, Fwa and Tan (*2*) have shown that the following formula is applicable for density measurement of solid cylindrical specimens having diameters from 75 to 150 mm:

$$\ln C_R = \ln F - \mu c d \rho \quad (3)$$

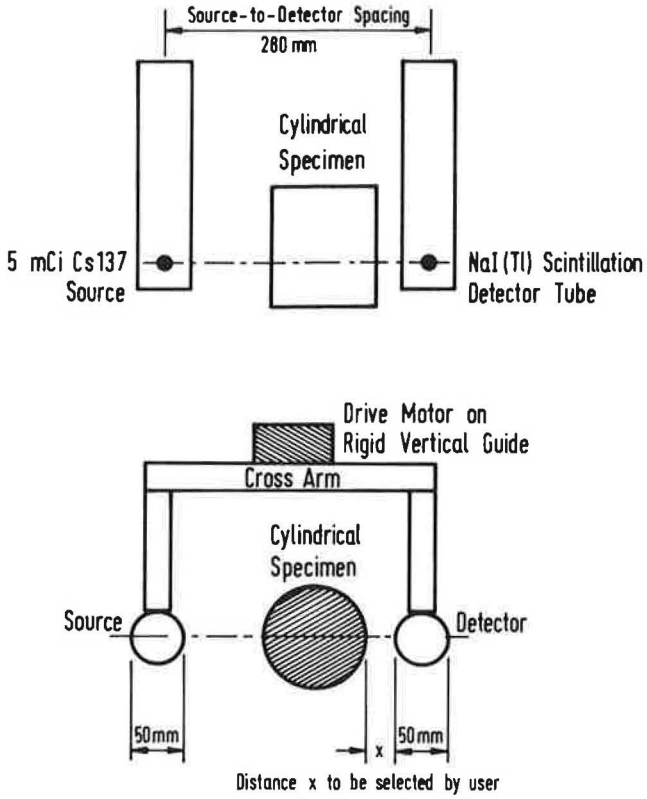

FIGURE 1 Experimental setup of twin-probe gamma-ray gauge: *top*, elevation view; *bottom*, plan view (not to scale).

where c is the diameter correction factor to account for circumference curvature of a cylindrical specimen and d is the diameter of the specimen.

For measuring the density of bituminous mixtures prepared with asphalt of a given grade and aggregates of a given source and adopting a fixed geometry of the experimental setup of the gauge as depicted in Figure 1, the factors F and μ can be taken as constants. Equation 3 may then be simplified as follows for testing with specimens of the same size:

$$\ln C_R = k_1 - k_2 \rho \tag{4}$$

where k_1 and k_2 are constants that can be calibrated from measurements of bituminous specimens of known densities. Once calibrated, Equation 4 is used to calculate the density of a specimen from the count rate readings of the twin-probe gauge.

CONSIDERATIONS IN DENSITY MEASUREMENT OF BITUMINOUS MIXTURES

For meaningful interpretation of density measurements from the count rates of the twin-probe gauge, the operational features of the gauge and the characteristics of the composite structure (such as aggregate gradation and air void percentage) of bituminous mixtures must be considered.

Zone of Measurement

The so-called zone of measurement refers to the volume of specimen material covered in a density determination using the twin-probe gauge. The boundaries of the zone of measurement are dependent on the geometry of the gauge and the position of specimen between the source and detector. For the twin-probe setup in this study, the NaI(Tl) crystal in the scintillation detector is a cylinder 40 mm in diameter and 12 mm thick. The 5-mCi cesium-137 mass can be taken to be a point source. The measurement path of the twin-probe gauge may then be represented by a pyramid with a rectangular base of 12 × 40 mm and a height of 280 mm, as depicted in Figure 2 (*left*). Figure 2 (*right*) indicates that the mass of specimen material exposed to the gamma-radiation measurement is given by the intersection of the path of measurement and the specimen. This is defined by the volume *abcdefgh*. For a 100-mm-diameter cylindrical specimen placed at a distance x = 10 mm from the detector (see Figure 1 for definition of x), Figure 3 shows the plan view of the zone of measurement.

It is clear that the volume and mass of a specimen covered in each density measurement by the twin-probe gauge are considerably smaller than those involved in a conventional density measurement by means of the water-displacement principle. This localized density determination capability of the twin-probe gauge offers two obvious advantages: (a) locational variations of density in a plane perpendicular to the

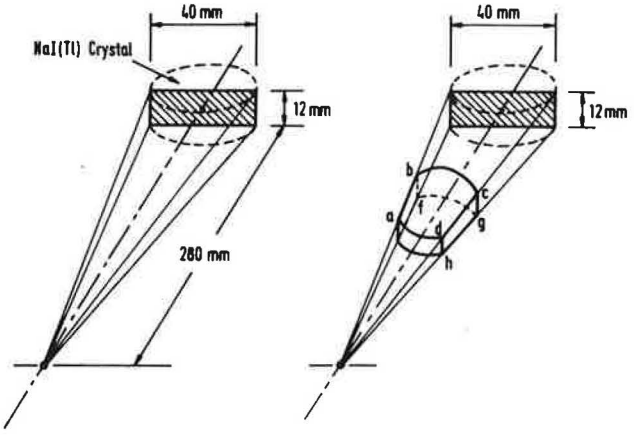

FIGURE 2 Zone of measurement in twin-probe nuclear gauge density determination: *left*, path of measurement; *right*, volume of specimen measured (not to scale).

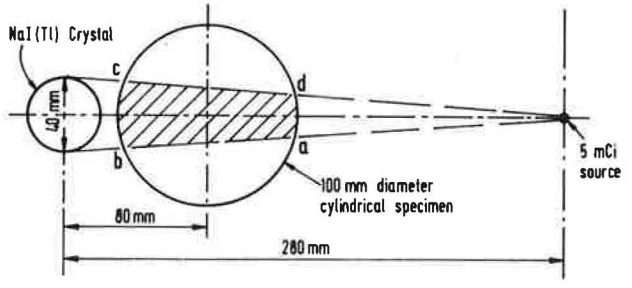

FIGURE 3 Plan view of zone of measurement (*abcd*) for cylindrical specimen.

measurement path can be identified; this allows one to determine the horizontal and vertical distribution patterns of density of a laboratory-compacted specimen or a field-extracted sample; and (b) directional variations in a plane parallel to the measurement path can also be determined. For a cylindrical specimen as shown in Figure 3, this is achieved simply by rotating the specimen horizontally so that different zones of measurement can be covered.

Relating Gauge Measurements to Bulk Density

In laboratory testing of bituminous mixtures for pavement engineering applications, reference is often made of the bulk density of cylindrical laboratory-prepared specimens or field cores. There is therefore the need to relate nuclear gauge density measurements to the bulk density measured by the conventional water-displacement method. In the event that the specimen measured is homogeneous in nature and has uniform density distribution, gauge-measured densities can be directly related to bulk densities. This is not likely with a bituminous mixture because its three basic constituents—aggregates, air, and asphalt—differ greatly in density. Depending on the type of mix and gradation of aggregates, the density distribution in a bituminous mix can be far from uniform.

One possible approach to obtain bulk density from gauge density readings is to make multiple measurements to cover the entire volume of the specimen, with no overlapping of zones of measurement. This approach, however, is not practical for cylindrical specimens because the change in geometry in each measurement requires a separate calibration of Equation 4. In addition, considerable errors due to increased curvature effects are expected because measurements are made away from the centerline of a cylindrical specimen (*1*).

The approach adopted in this study involves making nuclear density measurements from selected directions spaced at equal angles about the center of the specimen tested. Figure 4 shows the measurement directions for different cases. In each case, an estimate of bulk density is computed as the mean of the gauge-determined densities obtained from different directions. In general, it is likely that the more nonuniform the density distribution of a specimen, the higher is the number of measurement directions needed to arrive at a sufficiently accurate assessment of its bulk density.

Gauge Calibration

For density measurement of cylindrical specimens of the same diameter, the calibration coefficient k_2 in Equation 4 is a function of μ, the material mass absorption coefficient. For common civil engineering materials composed mainly of carbon, oxygen, aluminum, silicon, and calcium, with only a small amount of heavy elements such as iron, μ can be taken as a constant (*3–6*). This means that the density calibration of these materials, according to Equation 4, will lie on a straight line on a $\ln(C_R)$-versus-density plot. Using the twin-probe nuclear gauge described in this study, the authors (*1,2*) have verified this linear relationship experimentally using cylindrical specimens of aluminum (bulk density = 2.70 g/cm³),

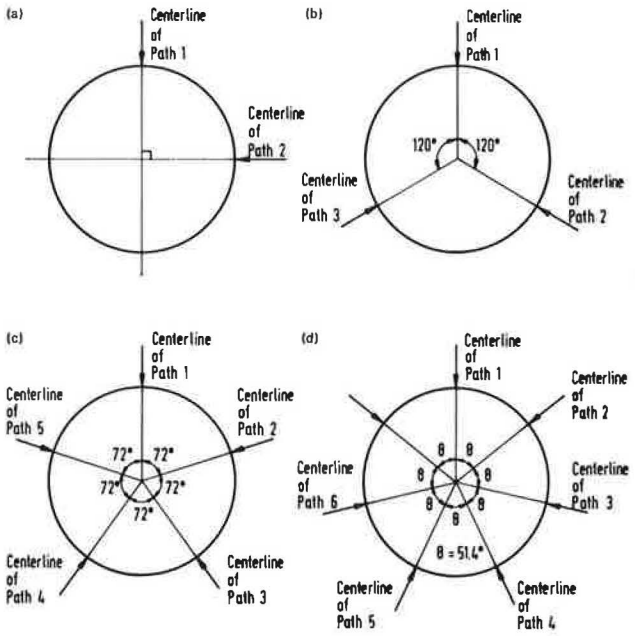

FIGURE 4 Gamma-ray density measurement in more than one direction (arrows indicate centerline and direction of measurement path): *a*, for two directional measurements; *b*, for three directional measurements; *c*, for five directional measurements; *d*, for seven directional measurements.

glass (2.51 g/cm³), hardened portland cement (1.83 g/cm³), perspex (1.18 g/cm³), asphalt (1.00 g/cm³), and paraffin wax (0.83 g/cm³). A calibration plot for 100-mm-diameter cylindrical specimens is shown in Figure 5. Source-to-detector spacing is 280 mm and specimen-to-detector gap is 10 mm. The corresponding calibration equation is

$$\ln C_R = -0.01706 - 0.55166\,\rho \qquad (5)$$

This fitted equation has a statistical coefficient of multiple determination, r^2, equal to .999.

In a separate study on nuclear density measurements of granular materials, Tan and Fwa showed that the calibration

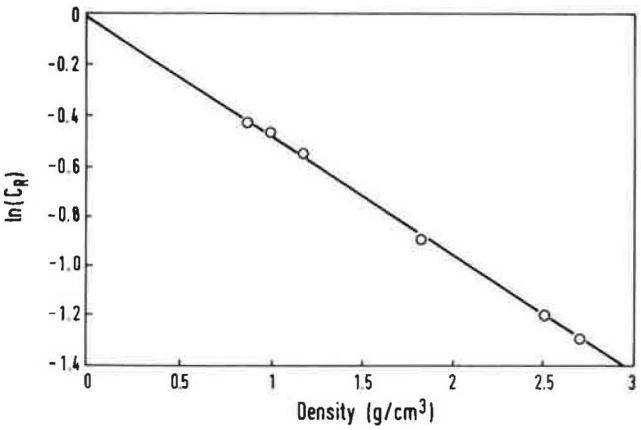

FIGURE 5 Calibration plot of twin-probe gamma-ray gauge.

based on Equation 5 was also valid for density measurements of granite aggregates and siliceous sand masses with different porosities (7). Because bituminous mixes are mixtures of asphalt and aggregates, both of which follow the calibration relationship of Equation 5, it is logical to expect the same relationship to be applicable to these mixes. Three types of bituminous mix are investigated in this study to verify this.

DENSITY MEASUREMENTS AND ANALYSIS

This section describes the tests performed to determine the precision and accuracy characteristics of the gamma-ray probe in density measurements of compacted bituminous mixes. A dense-graded mix and an open-graded mix, with aggregate gradations as described in Table 1, were prepared with asphalt contents of 5.5 and 7.0 percent, respectively. The third mix type was a sand asphalt prepared using an asphalt content of 8 percent and natural siliceous sand with a nominal maximum size of 2.36 mm. These mixes were chosen to cover the range of density commonly found for compacted bituminous mixtures.

In making the precision and accuracy assessments, the following aspects were examined for each of the three mixes: (a) repeatability of density measurements for a fixed path of measurement, (b) number of directional measurements required to achieve a desired level of accuracy, and (c) comparison with bulk densities determined by the conventional water-displacement method.

TABLE 1 Aggregate Gradations of Dense- and Open-Graded Mixes

Sieve Size (mm)	Percent Passing (Dense-Graded Mix)	Percent Passing (Open-Graded Mix)
25	100	100
19	100	95
13	95	75
9.5	85	55
4.75	70	27
2.36	50	10
1.2	37	5
0.3	19	0
0.075	6	0

Repeatability of Density Measurements

Three specimens of each of the three mix types were tested for repeatability of nuclear gauge density measurements. For each specimen, a measurement path was arbitrarily chosen and 40 readings of 1-min counts were obtained. Figure 6 shows typical frequency distribution plots of 1-min counts for the three mix types. Also shown in the same figure are the corresponding frequency distributions of densities, in which each density was computed from a 1-min count using the calibration relationship of Equation 5. It can be seen that both the count rate and density distributions are approximately Gaussian.

Table 2 summarizes the statistical characteristics of nuclear density measurements for single measurement paths. The results show that the sand asphalt specimens had the lowest density, followed by open-graded and dense-graded specimens in the order of increasing density. The corresponding standard deviations in density from the sand asphalt to dense-graded specimens varied from 0.009 to 0.012 g/cm³. This follows the general trend in nuclear density measurements, that precision improves as the count rate increases (or as the density decreases) (2).

On the basis of the Gaussian theory, a precision statement can be made for single-path density measurements of each of the three mix types. This is shown in Table 2, in which the ranges of error associated with different numbers of repeated 1-min counts were computed. For the three bituminous mixes, it may be concluded that a minimum of four 1-min counts are required for each measurement path to give a precision on the order of ±0.01 g/cm³ at a confidence level of 95 percent. The level of precision achieved is of the same order of magnitude as those obtained for the solid materials shown in Figure 5. This precision is adequate for most engineering applications. Therefore, four 1-min counts are recommended for each measurement path and used in all gamma-ray density measurements in this study.

Required Number of Directional Measurements

The presence of different sizes of aggregates and air voids in the mass of a bituminous specimen makes it necessary to

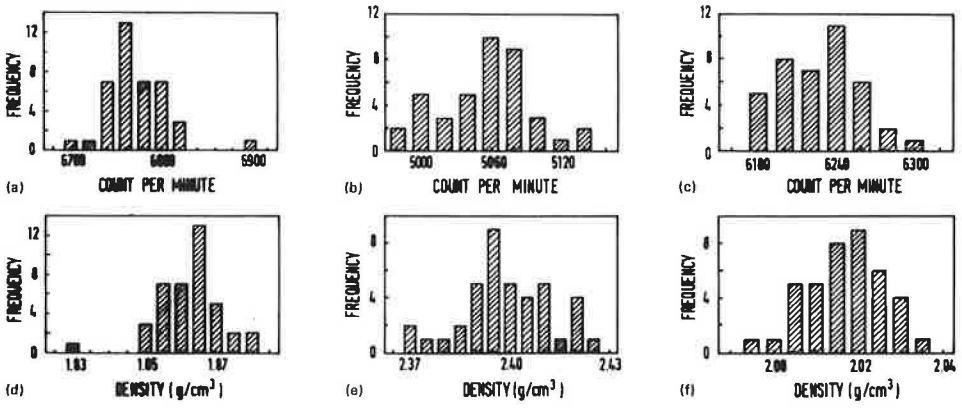

FIGURE 6 Count and density distribution for bituminous mixes: *a*, sand asphalt mix count distribution; *b*, dense-graded mix count distribution; *c*, open-graded mix count distribution; *d*, sand asphalt density distribution; *e*, dense-graded mix density distribution; *f*, open-graded mix density distribution.

TABLE 2 Characteristics of Single-Path Measurements of Density by Twin-Probe Gamma Ray Gauge

Type of Mix	Mean One-Minute Count	Path Density (g/cm^3)		Precision Characteristics	
		Mean	Std Dev	n *	e **
Sand Asphalt	6,761	1.821	0.0088	2	±0.012
				3	±0.010
				4	±0.008
Open-Graded Mix	6,217	1.974	0.0090	2	±0.012
				3	±0.010
				4	±0.009
Dense-Graded Mix	5,047	2.352	0.0126	2	±0.018
				3	±0.014
				4	±0.012

*n is the number of repeated one-minute counts.
**e is the range of error in density at confidence level of 95%, expressed in units of g/cm^3.

perform more than one directional measurement to obtain a representative assessment of the bulk density of the specimen. In general, one would expect that the less uniform the density distribution of a specimen is, the more directional measurements will be needed.

Following the measurement patterns of Figure 4, all the three specimens of each of the three mix types were subjected to 2-, 3-, 5-, 7-, 11-, and 15-path directional measurements of densities. For each pattern of directional measurements, Path 1 was first randomly selected, followed by fixing of the directions of the remaining paths according to the arrangement in Figure 4 so that all the measurement paths were equally spaced on the perimeter of the specimen. This procedure was repeated 30 times per pattern for each specimen. The sample mean and standard error for each set of 30 density measurements were then computed.

The results of the analysis are summarized graphically in Figure 7. The coefficient of sample variation, CV, calculated by dividing the standard error by the mean, is plotted against the number of directional measurements. It is observed that whereas the mean did not vary much with the number of directional measurement paths for all the three mix types, the variability of measurements as represented by the range of CV decreased rapidly from path size of two. The variations in CV began to stabilize at a path size of about five for the sand asphalt and dense-graded mix and at a path size of about seven for the open-graded mix.

It is interesting to note that the mean CV of the three bituminous mixes provides a quantitative measure of the degree of nonuniformity of their density distributions. The sand asphalt specimens, with their mean CV in the order of 0.4 percent, had the most-uniform density distributions. The density distributions of the dense-graded specimens were less uniform, giving a mean CV of about 1.0 percent. The open-graded specimens, having mean CV of about 2.3 percent, were the least uniform in density distribution among the three mix types.

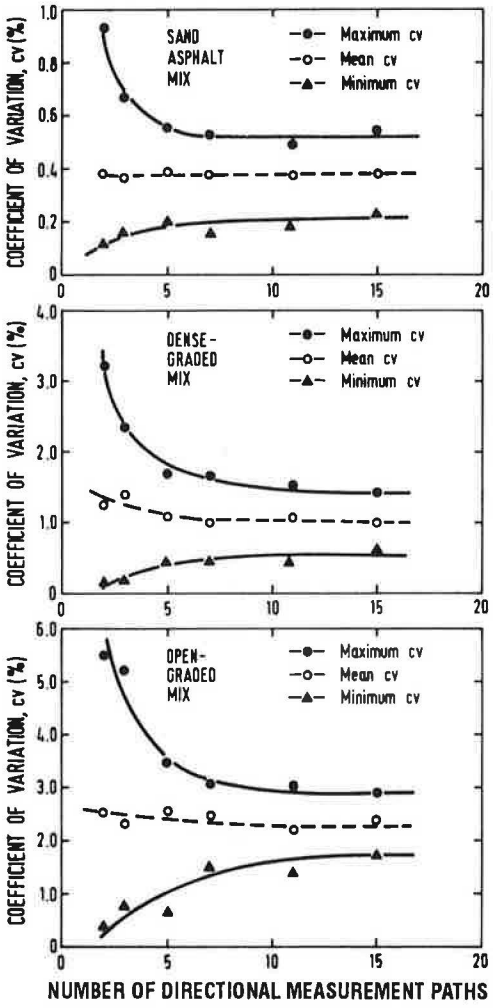

FIGURE 7 Variations of density measurements with number of measurement paths: *top*, sand asphalt mix; *middle*, dense-graded mix; *bottom*, open-graded mix.

Procedure for Estimating Bulk Densities

From the precision analyses presented in the preceding sections, the requirements for nuclear gauge density measurements of bituminous mixes outlined in Table 3 were adopted. Using the results of mean CV obtained earlier for each of the three mix types, estimates of the probable error were computed. Using five directional measurement paths each, the precisions obtained for the sand asphalt and dense-graded specimens were respectively within ±1 percent. For open-

TABLE 3 Requirements Adopted for Estimating Bulk Densities Using Twin-Probe Nuclear Gauge

Type of Mix	Number of Directional Measurement Paths	Number of One-Minute Counts Counts per Path	Range of Error in Density at Confidence Level of 95%
Sand Asphalt	5	4	±0.35%
Dense-Graded Mix	5	4	±0.87%
Open-Graded Mix	7	4	±1.70%

graded specimens, a precision of ±1.70 percent was achieved with seven directional measurement paths. Additional directional measurement paths may be used if higher precision is desired. For example, to achieve ±1 percent precision for density measurement of the open-graded mix, the number of directional measurement paths required is 20.

Comparison with Water-Displacement Bulk Densities

The accuracy of bulk densities of bituminous mixtures determined using the twin-probe nuclear gauge can be assessed by comparison with the corresponding densities obtained by the commonly accepted water-displacement method. For consistency in testing the different mixes, ASTM D1188, which uses paraffin-coated specimens, was adopted. In addition to the nine specimens described in the preceding sections, eight other dense-graded specimens were included. These eight specimens, having the same aggregate gradations as the dense-graded specimens described in Table 1, were intentionally given different degrees of compactive effort during preparation to produce compacted mixtures of different densities.

The final results are plotted in Figures 8 and 9. In Figure 8, the test results are plotted with the twin-probe calibration line. It is seen that the calibration relationship fits reasonably well with the density measurements of the different types of bituminous mixes tested. In Figure 9, the bulk densities determined by the water-displacement method are plotted against the gauge-determined densities. The bulk densities determined by the two methods were highly correlated with a coefficient of correlation, r, equal to .968. Assuming the bulk density determined by the water-displacement method to be the true density, the plot suggests that the accuracy achievable by the gamma-ray gauge varies with the type of mix tested. In general, the relative order of the three mix types in terms of the accuracy achievable was similar to those reported in the precision analysis. The best accuracy was obtained with sand asphalt specimens, followed by those dense-graded specimens that were adequately compacted to yield densities higher than about 2.30 g/cm³. The nuclear gauge–determined densities of the open-graded specimens were comparatively least accurate. The order of accuracy obtained with undercompacted dense-graded specimens was comparable to that of the open-graded specimens.

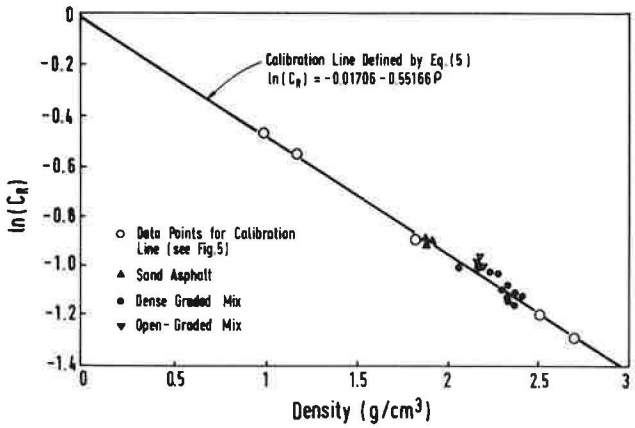

FIGURE 8 Plotting density data with twin-probe gauge calibration line.

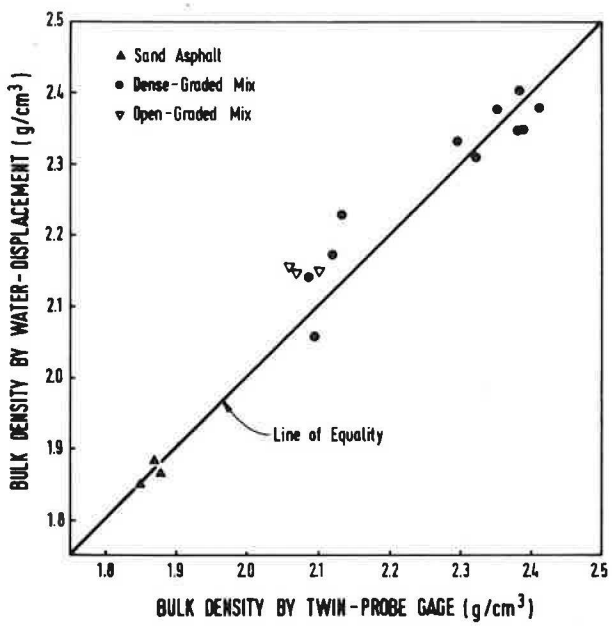

FIGURE 9 Comparison of gamma-ray density measurements with densities determined by water-displacement method.

There are two possible reasons that might have contributed to the differences in the accuracies of nuclear gauge–determined densities of different bituminous mixes. The relative uniformity of density distribution is believed to have a direct effect on the results. Another possible reason is the influence of air voids. Tan and Fwa have shown that the presence of voids in the zone of measurement of a coarse granular material tends

to cause the gamma-ray gauge to underestimate bulk density (*7*). This effect of voids appears to explain well the trend of the test results of open-graded specimens and undercompacted dense-graded specimens.

APPLICATION: DENSITY PROFILE BY GAMMA-RAY GAUGE

Because of the number of directional measurements and repeated 1-min counts needed, the bulk density measurement of a bituminous specimen by means of the twin-probe gauge takes 20 to 30 min. The most attractive feature of the probe, however, is its ability to measure density in a predetermined localized volume. A useful application of the twin-probe gamma-ray is to obtain the density profile of a layered field core for identifying its construction history or of a laboratory-compacted specimen for ensuring that the specimen is uniformly compacted at different depths. Being nondestructive, the gauge can also be used effectively to monitor changes in density of test specimens undergoing various treatments.

An example of density profile with depth obtained using the twin-probe gamma-ray gauge is illustrated in Figure 10. It is the density profile of a cylindrical specimen 250 mm tall and compacted in four layers. The number of compaction blows applied to each layer was varied to produce layers of different compacted densities. Three directional measurements, spaced 120 degrees apart, were made. For each directional measurement, density was determined at vertical intervals of 5 cm. The effects of different compactive efforts and the changes of density from layer to layer can be seen easily from the plot.

Although this example deals with layers of bituminous mixtures of the same mix design, the same experimental technique applies to the testing of field cores composed of layers of different mix types. However, depending on the mix types encountered, the number of directional measurements required may vary from layer to layer.

SUMMARY AND CONCLUSION

An evaluation of the feasibility of applying a twin-probe gamma-ray gauge for density measurements of cylindrical bituminous specimens has been presented. Sand asphalt and dense- and open-graded specimens were studied. Guidelines for gamma-ray density measurements of each mix type were recommended. From the experimental work and analyses performed in this study, the following recommendations and conclusions can be made:

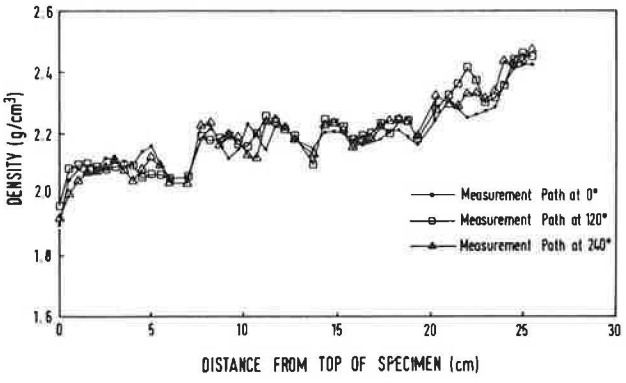

FIGURE 10 Example of density profile measurement using twin-probe gamma-ray gauge.

1. The gamma-ray technique is a reliable method of nondestructively measuring density of common bituminous mixtures used for road construction. The calibration relationship derived from referenced materials such as aluminum, glass, perspex, and paraffin wax blocks is valid for such density measurements.
2. Considering a single path of density measurement, the precision characteristics were found to be dependent on gamma-ray count rate and hence the density of the material measured. For the range of density (from 1.8 to 2.5 g/cm^3) tested in this study, four 1-min counts per measurement path were required to give a precision on the order of ± 0.01 g/cm^3 at a confidence level of 95 percent.
3. Because of nonuniformity of point density distribution within a bituminous mixture and the limited volume of material covered in each measurement path of the twin-probe gauge, more than one directional measurement of density is required for determining the bulk density of a cylindrical bituminous specimen.
4. The number of directional measurements required is a function of the degree of nonuniformity of density distribution of the material tested. Of the three mix types tested, sand asphalt specimens had the most-uniform density distribution, followed by dense-graded and open-graded specimens in order of increasing nonuniformity. Their corresponding coefficients of variations in density were 0.4, 1.0, and 2.3 percent for 15 directional measurements. It was suggested that for determining the bulk density of cylindrical specimens, five directional measurement paths be used for sand asphalt and dense-graded specimens and seven for open-graded specimens. The errors in density associated with this measurement scheme were ± 0.35, ± 0.87, and ± 1.70 percent at a confidence level of 95 percent for the three mixes, respectively.
5. The accuracy of gauge-determined densities measured against densities obtained from the water-displacement method varied with the type of mix tested. Test results suggest that better accuracy is achieved with specimens that have more-uniform density distribution and with specimens that are less porous. Gauge-measured densities of sand asphalt specimens were more accurate than those of dense- and open-graded specimens. Undercompacted dense-graded specimens, which were more porous than the well-compacted specimens of the same mix, also produced poorer accuracy in gamma-ray density measurements than open-graded specimens.
6. The results of this study indicate that the precision and accuracy of gamma-ray density measurements of bituminous mixtures vary with their mix design and degree of compaction. In measuring the density of a bituminous mixture using a gamma-ray device such as the twin-probe gauge, there is a need to establish a measurement scheme so that the desired precision and accuracy levels can be achieved. The experimental procedure described in this paper provides useful information and guidelines in this aspect.

REFERENCES

1. T. F. Fwa and S. A. Tan. Experimental Evaluation of a Twin-Probe Nuclear Gage for Laboratory Density Measurement. *Journal of Testing and Evaluation*, ASTM, (in preparation).
2. S. A. Tan and T. F. Fwa. Nondestructive Density Measurements of Cylindrical Specimens by Gamma-Ray Attenuation. *Journal of Testing and Evaluation*, ASTM, Vol. 19, No. 2, 1991, pp. 155–160.
3. D. G. Harland. A Radioactive Method for Measuring Variations in Density in Concrete Cores, Cubes and Beams. *Magazine of Concrete Research*, Vol. 18, No. 55, 1966, pp. 95–101.
4. P. A. Ruygrok. Evaluation of the Gamma and Neutron Radiation Scattering and Transmission Methods for Soil Density and Moisture Determination. *Geotechnical Testing Journal*, ASTM, Vol. 11, No. 1, 1988, pp. 3–19.
5. J. Kohl, R. D. Zenther, and H. R. Lukens. *Radioisotope Applications in Engineering*. Van Nostrand, Princeton, N.J., 1964.
6. E. L. Krinistsky. *X-Ray Measurement of Soil Densities in Models*. Paper S-72-1. U.S. Army Corps of Engineers Waterways Experiment Station, Vicksburg, Miss., 1972.
7. S. A. Tan and T. F. Fwa. Influence of Voids on Density Measurements of Granular Materials Using Gamma Radiation Techniques. *Geotechnical Testing Journal*, ASTM (in preparation).

Improved Rice Method for Determining Theoretical Maximum Specific Gravity of Asphalt Paving Mixtures

PRITHVI S. KANDHAL AND MAQBOOL A. KHATRI

The Rice method (ASTM D2041) is used for determining the theoretical maximum specific gravity of asphalt paving mixtures, which is one of the main test parameters used for mix design and construction quality control. The repeatability and reproducibility of the Rice method is not considered satisfactory, especially when highly absorptive aggregates are used in the mixture. Such aggregates can absorb water during the vacuuming phase of the Rice method. This necessitates the use of a supplementary (dry-back) procedure that is even more prone to testing errors. There is a need to improve the Rice method to avoid these problems. Two dense-graded asphalt paving mixtures (representing low- and high-absorption aggregates) and one AC-20 asphalt cement were used. Three factors (temperature, residual pressure, and vacuuming time) affecting the results from the Rice method were investigated at three levels each, involving some 108 tests. From these test data, optimum levels have been recommended for temperature, residual pressure, and vacuuming time. Use of these optimum levels is expected to improve the reproducibility of the Rice method, especially when highly absorptive aggregates are used in the asphalt paving mixtures. The improved Rice method is also likely to minimize the necessity of using the supplementary procedure.

Theoretical maximum specific gravity of hot mix asphalt (HMA) mixtures is used in all stages of HMA design, construction, and evaluation. The procedure for determining the theoretical maximum specific gravity of HMA mixtures was originally developed by Rice (*1*,*2*); it is standardized as ASTM D2041 (Theoretical Maximum Specific Gravity and Density of Bituminous Paving Mixtures). It is one of the main test parameters used for mix design and construction quality control. Besides the void parameters of an HMA mixture, the amount of asphalt cement absorbed by the aggregate is also computed by the use of theoretical maximum specific gravity as determined by ASTM D2041.

Although this is one of the most critical test parameters in the design of HMA mixtures, its repeatability and reproducibility have generally been unacceptable. In July 1983, the task force on revision of ASTM D2041 (the Rice specific gravity method) recommended that the water be made to boil (through suitable combinations of saturation temperature and pressure) in the vessel when subjecting the specimen to vacuum for removal of air. However, no test data were reported to justify the recommendation, and it was not made a part of the test method.

The situation is further complicated when highly absorptive aggregates are used in HMA mixtures and there is the potential of water's being absorbed by the aggregate during the vacuuming phase. The current ASTM method specifies a minimum vacuum level [maximum residual pressure of 30 mm of mercury (Hg) or less]. Therefore, one can use a high vacuum level and increase the potential for water absorption. The current ASTM test method suggests the use of a supplemental procedure to correct for this situation. However, this procedure is time-consuming, and its repeatability and reproducibility have not been established.

Alternative techniques for determining the theoretical maximum specific gravity have also been proposed and are in use. The U.S. Army Corps of Engineers developed and has used the bulk impregnated specific gravity in the design and control of asphalt paving mixtures (*3*,*4*). One limitation of this method, however, is the possible difficulty of removing air bubbles entrapped in the asphalt cement when both coarse and fine aggregates are added to molten asphalt.

Franco and Lee have recently evaluated the viability of using an air meter for determining the maximum specific gravity of HMA mixtures (*5*). The air meter has normally been used for determining the percent of air entrained in portland cement concrete. The so-called pressure method works on the principle of Boyle's law. A weighed sample of HMA mix is introduced into the bowl of the air meter (Type B air meter as specified in AASHTO T152) and water is introduced to fill the meter to the capacity (no attempt is made to remove the entrapped air). The filled air meter is weighed and the weight of water obtained. The air content of the meter is then determined in accordance with AASHTO T152. Back calculations are then performed, and the volume of the HMA mix is determined. Further work is needed to improve the design of the air meter so that its consistency and sensitivity are acceptable.

This study was aimed at refining the current Rice method (ASTM D2041). Two aggregates and one asphalt cement were used. Three factors—namely, temperature, residual pressure, and vacuuming time—were investigated to determine their optimum levels. The materials used in the study, the experimental plan, test results, and conclusions are presented in the following.

MATERIALS USED

Aggregates

All the materials used in this study were obtained from the Strategic Highway Research Program's (SHRP) Materials

National Center for Asphalt Technology, 211 Ramsay Hall, Auburn University, Auburn, Ala. 36849.

Reference Library (MRL). The following two different aggregates were used:

- RD—Frederick limestone (bulk specific gravity = 2.713, water absorption = 0.38 percent)
- RB—Watsonville granite (bulk specific gravity = 2.692, water absorption = 1.68 percent)

Aggregate RD was used in the first phase of the study in which three factors—temperature, residual pressure, and vacuuming time—were investigated for their optimum levels. This aggregate was selected because it had the lowest water absorption of all the SHRP MRL aggregates and its use would reduce the variation of test results due to water absorption during the vacuuming operation. Aggregate RB, which was used in Phase 2 of this study, was selected to represent a high-absorption aggregate. Initially, RC was tried, which is the highest-absorption SHRP MRL aggregate. However, during vacuuming at low residual pressures (high vacuum) while running the Rice method, the water in the flask became muddy because of suction of fines from the coated aggregate particles. As a result, the supplemental procedure was in error. Using a high-absorption aggregate such as RB was necessary for amplifying the difference in the values of the theoretical maximum specific gravity before and after running the supplemental procedure. The washed gradations of the mixes used are given in Table 1.

TABLE 1 Washed Gradations of Mixes Used

Sieve Size	Percent Passing for Aggregate	
	RB	RD
1/2 in	100.0	100.0
3/8 in	81.1	95.8
No. 4	54.1	50.3
No. 8	48.6	40.4
No. 16	35.0	28.7
No. 30	26.8	20.0
No. 50	18.5	14.7
No. 100	11.0	11.5
No. 200	6.1	9.5

Asphalt Cements

Only one asphalt cement (AAM-1, West Texas) was used in this study, and it was an AC-20. It was selected because AC-20 is the most widely used viscosity-graded asphalt cement in the United States.

TESTING PLAN

This study was divided in two phases. Phase 1 involved the use of RD, the SHRP MRL aggregate with the least water absorption, in order to avoid the supplemental procedure of the Rice method. The temperature, residual pressure, and vacuuming time were all investigated at three levels each. The levels of the factors tested were

- Temperature—69, 77, and 85°F;
- Residual pressure—16, 23, and 30 mm Hg; and
- Vacuuming time—5, 10, and 15 min.

The respective combinations of temperature and residual pressure—namely, 69°F and 16 mm Hg, 77°F and 23 mm Hg, and 85°F and 30 mm Hg—were selected to ensure that the water boiled continuously during the vacuuming phase of the Rice procedure. Three replicates were run at each treatment combination. The design was a 3^3 design with three replicates, giving a total of 81 tests. The replicates were considered as blocks.

For Phase 2, the factor temperature was dropped on the basis of the results from Phase 1. The other two factors, that is, residual pressure and vacuuming time, were included at three levels each. The levels used for these factors were the same as for Phase 1. Three replicates were run for each treatment combination and were treated as blocks. The design was a 3^2 design with three replicates, giving a total of 27 tests.

DISCUSSION OF RESULTS

The results for Phase 1 of the study are reported in Table 2. An analysis of variance (ANOVA) was carried out; it is re-

TABLE 2 Rice Specific Gravities Using Aggregate RD

Temperature, °F		69			77			85		
Res. Pressure, mm Hg		16	23	30	16	23	30	16	23	30
Vacuum Time, min	5	2.501	2.495	2.503	2.492	2.495	2.499	2.495	2.495	2.500
		2.493	2.498	2.501	2.491	2.495	2.492	2.491	2.494	2.493
		2.492	2.493	2.500	2.491	2.490	2.492	2.493	2.495	2.494
		2.495	2.495	2.501	2.491	2.493	2.494	2.493	2.495	2.496
	10	2.495	2.496	2.496	2.496	2.491	2.493	2.495	2.495	2.495
		2.496	2.498	2.496	2.493	2.490	2.496	2.497	2.494	2.501
		2.497	2.499	2.499	2.499	2.493	2.491	2.494	2.493	2.502
		2.496	2.498	2.497	2.496	2.491	2.493	2.495	2.494	2.499
	15	2.496	2.501	2.500	2.502	2.499	2.502	2.497	2.500	2.499
		2.496	2.499	2.500	2.497	2.495	2.500	2.497	2.497	2.496
		2.497	2.498	2.497	2.498	2.496	2.495	2.495	2.497	2.494
		2.496	2.499	2.499	2.499	2.497	2.499	2.496	2.498	2.496

ported in Table 3. Temperature (A), residual pressure (B), and vacuuming time (C) were all found to be significant at $\alpha = 0.05$. Only one interaction, $A \times C$ (temperature × vacuuming time), was found to be significant at $\alpha = 0.05$. By looking at the averages reported in Table 2 for each factor, it can be seen that average theoretical maximum specific gravity does not vary much at the various levels of all factors. The error variance is found to be 0.00001, giving a standard deviation of 0.00228. This gives a single-operator precision for the experiment of 0.007, which is less than the current ASTM value of 0.011. Moreover, the range of the values for the entire experiment is 2.490 − 2.502 = 0.012, which is about the same as the current ASTM single-operator precision.

For Phase 1 of the study, the objective was to maximize the value of the theoretical maximum specific gravity. The optimal conditions for all the factors are selected as follows.

Without Considering Interactions

The cumulative averages (average of 27 observations) for all the factors are shown in Table 4.

Observing the cumulative average values of the theoretical maximum specific gravity, the optimal levels of factors, based on the highest value, are selected as

- Temperature—69°F,
- Residual pressure—30 mm Hg, and
- Vacuuming time—15 min.

Considering Interaction $A \times C$

The cell averages for interaction $A \times C$ are as follows:

	Vacuuming Time (min)		
Temperature (°F)	*5*	*10*	*15*
69	2.497	2.497	2.498
77	2.493	2.494	2.498
85	2.494	2.496	2.497

Observing the cell averages, the optimal level for Factor C (vacuuming time) is confirmed to be 15 min. However, for Factor A (temperature), two levels are indicated: 69 and 77°F. Because there is not much variation in results, and moreover, because 77°F is a representative indoor temperature and is commonly used for most of the indoor testing, it was selected as the optimal temperature.

TABLE 3 ANOVA for Rice Gravities Using Aggregate RD

Source	df	SS	MS	F_o	$F_{Crit.}$
Total	80	0.00081	-	-	-
Temperature (A)	2	0.00009	0.00005	8.72	3.18 *
Res. Pressure (B)	2	0.00006	0.00003	5.42	3.18 *
Vacuum Time (C)	2	0.00012	0.00006	11.69	3.18 *
AxB	4	0.00003	0.00001	1.53	2.56
AxC	4	0.00006	0.00002	3.08	2.56 *
BxC	4	0.00004	0.00001	2.03	2.56
AxBxC	8	0.00008	0.00001	1.99	2.13
Error	52	0.00027	0.00001	-	-

* Significant at $\alpha = 0.05$.

TABLE 4 Cumulative Averages for All Factors

Level	Cumulative Average
Temperature (°F)	
69	2.497
77	2.495
85	2.496
Residual pressure (mm Hg)	
16	2.495
23	2.496
30	2.497
Vacuuming time (min)	
5	2.495
10	2.496
15	2.498

The optimal levels for the factors selected on the basis of Phase 1 of the study, therefore, are

- Temperature—77°F,
- Residual pressure—30 mm Hg, and
- Vacuuming time—15 min.

As a consequence of the results from Phase 1, it was decided to drop the factor temperature from the design for Phase 2 of the study. For Phase 2, the high-water-absorption aggregate RB was used.

The results from Phase 2 experiments are reported in Table 5. The reported results include the values for theoretical maximum specific gravity both before and after running the supplementary procedure. The ANOVAs for this phase are reported in Tables 6 and 7, respectively, for difference in theoretical maximum specific gravity values before and after running the supplementary procedure and theoretical maximum specific gravity values before running the supplementary procedure.

Differences

Here the Factor A (residual pressure) and the interaction $A \times B$ (residual pressure × vacuuming time) are found to be significant at $\alpha = 0.05$. The objective in this case was to minimize the differences. To determine the optimal levels, the cumulative averages for factor A are reported as

Level (mm Hg)	*Cumulative Average*
16	0.008
23	0.007
30	0.004

The optimal levels of factors, without considering interactions, are selected as

- Residual pressure—30 mm Hg, and
- Vacuuming time—Any level.

Now, because the interaction $A \times B$ was also significant, we should take a look at the cell averages:

Residual Pressure (mm Hg)	*Vacuuming Time (min)*		
	5	*10*	*15*
16	0.007	0.010	0.008
23	0.010	0.003	0.009
30	0.003	0.006	0.003

TABLE 5 Rice Specific Gravities Using Aggregate RB

Residual Pressure (A), mm Hg	Vacuuming Time (B), min.								
	5			10			15		
	Before	After	Difference	Before	After	Difference	Before	After	Difference
16	2.529	2.524	0.005	2.533	2.523	0.010	2.534	2.528	0.006
	2.527	2.520	0.007	2.524	2.514	0.010	2.531	2.524	0.007
	2.529	2.519	0.010	2.524	2.515	0.009	2.532	2.521	0.011
Avg.	2.528	2.521	0.007	2.527	2.517	0.010	2.532	2.524	0.008
23	2.518	2.508	0.010	2.532	2.529	0.003	2.530	2.521	0.009
	2.520	2.510	0.010	2.526	2.524	0.002	2.531	2.523	0.008
	2.523	2.513	0.010	2.526	2.522	0.004	2.536	2.525	0.011
Avg.	2.520	2.510	0.010	2.528	2.525	0.003	2.532	2.523	0.009
30	2.529	2.527	0.002	2.524	2.519	0.005	2.532	2.530	0.002
	2.522	2.518	0.004	2.527	2.519	0.008	2.528	2.526	0.002
	2.524	2.521	0.003	2.520	2.516	0.004	2.527	2.523	0.004
Avg.	2.525	2.522	0.003	2.524	2.518	0.006	2.529	2.526	0.003

Notes :

1. Before, After, and Difference refer to Before dry-back, After dry-back, and the difference of the two.

TABLE 6 ANOVA for Rice Gravity Differences Using Aggregate RB

Source	df	SS	MS	F	$F_{Crit.}$
Total	26	0.00026674	-	-	-
Res. Pr. (A)	2	0.00010496	0.00005248	23.09	3.63 *
Vac. Time (B)	2	0.00000230	0.00000115	0.51	3.63
AxB	4	0.00011215	0.00002804	12.33	3.01 *
Blocks	2	0.00001096	-	-	-
Error	16	0.00003637	0.00000227	-	-

* Significant at $\alpha = 0.05$.

TABLE 7 ANOVA for Rice Gravity Values Before Running Supplementary Procedure Using Aggregate RB

Source	df	SS	MS	F	$F_{Crit.}$
Total	26	0.00055000	-	-	-
Res. Pr. (A)	2	0.00005267	0.00002633	2.92	3.63
Vac. Time (B)	2	0.00021667	0.00010833	12.00	3.63 *
AxB	4	0.00009733	0.00002433	2.70	3.01
Blocks	2	0.00003889	-	-	-
Error	16	0.00014444	0.00000903	-	-

* Significant at $\alpha = 0.05$.

The factor level 30 mm Hg for Factor *A* (residual pressure) appears to be supported on the basis of interaction $A \times B$ as well. For Factor *B*, however, we could select any level. The optimal levels based on the differences, therefore, are

- Residual pressure—30 mm Hg, and
- Vacuuming time—Any level.

Values Before Running Supplementary Procedure

Here only Factor *B* (vacuuming time) is found to be significant at $\alpha = 0.05$. The objective in this case was to maximize the value of the theoretical maximum specific gravity before running the supplementary procedure or to eliminate the need for running the supplementary procedure, which is time-consuming and prone to testing errors. To decide the optimal levels, the cumulative averages for Factor *B* are reported as follows:

Level (min)	*Cumulative Average*
5	2.525
10	2.526
15	2.531

The optimal levels of factors are selected as

- Residual pressure—Any level, and
- Vacuuming time—15 min.

Combining the results then, the optimal levels of factors for Phase 2 are

- Residual pressure—30 mm Hg, and
- Vacuuming time—15 min.

Finally, as a result of the experiments conducted during Phases 1 and 2 of this study, the following levels of factors should be used when employing the Rice method to determine the theoretical maximum specific gravity of HMA mixtures:

- Temperature—77°F,
- Residual pressure—30 mm Hg, and
- Vacuuming time—15 min.

The use of these optimal levels of factors becomes even more important when one is dealing with absorptive aggregates, which tend to absorb water during the vacuuming phase and thus require a supplementary procedure to correct for this. The use of these levels will minimize the difference between the values of the theoretical maximum specific gravity obtained before and after running the supplementary procedure and may even eliminate the use of the supplementary

procedure for absorptive aggregates if these are adequately coated.

The current ASTM D2041 does specify the temperature to be 77°F. However, there is no restriction on the lower limit of the residual pressure (or, in other words, the upper limit of the vacuum level), which is important while one is dealing with highly absorptive aggregates. This has probably led to the poor reproducibility of the test method.

One more conclusion that has emerged from this study is that it is not necessary to make the water boil during vacuuming phase in order to get all the air out of the sample. This is concluded from the fact that the interaction of temperature and residual pressure was not found to be significant.

CONCLUSIONS AND RECOMMENDATIONS

On the basis of data obtained using two different aggregates and one asphalt cement, the following conclusions are drawn and recommendations made:

1. The following optimum levels of the factors temperature, residual pressure, and vacuuming time are recommended for use when using the Rice method for determining the theoretical maximum specific gravity of an HMA mixture:

- Temperature—77°F,
- Residual pressure—30 mm Hg, and
- Vacuuming time—15 min.

The use of these levels becomes even more important when one deals with absorptive aggregates, which tend to absorb water during the vacuuming phase and require the use of supplementary (dry-back) procedure to correct for the amount of water absorbed. Use of these optimum levels will minimize the difference between the values of the theoretical maximum specific gravity obtained before and after running the supplementary procedure and may even eliminate the use of the supplementary procedure for absorptive aggregates if the aggregate is adequately coated. Use of these same levels by all laboratories is also expected to improve the reproducibility of the Rice method.

2. It is not necessary to make the water boil during vacuuming phase of the Rice method in order to get all the air out of the sample. In fact, the use of lower partial vacuum (30 mm Hg residual pressure instead of 23 mm Hg, as required for boiling at 77°F) is even more important when aggregates of absorptive nature are handled.

3. Proposed modifications to the ASTM D2041 in view of these conclusions and revisions to the procedure are indicated in the following section. Curing of the HMA mix at 290°F for 4 hr before running the Rice method is based on previous research by the authors under SHRP Project A-003B. It should be noted that the proposed modifications are based on data from two mixes only. A multilaboratory round-robin study involving several mixes is recommended.

ADDITIONS AND REVISIONS TO ASTM D2041-90

The proposed revisions and additions to ASTM D2041-90 (Theoretical Maximum Specific Gravity of Bituminous Paving Mixtures) based on this study are given.

Section 6.1.2

- *Old*: The vacuum container size depends on the minimum sample size requirements given in 8.2. Avoid using a small sample in a large container.
- *New*: The vacuum container size depends on the minimum sample size requirements given in 7.2. Avoid using a small sample in a large container.

New Section and Note

- 7.3 For mix design and production control purposes, the sample should be cured in an oven at 290°F for at least 4 hr.
- Note 5: Curing in the oven at the specified temperature is especially important when absorptive aggregates are used. This will ensure the computation of realistic values for the amount of asphalt absorbed by the aggregate and void properties of the mix.
- Note 6: Curing of the mix as required in 7.3 may not be necessary during production if the mix is stored in a surge or storage silo for at least 3 hr. Curing time can also be reduced or eliminated during production if it can be demonstrated through a series of tests conducted after 0, 1, 2, 3, and 4 hr curing time.

Note 5

Renumber exiting Note 5 to Note 7.

Section 9.4 and New Note

- *Old*: Remove air trapped in the sample by applying gradually increased vacuum until the residual pressure manometer reads 30 mm of Hg or less. Maintain this residual pressure for 5 to 15 min. Agitate the container. . . .
- *New*: Remove air trapped in the sample by applying gradually increased vacuum until the residual pressure manometer reads 30 mm of Hg. Maintain this residual pressure within ±1 mm Hg for 15 min. Agitate the container. . . .
- Note 8: It has been found that by using this combination of residual pressure (30 mm Hg) and vacuuming time (15 min), the need for running the supplementary procedure (Section 11) can generally be avoided when testing a thoroughly coated mix.

Note 6

Delete existing Note 6.

Notes 7, 8, and 9

Renumber existing Notes 7, 8, and 9 to Notes 9, 10, and 11.

Section 13

Change all references to "Section 9" in the precision statements to "Section 11."

ACKNOWLEDGMENTS

This study was conducted by the National Center for Asphalt Technology (NCAT) at Auburn University under SHRP Contract A-003B on fundamental studies of asphalt aggregate interactions including adhesion and absorption.

REFERENCES

1. J. M. Rice. Maximum Specific Gravity of Bituminous Mixtures by Vacuum Saturation Procedure. *ASTM Special Technical Publication 191*, 1956.
2. J. M. Rice. New Test Method for Direct Measurement of Maximum Density of Bituminous Mixtures. *Crushed Stone Journal*, Sept. 1953.
3. W. C. Ricketts, J. C. Sprague, D. D. Tabb, and J. L. McRae. An Evaluation of the Specific Gravity of Aggregates for Use in Bituminous Mixtures. *Proc., ASTM*, Vol. 54, 1954.
4. *Investigation of the Penetration of Asphalt into Porous Aggregates as Related to and Affecting the Specific Gravity of the Aggregate. Miscellaneous Paper* 4-88. U.S. Army Corps of Engineers Waterways Experiment Station, Vicksburg, Miss., 1954.
5. C. A. Franco and K. W. Lee. Development of a Pressure Method to Determine Theoretical Specific Gravity of Bituminous Paving Mixtures. In *Transportation Research Record 1269*, TRB, National Research Council, Washington, D.C., 1990.

The opinions, findings, and conclusions expressed here are those of the authors and not necessarily those of SHRP, NCAT, or Auburn University.

Laboratory Tests for Assessing Moisture Damage of Asphalt Concrete Mixtures

M. STROUP-GARDINER AND J. EPPS

A synopsis of an extensive report prepared for the National Lime Association and FHWA is presented. Field projects originally constructed in the mid-1980s incorporating various methods of adding lime were used as the basis for the research effort. A total of 13 test sections constructed in four states were evaluated. Cores from the test sections and raw materials from the original suppliers for each project were obtained. The pavement condition surveys reported as part of the companion research effort were used to compare laboratory results with pavement performance. Laboratory testing included variations of existing moisture conditioning procedures: (a) no saturation, (b) partial saturation, and (c) full saturation. Results indicate that moisture-sensitive mixtures without lime will be significantly damaged even when the initial saturation step is eliminated. When lime is included in the mixtures, some level of saturation is needed to reduce significantly mixture strength. The increase in the number of freeze-thaw cycles from one to six follows the same trend—that is, mixtures without lime are significantly damaged, whereas mixtures with lime show only a moderate decrease in mixture strength with increasing numbers of freeze-thaw cycles. There is little difference in the mixture properties obtained for a given aggregate source when lime is introduced to either dry or prewet aggregate when preparing laboratory specimens. Little difference is noticed between the introduction of lime to prewet aggregate or lime with the binder inside the drum for field mixtures. The no-initial-saturation option provides the best agreement in relative ranking between conditioned resilient moduli values and the moduli values obtained for the cores. As the level of saturation is increased, the distinction between projects is lost.

The main purpose in assessing the moisture sensitivity of laboratory-prepared samples is to identify asphalt-aggregate mixtures that are susceptible to in-service moisture damage. However, any laboratory assessment of moisture sensitivity assumes that laboratory conditioning of laboratory-prepared samples accurately reflects the in-service environmental conditions and the as-constructed asphalt concrete. Current laboratory test methods have been developed from rational approaches, but little information is available that compares the various approaches and relates them to pavement performance.

This research program was designed to define the relationships between laboratory test method variables and pavement performance.

BACKGROUND

Current laboratory-conditioning procedures have been developed to represent both warm-wet and cold-wet climatic regions of the country. The two most commonly used laboratory simulations of these types of climates were developed by Root and Tunnicliff (*3*) and by Lottman (*4*). Both methods include some level of initial moisture saturation of the sample, followed by freezing (Lottman only), and subsequent warm-water thawing. The inclusion of a freeze-thaw cycle is based on regional climatic conditions. The second main difference between the two procedures is the result of a controversy over methods of saturating the sample before environmental conditioning.

Root and Tunnicliff have hypothesized that saturating samples to more than 90 percent of the sample void space can, by itself, damage the sample by creating excessive internal pressure (*3*). They also mention that saturation levels greater than this range may not be representative of actual field conditions. On the basis of these hypotheses, they have recommended saturation levels between 55 and 80 percent.

Lottman has indicated that damage due to saturation levels greater than 90 percent may be minimal and can be monitored by determining the swell (i.e., increase in sample volume) of the saturated sample (*4*). His procedure recommends a set level of vacuum pressure for a fixed time interval. Experience with this procedure has indicated that the specified 24 in. of vacuum for 30 min results in saturation levels consistently over 90 percent (*5*).

Additional research has indicated that increasing the number of freeze-thaw cycles used also affects test results (*5*). Typically, both mixture strength and retained strength ratios decrease as the number of cycles increases.

The testing program used to evaluate laboratory-prepared specimens was based on these test method variables.

RESEARCH PROGRAM

Objective

The main objective of the research was to establish guidelines for the laboratory assessment of moisture sensitivity of asphalt concrete mixtures. This was accomplished by first comparing test results obtained for the various laboratory test methods and then comparing these results to the fundamental properties (i.e., resilient moduli and tensile strength) of the cores.

Scope

A total of 13 test sections constructed by FHWA in Wyoming, Montana, New Mexico, and Georgia were used as the source

College of Engineering, University of Nevada, Reno, Nev. 89577.

of raw materials, cores, and estimates of pavement performance for this program (Figure 1). These sections were originally placed in the early 1980s to investigate both methods of adding lime and the benefits of using lime in asphalt concrete (*1*).

Raw materials were used to fabricate samples to the job mix formulas reported in the original FHWA report on the projects (*1*). Variables included in the laboratory assessment of moisture sensitivity included the number of freeze-thaw cycles (zero, one, and six), method of adding lime (dry aggregate, prewet aggregate), level of initial saturation (zero, 55 to 80 percent, and more than 90 percent). These results were then compared with the mixture properties (i.e., resilient modulus and tensile strength) of the cores.

BACKGROUND OF PROJECTS

Both the project descriptions and pavement condition surveys were reported in depth in the FHWA report for this project (*2*). A summary of this information is presented.

Project Descriptions

Wyoming

Two projects consisting of two test sections each were placed in September 1984 in Wyoming; all asphalt concrete was mixed in a drum plant. Project 1 was placed on US-14A between Garland and Byron. This project was new construction consisting of a 6-in. crushed aggregate base and a 3.5-in. layer of asphalt concrete. The top 1.5 in. of the asphalt concrete contained lime and was the test layer under investigation. Section 1 of this project contained lime added with the asphalt cement inside the drum. Section 2 had lime added to damp aggregate. The final surface was fog- and chip-sealed.

Project 2 was also new construction placed on Wyoming State Route 50 between Gillette and Pine Tree Junction. This project consisted of 9 in. of cement-treated base, followed by a 1-in. asphalt cement leveling course and a 2-in. wearing course; the wearing course was the test layer. Section 1 had lime added to damp aggregate, and Section 2 had lime added to dry aggregate inside the drum.

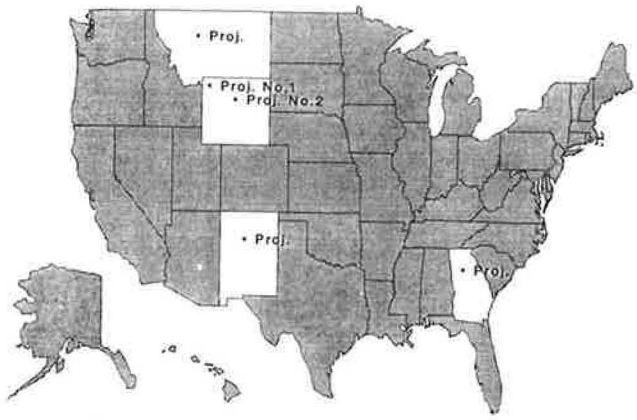

FIGURE 1 Location of original field test sections.

Montana

One overlay project consisting of two test sections was constructed in September 1984 on Interstate 15 between Craig and Cascade; a drum mix plant was used for both sections. The overlay consisted of a 3-in. asphalt concrete layer followed by an open-graded friction course. The top 2 in. of the asphalt concrete layer contained lime and were the test layers. Section 1 was prepared with a quicklime slurry added to the aggregate. Section 2 had lime added with the asphalt cement inside the drum.

New Mexico

One overlay project consisting of two test sections was constructed in July 1985 on New Mexico Route 76 between Truchas and Las Trampas; a drum mix plant was used to construct both test sections. The existing asphalt concrete was overlaid with 2.5 in. of new asphalt concrete containing lime, plus an open-graded friction course. Section 1 had lime added to damp aggregate. Section 2 had lime added with the asphalt cement inside the drum.

Georgia

Two overlay projects, one with a drum plant (Project 1, October 1984) and one with a batch plant (Project 2, September 1985), were constructed on Georgia State Route 20 in Gwinnett County beginning at the intersection with State Route 13. Four sections were constructed for Project 1: Section 1 had lime added to dry aggregate, Section 2 had lime added to damp aggregate, Section 3 had lime added with the asphalt cement inside the drum, and Section 4 had a lime slurry added to damp aggregate. Three additional sections were placed for Project 2: Section 5 had lime added to dry aggregate, Section 6 had lime added to damp aggregate, and Section 7 had a lime slurry added to damp aggregate.

Pavement Condition Surveys

Wyoming

Both sections constructed for Project 1 had a couple of low-temperature transverse cracks and a longitudinal crack at the centerline between two of the westbound lanes. There was no visible evidence of moisture damage. Although generally in good condition, Section 1 of Project 2 showed 12 low-temperature-induced transverse cracks as well as some raveling along the outside edge of the lane-line marker. Section 2 of Project 2 also showed 12 transverse cracks and some longitudinal cracking along the centerline. Surface raveling along the outside edge, along the centerline, and between the wheelpaths was also noted.

Montana

All sections were in excellent condition, except for a couple of thermally induced transverse cracks.

New Mexico

All sections were reported to be in excellent condition, except for a couple transverse cracks in Section 1; Section 2 had no cracks at all.

Georgia

All sections had slight transverse cracking. The alligator cracking in the sections was reported as follows:

- Drum Mix Plants
  - –Section 1: 11 to 15 percent,
  - –Section 2: Less than 10 percent,
  - –Section 3: 26 to 50 percent, and
  - –Section 4: None noted.
- Batch Plants
  - –Section 5: 26 to 50 percent,
  - –Section 6: 51 to 90 percent, and
  - –Section 7: 26 to 50 percent.

TESTING PROGRAM

The testing program used to develop the data presented in this report covers two areas of testing:

1. Assessment of moisture sensitivity of laboratory-prepared samples, and
2. Determination of current in-service mixture properties.

Testing of the laboratory-prepared specimens included various methods of estimating moisture damage; testing of the cores was limited to determining the current in-service mixture properties.

Sample Preparation

The job mix formulas reported during construction of each of the projects were used to prepare the specimens (*1*). Each aggregate source was sieved into 10 individual fractions, then recombined to meet the gradations. The binder content used was the percentage asphalt reported during construction quality-control testing. Samples were mixed and compacted in accordance with ASTM D1561, except that the compactive effort was reduced to produce air voids in the range of 6 to 8 percent. This range was more representative of the actual void contents reported immediately after construction.

Conditioning Procedures

Specimens were compacted and subjected to one of three conditioning procedures:

1. No saturation: Specimens were wrapped in plastic and placed in a 0°F freezer for a minimum of 15 hr. Specimens were then removed from the freezer, unwrapped, and placed in a 140°F water bath for 24 hr. Specimens were cooled to test temperature in a 77°F water bath for 2 hr.
2. 55 to 80 percent saturation: Specimens were partially saturated, and the level of saturation was determined. Once the desired level of saturation was achieved, the specimens were immediately wrapped in plastic and treated as described in the first procedure.
3. More than 90 percent saturation: Specimens were placed in a water bath and subjected to a vacuum of 30 mm of mercury (Hg) for 10 min. Specimens were then wrapped, frozen, and thawed as described.

The no-saturation option coupled with freeze-thaw conditioning was inherently included as a result of all factors' being considered in a full factorial experimental design.

Freeze-Thaw Cycles

One freeze-thaw cycle consisted of a minimum of 15 hr in a 0°F freezer, 24 hr in a 140°F water bath and 2 hr in a 77°F water bath. The time in the 77°F water bath was included in each cycle to minimize damage to the specimens as they were being rewrapped in plastic before their return to the 0°F freezer.

Methods of Adding Lime

Methods of adding lime to laboratory-prepared mixtures are designed to simulate, as closely as possible, the mixing of lime and aggregates during construction. In order to replicate the application of the lime to damp aggregate on the cold feed belt, lime is sprinkled over predampened aggregates, stirred, then used as usual in specimen preparation.

To simulate the injection of lime into the drum, just ahead of the binder, during construction, lime is sprinkled over dry aggregate. Specimens are then prepared as usual.

Measurements of Mixture Strength

Two measurements of mixture strength were determined: resilient modulus and tensile strength. Both tests were performed on the same sample because the first—resilient modulus—is considered a nondestructive test. Briefly, the resilient modulus is a ratio of the applied, repeated stress to the corresponding horizontal recoverable deformation. Testing was conducted at 77°F, 0.33 Hz, and a load duration of 0.1 sec. The tensile strength test subjects the specimen to a constant rate of strain of 2 in./min and measures the maximum stress at failure.

Moisture sensitivity is typically expressed as the ratio of either measurement after environmentally conditioning the specimen to the original strength. The resulting resilient modulus and tensile strength ratios are commonly used to describe the retained strengths of the mixtures.

EVALUATION OF LABORATORY RESULTS

Levels of Saturation

Three saturation levels before subjecting laboratory-prepared specimens to freezing and thawing were investigated: no sat-

uration, 55 to 80 percent saturation, and more than 90 percent saturation. The reader is reminded that although the no-saturation option did not saturate the specimens before freezing, the specimens were soaked and unwrapped, in the 140°F water bath during the thaw portion of the conditioning.

The resilient modulus ratio for no-saturation shows that the strength of mixtures without lime is substantially decreased just by exposure to water during the thaw stage of the conditioning procedure (Figure 2). A general trend for a decrease in resilient modulus ratio with increasing levels of saturation can also be seen.

A value of less than about 70 percent for the resilient modulus ratio, developed for a saturation level of specimens between 60 and 75 percent, has been suggested as an indication of moisture-sensitive mixtures. On the basis of this limit, only the Georgia (Project 1) and New Mexico mixtures would be acceptable as moisture-resistant mixtures without the addition of lime (specimens with 55 to 80 percent saturation).

If this same limit was applied to the results for the other levels of saturation, Wyoming Project 2 would be added to the list of acceptable projects for the no-saturation level, and none of the mixtures would be acceptable when saturation levels are greater than 90 percent.

Figure 3 shows that there is much less impact from the saturation level on the resilient modulus ratios for mixtures with lime. In fact, only the Wyoming mixtures showed any decrease in retained strengths when saturation was increased from 55 to 80 percent to more than 90 percent. When lime is added, only one project produced mixtures with a ratio substantially below 70 percent (Wyoming Project 2, 55 to 80 percent saturation).

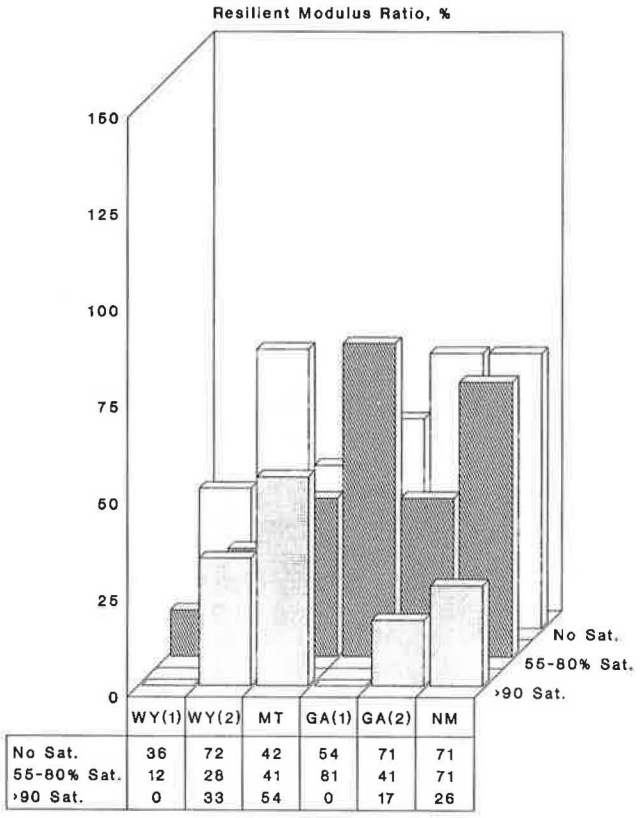

	WY(1)	WY(2)	MT	GA(1)	GA(2)	NM
No Sat.	36	72	42	54	71	71
55-80% Sat.	12	28	41	81	41	71
>90 Sat.	0	33	54	0	17	26

FIGURE 2 Impact of moisture on resilient modulus ratio for levels of saturation for mixtures with no lime (one freeze-thaw cycle).

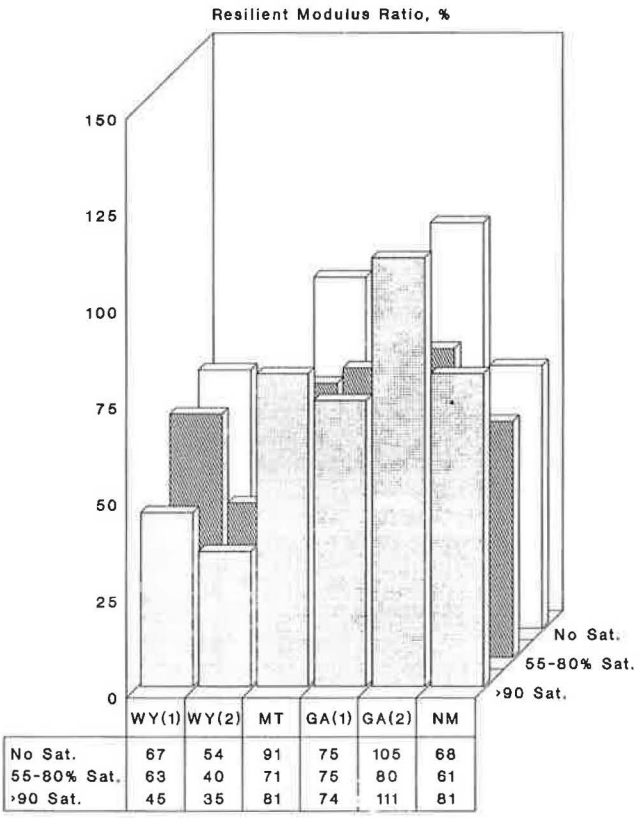

	WY(1)	WY(2)	MT	GA(1)	GA(2)	NM
No Sat.	67	54	91	75	105	68
55-80% Sat.	63	40	71	75	80	61
>90 Sat.	45	35	81	74	111	81

FIGURE 3 Impact of moisture on resilient modulus ratio for levels of saturation for mixtures with lime added to prewet aggregate (one freeze-thaw cycle).

This generally agrees with the pavement condition survey information noted in the previous section. No evidence of stripping was noticed for any of the projects except Wyoming (Project 2). As mentioned, Figure 3 shows that this was the only project with a resilient modulus ratio (40 percent) substantially below the suggested 70 percent limit. This would indicate that the 70 percent limit for indicating moisture sensitivity could be lowered to include mixtures with ratios in the 60s, and would be applicable to only mixtures tested with an initial saturation level between 55 and 80 percent.

Occasionally anomalies in the ratios are noticed. A comparison of Figures 2 and 3 shows that the ratio for Wyoming Project 2 is 72 with no lime but only 54 with lime (no saturation). If only ratios are considered as indicators of moisture sensitivity, then the mixture with lime would appear to be more sensitive to water. This contradiction of historical experience leads to a closer examination of values used to develop the ratios.

Figures 4 and 5 show that the original resilient modulus of the Wyoming Project 2 mixtures was 303 kip/in^2 (ksi) without lime and almost 500 ksi with lime, an increase in strength of approximately 65 percent. The wet resilient moduli for these projects were 218 and 267 ksi, respectively (no saturation). The mixture with lime still retains approximately 20 percent more strength than the mixture with no lime. When the wet

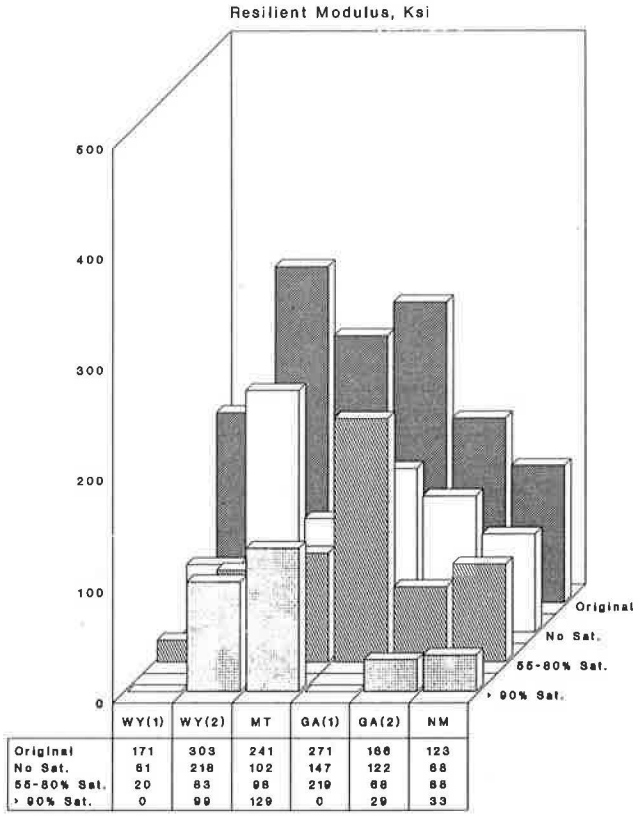

	WY(1)	WY(2)	MT	GA(1)	GA(2)	NM
Original	171	303	241	271	166	123
No Sat.	61	218	102	147	122	68
55-80% Sat.	20	83	98	219	68	68
> 90% Sat.	0	99	129	0	29	33

FIGURE 4 Comparison of resilient moduli after moisture conditioning at various levels of saturation conditioning (no lime, one freeze-thaw cycle).

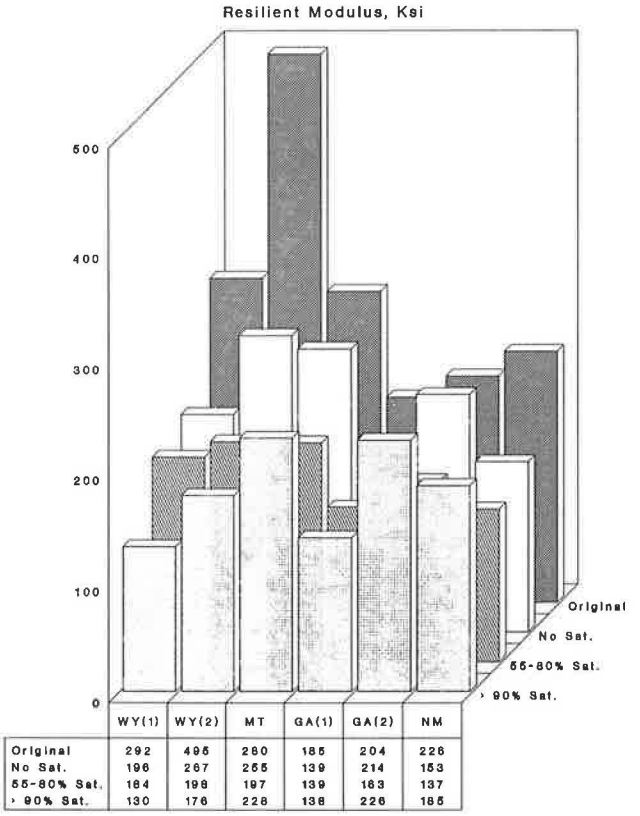

	WY(1)	WY(2)	MT	GA(1)	GA(2)	NM
Original	292	496	260	185	204	226
No Sat.	196	267	255	139	214	153
55-80% Sat.	164	198	197	139	163	137
> 90% Sat.	130	176	228	138	226	185

FIGURE 5 Comparison of resilient moduli after moisture conditioning at various levels of saturation conditioning (lime added to prewet aggregate, one freeze-thaw cycle).

strengths are considered alone, the benefit of adding lime to the mixtures can be seen.

The large initial increase in strength is concealing the benefit of adding lime when only the ratios are considered. For this reason, assessments of moisture sensitivity should include not only limits on the strength ratios, but also minimum values of wet strengths.

Figures 6 and 7 indicate that the tensile strength ratios follow the same trends as the resilient modulus ratios—that is, as the level of saturation increases, the ratios decrease substantially for mixtures without lime (Figure 6). The tensile strength ratio is relatively insensitive to saturation levels when mixtures contain lime (Figure 7).

Number of Freeze-Thaw Cycles

Figure 8 shows typical trends in the resilient modulus ratios that can be expected for mixtures without lime. At six cycles of conditioning, virtually all mixtures have failed.

Figure 9 shows, once again, that the addition of lime significantly improves the moisture resistance of the mixtures. An increase in the number of freeze-thaw cycles from one to six results in only a slight to moderate decrease in resilient modulus ratio.

Not all data are presented in this summary report, but these trends were consistent regardless of the level of saturation for resilient modulus and tensile strength ratios (*6*).

Methods of Adding Lime

Figure 10 shows that the addition of lime, in any manner, produces essentially the same wet resilient modulus values after one freeze-thaw cycle. There is, again, a substantial improvement over mixtures without lime. Figure 11 shows that this is also true when the number of freeze-thaw cycles is increased to six. The mixtures without lime have essentially failed; those with lime, added by either method, still have substantial wet strengths.

COMPARISON OF LABORATORY RESULTS WITH CORES FROM PROJECTS

Both the levels of saturation and methods of adding lime will be compared in this section. From the laboratory comparison of test results, one freeze-thaw cycle was considered adequate to indicate any substantial changes in mixture properties and will not be considered as a comparison variable in this section.

Levels of Saturation

Both resilient modulus and tensile strength values were obtained for cores from all of the field sections. A direct comparison between laboratory test results and core properties

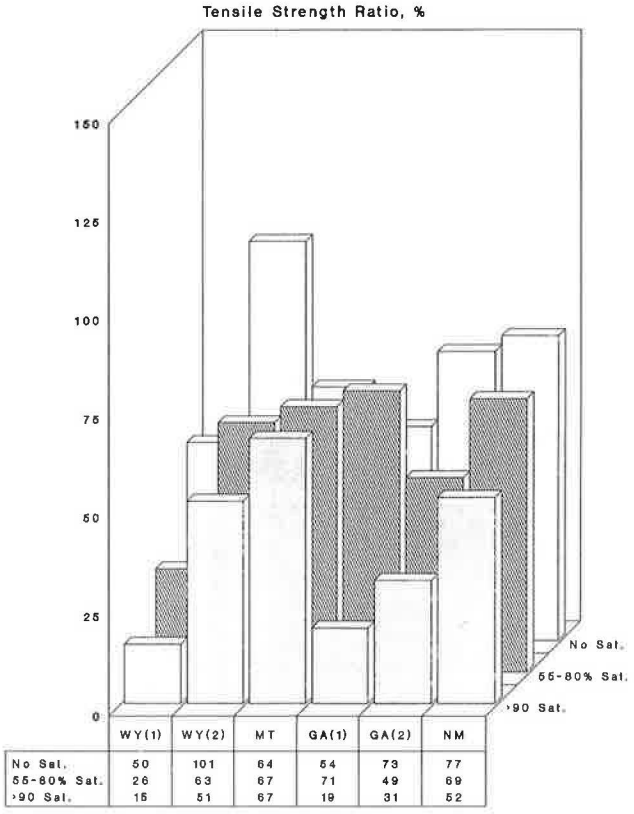

	WY(1)	WY(2)	MT	GA(1)	GA(2)	NM
No Sat.	50	101	64	54	73	77
55-80% Sat.	26	63	67	71	49	69
>90 Sat.	15	51	67	19	31	52

FIGURE 6 Impact of moisture on tensile strength ratios for various levels of saturation for mixtures with no lime (one freeze-thaw cycle).

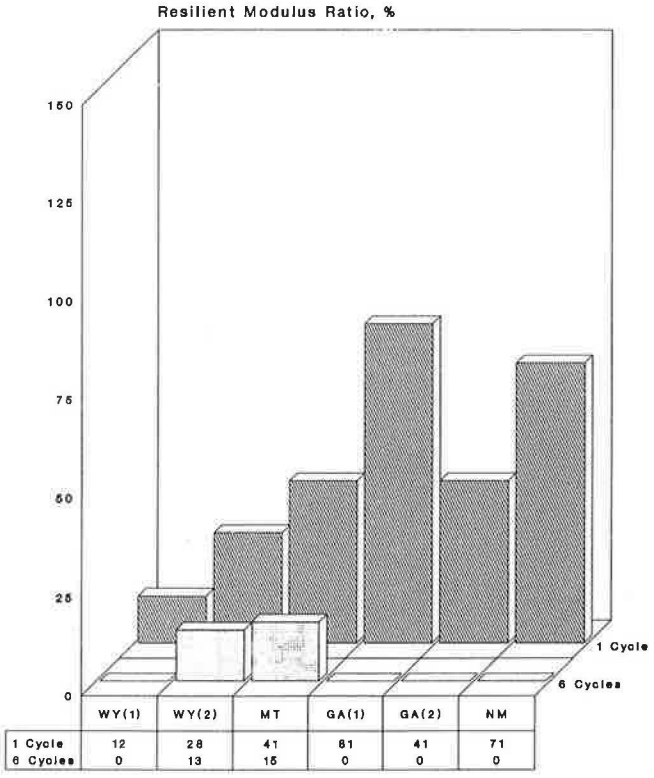

	WY(1)	WY(2)	MT	GA(1)	GA(2)	NM
1 Cycle	12	28	41	61	41	71
6 Cycles	0	13	15	0	0	0

FIGURE 8 Impact of number of freeze-thaw cycles on resilient modulus ratio (no lime, 55 to 80 percent saturation).

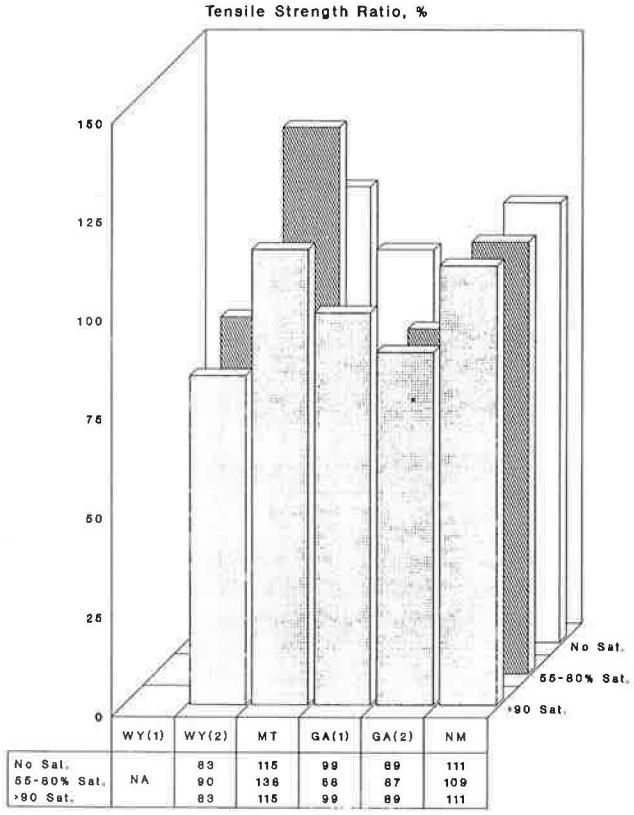

	WY(1)	WY(2)	MT	GA(1)	GA(2)	NM
No Sat.		83	115	99	89	111
55-80% Sat.	NA	90	136	66	87	109
>90 Sat.		83	115	99	89	111

FIGURE 7 Impact of moisture on tensile strength ratio for levels of saturation for mixtures with lime added to prewet aggregate (one freeze-thaw cycle).

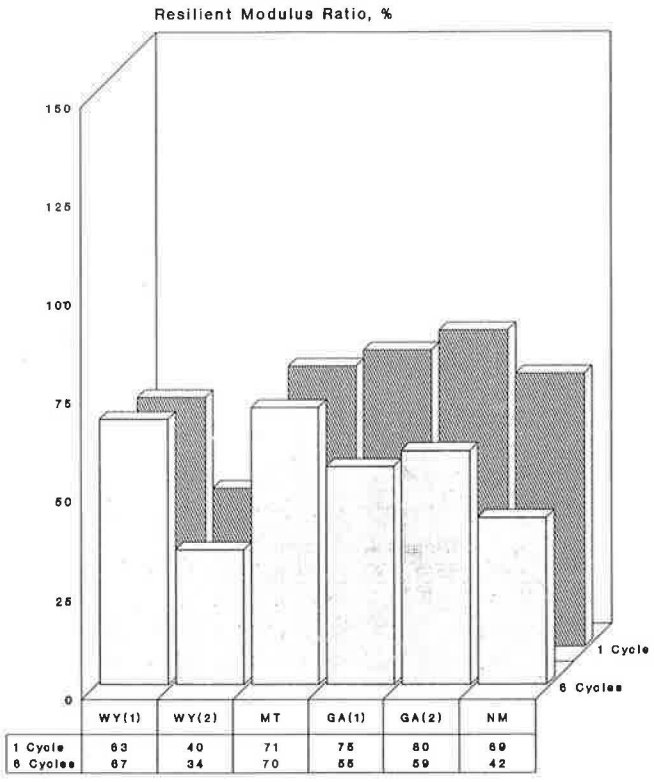

	WY(1)	WY(2)	MT	GA(1)	GA(2)	NM
1 Cycle	63	40	71	75	80	69
6 Cycles	67	34	70	55	59	42

FIGURE 9 Impact of number of freeze-thaw cycles on resilient modulus ratio (lime added to prewet aggregate, 55 to 80 percent saturation).

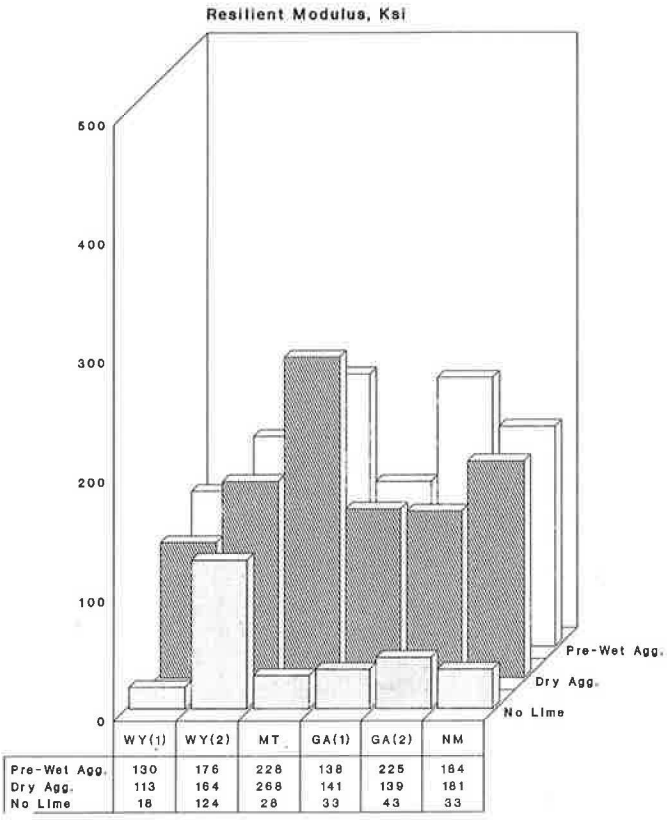

FIGURE 10 Impact of various methods of adding lime on moisture sensitivity of mixtures (55 to 80 percent saturation, one freeze-thaw cycle).

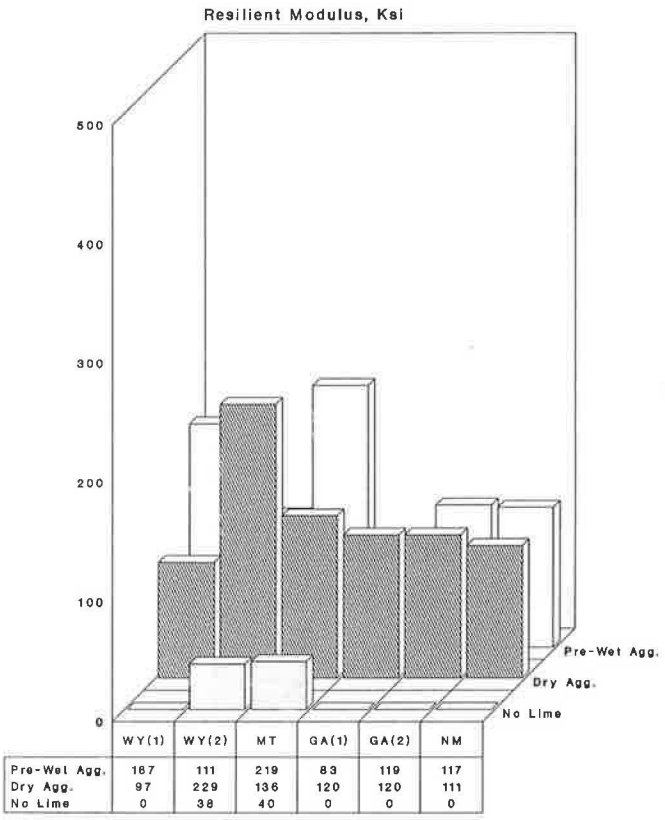

FIGURE 11 Impact of various methods of adding lime on moisture sensitivity of mixtures (55 to 80 percent saturation, six freeze-thaw cycles).

can be made for 9 of the 13 sections constructed. This reduction in the data base is because neither the particular lime slurry nor the lime blended with the binder could be reproduced in the preparation of laboratory specimens.

In theory, if the laboratory estimate of moisture damage is accurate, conditioned resilient modulus and tensile strengths should be reflected by the core properties several years after construction. Figures 12 and 13 show that this is true for these sections. What is interesting is that the results for the no saturation and 55 to 80 percent saturation reflect the core properties. In fact, the no-saturation option appears to best reflect the discrete differences between the projects. As the levels of saturation increase to above 90 percent for the laboratory-prepared specimens, the differences between the projects become less evident.

This leads to the conclusion that each mixture has a unique affinity for water, and hence subsequent moisture damage. All that is required to induce moisture damage is to expose the compacted specimen to warm water after it has been frozen. This affinity for water can be accentuated if the specimens are initially saturated; however, the subtle distinctions between projects can be camouflaged by high levels of saturation.

Methods of Adding Lime

These figures also provide a means for comparing methods of adding lime. Figure 12 presents data for both laboratory-prepared specimens and cores for mixtures with lime added to prewet aggregate. The first fact that is obvious is that the cores produce stiffer mixture properties than the laboratory specimens. The higher core stiffness is, as expected, attributable to the decrease in air voids (known to increase resilient moduli) from traffic and stiffening of the binder due to oxidation and ultraviolet light. The second fact is that the trend (or ranking) shown by the core properties is evident in the laboratory-prepared specimens when either the no-saturation or the 55-to-80-percent-saturation option is used. This would indicate that the laboratory method of introducing lime into the laboratory samples reasonably represents field conditions.

Figure 13 provides the same comparison for mixtures with lime added to dry aggregate. Again, the same trends as discussed are apparent.

Four of the 13 field sections can provide a direct comparison of methods of adding lime in the field. Figures 14 and 15 show a comparison of resilient modulus and tensile strengths, respectively, for lime added in the drum with the binder and lime added to damp aggregate on the cold feed belt. The data show that both methods of introducing the lime during construction generally produce mixtures with similar properties; this is generally more true of the tensile strengths than of the resilient modulus. In one case there is little impact on the moduli, in two cases lime added with the binder produced significantly higher moduli, and in another case the moduli increased when the lime was added to damp aggregate.

The use of either a drum or batch plant does not appear to alter this conclusion. Figure 16 shows that the Georgia

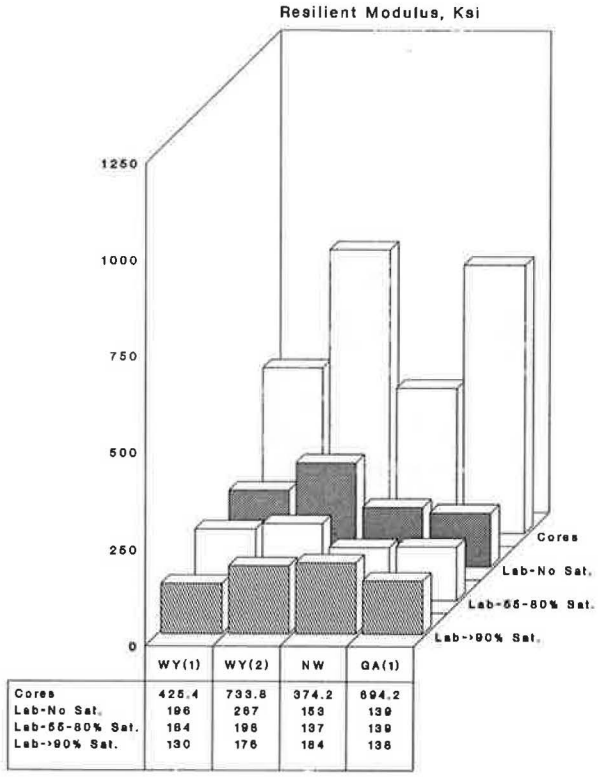

	WY(1)	WY(2)	NW	GA(1)
Cores	425.4	733.8	374.2	694.2
Lab-No Sat.	196	267	153	139
Lab-55-80% Sat.	184	198	137	139
Lab-→90% Sat.	130	176	184	138

FIGURE 12 Comparison between cores and lab estimate of resilient modulus after moisture damage (lab samples: one freeze-thaw cycle, lime added to prewet aggregate; cores: unconditioned value, lime added to damp aggregate).

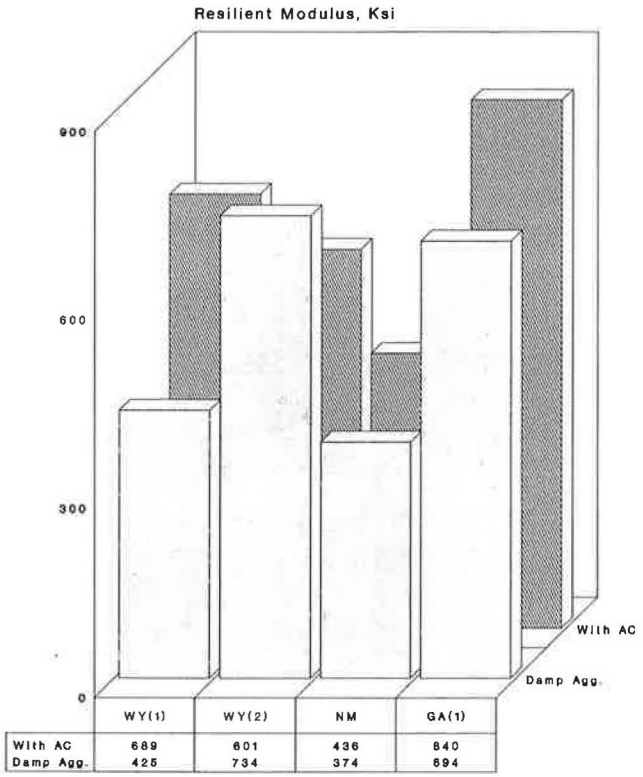

	WY(1)	WY(2)	NM	GA(1)
With AC	689	601	436	840
Damp Agg.	425	734	374	694

FIGURE 14 Comparison of methods of adding lime for field sections.

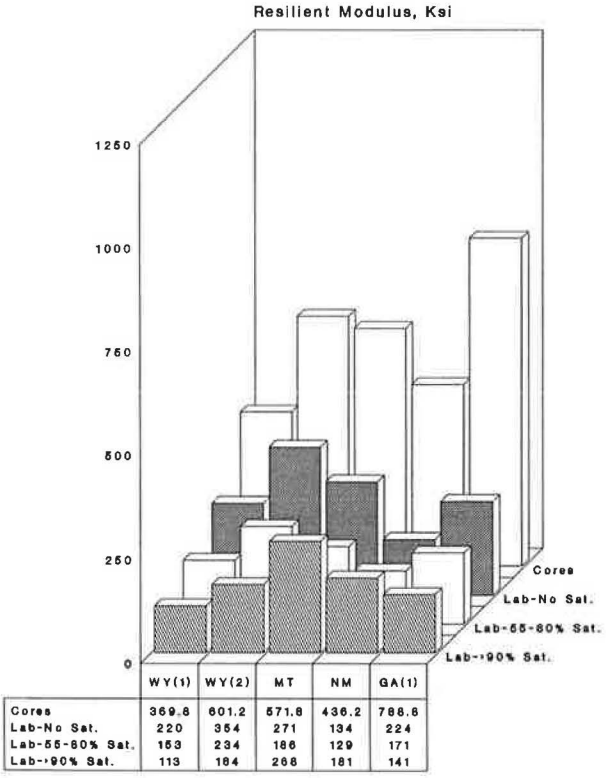

	WY(1)	WY(2)	MT	NM	GA(1)
Cores	369.8	601.2	571.8	436.2	788.8
Lab-No Sat.	220	354	271	134	224
Lab-55-80% Sat.	153	234	186	129	171
Lab-→90% Sat.	113	184	268	181	141

FIGURE 13 Comparison between cores and lab estimate of resilient modulus after moisture damage (lab samples: one freeze-thaw cycle, lime added to dry aggregates; cores: unconditioned value, lime added to asphalt concrete).

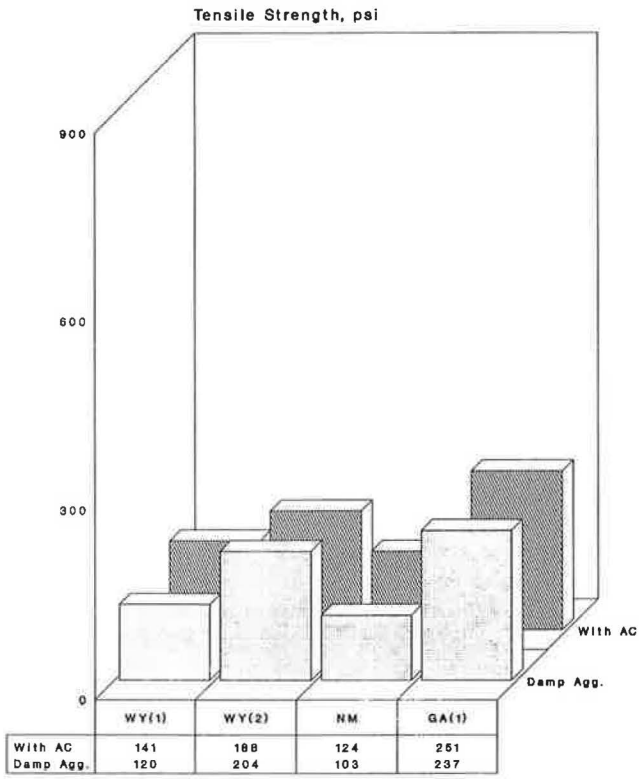

	WY(1)	WY(2)	NM	GA(1)
With AC	141	188	124	251
Damp Agg.	120	204	103	237

FIGURE 15 Comparison of methods of adding lime for field sections.

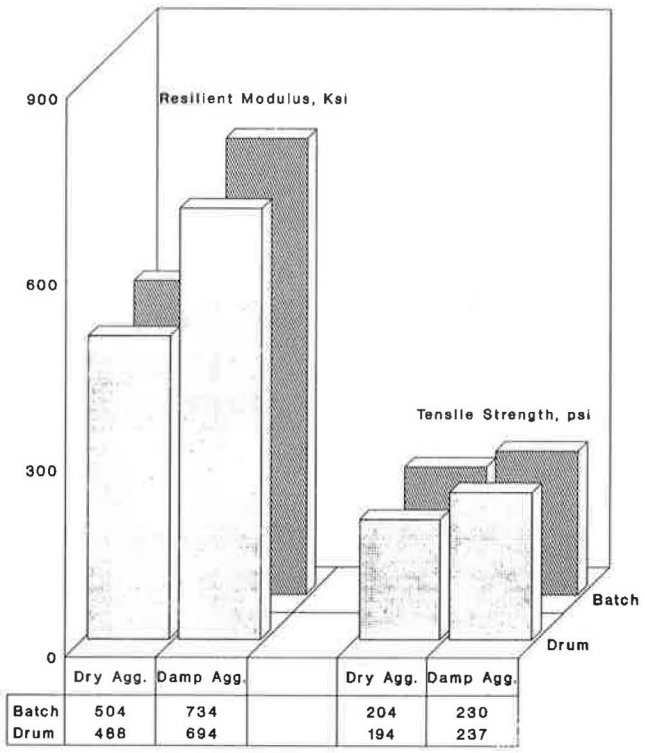

FIGURE 16 Comparison of resilient modulus and tensile strength between drum and batch plants (Georgia cores).

projects constructed with both plants show virtually no difference in either resilient modulus or tensile strength.

SUMMARY

The following conclusions can be drawn from the data presented in this paper:

1. Mixtures without lime will exhibit a significant loss of both resilient modulus and tensile strength even though the initial saturation step is eliminated.
2. Mixtures with lime require some level of initial saturation in order for the resulting impact of moisture on resilient modulus and tensile strength to be significant.
3. When the number of freeze-thaw cycles is increased from one to six, mixtures without lime generally do not survive the testing sequence. The impact of the increased numbers of cycles is substantially reduced for mixtures with lime.
4. Lime added to either dry or prewet aggregate for laboratory-prepared specimens produces mixtures with similar resilient moduli values for a given aggregate source.
5. Laboratory methods of adding lime to either prewet aggregate or to dry aggregate appear to reasonably simulate the field application of lime to damp aggregate on the cold feed belt and lime added with the binder in the drum, respectively.
6. When laboratory test results after various methods of moisture conditioning are compared to moduli (unconditioned) cores obtained from in-service pavements, the following conclusions can be drawn: (a) the relative ranking of the resilient moduli values for the various projects is consistent between test methods using no initial saturation and 55 to 80 percent saturation—there is less agreement for the more-than-90-percent-saturation option because of the decrease in differences evident between the projects; and (b) as the level of initial saturation is increased, the distinction between the various projects is reduced. The no-initial-saturation option best replicates the distinction observed between the projects.
7. Using one freeze-thaw cycle for conditioning laboratory-prepared specimens reflects pavement performance when either no or 55 to 80 percent saturation is used.
8. A limited comparison of methods of adding lime during construction indicates mixtures with either lime added to prewet aggregate or lime added with the binder inside of the drum produce mixtures with similar properties. No difference was noticed between either drum or batch plants.

RECOMMENDATIONS

From the findings presented in this report, the following recommendations are made:

1. The initial saturation level step can be eliminated when specimen is frozen before the warm-water soaking.
2. If initial saturation is used, saturation levels should be no more than 80 percent.
3. One freeze-thaw cycle is sufficient for estimating pavement performance.

ACKNOWLEDGMENTS

The authors would like to thank FHWA for its commitment to improving relationships between laboratory testing and field performance. The authors would also like to thank the members of the National Lime Association for their support and help in completing this extensive research program.

REFERENCES

1. D. G. Tunnicliff and R. E. Root. *Introduction of Lime into Asphalt Concrete Mixtures*. Report FHWA/RD-86/071. FHWA, U.S. Department of Transportation, July 1986.
2. S. W. Hudson, F. N. Finn, H. J. Treybig, J. A. Epps, V. Anderson, and M. A. Diaz. *AC Striping Problems and Corrective Treatments*. Report FHWA/R-90/049. FHWA, U.S. Department of Transportation, May 1990.
3. D. G. Tunnicliff and R. E. Root. *NCHRP Report 274: Use of Antistripping Additives in Asphaltic Concrete Mixtures*. TRB, National Research Council, Washington, D.C., Dec. 1984.
4. R. P. Lottman. *NCHRP Report 246: Predicting Moisture-Induced Damage to Asphaltic Concrete-Field Evaluation*. TRB, National Research Council, Washington, D.C., May 1982.
5. J. Coplantz and D. Newcomb. Water Sensitivity Test Methods for Asphalt Concrete Mixtures: A Lab Comparison. In *Transportation Research Record 1171*, TRB, National Research Council, Washington, D.C., 1988.
6. M. Stroup-Gardiner and J. Epps. *Relationship Between Moisture Conditioning of Laboratory Samples and Pavement Performance*. Report 1-953-1. University of Nevada, Reno, Jan. 1991.

Structure-Fracture Toughness Relationships of Asphalt Concrete Mixtures

H. AGLAN, I. SHEHATA, L. FIGUEROA, AND A. OTHMAN

A methodology to characterize the resistance of asphalt concrete mixtures to fatigue crack propagation has been developed to construct fundamental structure-fracture toughness relationships. Experimental techniques to evaluate parameters controlling the crack propagation process are presented. These parameters include crack driving force and the change in work done on the crack tip damage (active zone). A linear relationship between the width of the active zone and the crack length is assumed in order to quantify the amount of damage at each crack length. A constitutive equation is used to extract the specific energy of damage (γ'), a material parameter characteristic of the asphalt concrete mixture's resistance to crack propagation, and a dissipative coefficient (β'). The capability of this approach to discriminate the subtle effect introduced by different chemical structures of asphalts on γ' is demonstrated on Elvax-modified AC-5 and AC-20 concrete mixtures. The validity of the current approach to describe the fatigue behavior of asphalt concrete mixtures over the entire range of energy release rate is verified. The practical utilization of this methodology is evident. It forms a basis on which structure- or processing condition–fracture toughness relationships of asphalt concrete mixtures can be constructed. Such relationships can guide the development of asphalt concrete mixtures with superior crack resistance and aid in the design of primary and secondary pavements.

The limitation of fatigue cracking in paving mixtures and flexible pavement systems is a major design criterion in various transportation facilities and military airfields. The repetitive nature of traffic loading on pavements in service has led to laboratory investigations of their performance under cyclic loading. These investigations have been carried out through two main approaches: a phenomenological approach and a fracture mechanics–based approach.

The phenomenological approach that is based on the endurance concept using Wohler techniques (*1*, p. 199) has been used by various researchers (*2*, p. 188; *3*; *4*, p. 310; *5*). It correlates the number of cycles to failure (N_f) to the applied stress (σ) or strain (ε) through empirical constants. A familiar relationship of this approach that represents the fatigue response is expressed as

$$N_f = C_1 (1/\varepsilon)\, C_2 \tag{1}$$

where C_1 and C_2 are regression constants. Because of its simplicity, this approach has been widely adopted. However, it carries severe limitations. It does not address the number of cycles to failure for both crack initiation and propagation of which the relative magnitude of each is extremely important from a structural design viewpoint. Moreover, the constants C_1 and C_2 are indeed regression constants and are influenced by many variables such as the type and rate of loading. Therefore, they are not material constants.

The fracture mechanics approach adopted by many workers essentially deals with crack propagation (*6–8*). This approach identifies the crack driving force (X) and correlates it with the average crack speed (da/dN) in a power law based on the equation derived by Paris (*9*, p. 528; *10*). This equation is given as

$$da/dN = A(X)^n \tag{2}$$

X can be the stress intensity factor K (*11*) or the stress intensity factor range ΔK. The parameters A and n are empirical constants.

Alternatively, the elastic energy release rate may be invoked as the crack driving force for linear elastic conditions with limited crack tip plasticity. This is expressed as

$$G = K^2(1 - \nu^2)/E \tag{3}$$

For elastic-plastic conditions the energy release rate J can be obtained (*12*) from the load displacement curve associated with crack extension, based on the J-integral proposed by Rice (*13*, p. 379). To include unloading effects, J may be evaluated from the change in potential energy (the area above the unloading curve) with respect to the crack length, divided by the thickness of the specimen (*14*). Again A and n in Equation 2 are empirical constants that may under some conditions be constant but that are not material properties. This view is shared by many researchers. It is stated by Majidzadeh et al., who are advocates of the power law type analysis, that at low temperature for sand asphalt and asphaltic concrete beams, A in Equation 2 becomes a material constant (*6*). However, at high temperature, A and n can no longer be considered as material constants.

Schapery developed a theoretical analysis to link material properties such as the creep compliance, tensile strength, and fracture energy to determine the A and n in the Paris equation for viscoelastic materials (*15–17*). This theoretical relationship has been examined using asphalt concrete mixtures by researchers including Little et al. (*14*) and Germann and Lytton (*8*). Little et al. found that the crack speed of various

H. Aglan and I. Shehata, Department of Mechanical Engineering, Tuskegee University, Tuskegee, Ala. 36088. L. Figueroa and A. Othman, Department of Civil Engineering, Case Western Reserve University, Cleveland, Ohio 44106.

asphalt concrete specimens at two different crack lengths (1 and 2 in.) were identical when they were calculated from either the viscoelastic analysis or the linear elastic approach. They concluded that both analyses yield the same results when using A and n from either approach to determine the crack speed. Germann and Lytton found that the calculated values of A and n agree fairly well with those determined experimentally for samples with high asphalt content. At lower asphalt content, the theoretical and experimental values differ significantly.

Even if A and n can be related to some material properties as Schapery suggested, they are still used in a power law relationship that at best can describe only a linear region of fatigue crack propagation; that is, it will not describe fatigue crack propagation over the entire range of the crack driving force.

Thus, it appears that the phenomenon of fatigue cracking in paving mixtures has been treated in a rather empirical manner. Both the phenomenological approach and the fracture mechanics–based approach use regression constants that usually cannot be considered as material parameters. Evidently material parameters are needed to discriminate the effects introduced by the different chemical structures of asphalts, asphalt content, the type of additive used, additive dosage, aging, gradation size, and frequency. Such parameters ought to account for micromechanical effects, that is, the magnitude of matrix cracking and cracking at the matrix-aggregate interface.

The present work outlines an innovative approach to characterize the resistance of asphalt concrete mixtures to fatigue crack propagation (FCP). The philosophy behind this approach is that the resistance of asphalt concrete mixtures to crack propagation depends on the energy expended on irreversible processes (damage) in the vicinity of the crack tip. On this basis, the objective of crack propagation studies is to identify and determine parameters responsible for a mixture's resistance to crack propagation.

THEORETICAL

A fundamental equation has recently been developed (*18*, p. 97) and successfully applied to characterize the resistance of highly strained nonlinear materials to FCP (*19*, p. 167; *20*, p. 98; *21*, p. 285). This equation expresses the rate of FCP as

$$da/dN = \dot{D}/(\gamma^* R_1 - J) \tag{4}$$

where

da/dN = cyclic rate of FCP,
$\dot{D}$ = cyclic rate of energy dissipation on material transformation associated with active zone evolution,
J = crack driving force (energy release rate),
R_1 = resistance moment that accounts for the amount of damage associated with crack advance, and
γ^* = specific energy of damage.

The last one, γ^*, is a material parameter characteristic of its resistance to crack propagation that is to be extracted from the results of FCP experiments.

Crack Driving Force

The crack driving force can be evaluated at increments of crack length from either the area above the unloading curve (potential energy) or the area under the loading curve (strain energy). Current analysis of the FCP data obtained from experiments conducted on various asphalt mixtures shows that invoking the potential energy principle to evaluate the crack driving force J is more appropriate in stress controlled fatigue. Moreover, because undetected crack propagation may occur during loading, the area above the unloading curves is a more reliable presentation of the potential energy. Thus,

$$J = (\partial P/\partial a)/B \tag{5}$$

where

P = potential energy (area above the unloading curve),
B = specimen thickness, and
a = crack length.

Resistance Moment

The resistance moment, R_1 in the proposed model, accounts for the amount of damage associated with the crack advance. Video monitoring of crack propagation in various asphalt concrete mixtures reveals damage in the form of "minicracks" emanating from the main crack as shown in Figure 1. Postfailure microscopic analysis of the fractured specimens shows that the minicracks exist on both surfaces of the tested specimens as well as inside the specimens. An important feature of the minicracks is that they mainly exist in the matrix or at the aggregate-matrix interface. This phenomenon of minicracking has been observed in pavement in service under fatigue loading (*22*).

It has also been observed that the amount of transformed (damaged) material (due to minicracks) in the vicinity of the crack tip increases with the crack advance. Following the Irwin plastic zone size (*23*,*24*) it can be assumed that the width of the transformed material ahead of the crack tip (active zone) is a linear function of the crack length, a, up to its critical length, a_c. This has been shown to be true in various other

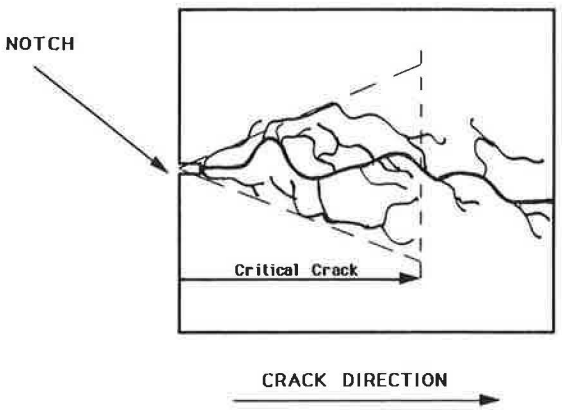

FIGURE 1 Postfailure assembly of damage in form of minicracks in AC-20 asphalt concrete specimen after fatigue.

materials, for example, metals (*25*), polymers (*26*, p. 263; *27*, p. 1377), and polymer composites (*28*, p. 381). Thus, the resistance moment can be evaluated as follows:

$$R_1 = (\partial V/\partial a)/B \tag{6}$$

where V is the volume of the damaged material (active zone) at crack length a.

$$V = (ahB)/2 \tag{7}$$

where h is the width of the active zone and is expressed as

$$h = Ca \tag{8}$$

where C is a constant. Thus,

$$V = (CBa^2)/2 \tag{9}$$

On this basis,

$$R_1 = (CBa)/B = Ca \tag{10}$$

$$C = 2\tan(\phi/2) \tag{11}$$

where ϕ is the active zone angle. Therefore, $\gamma^* R_1$ in Equation 4 can be evaluated as

$$\gamma^* R_1 = \gamma^* Ca = \gamma' a \tag{12}$$

where γ' replaces $\gamma^* \cdot \gamma'$ is a material constant characteristic of the material's resistance to crack propagation.

Energy Dissipation

The quantity $\dot{D}$ in the aforementioned model is the cyclic rate of energy dissipation on submicroscopic processes leading to damage formation. It has previously been shown (*19*) that for a strain control fatigue experiment, the value of $\dot{D}$ in Equation 4 can be expressed as

$$\dot{D} = dD/dN = \beta J^2 \tag{13}$$

where β is the coefficient of energy dissipation that expresses the portion of the change in work per cycle expended on damage formation for strain control. For stress-controlled experiments, it is found that the value of $\dot{D}$ can be extracted from the area of the hysteresis loop. This is approached as follows:

$$\dot{D} = dD/dN = \beta'\, dW_i/dN = \beta' \dot{W}_i \tag{14}$$

where β' is the coefficient of energy dissipation on submicroscopic processes associated with the stress control loading configuration. The relationship between β and β' for the same material has yet to be developed. It is expected that both β and β' may be dependent on temperature, strain rate, and a characteristic time of the process (*29*). The quantity $\dot{W}_i$, which is the "change in work," is measured directly as the area of the hysteresis loop at any crack length, a, minus the area of the loop just before crack initiation. In viscoelastic materials, $\dot{W}_i$ includes work expended on damage processes associated with crack growth and history-dependent viscous dissipation processes, both of which are irreversible. In the current analysis, the quantity $\dot{D}$ in Equation 14, which is the rate of energy dissipation on submicroscopic processes leading to damage formation, is expressed as a portion of this total change in work, $\dot{W}_i$. This value has successfully been evaluated for various asphalt concrete mixtures and will be employed in the current study.

EXPERIMENTAL

Asphalt concrete beams 15 in. long, 2 in. wide, and 3.5 in. high were prepared in substantial agreement with ASTM D3202-83. Two types of asphalt were considered in this study: Elvax-modified AC-5 and AC-20. The beams were prepared at an asphalt content of 8 percent by dry weight and a target asphalt concrete unit weight of 149 pcf. The following gradation was used:

Sieve	*Total Passing (%)*
½ in.	100
⅜ in.	95
No. 4	59
No. 16	28
No. 50	9
No. 200	0

The AC-5 specimens were modified with 6 percent Elvax (percentage of the asphalt content). The aggregate, the asphalt cement, the mold, and the compaction hammer were all preheated to 300°F before blending and compaction. Beam compaction was achieved in accordance with the Marshall hammer method (ASTM D1559-89). Beams were allowed to cool off in the compaction mold and were usually tested 7 days after preparation and conditioning. Conditioning consisted of subjecting each beam to a constant temperature of 140°F for 1 day. The air void content for the specimens was approximately 1.3 percent, and the voids in mineral aggregate (VMA) was about 20 percent.

Four-point bend fatigue testing on notched beams of each mixture was conducted on a pneumatic testing machine. The support span was 10.2 in. and the midspan (between the inner load points) was 3.4 in. An initial straight notch with a total depth of 0.25 in. was inserted at the middle of the specimens with a 0.156 in. saw with a round tip of radius 0.094 in. The tests were conducted at a constant frequency of about 0.5 Hz under load control with a constant maximum load of 65 lb. Each cycle consisted of a 0.2-sec load duration. The specimens were cycled from zero to the maximum load. All tests were conducted at 70°F. Multiple identical specimens (three from each mixture) were tested under the same set of experimental conditions. A hysteresis loop was recorded at ¼-in. intervals of crack growth. Software has been developed to digitize graphical data and to calculate pertinent areas within the load-deflection curves obtained during fatigue testing. These areas are considered important in the current analysis of asphalt concrete under fatigue loading. A traveling video camera equipped with a zoom lens was used to monitor the crack propagation and capture any damage events associated with the fracture process.

RESULTS

Substituting Equations 12 and 14 into Equation 4 yields the following relationship:

$$da/dN = [\beta' \dot{W}_i/(\gamma' a - J)] \quad (15)$$

Equation 15 calls on the accurate measurement of the crack speed (da/dN), the crack driving force (J), and the change in work ($\dot{W}_i$). On this basis, the specific energy of damage (γ') and the dissipation coefficient (β') can be extracted from Equation 15. Analysis of results of FCP experiments generated for typical specimens of the modified AC-5 and AC-20 paving mixtures are presented in the following sections. The average values of γ' and β' were then obtained based on the three tested specimens from each mixture.

Crack Speed

In order to determine the crack speed, the crack length is monitored with respect to the number of cycles. This monitoring is a well-established procedure, and many techniques are available to measure the crack length in FCP experiments. In the current experiment, an accurate transparent flexible scale was attached to the specimens to measure the crack length. Typical curves for crack length (a) versus the number of cycles (N) for the modified AC-5 and AC-20 asphalt mixture specimens are shown in Figures 2 and 3, respectively. In the modified AC-5 specimen (Figure 2), a crack initiated at about 2,000 cycles and advanced in a stable manner, reaching ultimate failure at about 3,600 cycles. In the AC-20 specimen, crack initiation started at about 1,400 cycles. The crack then advanced faster than in the modified AC-5, reaching ultimate failure at about 2,700 cycles. The slope of the curves in Figures 2 and 3 is the average crack speed at the corresponding crack length. The number of cycles for both crack initiation and propagation is larger for the modified AC-5 mixture than for the AC-20 mixture. The initiation and propagation life times

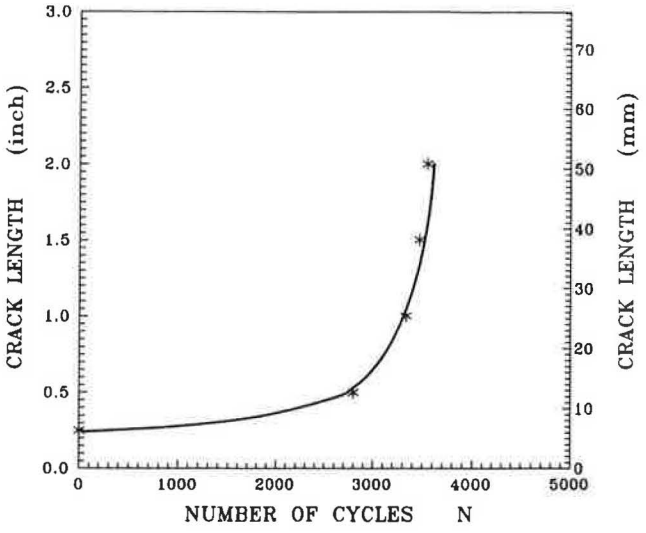

FIGURE 2 Crack length versus number of cycles in modified AC-5 asphalt concrete mixture.

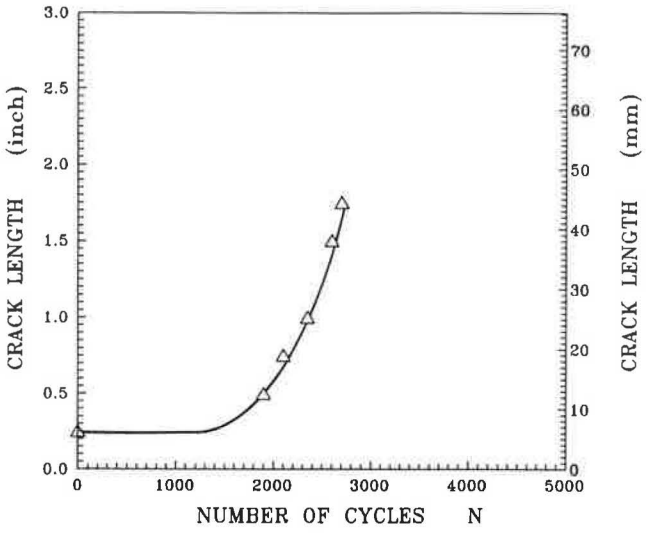

FIGURE 3 Crack length versus number of cycles in AC-20 asphalt concrete mixture.

of the modified AC-5 are about 1.4 and 1.2 times higher than the AC-20, respectively.

Energy Release Rate

Invoking the potential energy principle, Equation 5 is used to evaluate the energy release rate (J) at increments of crack length for the modified AC-5 and AC-20 specimens. This is shown in Figure 4 for typical specimens of each asphalt mixture. It is evident from Figure 4 that the value of J for the modified AC-5 mixture is always higher than that of the AC-20 for the same crack length.

As it is shown in Figure 4, the energy release rate for the modified AC-5 mixture evolves at a faster rate with respect to the crack length than that of the AC-20 asphalt concrete

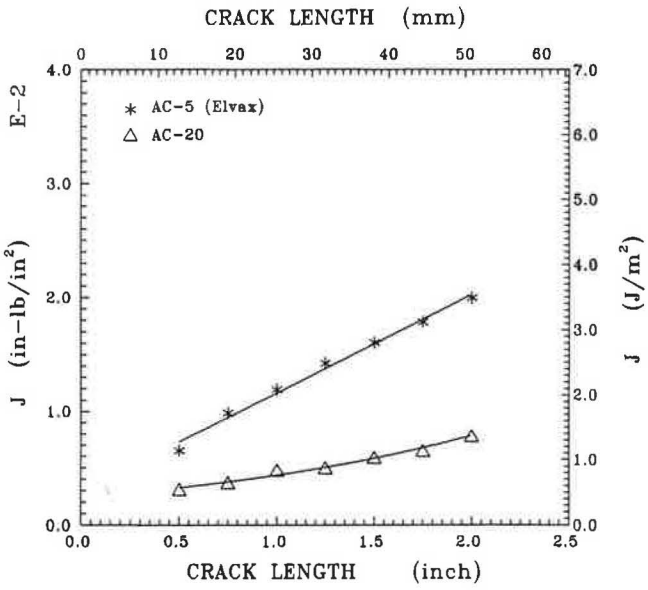

FIGURE 4 Energy release rate (J) versus crack length for modified AC-5 and AC-20 asphalt concrete mixtures.

mixture. The ductile fracture behavior of the AC-5 mixture causes a larger increase in the resistance of this mixture to crack propagation with the crack length. As a result, the energy release rate (J) must increase in order to maintain crack growth. The slow evolution of J with respect to the crack length in the case of the AC-20 mixture is indicative of the "brittle" fracture behavior of this mixture in comparison with the AC-5. Since the energy release rate is always higher for the modified AC-5 mixture, it is expected to be tougher than the AC-20 mixture.

Change in Work

The change in work ($\dot{W}_i$) for the modified AC-5 and AC-20 specimens is evaluated from the area of the hysteresis loops at increments of crack length. The evolution of the quantity $\dot{W}_i$ with the crack length for typical specimens of both materials is shown in Figure 5. The value of $\dot{W}_i$ for the modified AC-5 specimen is higher than that of the AC-20 specimen at each crack length. Thus, it appears that more total work has been expended on both damage formation and history-dependent viscous dissipation processes within the active zone of the modified AC-5 mixture.

DISCUSSION OF RESULTS

The new methodology developed through the work outlined will be used to determine the parameters that characterize the resistance of the two asphalt concrete mixtures to crack propagation. These parameters (γ' and β'), which control the fracture process, can be determined by rearranging Equation 15. Thus,

$$J/a = \gamma' - \beta'\{\dot{W}_i/[(da/dN)a]\} \quad (16)$$

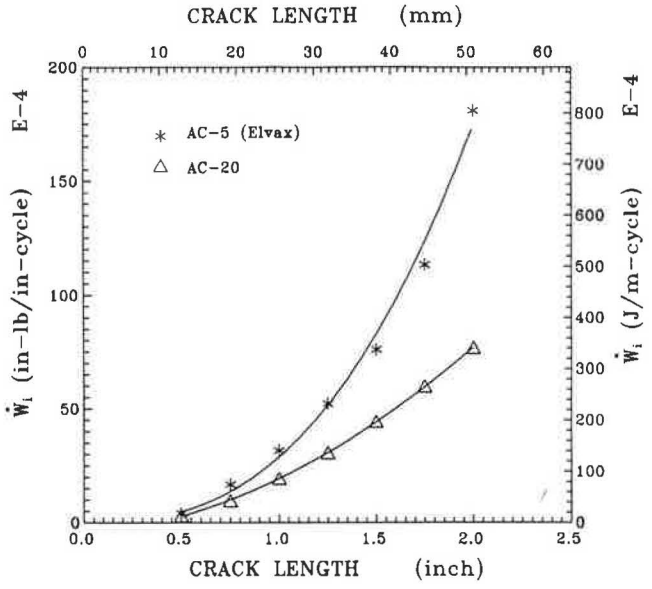

FIGURE 5 Change in work ($\dot{W}_i$) versus crack length for modified AC-5 and AC-20 asphalt concrete mixtures.

If the experimental results of each asphalt mixture tested are in accord with the proposed model, a plot of J/a versus $\{\dot{W}_i/[(da/dN)a]\}$ should give a straight line with γ' the intercept and β' the slope. Indeed, when the results of the experiments previously presented were plotted on the basis of Equation 16, the experimental points for both the modified AC-5 and AC-20 mixtures make nearly a straight line. This is shown in Figures 6 and 7 for a typical specimen of the modified AC-5 and AC-20 mixtures respectively. Thus, it is safe to conclude that the model is in accord with the results of the experiments.

Curves plotted on the basis of Equation 15 using the obtained values of γ' and β' with the experimental results are shown in Figures 8 and 9 for the typical specimens of the modified AC-5 and AC-20 mixtures, respectively. The theoretically obtained curves describe the experimental results very well. This has also been found to be true for the other two specimens of each asphalt mixture. It has been observed that the fatigue crack propagation kinetics of all of the tested specimens of the two asphalt concrete mixtures under consideration display the familiar S-shaped character. Three stages of crack propagation kinetics are obvious. The threshold stage

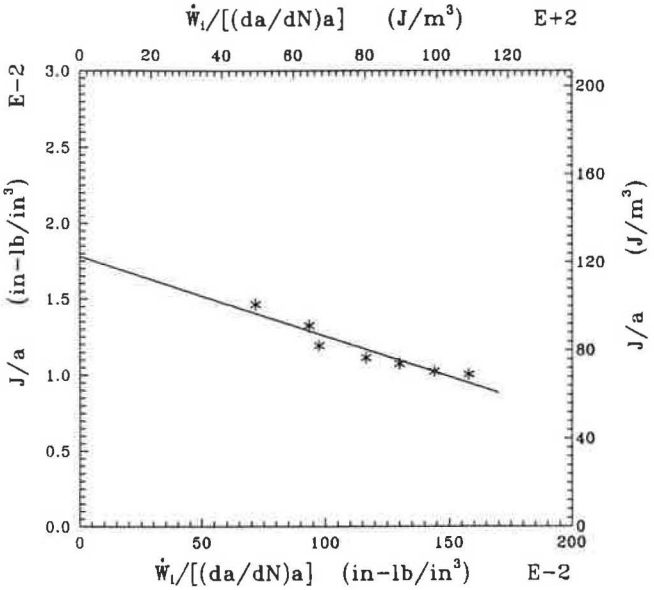

FIGURE 6 FCP behavior of modified AC-5 mixture plotted in form of proposed model to obtain γ' and β'.

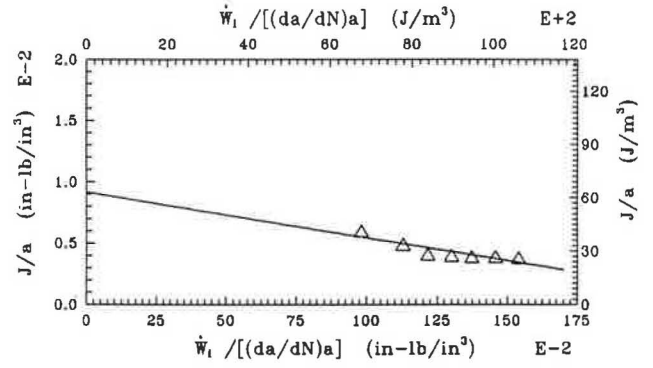

FIGURE 7 FCP behavior of AC-20 mixture plotted in form of proposed model to obtain γ' and β'.

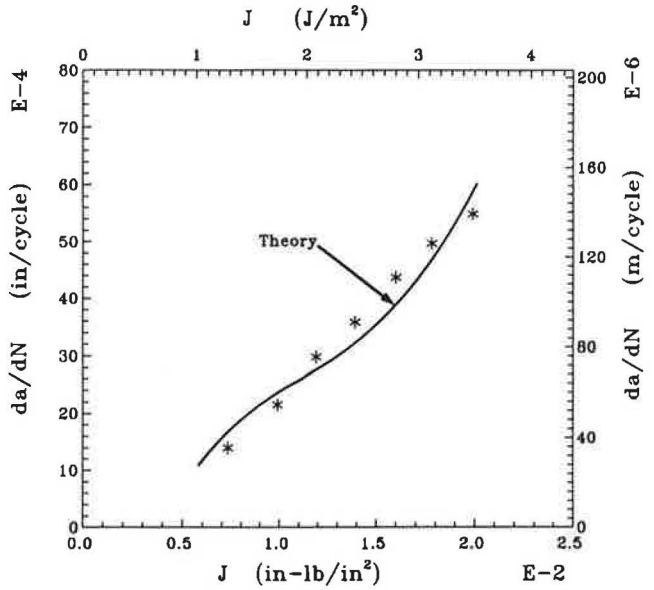

FIGURE 8 Theoretically predicted FCP speed based on proposed model (with experimental data) for modified AC-5 mixture.

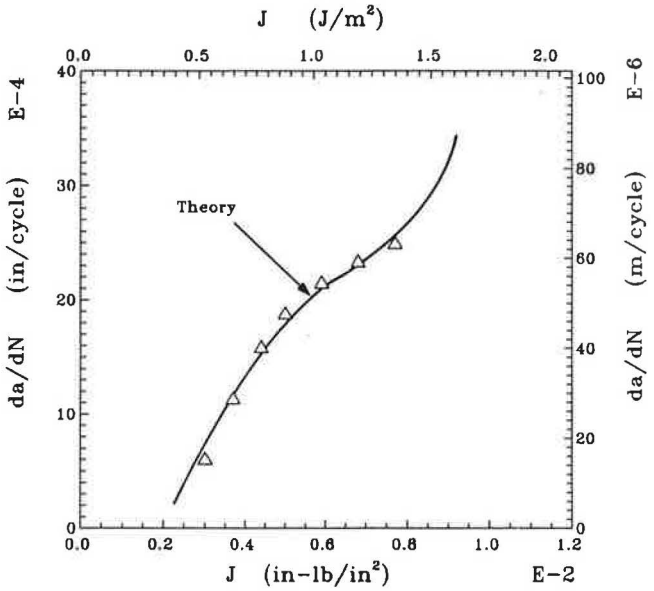

FIGURE 9 Theoretically predicted FCP speed based on proposed model (with experimental data) for modified AC-20 mixture.

is followed by a stage of reduced acceleration and then the stage of unstable crack propagation. This behavior indicates the evolution of crack tip damage.

The average values of γ' and β' for the three Elvax-modified AC-5 specimens tested are $1.79 \pm 0.09 \times 10^{-2}$ (in.-lb/in.^{3}) and $4.8 \pm 0.37 \times 10^{-3}$, respectively. The average values of γ' and β' for the AC-20 specimens are $1.17 \pm 0.41 \times 10^{-2}$ (in.-lb/in.^{3}) and $2.71 \pm 0.70 \times 10^{-3}$, respectively. As can be seen, the average value of γ' is higher for the modified AC-5 mixture than for the AC-20. Thus, more energy is required to cause a unit volume of the AC-5 to change from undamaged to damaged material. On this basis AC-5 is more resistant to crack propagation than AC-20. The larger value of β' for the modified AC-5 mixture reflects the larger percentage of energy expended on dissipative processes and damage growth within the active zone. The standard deviation in the values of γ' and β' for the AC-5 are surprisingly low for this type of heterogeneous material. The large standard deviation for the AC-20 mixture values probably can be attributed to the "brittleness" of the AC-20 compared with the AC-5. To compare the data further, the two curves of Figures 8 and 9 are plotted together in Figure 10. It is evident that the modified AC-5 mixture is superior to the AC-20 mixture, as is reflected by the larger value of γ'.

It should also be mentioned that the fracture processes are not as sensitive to β' as they are to γ'. The denominator of Equation 15 is the energy barrier that controls the fracture process. As can be seen from analysis of the AC-5 mixture, $\dot{W}_i$ and β', which make up the numerator of Equation 15, are higher than for the AC-20. Nevertheless, da/dN is lower. This attests to the sensitivity of the fracture processes to the value of $(\gamma' a - J)$, and in turn γ' rather than β'. Therefore γ' is a candidate material parameter characteristic of the material's resistance to fracture and β' is a dissipative coefficient. The dependency of β' on the strain rate, temperature, and time characteristic of the process is still unresolved and will be the subject of further research.

CONCLUDING REMARKS

A methodology has been developed and successfully applied to characterize the resistance of asphalt concrete mixtures to fatigue crack propagation. This methodology reasonably describes fatigue crack propagation behavior of the pavements over the entire range of the energy release rate. Parameters controlling the fracture process were extracted from fatigue crack propagation experiments on two asphalt concrete mixtures (Elvax-modified AC-5 and AC-20) with defined chem-

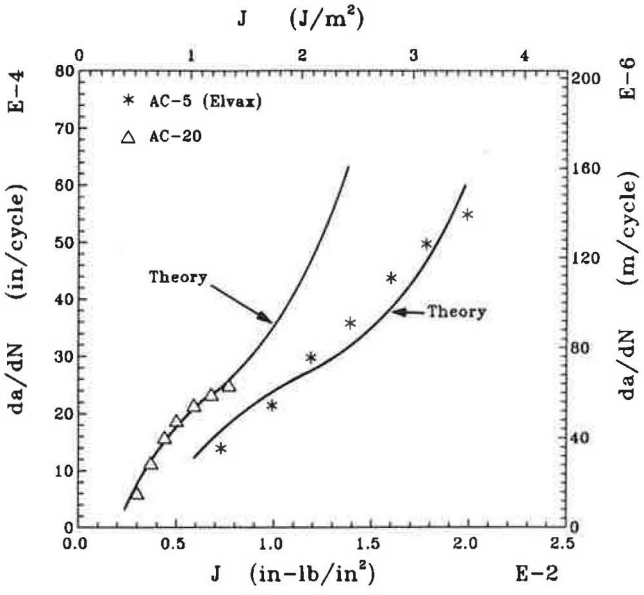

FIGURE 10 Theoretically predicted FCP speed for modified AC-5 and AC-20 mixtures (with experimental data).

ical structures. These are the specific energy of damage (γ'), a candidate material parameter characteristic of the mixtures resistance to FCP, and β', a dissipative coefficient.

The current study reveals that γ' reflects the toughness of the material. A higher value of γ' gives a lower crack speed over the entire range of the energy release rate. Although β' represents the portion of the change in work expended on damage processes, it does not play as important a role in controlling the fracture process as γ' does. Knowing γ' and β' for an asphalt concrete mixture can serve an important practical purpose. Useful relationships can be established between γ' and β' and structure and processing conditions. Such relationships can guide the development of asphalt mixtures with superior resistance to cracking. Research activities to achieve this goal are currently in progress.

ACKNOWLEDGMENTS

The authors gratefully acknowledge the financial support of the U.S. Army Corps of Engineers Waterways Experiment Station, Vicksburg, Mississippi. The guidance and direction of William N. Brabston of the Army Corps of Engineers is also gratefully appreciated.

REFERENCES

1. A. Wohler. *English Abstract in Engineering*, Volume II. 1871.
2. C. L. Monismith, K. E. Secor, and E. W. Blackmer. Asphalt Mixture Behavior in Repeated Flexure. *Proc., Association of Asphalt Paving Technologists*, Vol. 30, 1961.
3. C. L. Monismith. *Asphalt Mixture Behavior in Repeated Flexure*. Report TE 64-2. University of California, Berkeley.
4. P. S. Pell. Fatigue Characteristics of Bitumen and Bituminous Mixes. *Proc., 1st International Conference on the Structural Design of Asphalt Pavements*, 1963.
5. P. S. Pell and I. F. Taylor. Asphalt Road Materials in Fatigue. *Proc., Association of Asphalt Paving Technologists*, 1969, pp. 423–458.
6. K. Majidzadeh, E. Kauffmann, and C. Saraf. Analysis of Fatigue of Paving Mixtures from the Fracture Mechanics Viewpoint. In *ASTM Special Technical Publication 508*, ASTM, Philadelphia, Pa., 1972, pp. 67–83.
7. K. Majidzadeh and D. Ramsamooj. *Applications of Fracture Mechanics for Improved Design of Bituminous Concrete*. Report FHWA-RD-76-91. FHWA, U.S. Department of Transportation, June 1976.
8. P. F. Germann and R. L. Lytton. *Methodology for Predicting the Reflection Cracking Life of Asphalt Concrete Overlays*. Report TT 2 8-75-207-5. Texas Transportation Institute, Texas A&M University, College Station, 1979.
9. P. C. Paris and F. J. Erdogan. A Critical Analysis of Crack Propagation Laws. *Journal of Basic Engineering* (Transactions of American Society of Mechanical Engineers), Vol. 85D, 1963.
10. P. C. Paris and C. G. Sih. Stress Analysis of Cracks. In *ASTM Special Technical Publication 381*, ASTM, Philadelphia, Pa., 1965, pp. 30–81.
11. H. Tada, P. Paris, and G. Irwin. *The Stress Analysis of Cracks Handbook*. Paris Production, Inc., St. Louis, Mo., 1985.
12. J. Begley and J. Landes. The J-Integral as a Fracture Criterion. In *ASTM Special Technical Publication 514*, ASTM, Philadelphia, Pa., 1972, pp. 1–20.
13. J. Rice. A Path Independent Integral and the Approximate Analysis of Strain Concentration by Notches and Cracks. *Journal of Applied Mechanics* (Transactions of American Society of Mechanical Engineers), Vol. 35, 1968.
14. D. Little et al. *Investigation of Asphalt Additives*. Report FHWA-RD-87-001. FHWA, U.S. Department of Transportation, Nov. 1986.
15. R. A. Schapery. A Theory of Crack Initiation and Growth in Viscoelastic Media—I. Theoretical Development. *International Journal of Fracture*, Vol. 11, 1975, pp. 141–159.
16. R. A. Schapery. A Theory of Crack Initiation and Growth in Viscoelastic Media—II. Approximate Methods of Analysis. *International Journal of Fracture*, Vol. 11, 1975, pp. 369–388.
17. R. A. Schapery. A Theory of Crack Initiation and Growth in Viscoelastic Media—III. Analysis of Continuous Growth. *International Journal of Fracture*, Vol. 11, 1975, pp. 549–562.
18. A. Chudnovsky. Crack Layer Theory. *Proc., 10th U.S. Conference on Applied Mechanics*, American Society of Mechanical Engineers, Houston, Tex., 1986.
19. H. Aglan, A. Chudnovsky, et al. Crack Layer Analysis of Fatigue Crack Propagation in Rubber Compounds. *International Journal of Fracture*, Vol. 44, 1990.
20. H. Aglan and A. Moet. The Resistance of Rubber Compounds to Brittle Crack Propagation. *Rubber Chemistry and Technology*, Vol. 62, 1989.
21. H. Aglan and A. Moet. Crack Tip Damage in Rubber Compounds. *International Journal of Fracture*, Vol. 40, 1989.
22. R. L. Terrel. Fatigue Behavior: Field Observations and Analytical Predictions. In *ASTM Special Technical Publication 508*, ASTM, Philadelphia, Pa., 1972, pp. 117–143.
23. G. R. Irwin. *Fracture I, Handbuch der Physik VI*. Springer, 1958, pp. 558–590.
24. F. A. McClintock and G. R. Irwin. Plasticity Aspects of Fracture Mechanics. In *ASTM Special Technical Publication 381*, ASTM, Philadelphia, Pa., 1965, pp. 84–113.
25. I. Mustapha. Ph.D. thesis. Case Western Reserve University, Cleveland, Ohio, 1989.
26. J. Botsis, A Chudnovsky, and A. Moet. Fatigue Crack Layer Propagation in Polystyrene, Part I: Experimental Observations. *International Journal of Fracture*, Vol. 33, 1987.
27. N. Haddaoui, A. Chudnovsky, and A. Moet. Ductile Fatigue Crack Propagation in Polycarbonate. *Polymer*, Vol. 27, 1986.
28. P. X. Nguyen, A. Chudnovsky, and A. Moet. Enhanced Fatigue Resistance of Glass Reinforced PVC Composites. *SPE-ANTEC*, 1985.
29. A. Chudnovsky. *Crack Layer Theory*. NASA Contractor Report 174634. National Aeronautics and Space Administration, Washington, D.C., March 1984.

New Laboratory Testing Technique for Asphalt Concrete

OTTO J. SVEC AND DAVID ELDRED

The Institute for Research in Construction, National Research Council of Canada, recently developed new laboratory equipment for testing mechanical properties of asphalt concrete. Tensile and shear (static or dynamic) loading can be applied to slab samples of asphalt pavement. The concept and the first prototype of this testing equipment are described, along with results of an experimental evaluation and testing program. The laboratory testing was carried on slab specimens extracted from the pavement of a field trial section partly reinforced by a geogrid.

Testing of the mechanical properties of asphalt concrete (AC) has been traditionally focused on compressive, tensile and bending strengths. Many tests are used to quantify these properties in static or dynamic (fatigue) modes. These testing techniques have been steadily improving in quality and sophistication, in an effort to better understand and evaluate the behavior of AC. For recent advances on asphalt laboratory testing, an interested reader is referred to the *Proceedings of the Fourth International RILEM Symposium* (*1*). Past emphasis has been on compressive, tensile, and bending strength testing. The shear strength of AC has rarely been examined, perhaps because of its simplicity. An exception is testing done using the gyratory equipment, as described by Ruth et al. (*2*). In the vast majority of laboratory testing today, a single deformation component is normally applied, resulting in a single stress component or a limited combination of stresses, for example, compressive and tension. A combination of deformation in different directions leading to a combination of stresses—for example, tensile and shear—is seldom used to evaluate the behavior of AC.

To examine the importance of combining various strains and stresses in AC testing, consider an asphalt overlay on top of a cracked AC or portland cement concrete (PCC) pavement. Furthermore, consider a moving vehicle on the overlay, which covers a crack in the old pavement underneath (Figure 1). As the wheel of the vehicle moves from one side of the crack to the other (i.e., from one independent slab to the other), the asphalt overlay is loaded with considerable shear strain and stress. This large shear stress is imposed twice in the opposite direction with every pass of the wheel. At the bottom of the overlay at the edges of the crack, a high concentration of compressive stress develops under the wheel load. Furthermore, if the crack is wide and the subgrade underneath the old asphalt deteriorated and weak, the new asphalt also becomes stressed in bending (Figure 2). There is yet another serious factor in this process: the development of tensile stress due to thermal contraction, as shown in Figure 3. All these combined actions near the crack in the old pavement contribute to the development of a "reflection" crack propagating upward to the asphalt overlay, causing premature deterioration of rehabilitated pavements (*3*).

To properly evaluate various rehabilitation measures and their ability to reduce reflection cracking and other distress phenomena in asphalt pavements (e.g., overlays and the use of geogrids as crack retardants and stress reinforcement in pavements), a combination of tensile and shear stresses must be considered. Therefore, the Institute for Research in Construction (IRC) has recently developed a testing table called Construction Material Testing System (CMTS); it can combine tensile and shear (static or dynamic) loading applied to asphalt concrete slabs. Besides general material testing (e.g., tensile, compressive, shear, and flexural strength), this equipment has also been designed to evaluate the performance of various crack rehabilitation techniques.

This paper describes the new CMTS and its functions and performance. The testing results of plain and reinforced asphalt slabs in combined tensile and dynamic shear modes are presented along with some interesting implications.

BACKGROUND

One of the major expenses incurred by transportation departments around the world is the rehabilitation of their road networks. A significant part of these funds is associated with sealing cracks, rehabilitating badly cracked locations with other techniques, and placing asphalt concrete overlays over entire road sections.

Overlays over cracked or jointed PCC, or over cracked AC, pose the problem of reflection cracking. Other locally applied rehabilitation measures—such as deep patching, milling and machine patching, crack filling and sealing, and using geogrids, geotextiles, and special rubber mixes—are all susceptible to deterioration at varying rates. This deterioration depends on climatic temperature and moisture effects, the resistance of a particular repair method of fatigue due to traffic, and the overall structural integrity of the pavement structure below. Therefore, a realistic, comprehensive, yet practical laboratory testing technique is needed to evaluate performance, life span, and economic implication of individual asphalt pavement repair methods.

Reflection cracking in a broad sense can be described as the result of stress concentration caused by horizontal and vertical movements at joints or cracks in the pavement (*4*,*5*). Horizontal movement and corresponding tensile stress are caused by low-temperature shrinkage; vertical movement and

Institute for Research in Construction, National Research Council of Canada, Ottawa, Ontario, Canada K1A 0R6.

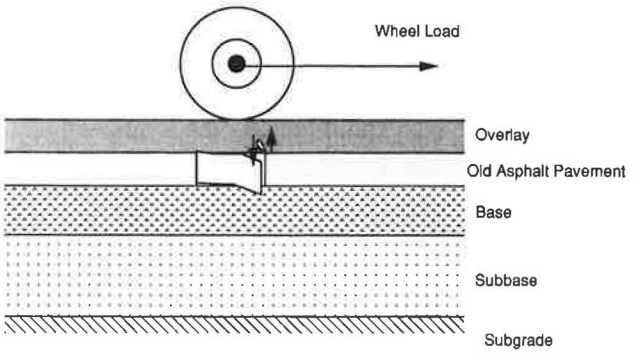

FIGURE 1 Shear stress in overlay due to crack in old asphalt.

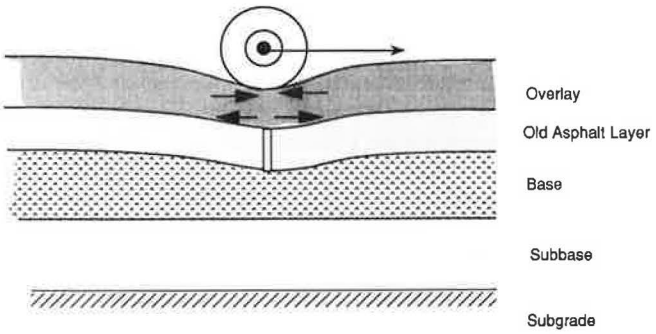

FIGURE 2 Bending stress in overlay.

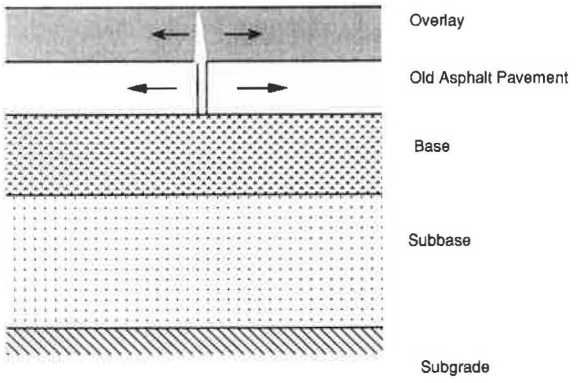

FIGURE 3 Crack formation in overlay due to thermal shrinkage.

corresponding shear stress are caused by the traffic load. A contributing factor to the development of tensile stresses is the high thermal conductivity of subgrade; contributing to the development of shear stresses is a weak pavement structure. Furthermore, a contact stress concentration develops under the crack edges between the old asphalt pavement and the granular base, causing the granular base to settle in that area. As a result (and dependent on the extent of the settlement), bending of the overlay occurs. Consequently, the overlay above the crack in the old pavement is stressed by shear, tensile, and bending stresses simultaneously.

It is clear that to fully understand the process of reflection cracking and to propose effective measures for arresting this type of cracking, laboratory testing using dynamic shear and tensile stress loading simultaneously must be carried out. Similarly, to evaluate properly various rehabilitation measures applied to cracked PCC or AC, such combined loading must be used.

The objective of the presented research work was to develop CMTS and to carry out its initial evaluation. The testing program was focused on resistance of AC to the combined effect of tensile stress and dynamic shear loading. In addition, to further illustrate the importance of this type of testing in evaluating the use of geogrids in improving the material resistance to failure under these loading conditions, plain AC was compared with AC reinforced by a geogrid. This program has been carried out using asphalt concrete slab specimens extracted from an experimental overlay that was constructed on the campus of the National Research Council of Canada.

TENSILE AND SHEAR TESTING TABLE (CMTS)

The concept of CMTS is rather simple; it is shown schematically in Figure 4. The system resembles a table consisting of two halves: one half of the table can move horizontally, and the other half can move vertically. When an asphalt specimen is fixed to the top of this table (i.e., to both halves, Figure 4), the horizontal movement of one half will generate tensile stress in the specimen, and the vertical movement of the other half will generate shear stress. Depending on the AC slab fixation to the table and on other boundary conditions, the vertical movement may also translate to a bending movement.

The main components of this new testing table are two thick sheets of steel 60.0 × 60.0 × 2.5 cm (24 × 24 × 1 in.), as shown in the overall photograph of CMTS (Figure 5). As described, one half of this table moves in the horizontal direction (referred to as the "horizontal plate"), and the other moves in the vertical direction ("vertical plate"). Horizontal movement is facilitated by the use of four linear bearings mounted on the bottom of the horizontal plate, moving along two heavy horizontal rods. Vertical movement is arranged by using two large commercially available tool-making die plates. The vertical dynamic (cycling) movement is provided by a hydraulically driven loading jack, as seen in Figure 5. The horizontal movement of the horizontal plate (i.e., the strain rate) is controlled through a variable-speed electric motor and set of gears.

Undesirable horizontal movement of the vertical plate, caused by large horizontal forces transmitted through the AC slab during testing, is restricted by two ball bearings mounted on consoles and acting on the vertical plate. Similarly, undesirable vertical movement of the horizontal plate, caused by vertical force transmitted to this plate through the AC specimen, is restricted by a similar arrangement. Furthermore, the weight of the vertical plate is counter-balanced by a dead load, so stresses caused by the weight of this plate are not transmitted to the tested specimen.

To facilitate testing, slab specimens are glued onto two steel plates (away from the testing table). These plates are held together by two aluminum handles attached to the side of the plates by a set of screws. After the glue is set, this assembly is placed on the testing table and firmly bolted to the horizontal and vertical plates of the CMTS. The handles are then removed, and the sample is ready for testing. In this way,

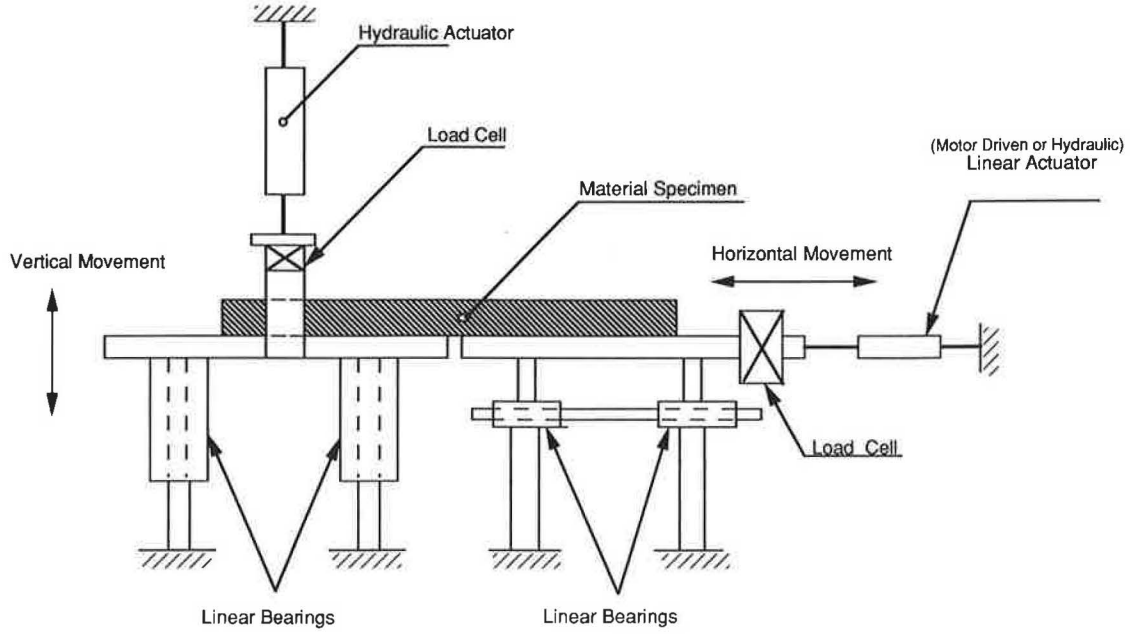

FIGURE 4 Concept of CMTS.

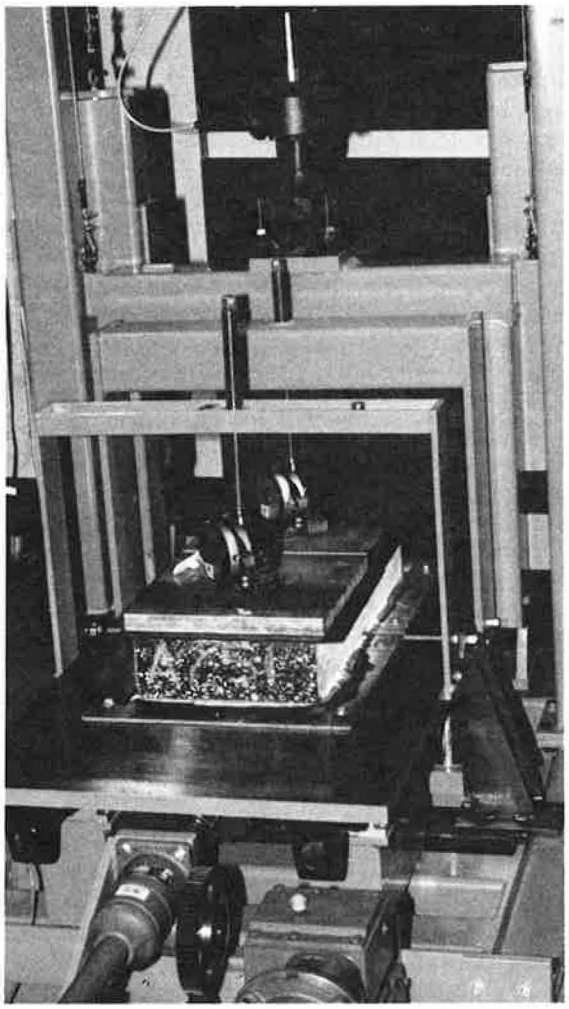

FIGURE 5 CMTS: thick AC slab ready for testing.

any number of samples can be prepared before the testing without tying up the CMTS.

A high-speed PC data acquisition system monitors the load cells, displacement transducers, and temperature sensors. Data processing computer programs are then used for data analysis and graphical output of the test results.

The CMTS will soon be relocated into a large cold room so that the effect of temperature changes (to $-40°C$) can be included in future research programs. The intellectual property of the CMTS has been protected. Interested companies or other agencies, however, can contact the authors for a licensing agreement.

LAYOUT OF FIELD TRIAL

As mentioned, the main objective of this project was to test the CMTS, using plain and geogrid-reinforced AC slabs. To obtain realistic samples, the AC slabs were extracted from a road test section constructed with standard paving equipment. The field preparation was carried out on the campus of the National Research Council of Canada in Ottawa, Ontario, on May 3, 1991. The selected site was a very lightly trafficked service road, thus allowing total closure of the site (half of the road) to traffic and eliminating operational disruption. The size of the test section was 15 m (50 ft) long and 3 m (10 ft) wide.

Before the asphalt was placed, the site was cleaned and then the old asphalt spread with a thin layer of sand. The purpose was to seal small existing cracks and to even out some irregularities. At the same time, the thin layer of sand prevented the new asphalt from adhering to the old, thus allowing easy removal of the asphalt slab samples from the site. A standard hot asphalt mix known as HL4 designed by the Ministry of Transportation of Ontario was used.

Once preliminary preparations were completed, the asphalt spreader was then backed over the sand in order to lay down a lift of HL-4 asphalt mix approximately 37 mm (1.5 in.) thick over the first half of the total length [i.e., first 7.5 m (25 ft)]. The thickness of the lift in the second half (i.e., the next 7.5 m) was increased to 50 mm (2 in.). One meter at the beginning of the first layer was used as a ramp for the compactor, resulting in the total area of 14 × 3 m available for testing. A portion of this uncompacted first lift was then covered with a 3-ton polyester geogrid. The second lift was laid over the entire test section, consisting of 37 mm over the first 7.5 m and 50 mm over the second 7.5 m. The entire area was then compacted by a standard Dynapac compactor and then by a rubber tire roller using an appropriate number of passes. The final compacted section measured approximately 7.5 m × 3.0 m × 75 mm (25 ft × 10 ft × 3 in.) and 7.5 m × 3.0 m × 10 mm (25 ft × 10 ft × 4 in.). More than 200 cores were extracted from this section in order to characterize its various parts—thin, thick, plain, and reinforced subsections—according to density and indirect tensile strength. In addition, many slabs 30 × 60 cm (12 × 24 in.) were cut and transported to the laboratory for testing. Great care was exercised in lifting slabs from the pavement to avoid any damage. This was accomplished by supporting the slabs at all times with thick plywood sheets.

LABORATORY TESTING

As discussed, many times a combination of the tensile stress and the shear stress can be critical to the integrity of the asphalt layer. In addition to the plain AC, this loading condition also poses another very important question: How will AC reinforced by a geogrid respond to such a stress combination? To understand fully the effect of the combined tensile and shear loading on AC, plain and reinforced, an entire range of the stress combination was applied to the test specimens. Because AC is a viscoelastic-plastic material that creeps in time with load, there are three possibilities for applying the tensile stress: constant strain, constant stress, and stress relaxation. The constant strain test (i.e., horizontal movement only) does not pose a problem, except that the resulting tensile stress is a function of the strain rate. Therefore, it is important to consider the rate of applied strain. Such direct tensile stress tests on slab specimens are used in many laboratories, usually under uninterrupted constant strain rate control. A stress relaxation test is also easy to perform: rapidly apply a tensile stress and allow the stress to relax. Once movement of the horizontal plate is stopped, the tensile stress in the AC slab will drop rather quickly. For a constant stress test, the horizontal movement of the table must continue, but its speed (i.e., the strain rate) must be controlled to compensate for stress relaxation of AC and failure progression (cracks propagation) during testing. Considering these possibilities, a range of the tensile and shear stress combinations was determined as follows:

- Tensile stress only (i.e., direct tensile test based on constant strain);
- Initial tensile stress with relaxation (i.e., constant displacement) combined with a dynamic shear;
- Constant tensile stress without relaxation and combined with a dynamic shear; and
- Dynamic shear only.

During these tests the forces and displacements are monitored by high-speed data acquisition equipment. In addition, the crack initiation, development, and propagation is continuously being observed and recorded using photo and video cameras. The video recording is particularly effective during the cycling of the vertical plate because the progressive nature of failure of the AC can be easily followed.

RESULTS

The testing program reported in this paper has been carried out at a room temperature of 22°C using the following types of test:

1. Direct tensile stress, in which only the horizontal plate is moving in a constant strain rate mode; and
2. Constant tensile stress combined with dynamic shear, in which the movement of the horizontal plate is load-controlled and the cyclic movement of the vertical plate is displacement-controlled (±1.27 mm/±0.05 in.).

An aspect of stress relaxation was also included in the direct tensile stress test in order to investigate the characteristic creep behavior of AC: soon after peak load was observed, the movement of the horizontal plate was arrested for a short period of time, until the load decreased by 50 percent (usually 30 sec), and then horizontal displacement recommenced. As Figures 6 and 7 indicate, the load rapidly increased to another peak, reaching the envelope of a continuous test. After this secondary peak, the load continued along a load displacement curve similar to that expected for a test without stress relaxation.

Figure 6 depicts typical load-versus-displacement relationships of thin AC slabs, plain and geogrid-reinforced; Figure 7 shows the same relationships for thick AC slabs. One might argue that instead of load, tensile stress should be used for comparison purposes as in Table 1, because cross sections of samples are not identical. This comparison would be realistic only up to the load displacement peak, at which massive cracking failure occurs. After this failure, the area of the cross section cannot be determined because of the propagation of cracks. Moreover, in the case of reinforced samples, the load, after the failure of AC, is transmitted only by the geogrid and the stress definition becomes meaningless. It is clear from Figure 6 that the plain AC slabs lost their entire strength at about 20 mm (0.8 in.) of total displacement, at which point the slabs failed and were practically pulled apart. On the other hand, the AC slabs reinforced by a geogrid behaved quite differently. In Figure 6 the first part of the R143 load deformation curve—that is, up to about 12 mm (0.4 in.) of displacement—is similar to that of plain AC. Following this, however, the "strength" of the slab increased and continued to resist horizontal deformation up to a total displacement of about 35 mm (1.4 in.). This observation indicates that during the first part of the test, load is activated by the strength of the AC alone. After a partial failure of the AC and a sufficient

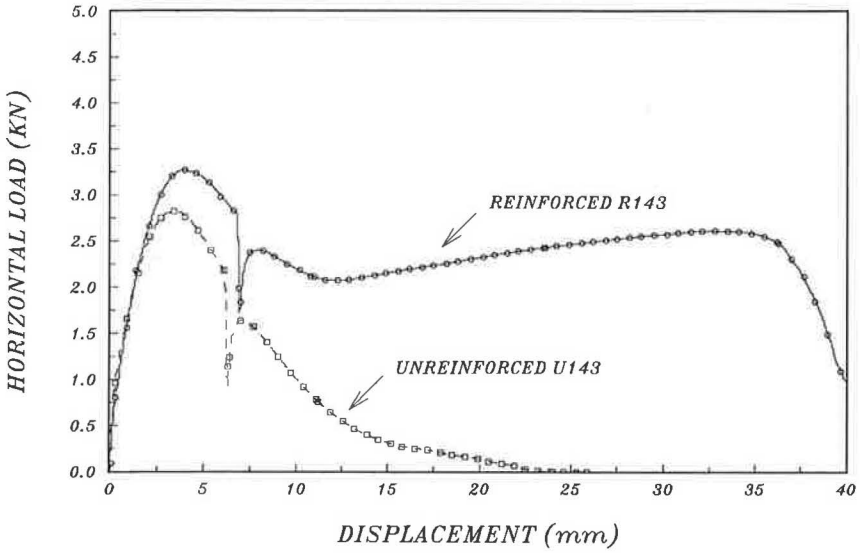

FIGURE 6 Interrupted constant strain rate tensile test, thin AC slabs (approximately 60 mm).

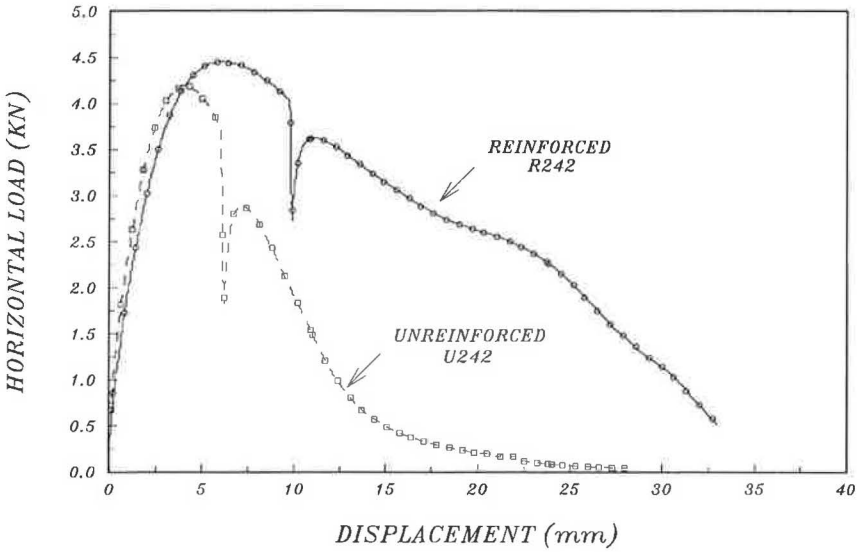

FIGURE 7 Interrupted constant strain rate tensile test, thick AC slabs (approximately 90 mm).

TABLE 1 Direct Tensile Stress, Strain Rate: 4 mm/min (0.15 in./min)

Sample		Plain				Sample	Reinforced			
		Depth (mm)	Peak Load (kN)	Peak Stress (MPa)	Peak Displ. (mm)		Depth (mm)	Peak Load (kn)	Peak Stress (MPa)	Peak Displ. (mm)
Thin	U143	60.4	2.81	0.153	3.7	R142	58.6	3.31	0.185	4.2
	U142	61.2	3.08	0.167	3.2	R143	71.4	3.27	0.185	4.0
		60.8	2.94	0.160	3.5	-	65.0	3.29	0.186	4.1
Thick	U243	92.2	3.18	0.122	4.5	R242	96.0	4.46	0.149	6.2
	U242	85.8	4.19	0.150	4.0	R243	96.7	4.97	0.172	5.5
Average		89.0	3.68	0.136	4.3		96.3	4.72	0.160	5.9

deformation, load is transferred to the geogrid and it becomes the only stress-resisting structural element. In other words, the second part of Curve R143 in Figure 6 represents the tensile strength of the geogrid and its interlock within the AC. The behavior of thick samples shown in Figure 7 is similar to that of thin samples shown in Figure 6, except that the load does not increase after being transferred to the geogrid. In this case, the interlock between the geogrid and the AC was not as effective as in the case of the thin samples.

The results of all the direct tensile strength tests carried out using four plain AC slabs and four reinforced AC slabs are also summarized in Table 1. It can be seen not only that is the peak stress higher for reinforced AC, but also that the peak displacement is considerably larger. These data indicate that a reinforced AC at room temperature (22°C) does not fail in tension in an abrupt manner (i.e., deforming as an elastic body up to a breaking point). Instead, the failure is initiated through small cracks and, at the same time, the geogrid begins to activate.

The second part of the testing program was carried out, combining horizontal tensile stress with vertical shear stress. For these tests, small loading frames were attached to both horizontal and vertical plates (i.e., across and above the plates) so that a vertical static load could be applied to the top of both sample halves (Figure 5). Relatively uniform stress distribution was accomplished by using thick (25 mm) aluminum 300 × 300 mm plates resting on thin (0.6 cm) sheets of rubber. The load was applied through a large screw and a loading cell. The main reason for this arrangement was to eliminate vertical tensile stress on the glued bottom of the slabs during the vertical cyclic movement of the vertical plate. The overall procedure for these tests followed these steps:

1. Horizontal load was applied at the rate of 4 mm/min (0.15 in./min) up to 1.11 kN (250 lbf) for thin samples and 1.78 kN (400 lbf) for thick samples. At this stage the movement of the horizontal plate was stopped.
2. Immediately after, the plates on top of the sample were loaded through the screw–load cell arrangements by 4.45 kN (1,000 lbf) resulting in 47.9 kPa pressure between the loading plates and the surface of the AC slabs.
3. As soon as the sample was loaded by the top plates, the vertical plate started to cycle in vertical movement with a frequency of 2.5 Hz and ± 1.25 mm (0.05 in.) from the zero position. At the same time movement of the horizontal plate resumed in order to maintain a constant tensile load of 0.67 kN (150 lbf) for thin samples and 1.11 kN (250 lbf) for thick samples.
4. After failure, defined as a single continuous crack from top to bottom and across the sample, the cycling of the vertical plate was stopped.
5. The movement of the horizontal plate continued at the top constant strain rate (only for reinforced slabs) in order to evaluate the geogrid-AC interlock. This determination can be seen as large peaks at the end of the graphs (Figures 8 and 9).

Figures 8 and 9 represent time versus horizontal force for plain and reinforced AC under conditions of combined constant tensile stress and dynamic shear stress for thin (approximately 60 mm) and thick (approximately 90 mm) AC slabs, respectively. It should be noted that measured force is used in this paper, i.e., not converted into stress. The reason is that as cracks initiate and later propagate, the area of the slab cross section is essentially indeterminate.

The first three test steps usually take 30 to 50 sec. After that, the vertical plate starts to cycle, not only imposing large shear stress in the central cross section of the slab, but also generating a horizontal force. The total horizontal force in these figures consists, therefore, of two components: one is caused by the movement of the horizontal plate and the second is generated by movement of the vertical plate. This can easily be seen on all four graphs in Figures 8 and 9. The fluctuation of horizontal force due to the cycling of the vertical

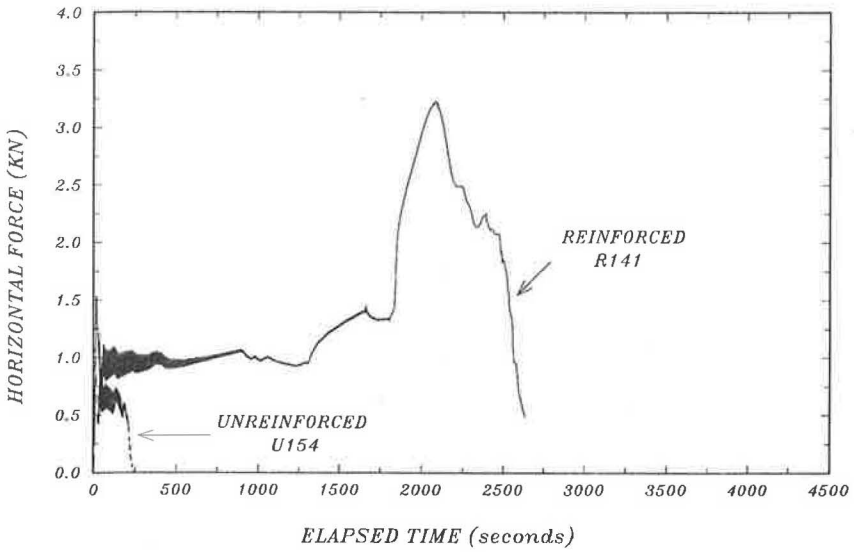

FIGURE 8 Combined tensile and shear stress test, thin AC samples (approximately 60 mm).

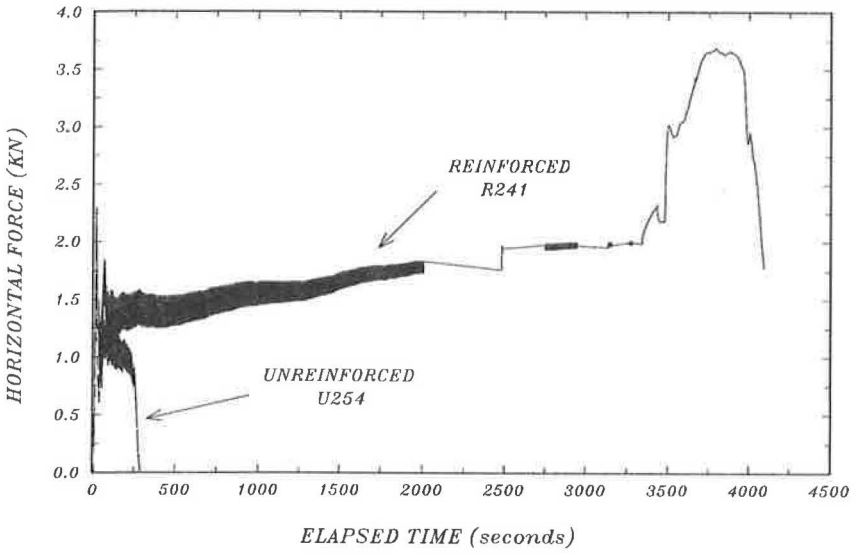

FIGURE 9 Combined tensile and shear stress test, thick AC samples (approximately 90 mm).

plate is quite large at the beginning of the test, but slowly diminishes with cycling as the slab loses its strength.

FAILURE MODES

The close observation of crack initiation and propagation, including an overall mode of failure, revealed several interesting facts.

Unreinforced AC

Cracks begin in the central region and at the bottom of the AC slabs, where tensile stress is the highest. These cracks are at the end of the mounting plates and the glue, where the highest stress concentration exists. The bottom cracks propagate upward very quickly and soon are joined by surface cracks propagating downward, as seen in Figure 10. Both thin and thick slabs fail between 400 and 500 cycles.

FIGURE 10 Failure mode-cracking pattern for unreinforced AC slab during combined tensile and shear stress test.

Geogrid-Reinforced AC

The first cracks appear at the bottom of the slabs. Besides the vertical cracking, the slabs also crack horizontally at the bottom just above the glue. This is not a failure of the AC; instead, the slabs are being lifted from the mounting plates because of the vertical movement of the vertical plate. As a result, the slabs lose bond 5 to 6 cm from the edge of the mounting plates.

The vertical cracks propagate upward with continued cycling to the level of the geogrid, where they are arrested. A simplified finite element modeling of this test was carried out to explain some aspects of the failure mechanism. This analysis showed that in the middle of the slab height, for these types of boundary conditions and loading, the shear stress is the highest. This fact coincides with observations of these tests, revealing horizontal cracking at the level of the geogrid. Sometimes this cracking occurs as a change in the direction of cracking from vertical to horizontal, yet sometimes these horizontal cracks are self-initiated before they are joined by the bottom vertical cracks. This type of failure progresses slowly and usually takes about 5,000 cycles and large horizontal deformation before further vertical cracking occurs at the top of the samples (Figure 11, thin sample). Horizontal cracking or delamination at the level of the geogrid indicates poor interlock between the geogrid and asphalt concrete; it also indicates poor asphalt mix and geogrid design. Such delamination could be a serious problem leading to pavement failure, that is, to the disintegration of the asphalt concrete

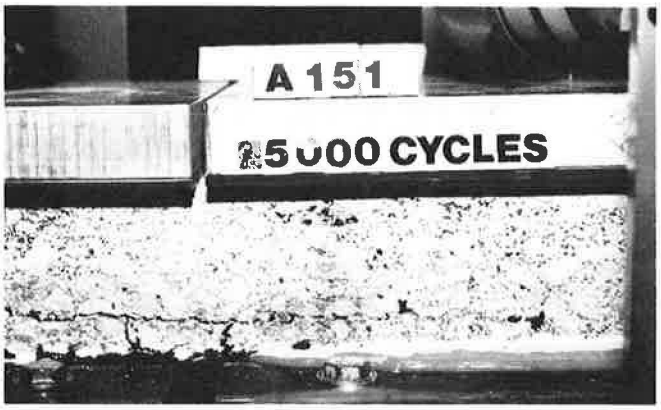

FIGURE 11 Horizontal cracking at level of geogrid due to shear load, thin AC slab.

layer above the geogrid. It is clear that there is a need to develop an "integrated" design encompassing the design of the geogrid with the mix. For a geogrid applied to an overlay, the presented testing technique will be useful in developing an optimum overlay thickness.

CONCLUSIONS

This paper describes the development of a new piece of laboratory equipment: CMTS. The first application has been for testing the mechanical properties of asphalt concrete. The main advantage of the CMTS is its ability to combine tensile and dynamic shear stresses in a single test. The results of the first testing program presented here demonstrate the importance of considering the combination of tensile shear loading, which very often occurs in real pavement. The main conclusions can be summarized as follows:

1. The failure mechanism of unreinforced asphalt concrete due to the tensile loading begins at the bottom of the layer. This is caused by the fact (confirmed by finite element stress analysis) that shear stress is highest at the bottom due to fixation (i.e., gluing in the experiment or, in a real situation, the bond between an overlay and the surface of the old pavement). In pavement, cracks may also be initiated at the surface, if construction cracking caused by steel drum compactors (known as checking) is present.
2. Dynamic shear stress greatly accelerates tensile cracking, leading to a fast progressive failure of unreinforced asphalt concrete.
3. The presence of a geogrid can arrest bottom vertical cracks and considerably slow failure. This is true only if a good interlock between the geogrids and asphalt concrete is achieved during construction. Because dynamic shear stress can generate horizontal cracking on the geogrid level, the development of a proper construction technique for reinforced asphalt pavement is of paramount importance.
4. It is expected that the type of testing developed here will assist in evaluating the interlock characteristic of a reinforced asphalt concrete.

This paper represents only the first phase of the research program carried out on the new testing equipment combining shear and tensile stresses. The second phase is already on its way to confirm findings presented in this paper and to evaluate new testing procedures (including effects of loading types, loading rates and different boundary-fixation conditions) on large numbers of lab experiments.

ACKNOWLEDGMENTS

The authors acknowledge help and advice during laboratory testing from A. O. Abd El Halim of Carleton University in Ottawa. Mario Gervais, a graduate student at Carleton University, assisted with the test program. A colleague, Keyvan Sepehr, carried out the finite element analysis. Particular thanks and deep gratitude are due to Leo Mulvihill for contributing to the design and for fabricating the CMTS.

REFERENCES

1. Mechanical Tests for Bituminous Mixes, Characterization, Design and Quality Control (H. W. Fritz and E. Eustacchio, eds.). *Proc., 4th International RILEM Symposium*, Budapest, Hungary, Oct. 1990.
2. B. E. Ruth, M. Tia, and S. Sigurjonsson. Gyratory Testing for Bituminous Mix Evaluation. *Proc., 4th International RILEM Symposium*, Budapest, Hungary, Oct. 1990.
3. F. Hugo and P. Raath. The Prevention of Reflective Cracking in Asphalt Overlays. *Proc., Conference on Asphalt Pavements in South Africa*, Durban, South Africa, 1974.
4. B. F. McCullough and S. B. Seed. Field Validation of an Overlay Design Procedure To Prevent Reflection Cracking. *Proc., 5th International Conference on the Structural Design of Asphalt Pavements*, The Netherlands, Aug. 1982, pp. 780–791.
5. H. J. Treybig, B. F. McCullough, P. Smith, and H. Von Quintus. *Overlay Design and Reflection Cracking Analysis for Rigid Pavements, Volume 1—Development of New Design Criteria*. Research Report FHWA-RD-77-66. FHWA, U.S. Department of Transportation, Aug. 1977.

Development and Evaluation of Test System To Induce and Monitor Moisture Damage to Asphalt Concrete Mixtures

SALEH AL-SWAILMI, TODD V. SCHOLZ, AND RONALD L. TERREL

One of the major research goals of the Strategic Highway Research Program is to develop a relationship between asphalt binder properties and field performance for asphalt concrete mixtures. A part of this effort is concerned with development of a system and procedure to moisture-condition asphalt concrete specimens to determine whether an asphalt-aggregate mixture is susceptible to moisture-induced damage. The development of a computer-controlled loading and data acquisition subsystem used with moisture conditioning and environmental control subsystems is addressed. The three subsystems make up a state-of-the-art test system that is used to determine and measure the factors that most influence the amount of moisture damage. A brief overview of the three subsystems is given, as is a more detailed description of the development and evaluation of pertinent test parameters. Significant findings include (a) many factors affect the reliability of subsystems, and the computer-controlled loading and data acquisition subsystem provides an efficient tool for detecting factors causing variability in test results; (b) specimen instrumentation is simple, reliable, and accurate; (c) specimens 4 in. high and 4 in. in diameter were found to provide results of sufficient accuracy; and (d) specimen orientation was found to be very important.

A major goal of the Strategic Highway Research Program (SHRP) is to relate asphalt binder properties to field performance of asphalt concrete mixtures. Consequently, much of this research program has focused on the factors that influence field performance. Although many factors contribute to the degradation of asphalt concrete pavements, damage attributable to moisture is considered a key element in the deterioration of asphalt mixes.

With the recognition that moisture damage can significantly influence pavement performance, a part of the SHRP research effort has been concerned with the development of a system and procedure having a twofold purpose: (a) to determine whether an asphalt-aggregate mixture is susceptible to moisture-induced damage, and (b) to moisture-condition asphalt concrete specimens to be tested for mixture properties including thermal cracking, fatigue, and permanent deformation (rutting).

Previous work on the development of a moisture-conditioning procedure has been documented elsewhere (*1*,*2*). This paper addresses the development and evaluation of the test system composed of a computer-controlled closed-loop loading and data acquisition subsystem that is used with fluid conditioning and environmental cabinet subsystems. The three subsystems make up a state-of-the-art test system used to determine and quantify the factors that most influence the amount of moisture damage that occurs in asphalt concrete mixtures.

A brief overview of the three subsystems, collectively referred to as the environmental conditioning system (ECS), is followed by a more detailed description of the development and evaluation of pertinent test parameters. Provided are details about factors that affect the measurement of resilient modulus (height-to-diameter ratio, deformation measurement, etc.), permeability measurement, and overall water sensitivity evaluation (saturation level, conditioning temperature, etc.). It is shown that considerable effort was required to "debug" the overall test system so that a reliable system producing repeatable results emerged.

TEST SYSTEM

The ECS was designed and fabricated to assist in determining the most important factors in the performance of mixtures in the presence of moisture. The test setup permits evaluation of air voids and behavior of mixtures in several ways, including

- Saturation versus wet (partial saturation),
- Water versus vapor as a conditioning fluid,
- Permeability versus air void content,
- Freezing versus no freezing,
- Volume change effects (i.e., oversaturation),
- Effects of time on rate of saturation or desaturation,
- Continuous monitoring using resilient modulus (M_R),
- Repeated loading versus static loading, and
- Coating and stripping.

The ECS can be used to evaluate these factors in terms of the effectiveness of currently used testing procedures, and it can lead to the development of a new testing procedure. In addition, the ECS can be used to validate concepts developed by others involved in SHRP asphalt research. As noted, the ECS can test a wide range of factors, but it is recognized that all of this capability may not be required in the final version of the SHRP-ECS test to be used for routine testing.

The ECS was designed and fabricated to provide a means of simulating various conditions within an asphalt pavement. Figure 1 shows the ECS and its subsystems: the fluid-conditioning subsystem, the environmental cabinet subsystem, and the loading subsystem.

Department of Civil Engineering, Oregon State University, Corvallis, Oreg. 97331.

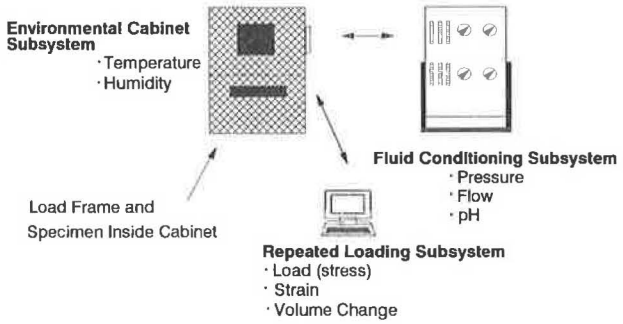

FIGURE 1 Overview of ECS.

Fluid-Conditioning Subsystem

This system was designed to test the air and water permeability of asphalt concrete mixtures as well as to provide fluid (water, water vapor, or air) conditioning.

As shown in Figure 2, the test specimen is placed in a load frame. Two differential pressure gauges, connected immediately before and after the specimen, measure the pressure gradient across the specimen, which is controlled by a vacuum regulator.

Environmental Cabinet Subsystem

The heart of the system is a Despatch Industries 16000 Series high- and low-temperature and humidity environmental-conditioning cabinet. The environmental chamber simulates high and low temperatures and humidity levels.

Loading Subsystem

The repeated loading subsystem is an electropneumatic closed-loop system made up of a personal computer with software and an analog-to-digital/digital-to-analog interface card, a transducer signal conditioning unit, a servovalve amplifier and power supply, and a load frame.

Figure 2 shows a schematic of the load frame, which includes a double-acting pneumatic actuator (piston) and servovalve. The servovalve, serviced by compressed air and driven by a computer software program, drives the piston. Loads are delivered by the piston through its load ram to a load cell mounted on the specimen cap, which rests atop the test specimen. The signals from the load cell and linear variable differential transducers (LVDTs) mounted on the specimen are collected by the computer software program and converted to engineering units of stress and strain allowing the calculation of the M_R. Although the software can deliver a variety of loads and waveforms, tests in the ECS have been almost exclusively conducted using a haversine pulse load with a pulse load duration of 0.1 sec, a pulse load frequency of 1 Hz, and a pulse load magnitude of 600 lb.

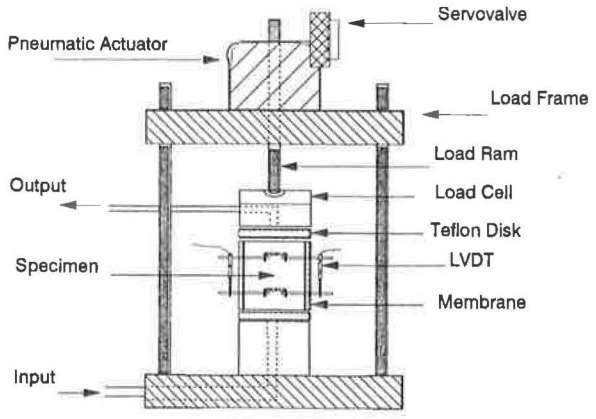

FIGURE 2 Load frame inside environmental cabinet for evaluating water sensitivity.

SYSTEM DEVELOPMENT AND EVALUATION

As stated earlier, the intent of this paper is to describe the development and evaluation of the ECS. Generally, before a full-scale test scheme is started, many questions and details must be evaluated when a testing device is developed. Likewise, before the ECS was used as a testing device for the water sensitivity program at Oregon State University, it was subjected to detailed investigation and refinement to prove its reliability and reproducibility in three aspects: resilient modulus measurement, permeability measurement, and water-conditioning evaluation.

Resilient Modulus Measurement

Many test procedures and types of test equipment have been developed and used in several laboratories and agencies to evaluate the structural properties of the asphalt concrete mixtures. The resilient modulus of compacted asphalt mixtures can be obtained by using either repeated-loading triaxial test or repeated-loading indirect tensile test. These two procedures have been standardized by ASTM as the Standard Test Method for Dynamic Modulus of Asphalt Mixtures (ASTM D3497) and the Standard Test Method of Indirect Tension Test for Resilient Modulus of Bituminous Mixtures (ASTM D4123).

In the ECS, the resilient modulus is defined as the ratio of the applied differential axial stress to the corresponding recoverable (elastic) axial strain. The vertical stress is applied axially by the use of an electropneumatic closed-loop testing system. Applied stress is monitored by a load cell placed on the top of the specimen. Recoverable axial strain is monitored by LVDTs. Stresses and strains are recorded and analyzed by the computer and software package.

For axial loading the appropriate specimen height, as recommended in ASTM D3497, should be at least 8 in. for a specimen with a 4 in. diameter. However, it was not feasible to water-condition these tall specimens. To compromise between the ASTM D3497 requirement and typical pavement layer thicknesses, a ministudy was conducted to investigate the effect of height-to-diameter (L/D) ratio, on resilient modulus. In addition, other ministudies were conducted to investigate other details, including the effect of glue type for strain gauges (strain gauges were later replaced by LVDTs), and

the repeatability of ECS resilient modulus and necessity of using Teflon disks.

Test Specimen Preparation

One mix was used for preparing three specimens 4 in. in diameter and 7 in. high. After density was determined, a vertical alignment jig was used with capping compound to maintain caps perpendicular with the specimen axis according to the requirements of ASTM C617 (Capping Cylindrical Concrete Specimens). After testing the specimens with the full height, 1.0 in. was trimmed from each end with a diamond saw. Capping and testing were repeated for the new 5-in. specimens. Finally, 1.25 in. was trimmed from each end of the 5-in. specimen, which resulted in 2.5-in. specimens that were exposed to the same capping and testing procedure. Trimmed specimen densities and air void calculations were monitored for the three heights.

Test Equipment and Instrumentation

In this ministudy, an MTS electrohydraulic closed-loop system was used for the dynamic compression loading and stresses were monitored by chart recorder. Recoverable axial strain was measured by two techniques:

1. LVDTs attached to the specimen by a pair of clamps that were cemented to the specimen by plates, maintaining a 2-in. gauge length. Deformations were measured by chart recorder.
2. A pair of strain gauges 1 in. long and a strain indicator for recording strains.

The specimens were loaded using two modes: (a) continuous repeated loading of haversine wave form, and (b) continuous repeated loading of square wave form. A dynamic load of 600 lb was used after the specimens were seated with a 60-lb static load.

Effect of L/D Ratio on Resilient Modulus

Figures 3, 4, and 5 show the relationship between resilient modulus and specimen thickness for the three similar specimens (three test replications). Moduli of the specimens with 2.5-in. thickness are significantly higher than the moduli of the specimens with 5- and 7-in. thicknesses. The wave form (haversine or square) and strain measurement device (LVDTs or strain gauges) have no effect on the trend or general relationship, but they do affect the magnitude: for the same method of strain measurement and load level, the M_R from the square wave mode is higher than the M_R from the haversine wave form.

For the same wave form, strain gauges detect less strain, which resulted with a higher M_R than that from the LVDTs. Strain gauges may not indicate the total strain as the LVDTs do because large stones behind the strain gauges may not transmit the total strain. In contrast, LVDTs with total slippage controlled measure the cumulative strain between two points, which may be more realistic. In addition, during the ECS testing program it has been noticed that the strain gauges mounted on specimens with high air voids (such as 10 percent) experienced major wrinkles under the effect of repeated load-

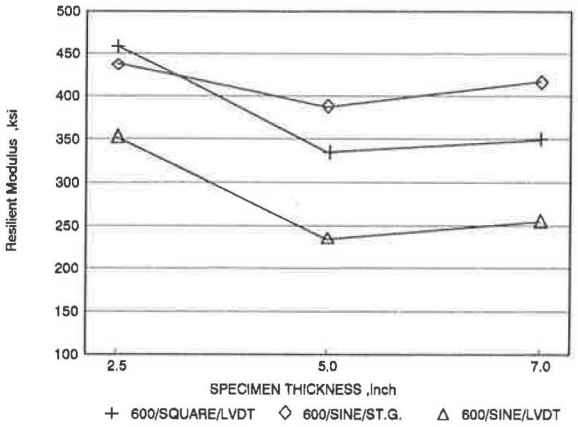

FIGURE 3 Relationship between M_R and specimen thickness for two testing conditions, Specimen 1.

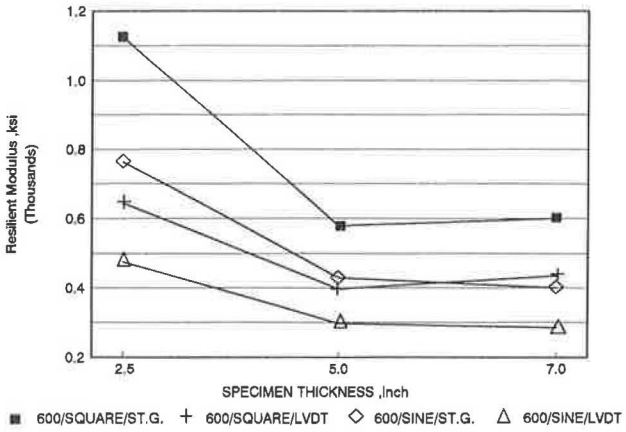

FIGURE 4 Relationship between M_R and specimen thickness for two testing conditions, Specimen 2.

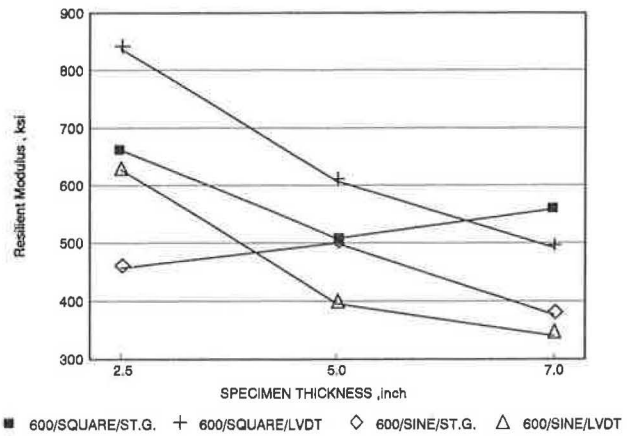

FIGURE 5 Relationship between M_R and specimen thickness for two testing conditions, Specimen 3.

ing with hot-water conditioning. The deformed strain gauges were most likely caused by total deformation due to compaction. Because of such deficiencies associated with the strain gauges and because of their cost, it was decided to switch to LVDTs after a significant part of the ECS testing program, particularly the low-air-void specimens, was completed using strain gauges.

Finally from this investigation, it was concluded that specimen thickness has a crucial effect on resilient modulus value and the specimen closest in thickness to 8 in. (L/D = 2.0) gives the closest to "true" resilient modulus. For the ECS, it is sufficient to monitor relative change in resilient modulus during water conditioning, which indicates the real strength (M_R) change. This concept of relative M_R using a 4-in. specimen has been used as a compromise for an 8-in. specimen (4-in. specimens are easier to produce and test and are more representative of actual pavement lift thicknesses). Thus, a specimen 4 in. high was recommended and is used for the ECS testing.

Since the resilient modulus value from the ECS is not the true or familiar M_R, the term "ECS-M_R" will be used in this paper for 4-in. specimens. Therefore, there are two important differences between the ECS-M_R and the dynamic modulus defined in ASTM D3497: (a) the height of the specimen is 4 in. instead of 8 in., and (b) the specimen is encapsulated in a rubber membrane throughout the test. In addition to ECS-M_R, a diametral M_R is measured for each specimen before the ECS testing process to be used for reporting the initial specimen strength. All values of M_R in this report stand for ECS-M_R unless otherwise noted.

Effect of Strain Gauge Glue Type

The ECS testing program started with strain gauges that were subjected to a detailed investigation before the full-scale test scheme was begun. The main factor to be evaluated was the effect of glue type on strain gauge performance. To accomplish this investigation, six strain gauges (X_1, X_2, X_3, Y_1, Y_2, and Y_3) were bonded on a plastic specimen 7.5 in. high and 4 in. in diameter. The strain gauges were divided into two groups, and each group was mounted at midheight opposite to the other group. The two groups are (a) X_1, X_2, and X_3 bonded on Side X; and (b) Y_1, Y_2, and Y_3, bonded on Side Y. Three types of glue were used for bonding the strain gauges according to the following identification:

- X_1 and Y_1: 1-in. strain gauge with cyanoacrylate ("superglue");
- X_2 and Y_2: 1-in. strain gauge with Ca-200LS glue; and
- X_3 and Y_3: 1-in. strain gauge with Testor's "airplane" glue.

Specimens were subjected to dynamic repeated loading by using the MTS and strains were monitored by strain indicator. Figure 6 shows resilient modulus results from each strain gauge. The difference between glue types is not significant. The M_R on Side X was higher than M_R on Side Y due to an eccentricity problem that was later corrected. As a result of this experiment, superglue was selected for future strain gauge application because it needs a very short time to cure.

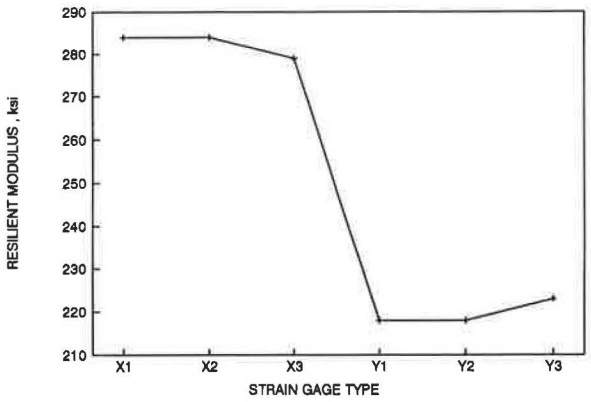

FIGURE 6 Effect of strain gauge mounting glue on M_R.

Repeatability of ECS-M_R and Effect of Teflon Disks

Six specimens were used to investigate the repeatability of ECS-M_R and the effect of friction between the specimen and the top cap and bottom base. Teflon disks were used because of the concern that the shorter (4-in.) specimens are affected by the load platens to a greater extent than for taller specimens. The following specimens were used in the study:

- 1 PLAS and 2 PLAS: plastic, 4 in. in diameter and 2.5 in. high;
- 54TB and 62TB: asphalt concrete, 4 in. in diameter and 2.5 in. high; and
- TG61 and WG77: asphalt concrete, 4 in. in diameter and 4 in. high.

Strain gauges 1 in. long were used on specimens 2.5 in. high, and strain gauges 2 in. long were used on the 4-in. specimens. The ECS was used to conduct resilient modulus tests. Two types of ⅛-in.-thick Teflon disk were used: solid and perforated. Tests were performed on each specimen according to the following combinations:

- No disks: No disks were used;
- One disk: One solid Teflon disk, top and bottom;
- Perf. disk: One perforated Teflon disk, top and bottom;
- Two disks: Two solid Teflon disks, top and bottom;
- One disk: One solid Teflon disk, top and bottom; and
- Diff. Or: One solid disk top and bottom with different orientation by rotating the specimens 180 degrees around its vertical axis.

The one-disk setup was conducted twice to show the repeatability of ECS-M_R for the test setting that represents the ECS testing program standard. Figure 7 shows the ECS-M_R for all test setups from each specimen. For all six specimens, the repeatability of one disk setting is very high. Teflon disk and test orientation does not affect the results for the plastic specimen because of Teflon's near frictionless surfaces and high uniformity. Teflon disks and test orientation have a significant effect on ECS-M_R of 2.5-in. asphalt concrete specimens, 54TB and 62TB. The effect of Teflon disks and test orientation on ECS-M_R from 4-in. asphalt concrete specimens is not significant.

It was found necessary to use perforated spacers between the specimen and top cap and base plate to collect any stripped

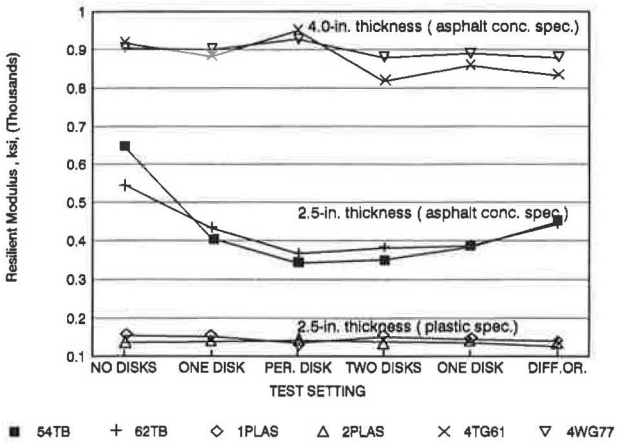

FIGURE 7 Variability of ECS-M_R for different test conditions.

asphalt that might stick on the bottom of the top cap during the water conditioning process and change its serviceability condition. Perforated Teflon disks, top and bottom, are recommended to be used with the ECS testing program.

Permeability Measurement

Permeability K, as defined by Kumar and Goetz (*3*), is the volume of fluid Q of unit viscosity μ passing in unit time Δt through a unit cross section A of a porous medium of length L under the influence of a unit pressure gradient ΔP.

$$K = \frac{Q\mu L}{A\Delta P\Delta t}$$

There is a general belief that permeability is a better measure of durability than percentage air voids because permeability measures fluid accessibility through the asphalt pavement. Some air voids may not be accessible by water. In the ECS testing program, a relationship is hypothesized between permeability and water damage.

For the air or water flow to pass only through the specimen during the permeability test, the outer surface of the specimen wall must be sealed to close off surface voids. Goode and Lufsey (*4*) used paraffin for sealing to prevent leakage between the specimen wall and the membrane. However, this method destroys the specimen for further use by contaminating the asphalt.

Another method is to place the specimen in a cylindrical rubber membrane fastened to a hollow metal cylinder with hose clamps. This method does not totally prevent leakage between the specimen wall and the membrane, especially with mixtures having coarse surface texture. Another disadvantage of this method is that air pressure in the membrane may cause deformation of the specimen.

Kumar and Goetz (*3*) developed a different technique to prevent leakage. The specimen is placed between lower and upper collars and coated with silicone rubber sealer all around the specimen and part of both collars in order to bind the collars to the specimen. This method prevents the leakage through the specimen wall, but it is rather involved and time-consuming.

In the modified procedure developed at Oregon State University, the middle third of the specimen's surface is coated with silicone and then enveloped with a cylindrical rubber membrane 1.5 in. high (a wide rubber band, cut from a membrane) to provide a smooth surface as shown in Figure 8. After curing for a few hours, the specimen is fitted with a cylindrical rubber membrane, long enough to envelop the sample base and sample top cap. This procedure has been adopted after investigating three levels of silicone seals on the surface of the specimen and under the rubber membrane. Test results from six specimens showed that the "standard" procedure of a single seal at the midpoint was adequate, as shown in Figure 9.

Water Sensitivity Evaluation

An intensive testing program was conducted by using the ECS at Oregon State University. The controlled variables and their treatment levels in a factorial design experiment include

1. Temperature with three treatment levels: hot (60°C), ambient (25°C), and freeze (−18°C).
2. Permeability with three treatment levels depending on the air voids (AV): low (% AV ≤ 6), pessimum (6 < % AV < 14), and high (% AV ≥ 14).
3. Wet conditioning with three treatment levels: dry (No water conditioning) moist [running water through the speci-

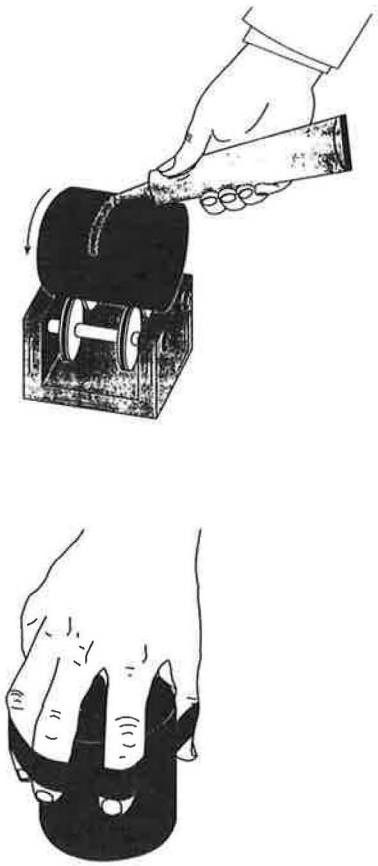

FIGURE 8 Permeability sealing of compacted asphalt mixtures using silicon sealer and rubber membrane.

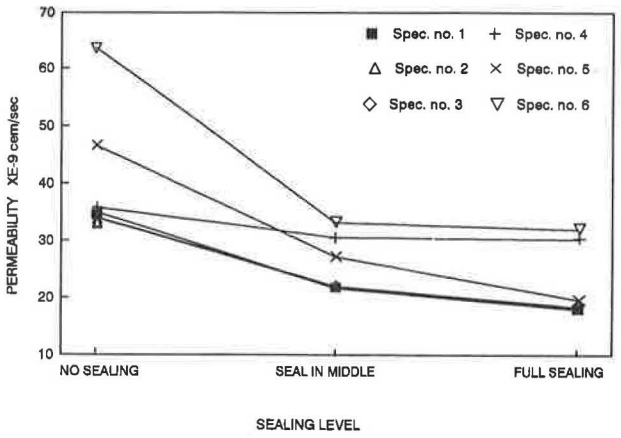

FIGURE 9 Effect of sealing level on permeability.

mens at 25°C under 10 in. of mercury (Hg) vacuum for 30 min], and saturated (running water through the specimen at 25°C under 20 in. of Hg vacuum for 30 min).

The complete study has been documented by Al-Swailmi and Terrel (*1*). Because of space limitations, only two water-conditioning tests will be discussed to show the capability of the ECS in detecting asphalt concrete response under the effect of water conditioning.

Materials

Two aggregates and two asphalts were used from the SHRP Materials Reference Library (MRL) at the University of Texas (Austin) as follows:

1. Aggregates: granite, RB, nonstripper and gravel, RL, a known stripper.
2. Asphalts: AAG-1 and AAK-1. These were selected because of their different compositional and temperature-susceptibility characteristics.

These four asphalt-aggregate combinations were used to fabricate mixtures.

Test Procedure

The water-conditioning procedure is summarized for a typical test and includes several steps, depending on the mixture and variables being evaluated.

1. A specimen 4 in. in diameter and 4 in. high is mixed and compacted.
2. Physical measurements (density, voids, etc.) are determined.
3. Circumferential silicon seal is applied, and specimens are mounted in load frame.
4. LVDTs are mounted.
5. Preconditioned resilient modulus is determined.
6. Permeability (air) is measured.
7. Specimen is wetted according to desired procedure and permeability (water) is measured.
8. Conditioning cycles are begun according to the desired sequence. Table 1 shows a typical conditioning chart that includes the variables for each test.
9. The resilient modulus (M_R) and water permeability (K) are measured at 25°C after each cycle.
10. Upon completion of conditioning, the specimen is split open and the degree of stripping determined.

Effect of Saturation Level

One of the capabilities of the ECS is to isolate and evaluate a single factor among a wide range of factors. In the ECS water-conditioning procedure, the degree of saturation is defined by a standardized vacuum level. The wetting vacuum level, before the water-conditioning cycling, is either 10 in. Hg for moist or 20 in. Hg for saturated. A vacuum level of 10 in. Hg is then maintained during conditioning. Vacuum level appears to be more representative for the ECS procedure because retaining some vacuum (10 in.) during water conditioning maintains a constant level of saturation better than for static immersion conditioning.

For evaluation of the saturation level, 2 two-specimen sets were compacted for one air void level from the same asphalt-aggregate mix, RL–AAK-1. One set was then wetted to achieve the moist condition, and the second set was wetted to achieve the saturated condition. All specimens were then subjected to the same water-conditioning procedure, same temperature level, and repeated loading, as shown in Table 1. Figure 10 shows the retained modulus (average of each set) obtained by dividing the M_R after each conditioning cycle by the original dry M_R. The specimens subjected to the higher wetting level (i.e., saturated) experienced more water damage.

TABLE 1 Conditioning Chart for Figure 10

CONDITIONING FACTOR		CONDITIONING STAGE			
		WET *	CYCLE-1	CYCLE-2	CYCLE-3
Vacuum (in. Hg) :	Saturated	20	10	10	10
	Moist	10	10	10	10
Ambient Temp.(C) **		25	60	60	60
Duration (hr.)		0.5	6	6	6

* WET : Wetting the Specimen Prior Conditioning Cycles
** Inside the Environmental Cabinet

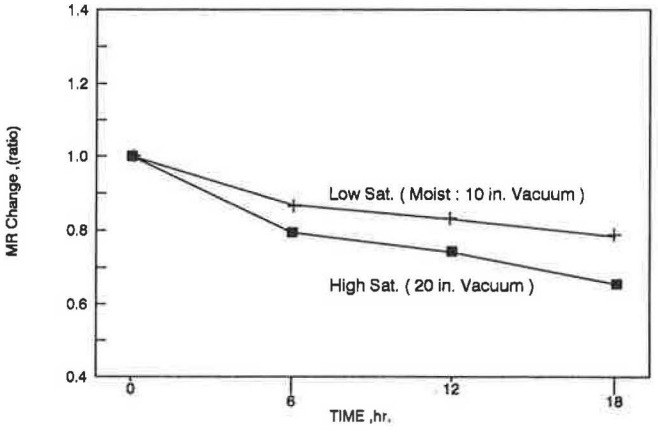

FIGURE 10 Effect of vacuum level on M_R: hot-saturated and hot-moist conditionings with continuous repeated loading.

Effect of Conditioning Temperature

To evaluate conditioning temperature 2 two-specimen sets were compacted to the same air void level using the same asphalt-aggregate combination, RL–AAK-1. Before conditioning, the specimens were tested for M_R at 25°C. Both sets were then subjected to the same wetting procedure to achieve a saturated level (i.e., pulling 25°C water under a vacuum level of 20 in. of Hg for 30 min). After wetting, one set was subjected to three 6-hr "hot cycles" at a temperature of 60°C with continuous repeated loading while a vacuum of 10 in. of Hg was maintained. Between cycles the specimen temperature was reduced to 25°C and the M_R was measured. The second set was tested in the same manner except the specimen temperature remained constant at 25°C throughout. Figure 11 shows that the specimens subjected to the hot cycles (60°C) experienced a significantly higher degree of water damage than did the specimen cycled at ambient temperature (25°C).

SUMMARY AND CONCLUSIONS

The development of the ECS required considerable effort to mitigate the problems associated with seemingly minor details (e.g., L/D ratio, strain gauges versus LVDTs, amount of silicone sealing required) such that a reliable and practical system producing repeatable results emerged. Although the following conclusions (which are based on data to date) appear warranted, it should be noted that this is an ongoing study and that the conclusions should be regarded as tentative.

As for the loading subsystem, the effect of the height-to-diameter ratio was shown to have significant import in the determination of resilient moduli of asphalt concrete specimens. Resilient modulus tests indicated that specimens having an L/D ratio of less than unity showed greater variability and significantly greater magnitudes than did specimens having L/D ratios greater than unity. Furthermore, it was shown that modulus tests on specimens having an L/D ratio of 5/4 had essentially the same variability and magnitude as those for specimens with L/D ratios of 7/4. With these results and the expectation that most production laboratories can easily produce 4-in.-high specimens (but may need to retool to produce specimens of greater height), a 4-in. height and 4-in. diameter were selected as a standard.

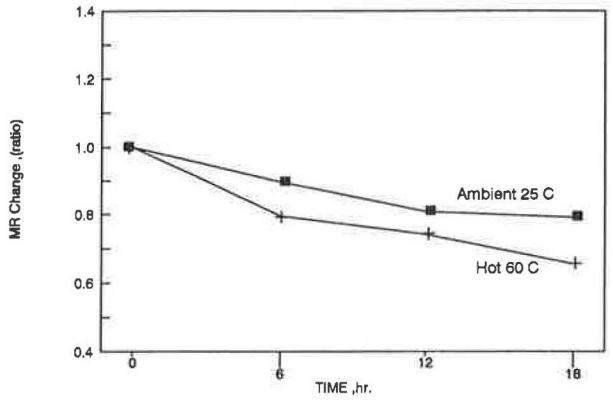

FIGURE 11 Effect of conditioning temperature on M_R.

Comparisons between LVDTs and strain gauges showed little or no significant difference on dry specimens. However, the use of strain gauges presented problems of practicality during actual testing. That is, the strain gauges wrinkled under the effect of repeated loading with hot-water conditioning. Therefore, the use of LVDTs was adopted for strain measurement during the resilient modulus tests. Although the use of strain gauges for the ECS was abandoned, tests on the type of glue used to bond the gauges to the specimens showed no significant difference between glue types, thus cyanoacrylate ester (superglue) was recommended for such application, because of its quick drying time.

Tests evaluating the use of Teflon disks (used to minimize shear stresses at the top and bottom of the specimen during modulus testing) indicated that perforated disks are suitable and that no significant difference exists between the type or number of disks. Duplicate tests using one disk at each interface indicated that the ECS-M_R is indeed repeatable.

As for permeability measurement, it was shown that partially sealing the specimen (sealing the middle third) with silicone cement is adequate; that is, fully sealing the specimen is unnecessary—the two methods indicate no significant difference.

Finally, regarding evaluation of the overall system, it was shown that the system is sufficiently sensitive to detect the level of damage due to water in terms of saturation level and conditioning temperature. In short, the ECS has been demonstrated to be suitable for and capable of determining the effect of water damage for a range of asphalt concrete mixtures.

ACKNOWLEDGMENTS

The research was supported by SHRP, a unit of the National Research Council that was authorized by Section 128 of the Surface Transportation and Uniform Relocation Assistance Act of 1987. The authors are grateful for the opportunity to work on this important project.

REFERENCES

1. S. Al-Swailmi and R. L. Terrel. Evaluation of Water Damage of Asphalt Concrete Mixtures Using the Environmental Conditioning System (ECS). *Journal of the Association of Asphalt Paving Technologists*, 1992.
2. C. Curtis, R. L. Terrel, L. M. Perry, S. Al-Swailmi, and E. J. Brannon. Asphalt Aggregate Interactions. *Journal of the Association of Asphalt Paving Technologists*, 1991.
3. A. Kumar and W. H. Goetz. Laboratory Measurement of Permeability of Compacted Asphalt Mixtures. In *Transportation Research Record 659*, TRB, National Research Council, Washington, D.C., 1977.
4. J. F. Goode and L. A. Lufsey. Voids, Permeability, Film Thickness versus Asphalt Hardening. *Proc., Association of Asphalt Paving Technologists*, Vol. 34, 1969, pp. 430–462.

Effects of Test Parameters on Resilient Modulus of Laboratory-Compacted Asphalt Concrete Specimens

RICHARD L. BOUDREAU, R. GARY HICKS, AND ARTHUR M. FURBER

The resilient modulus of a laboratory-compacted asphalt concrete specimen is dependent on many factors, including the test system used, the test operator, the method of compaction, the level of compaction, and parameters or conditions in the test procedure such as temperature, load frequency, load duration, and load-induced diametral strain level. The results of a parametric study involving resilient modulus testing of two dense-graded hot-mix asphalt concrete mixtures compacted to two levels of air voids are presented. Three replicated test specimens were prepared for each mix at each air void level using the Marshall method of compaction. The concern was to select one combination of test temperature, load frequency, load duration, and induced diametral strain that would lead to repeatable modulus results among the replicated specimens within each group while being sensitive enough to detect differences between the two mix types and levels of air void contents of similar mix types. A pneumatic test system was used to measure resilient modulus. On the basis of a statistical analysis of the test results, it was concluded that the test conditions consisting of 0.1-sec load duration, 0.33 Hz load frequency, 50 to 75 $\times$ 10^{-4} percent induced strain (50 to 75 μstrain) at 60°F would best satisfy the repeatability criteria.

Various testing machines are available that can directly measure the resilient modulus (M_R) of an asphalt concrete (AC) specimen using repeated-load techniques. Variability in the M_R arguably can be attributed to the operation of different machines by different operators, the variations in mix designs, and the level of compaction of the AC specimens, but perhaps the most severe variable contributing to such errors is the combination of test conditions selected to perform the test.

ASTM has recommended a range of test temperatures, load duration and frequency, and induced diametral strain in the standard test method ASTM D4123. These conditions are

Temperature—41, 77, and 104°F;
Load duration—0.1 to 0.4 sec;
Load frequency—0.33, 0.5, and 1.0 Hz; and
Load/strain level—induce 10 to 50 percent of the tensile strength.

M_R can be measured as total or instantaneous, which differ in the interpretation of recoverable strain on load release; it is described in more detail in the ASTM test procedure. All of these factors can greatly influence the M_R of an asphalt concrete mixture.

R. L. Boudreau, Law Engineering, Inc., 1386 Mayson Street, Atlanta, Ga. 30324. R. G. Hicks, Oregon State University, Covell Hall 106, Corvallis, Oreg. 97331. A. M. Furber, Pavement Services, Inc., 2510 Southwest First Avenue, Portland, Oreg. 97201.

The concern of the laboratory study presented in this paper is to evaluate the effects of the M_R test conditions on replicated specimen groups. The primary objective is to develop a singular set of test conditions that leads to the most repeatable M_R results within a set of replicated specimens. The secondary objective is to evaluate the potential of the test conditions selected to differentiate between M_R results of replicated specimen groups with subtle variations in mix constituents and levels of compaction.

EXPERIMENT DESIGN

To satisfy these objectives, several variables were used in the study. These test variables can be divided into two general groups: (a) material variables (two aggregate types and two air void contents), and (b) procedural variables (ASTM test conditions as defined).

Material Variables

The specimens tested were laboratory Marshall-compacted, dense-graded hot-mix AC specimens made up of aggregates from two Oregon sources. Aggregate A is a crushed, river-run basalt aggregate. Aggregate B is a crushed hillside basalt aggregate. By visual observation, Aggregate B generally exhibits greater fractured faces, angularity, and surface roughness than Aggregate A.

An AR-4000W grade asphalt was batched with each aggregate at the optimum content recommended by the Oregon Department of Transportation (ODOT), as shown in Table 1.

Two levels of compaction were used for each aggregate type to achieve 4 and 10 percent air voids. The group prepared with Aggregate B at 4 percent air voids also contained 1 percent hydrated lime, which was slurried with the aggregate and dried before batching. The lime was used with Aggregate B only to aid in the evaluation of the effectiveness of lime as an antistripping additive, which is not evaluated in this paper. The air void contents were determined by the standard procedure given in ASTM D3203, (Percent Air Voids in Compacted Dense and Open Bituminous Paving Mixtures) and reported as a percentage of total specimen volume. Bulk specific gravities were determined using ASTM D2726 (Bulk Specific Gravity and Density of Compacted Bituminous Mixtures Using Saturated Surface-Dry Specimens); maximum

TABLE 1 ODOT Mix Designs for Dense-Graded C-Mix (HVEEM)

Sieve Size	Percent Passing (percentages of total aggregate by weight) Aggregate A	Aggregate B	ODOT Specifications
3/4"	100	100	100
1/2"	98	99	95 - 100
3/8"	81	87	
1/4"	65	66	60 - 80
#10	32	33	26 - 46
#40	12	16	9 - 25
#200	5.0	4.8	3 - 8
Optimum Asphalt Content*, %	6.0	6.7	4 - 8

* Percent of total mix by weight

specific gravities were determined using ASTM D2041 (Theoretical Maximum Specific Gravity and Density of Bituminous Paving Mixtures).

The purpose of using varying air void contents for the test program was to detect if the test procedure would be sensitive enough to differentiate between M_R values of varying voids. The expected trend is a decrease in M_R with an increase in air voids (*1*,*2*).

Procedural Variables

The pneumatic test system shown in Figure 1 was used in this study. As described, the operator of the repeated-load diametral test system can control a fairly wide range of values for the load duration, frequency, and amplitude, along with the testing temperature. Each test specimen, therefore, was subjected to a series of tests over a range of controlled conditions as shown in Table 2. The range was selected in order to investigate the full range of test conditions specified by ASTM D4123. Table 2 illustrates that 13 out of a total of 81 test combinations were selected for the evaluation. The selection of the 13 conditions was made on the assumption that trends of M_R with respect to duration, frequency, and strain level are the same for any given material at any temperature. Therefore, the effects of duration and frequency were observed at only one temperature (77°F) and one induced strain level (75 μstrain) and the effects of

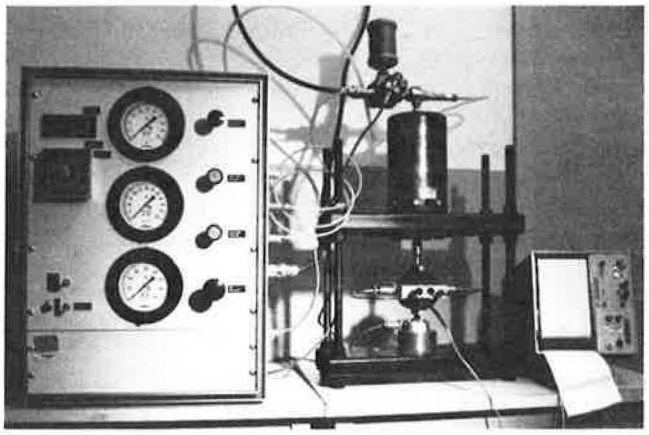

FIGURE 1 Pneumatic test system.

TABLE 2 Matrix of Test Conditions in Study

Temperature (°F)		41			77			104		
Microstrain		50	75	100	50	75	100	50	75	100
Duration (hz.)	Frequency (sec.)									
0.1	0.33					X				
	0.5	X	X	X	X	X	X	X	X	X
	1.0					X				
0.2	0.33									
	0.5					X				
	1.0									
0.4	0.33									
	0.5					X				
	1.0									

temperature and induced strain level were observed at only one load duration (0.1 sec) and one load frequency (0.5 Hz). If this assumption is correct, the *F*-ratio for the two-way interaction should not be significant.

ANALYSIS PROCEDURE

The experimental design used to analyze the test results was a completely randomized design (CRD), and a two-way analysis of variance (ANOVA) was selected as the statistical tool to aid in the evaluation of the results (*3*). For this design the procedural variables or conditions were assigned as Factor *A*, and the material variables, or simply materials, were assigned as Factor *B*. Therefore, 13 levels of Factor *A* and 4 levels of Factor *B* for a total of 52 treatments ($A \times B$ interactions) could be evaluated.

An assumption of ANOVA is that experimental errors are random, independent, and normally distributed about zero mean with common variance (*3*). The *F*-ratio, a statistic computed from the ANOVA error terms, is the ratio of two independent estimates of the same variance. Where the *F*-ratio is used, a null hypothesis of equal factor means is assumed. In general terms, the ratio represents a comparison between a biased estimated variance (mean square for factors, *MSA*, *MSB*, or *MSAB*) of the experiment and an unbiased estimate of variance (mean square for error, *MSE*) of the experiment. The hypothesis of equal means is rejected in favor of unequal means if the computed *F*-ratio is larger than critical *F*-ratios for any combination of degrees of freedom and significance levels associated with a given experiment. Critical *F*-ratios are tabularized in most statistics textbooks.

The total and instantaneous M_R were measured; therefore, two ANOVA tables were generated that were similar to the one in Table 3. A comparison of precision between the two measurements can be made using the coefficient of variation, CV, (*4*, p. 13) which is defined by Equation 1:

$$CV = [(MSE)^{1/2}/x..) * 100 \text{ percent} \quad (1)$$

where $x..$ is the grand mean of all observations.

TABLE 3 Experimental Design ANOVA

Source of Variation	Degrees of Freedom	Sum of Squares	Mean Square	F-ratio
Conditions (Factor A)	k-1	SSA	MSA	F_A
Materials (Factor B)	l-1	SSB	MSB	F_B
Treatments (A x B)	(k-1)(l-1)	SSAB	MSAB	F_{AB}
Error	kl(m-1)	SSE	MSE	
Total	klm-1	SSTot		

Variable definitions:

k = No. of levels of conditions = 13

l = No. of levels of materials = 4

kl = No. of treatments (each one a combination of test conditions and materials level) = 52

m = No. of observations of each treatment = 3 replicates

Calculations:

CT = $CT = \text{Correction term} = klm(x..)^2$ where x.. = Grand mean of all observations

SSA = $ml\Sigma A^2_k - CT$ x = each observation

SSB = $mk\Sigma B^2_l - CT$

SSAB = $m\Sigma\Sigma AB^2_{kl} - SSA - SSB - CT$

SSTot = $\Sigma\Sigma\Sigma x^2_{klm} - CT$

SSE = SSTot - SSA - SSB - SSAB

Mean squares are determined by dividing the sum of squares by their associated degrees of freedom.

F-ratios are determined by dividing the mean squares by the mean square for error.

RESULTS

M_R tests were performed on each test specimen (4 groups × 3 replicates/group = 12 total specimens) using the repeated-load test system. The H&V pneumatic device shown in Figure 1 was used in this study. The specimens were tested at each of the 13 test conditions identified in Table 2, and corresponding total and instantaneous M_R values were recorded. The values were averaged for the three replicated specimens in each group (i.e., A4 = Aggregate A, 4 percent air voids, A10 = Aggregate A, 10 percent air voids, BL4 = Aggregate B treated with lime, 4 percent air voids, and B10 = Aggregate B, 10 percent air voids), and the results are presented in Figures 2 through 9 to illustrate the general M_R trends with respect to each test condition. Each figure representing the total M_R response is grouped with a similar figure representing the instantaneous M_R response. By general observation, the modulus decreases with increasing temperature and load duration. It is apparent that these general trends are consistent within the different material groups (shown by approximate parallel lines) for the total M_R response and inconsistent (shown by intersecting lines) for the instantaneous M_R response. The total and instantaneous M_R responses were observed to be independent of load frequency and induced strain levels; therefore, they are not shown graphically. The coefficient of variation for each observation (average of three replicates) was found to be generally greater for the instantaneous M_R response. This was expected in that the interpretation of the instantaneous measurement deflection is more judgmental than the total measurement of deflection, which leaves a greater chance for error when obtaining instantaneous M_R results (ASTM D4123).

It should be noted that tests performed at 104°F were only marginally successful for the 4 percent air void samples and could not be performed for the 10 percent air void samples. This temperature was found to be too warm, and all samples

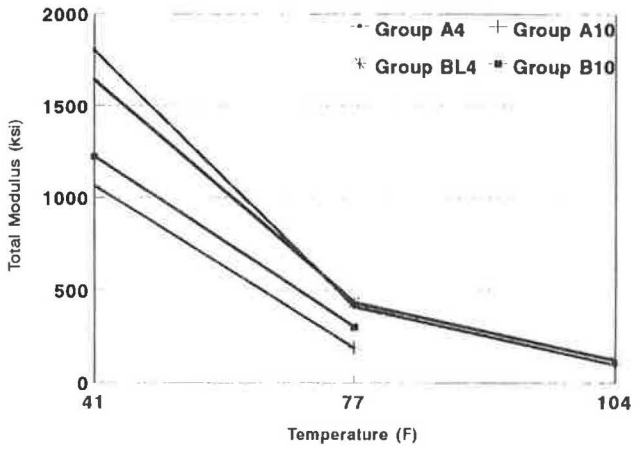

FIGURE 2 Temperature effects at 50 μstrain: total modulus.

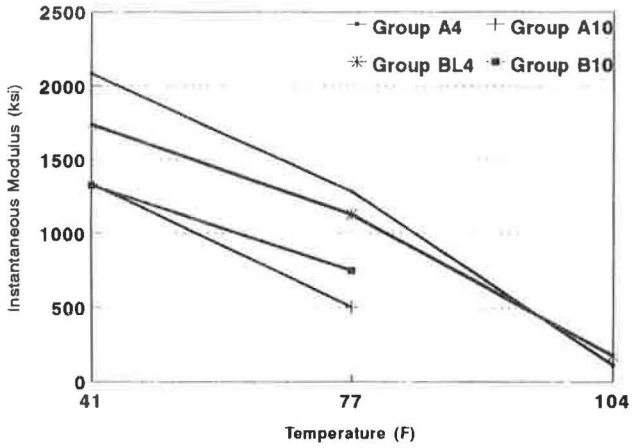

FIGURE 3 Temperature effects at 50 μstrain: instantaneous modulus.

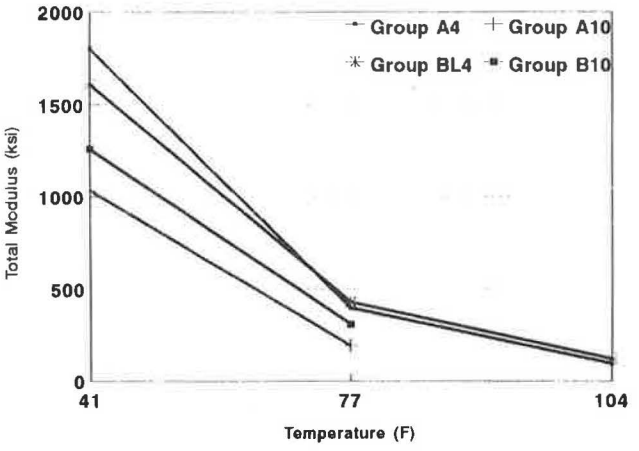

FIGURE 4 Temperature effects at 75 μstrain: total modulus.

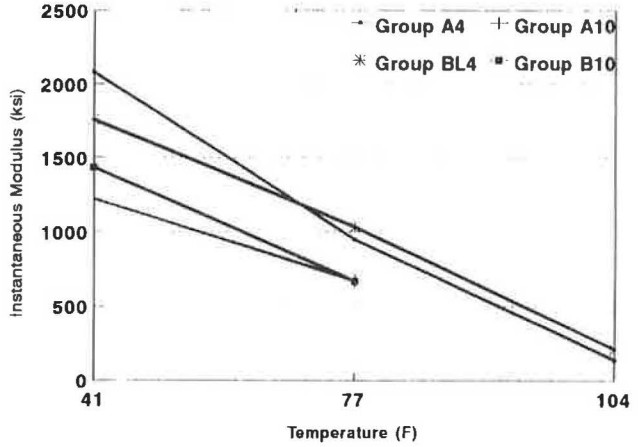

FIGURE 5 Temperature effects at 75 μstrain: instantaneous modulus.

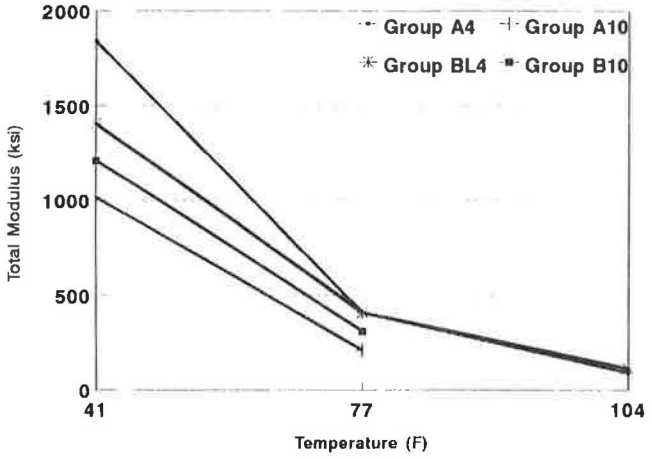

FIGURE 6 Temperature effects at 100 μstrain: total modulus.

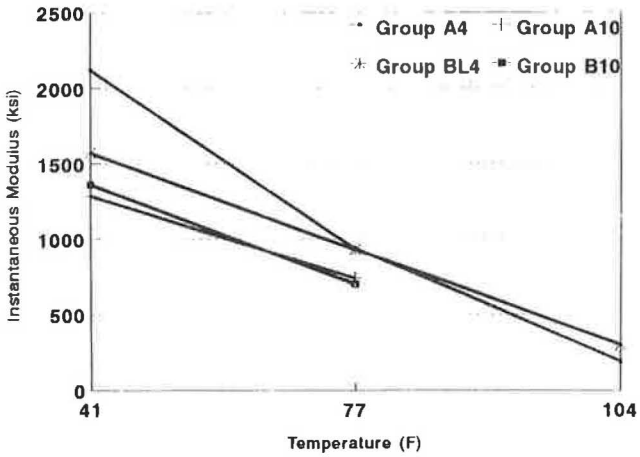

FIGURE 7 Temperature effects at 100 μstrain: instantaneous modulus.

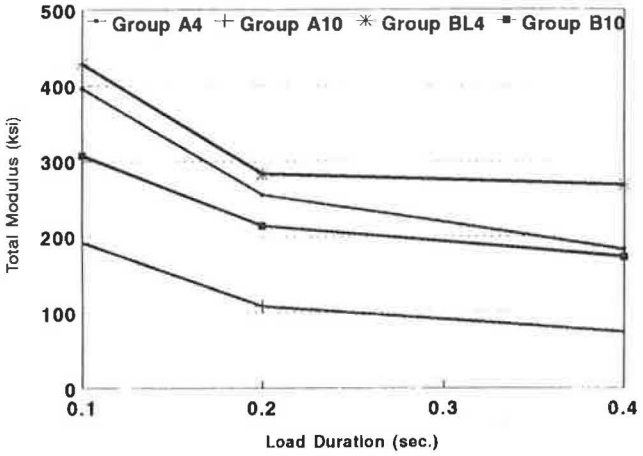

FIGURE 8 Load duration effects: total modulus.

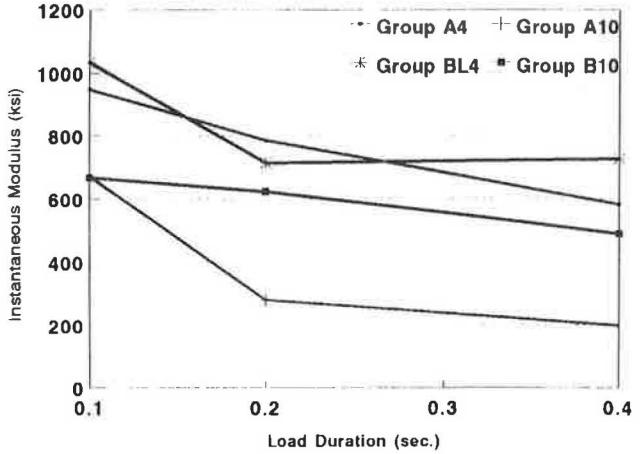

FIGURE 9 Load duration effects: instantaneous modulus.

exhibited flow (excessive permanent deformation) with only a 10-lb static seating load. Therefore, the 104°F test temperature was removed from consideration as a practical temperature, and the ANOVA in Table 3 was adjusted accordingly to reflect that only 10 levels of testing condition, Factor *A*, were considered in the analysis rather than the 13 levels originally planned.

DISCUSSION OF RESULTS

Two ANOVAs were performed at the conclusion of the M_R testing, one for the instantaneous measurement of M_R and the second for the total measurement of M_R. The ANOVAs resulted in a highly significant interaction (a significant *F*-ratio of the *AB* interaction), suggesting that Factors *A* and *B* do not act independent of each other. Unfortunately, inferences drawn from the test data at the 77°F testing temperature (i.e., general trends of M_R with respect to load duration, frequency and induced strain level) do not necessarily hold true at the 41°F testing temperature.

Because Factors *A* and *B* do not act independent of each other, the results can be summarized in a two-way table of *AB* means as shown in Tables 4 and 5 for the instantaneous and total measurements, respectively, and comparisons of *AB* means can be made.

At the onset of the experiment, both measurements were expected to detect significant differences between material

TABLE 4 Mean Instantaneous M_R of Four Types of Material Under Different Levels of Settings [ksi ($n=3$)]

	CONDITIONS*									
	1	2	3	4	5	6	7	8	9	10
Temperature(°F)	41			77						
Frequency (hz.)	0.5			0.5	0.33	0.5			1.0	0.5
Duration (sec.)	0.1			0.1	0.1	0.1	0.2	0.4	0.1	0.1
Microstrain	50	75	100	50	75					100
MATERIALS**										
A4	2085	2083	2121	1283	1109	948	785	582	866	935
BL4	1743	1758	1571	1125	867	1033	714	726	921	928
A10	1336	1223	1284	503	576	672	281	199	820	738
B10	1327	1435	1362	746	759	668	624	490	772	699
Average	1623	1625	1585	914	828	830	601	499	845	825

* Conditions are combinations of temperature, load frequency and duration, and microstrain level.
** Materials are combinations of aggregate type, air void content and additive type.

TABLE 5 Mean Total M_R of Four Types of Material Under Different Levels of Settings [ksi ($n=3$)]

	CONDITIONS*									
	1	2	3	4	5	6	7	8	9	10
Temperature(°F)	41			77						
Frequency (hz.)	0.5			0.5	0.33	0.5			1.0	0.5
Duration (sec.)	0.1			0.1	0.1	0.1	0.2	0.4	0.1	0.1
Microstrain	50	75	100	50	75					100
MATERIALS**										
A4	1801	1801	1840	410	398	396	256	183	392	409
BL4	1642	1610	1406	433	504	429	283	268	436	409
A10	1063	1033	1017	187	175	192	108	74	231	211
B10	1224	1259	1211	300	353	306	214	173	344	310
Average	1433	1426	1369	333	358	331	215	175	351	335

* Conditions are combinations of temperature, load frequency and duration, and microstrain level.
** Materials are combinations of aggregate type, air void content and additive type.

groups at any test condition combination. Differences between material groups at any test condition combination can be made using the t-test statistic. The t-test tests the hypothesis that means are equal against the alternative that the means are different (5). The t-statistic is computed as follows:

$$t = (x_{ij} - x_{i'j'})/(2MSE/m)^{1/2} \quad (2)$$

where

x_{ij} = mean M_R at the ith level of material and the jth level of conditions,
$x_{i'j'}$ = mean M_R at the ith′ level of material and the jth′ level of conditions ($x_{ij} \neq x_{i'j'}$),
$(2MSE/m)^{1/2}$ = standard error for differences between AB means,
MSE = mean square for error of the appropriate experiment, and
m = number of replications at each AB level.

The computed t-statistic is compared to a tabularized critical t-value at the appropriate level of significance and associated degrees of freedom. These critical t-values can be found in most statistics textbooks. Differences of material means at each level of setting combinations were compared in Tables 4 and 5, and the means that were not significantly different were marked with links as shown. A link drawn on the left side of the column indicates that the particular combinations

of test conditions uniquely defining that column did not result in M_R values that could successfully differentiate between mixtures composed of different aggregates at the same level of air voids. Likewise, a link drawn on the right side of the column indicates that the particular combinations of test conditions uniquely defining that column did not result in M_R values that could successfully differentiate between similar mixtures compacted to different levels of air voids. These comparisons were made at the 0.05 α-level. The tables illustrate that differences between material groups are most apparent at 41°F. It is also apparent from these tables that the total M_R measurement differentiates between material changes better than the instantaneous M_R measurement at the lower temperature. Also, the computed CV of the total M_R experiment was 11.9 percent as compared with the 12.5 percent CV computed from the instantaneous experiment, suggesting that the total measurement is relatively more precise.

The conclusions, from the ANOVA, strongly suggest 41°F as the preferred testing temperature. The conclusion is supported by the fact that at this temperature, the test procedure yields M_R values that differ significantly between material changes. The test procedure does not give a strong differentiation of M_R results at 77°F.

The 41°F test procedure requires special conditions, namely, a cold environment in which to work. The closer the test temperature is to ambient temperature, the more practical the test will be. If the test temperature is significantly different than ambient, heat loss or gain becomes a problem and an individual test can take an impractical amount of time. Therefore, a temperature between 41° and 77°F needed to be explored as a practical alternative.

This was done with samples compacted to 4 and 8 percent air voids for each aggregate type (sample groups therefore consisted of A4, B4, A8, and B8, as defined). Four replicates were compacted and tested for total M_R at temperatures of 41, 50, 60, and 77°F. A summary of the test results is shown in Table 6. An ANOVA was done by partitioning the temperatures as blocks in a randomized block design and selecting the four material groups as treatments (*6*). These results are presented in the ANOVA Table 7. The ANOVA table shows that there exists highly significant differences between treatment means, and blocking was successful in removing one source of variation from the experimental error (shown as significant *F*-ratios).

TABLE 6 Supplemental Temperature Study: Total M_R ksi ($n=4$)

	Blocks of Temperature			
	1	2	3	4
Treatments	41°F	50°F	60°F	77°F
A4	2595	1882	1271	496
B4	2717	2213	1686	771
A8	1768	1189	725	208
B8	1831	1421	960	322
block mean =	2228	1676	1160	449
SS(Tr)j =	74135	633310	517904	180039
MS(Tr)j =	247712	211103	172635	60013
F(Tr)j =	13.53	11.53	9.43	3.28

TABLE 7 Supplemental Temperature Study, ANOVA

Source of Variation	Degree of Freedom	Sum of Squares	Mean Square	F-ratio
Treatments	3	1909595	636532	34.76**
Blocks	3	6886178	2295393	125.36**
Error	9	164793	18310	
Total	15			

** Significant at the 0.01 α-level

The primary concern in this supplemental temperature study was to determine if some intermediate temperature between 41 and 77°F would lead to M_R values that strongly differentiate between treatment means. This was done by computing the individual contribution of variability among blocks (MST_{bl}) to the overall variability of the experiment (MSE), shown as a partial *F*-ratio identified as $F(\mathrm{Tr})_j$ of Table 6. This analysis suggests choosing the largest *F*-ratio among blocks, which implies the largest contribution to the overall experimental variability, or in other words, the block (temperature) that results in M_R values most different with respect to material groups.

The 41°F temperature again leads to the most discriminate M_R values, shown as a high partial *F*-ratio $[F(\mathrm{Tr})_j]$ in Table 6. However, by elevating the test temperature to 50 and 60°F, the results still appear to discriminate highly between material groups; at 77°F, this generalization does not seem warranted. The relationship between 41 and 77°F with respect to material sensitivity is consistent with those found earlier.

CONCLUSIONS AND RECOMMENDATIONS

Conclusions

From this study, the following conclusions can be made:

1. M_R results obtained shown a high degree of material sensitivity at 41°F and a low degree at 77°F.
2. The total measurement led to results with a higher degree of material sensitivity than the instantaneous measurement did. The total measurement is also comparatively more precise than the instantaneous measurement.
3. There is evidence that indicates little change in the ability of the test procedure to differentiate between material changes when total M_R is tested at 41, 50, or 60°F. This is shown in the partial *F*-ratio row of Table 6.
4. There is insufficient evidence that indicates differentiation between material changes at 77°F testing temperature, shown as a low partial *F*-ratio in Table 6.

Recommendations

From the evaluation of these study results, it is recommended that the test conditions of 0.1-sec load duration, 0.33 Hz load frequency, 50 to 75 μstrain, and 60°F be used as the standard procedure to be used with the repeated-load test system and

the M_R reported as a total M_R. These test conditions are critical when a relative comparison of two or more mix types is to be made or when subtle differences of one mix type are to be detected, such as strength sensitivity to gradation, asphalt content, and moisture damage.

REFERENCES

1. R. G. Hicks et al. *Identification and Quantification of the Extent of Asphalt Stripping in Flexible Pavements in Oregon—Phase II*. Report FHWA-OR-85-3. Materials Division, Oregon Department of Transportation, Salem, 1985.
2. E. L. Dukatz, Jr., and R. S. Phillips. The Effect of Air Voids on the Tensile Strength Ratio. *Proc., Association of Asphalt Paving Technologists*, Vol. 56, 1987, pp. 517–537.
3. J. Devore and R. Peck. The Analysis of Variance. In *Statistics—The Exploration and Anslysis of Data*, West Publishing Company, St. Paul, Minn., 1986, pp. 594–600.
4. R. G. Petersen. Completely Randomized Design. In *Design and Analysis of Experiments*, Marcel Dekker, Inc., New York, N.Y., 1985.
5. J. Devore and R. Peck. Inferences Using Two Independent Samples. In *Statistics—The Exploration and Analysis of Data*, West Publishing Company, St. Paul, Minn., 1986, pp. 373–374.
6. R. G. Petersen. Randomized Block Deisgn. In *Design and Analysis of Experiments*, Marcel Dekker, Inc., New York, N.Y., 1985, pp. 34–47.

Introduction to Strategic Highway Research Program–Long-Term Pavement Performance Asphalt Concrete Resilient Modulus Testing Program

WILLIAM O. HADLEY AND JONATHAN L. GROEGER

Research is under way in the Strategic Highway Research Program's Long-Term Pavement Performance (SHRP-LTPP) project to develop and implement a test procedure for resilient modulus testing of asphalt concrete. A comprehensive test procedure has evolved over the past 3 years and is moving toward full-scale production testing in early 1992. Readers with limited exposure with the SHRP-LTPP program are provided with a feel for the test procedure that has been developed and the various activities that have been undertaken in this program to ensure consistent and reliable results.

The overall goal of the Strategic Highway Research Program's Long-Term Pavement Performance Program (SHRP-LTPP) studies is "to increase pavement life by investigation of various designs of pavement structures and rehabilitated pavement structures, using different materials and under different loads, environments, subgrade soil and maintenance practices" (*1*). A major component of the LTPP research effort is the establishment of a national pavement data base (NPDB) containing inventory information and performance histories of pavements with various design features, materials, traffic loads, environmental conditions, and maintenance practices. The primary source of the information stored in the NPDB will be the inventory and monitoring data collected on a large number of pavement test sections on existing or in-service pavements forming the general pavement studies (GPS) portion of LTPP, as well as newly constructed or rehabilitated test sections included in the specific pavement studies portion of LTPP, which allows for more-intensive evaluation of selected factors (*1*).

The LTPP study is being conducted under the central leadership of the SHRP staff with technical assistance provided by Texas Research and Development Foundation under SHRP Contract (P-001). The inventory and field monitoring data are being collected through the efforts and supervision of four regional coordination office contractors in cooperation with the state/province highway agencies. Information obtained through LTPP field material sampling and field testing and laboratory testing contracts includes in situ density and moisture data, visual pavement layer information, and laboratory test data (materials characterization) for each pavement section. This information will be included in the NPDB (*1*).

Texas Research and Development Foundation, 2602 Dellana Lane, Austin, Tex. 78746.

A significant amount of data will be produced from the LTPP studies that can be used by the highway research community. One of the more important outputs from the materials characterization portion of the LTPP study will be resilient modulus (M_R) data from each layer of the pavement test sections. Relationships between this M_R data, other materials properties, and falling weight deflectometer data should be invaluable in evaluating the pavement performance of the LTPP sections.

This paper offers an overview of a specific SHRP-LTPP test procedure involving resilient modulus testing of asphalt concrete (AC) cores. It is intended to provide a discussion of the fundamentals of this test procedure and to identify the expected results to be achieved from the performance of this test.

OVERVIEW: SHRP-LTPP MATERIALS TESTING PROGRAM

The goal of the SHRP-LTPP field sampling and laboratory testing work is to recover, examine, and store pavement material samples obtained from designated pavement test sections and then to perform specified laboratory tests in order to define adequately the pavement layer structure and characterize material properties of the LTPP test sections. Laboratory tests are conducted for asphalt concrete, extracted aggregate from asphalt concrete, asphalt cement, bound base, subbase and subgrade, unbound granular base and subbase, subgrade, and portland cement concrete materials. The laboratory testing program includes a comprehensive testing process designed to produce an independent determination of pavement layering.

For each laboratory test, standard SHRP protocols have been developed for use by the laboratories. The intent of this process is to minimize the variability of material test data attributable to laboratory materials testing and handling techniques by standardizing these techniques as much as possible.

Many of the test procedures included in the SHRP program are based on standard AASHTO or ASTM specifications. However, several procedures, such as AC Core Examination and Thickness, were developed completely because AASHTO and ASTM lacked specifications. Still other protocols involve major modifications of the AASHTO or ASTM standards.

One such protocol, Resilient Modulus of Asphalt Concrete, represents a major modification to the existing ASTM D4123 procedure. The remainder of this paper will focus on this procedure.

AC RESILIENT MODULUS TESTING

Summary of Method

The SHRP protocol for AC resilient modulus testing (SHRP Protocol P07) describes procedures for determining M_R using repeated-load indirect tensile testing techniques. The procedure involves resilient modulus testing for a range of temperatures, loads, rest periods, and axis of loading. This test is completed on field cores obtained from SHRP test sections and is conducted through repetitive applications of compressive loads in a haversine waveform.

Development of Test Method

The development of the SHRP AC M_R test procedure has been under way for some time. An outline and a draft test procedure were originally developed by a group of materials-testing experts under the direction of SHRP (*2*). The first draft of Protocol P07 was essentially based on ASTM D4123-82 (1987) and preliminary findings of the asphalt-aggregate mixture analysis system study. The first production version of P07 was issued in July 1989. Subsequent revisions were instituted by the SHRP technical assistance contractor in November 1989, and the version currently in use for the resilient modulus pilot study was issued in July 1991. Further refinement of the test procedure, based on the results of a pilot study, is expected. This protocol was to be issued in its final form in early 1992. Resilient modulus testing of all LTPP AC specimens should be complete by middle to late 1992.

SHRP PROFICIENCY TESTING

Expert task group recommendations led to a decision in 1988 that a vital element in laboratory quality assurance would be the AASHTO accreditation program (AAP) (*3*). The laboratories under contract to SHRP were required to be accredited by AAP. Since the resilient modulus testing of asphalt is not covered under this program, it was decided that a separate proficiency-testing program would be developed to ensure the quality of the test data being collected (*3*).

Seventeen laboratories are participating in an asphalt concrete resilient modulus testing program that involves two separate test series for the verification of M_R system calibration and proficiency. The first portion involves the verification of the system calibration and proficiency by testing a set of four synthetic reference specimens (i.e., rubber, Teflon, polyurethane, and Lucite) provided by SHRP; the second portion involves establishment of further M_R proficiency on actual asphalt field cores.

In the first series, laboratory-generated M_R results for the synthetic specimens are compared with the anticipated range in M_R results to identify acceptable or unacceptable results. If the measured responses do not fall within the anticipated range, the agencies are advised to inspect their test system for problems with equipment (load cell, transducers, etc.), alignment, or specimen placement. Once system problems are corrected and acceptable M_R values are obtained, the testing agency is released to begin the second series of the proficiency program involving asphalt core proficiency testing. It should be noted that a number of laboratories had considerable difficulty in completing the initial proficiency test series.

The second proficiency test series involves M_R testing of asphalt cores obtained from the Pennsylvania State University test track. The participating laboratories were given two sets of core specimens and were asked to conduct resilient modulus testing using the SHRP Protocol P07 procedures including testing at 41, 77, and 104°F (5, 25, and 40°C). Similarly to the initial series, the M_R values generated by the participating laboratories were compared to a range of expected M_R values developed by SHRP quality-control personnel. If measured responses fall outside this range, the agencies are advised to inspect their load apparatus, transducer placement, and location for needed adjustments and to evaluate specimen marking, location, and placement techniques of laboratory personnel.

The initial round of testing within the synthetic proficiency series produced a range of resilient modulus values from 25 percent to an order of magnitude greater than the accepted values for the reference specimens. This illustrates that this testing program was indeed necessary and vital to the success of the LTPP program. The experience indicates that a less vigorous course of action may have resulted in the collection of unusable data at great cost to the highway community (*3*).

PILOT STUDY TESTING

The SHRP AC M_R pilot study was initiated to provide SHRP with answers to several questions concerning the AC M_R program. The objectives of this study are as follows:

- Provide SHRP laboratories with general resilient modulus testing experience before production testing of the specimens;
- Allow the laboratories a chance to institute and evaluate their inhouse quality-assurance and quality-control program before production testing;
- Encourage uniformity in M_R testing between the three SHRP contract laboratories;
- Determine the extent of construction variability present between ends of a test section;
- Determine areas in which Protocol P07 may be streamlined; and
- Determine if additional asphalt concrete property tests are required on samples undergoing resilient modulus testing.

As part of this pilot study, AC specimens were selected from 40 SHRP test sections representing all four SHRP regions, including 24 states and 4 Canadian provinces (see Figure 1). Approximately 480 specimens will undergo a battery of standard SHRP tests, including

- Core examination and thickness measurements,
- Bulk specific gravity,
- Maximum specific gravity,
- Asphalt content, and
- Resilient modulus.

Through the performance of this study and the analysis of the corresponding data, the objectives mentioned previously will be achieved.

Each SHRP contract laboratory must pass the AC proficiency and calibration testing program before they are cleared to begin pilot study testing. After clearance, each laboratory is given a list of the designated specimens for pilot testing. The order of testing of these samples has been randomized to minimize bias in the test results. The laboratory proceeds by testing each specimen in accordance with a defined process. The data from all of the samples will then be gathered and analyzed by the SHRP technical assistance contractor to achieve the stated objectives. It is anticipated that the results of this pilot study will have a significant chance of altering Protocol P07, since a critical analysis is going to be made of differences in modulus values for different rest periods on the same sample and of the effect of testing two axes of each sample. This pilot study testing program should yield valuable results and insights into the asphalt concrete resilient modulus test procedure.

RESILIENT MODULUS TEST

The repeated-load resilient modulus test of asphalt concrete cores is conducted through repetitive applications of compressive loads in a haversine waveform. The compressive load is applied along a vertical diametral plane of a cylindrical core of asphalt concrete (Figure 2). The resulting horizontal and vertical deformations of the core are measured, and resilient modulus is calculated using the applied load, specimen dimensions, and measured horizontal deformation information. In the current version of the M_R protocol, Poisson's ratios are assumed for the three test temperatures. However, the use of calculated Poisson's ratios developed from measured horizontal and vertical deformations in calculating the resilient modulus will be investigated in the pilot study.

Two separate resilient modulus values are obtained. One, defined as instantaneous resilient modulus, is calculated using

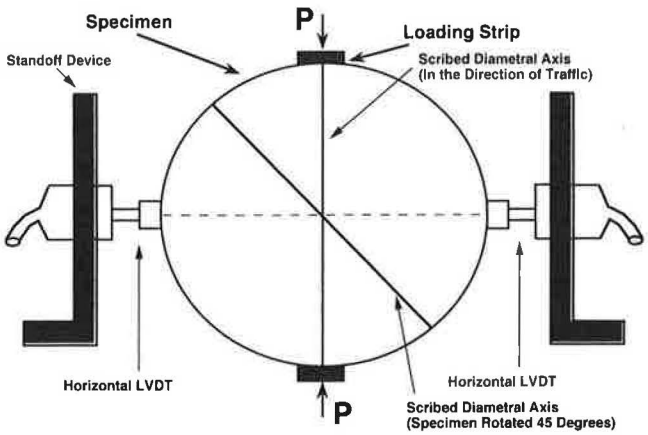

FIGURE 2 Proper loading and placement of horizontal transducers.

MOISTURE / TEMPERATURE / SUBGRADE TYPE / BASE THICKNESS	WET				DRY			
	FREEZE		NO FREEZE		FREEZE		NO FREEZE	
	F	C	F	C	F	C	F	C
LO	242401 (MD) 512004 (VA) 182008 (IN) 196150 (IA)	341638 (NJ) 541640 (WV) 261013 (MI) 271023 (MN)	223056 (LA) 052042 (AR) 412002 (AR)	124108 (FL) 479025 (TN)	382001 (ND) 836454 (MB) 307076 (MT) 901802 (SK)	322027 (NV) 829017 (BC) 201009 (KS) 327000 (NV)	067491 (CA) 404163 (OK) 062053 (CA) 062051 (CA)	321030 (NV) 404165 (OK) 371645 (NC) 068149 (CA)
HI	872811 (ON) 872812 (ON) 182009 (IN)	341033 (NJ) 341034 (NJ)	053071 (AR) 482108 (TX)	134112 (GA) 134113 (GA)	562017 (WY) 469187 (SD) 562020 (WY)	562019 (WY) 567772 (WY) 562037 (WY)	404154 (OK) 062004 (CA) 062647 (CA)	068201 (CA) 041062 (AZ) 041065 (AZ)

FIGURE 1 Pilot study experimental design.

the recoverable horizontal deformation that occurs during the unloading portion of one load-unload cycle. The other, defined as total resilient modulus, is calculated using the total recoverable deformation, which includes both the instantaneous recoverable and the continuing recoverable deformation during the rest period of one cycle.

For each resilient modulus test, the following general procedures are followed:

- The tensile strength is determined for a selected test specimen at 77 ± 2°F using the procedures described in this paper. The value of tensile strength determined by this procedure is then used to estimate the indirect tensile stress and the corresponding compressive load to be repetitively applied to the designated test specimens during the resilient modulus determinations.
- The test specimens are tested along two diametral axes at three rest periods (i.e., 0.9, 1.9, and 2.9 sec) and at testing temperatures of 41, 77, and 104 ± 2°F (5, 25, and 40°C ± 1°C). For each test temperature, repetitive haversine load pulses of 0.1-sec duration are applied to the individual test specimens with rest periods of varying duration between load pulses as described herein. The magnitude of load to be applied is based on a predefined percentage of the indirect tensile strength of a specimen. The general testing sequence includes initial testing at 41°F followed by testing at 77°F and final testing at 104°F.
- After completion of resilient modulus testing at 104°F, the test specimen is returned to 77°F and an indirect tensile strength test is performed in accordance with standard procedures to be outlined later. This test is performed to determine the tensile strength of the specific specimen actually used in resilient modulus testing.

In the pilot study, the resilient modulus test specimens subsequently are subjected to testing for maximum specific gravity and asphalt content using standard SHRP testing procedures.

TEST EQUIPMENT

Testing Machine

The machine used for SHRP resilient modulus testing is a top-loading, closed-loop, electrohydraulic testing machine with a function generator capable of applying a haversine-shaped load pulse over a range of load durations, load levels, and rest periods.

Temperature-Control System

The temperature-control systems are capable of attaining temperature control ranging from 41°F (5°C) to 104°F (40°C) while maintaining the specified temperature within ± 2°F (± 1.1°C). The system includes a temperature-controlled cabinet large enough to hold the load frame, one sample, and the horizontal and vertical deformation transducers. In most of the systems used by the SHRP testing laboratories, carbon dioxide is used to cool the chamber and electric heating elements are used to heat the chamber.

Specimen Holding and Loading Device

In addition to the closed-loop system, a diametral load guide device has been designed for SHRP testing. The loading device is a modified, commercially available (through special order) die set with upper and lower platens constrained to remain parallel during testing. The top platen is counterbalanced to minimize load effects for tests at elevated test temperatures. Attached to this load frame are two horizontal transducer holders positioned to provide a contact point of the transducer at the midheight of the specimen. These transducer holders are adjustable in order to "zero" the transducers before testing. Steel loading strips with a concave surface having a radius of curvature equal to a nominal 4.0-in.-diameter specimen are attached to the load frame to apply uniform loading to the diametral axis of the core. The outer edges of the loading strips have been rounded to remove sharp edges that might cut the core during testing.

This loading system has been designed to ensure that the load is applied evenly to the test specimen with no sample rocking or equipment flexure during testing.

Measuring and Recording System

The measuring and recording system includes sensors for measuring and recording horizontal and vertical deformations. The system is capable of recording horizontal deformations in the range of 0.000005 in. (0.00015 mm) of deformation (see Table 1).

The measuring or recording devices also provide real-time deformation and load information and are capable of monitoring readings on tests conducted to 1 Hz. Computer monitoring systems are used to generate real-time plots for viewing as the test progresses.

TABLE 1 Recommended Response Characteristics for Load Cell and Transducers

	Vertical	Horizontal
Measurement Transducers		
Max. Linear Stroke, mm	± 1.3	± 0.5
Max. Mechanical Travel, mm	4.0	1.5
Minimum Sensitivity, mv/v/mm	280	280
Nonlinearity, %FS	± 0.5	± 0.25
Min. Temperature Range, C	0 - 50	0 - 50
Load Cell		
Minimum Sensitivity, mv/v	2	
Nonlinearity, %FS	0.25	
Hysteresis, %FS	0.25	
Repeatability, %FS	0.10	
Maximum Deflection, mm	0.125	
Maximum Capacity, lb	800	

Horizontal Deformation Measurement

The transducers used to measure horizontal deformations are located at midheight and opposite each other along the specimen's horizontal diameter (Figure 2). Positive contact between the transducer tip and specimen is maintained during the test procedure. This is ensured by the use of spring-loaded transducers and the attachment of a suitable head as a contact point. In addition, the two horizontal transducers are wired so that each transducer can be read independently and the results summed during the test program.

Vertical Deformation Measurement

The two transducers used to measure vertical deformations are located on opposite sides of the upper platen of the load frame (Figure 3). These two transducers are equidistant from the actuator shaft and on a line coincident with the center of the two guideposts of the load frame and the center of the actuator shaft. The sensitivity of these measurement devices has been selected to provide the required level of deformation readout. A positive contact between the vertical transducers and the upper platen of the load frame is maintained during the test procedure. In addition, the two transducers are wired so that each transducer can be read independently and the results averaged during the test program.

Load Measurement

The repetitive loads are measured with an electronic load cell that meets the load requirements necessary for resilient testing (see Table 1).

SAMPLE HANDLING: PREPARATION AND MARKING

Size Requirements

Resilient modulus testing is being conducted on asphalt concrete specimens that are extracted from a single pavement layer and are more than 1.5 in. but less than 3.0 in. thick. The desired thickness for testing is 2.0 in. If the thickness of a particular AC layer scheduled for testing is 1 in. or more greater than the desired testing thickness of 2 in., then the 2-in. specimen to be used for testing is obtained from the middle of the AC layer by sawing the specimen. SHRP test samples that have projections or depressions higher or deeper than 0.1 in. are not tested unless no other suitable cores are available. In addition, specimens with ends that are skewed (either end of the specimen departs from perpendicularity to the axis by more than 0.5 degrees, or ⅛ in. in 12 in.) are not tested. Cores that have smooth, uniform curved surfaces as well as smooth and parallel top and bottom diametral faces are desired.

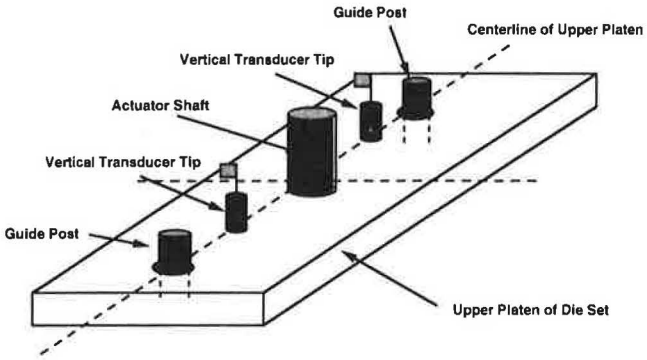

FIGURE 3 Placement of vertical transducers.

Specimens To Be Tested

Eight AC core locations have been designated for the P07 test on every flexible pavement test section in GPS study. If any of the test specimens obtained from the specified core locations are damaged or untestable, other cores that are in the same grouping but that have not been identified for other testing are substituted for M_R testing. Care is taken to ensure that high heat or other adverse conditions during storage do not deform the specimen or otherwise render it unfit for testing.

Preparation of Specimens Before Testing

Two diametral axes are marked on each test specimen to be tested using a suitable marking device (Figure 4). One axis shall be marked parallel to the traffic direction symbol (arrow) or "T" marked during the field coring operations. The other axis is marked at a 45-degree angle from the arrow (or T) placed on the specimen during field-coring operations. Slight adjustments in the marking locations are allowed to prevent the placement of the loading strips directly on exposed large-aggregate particles. The thickness of each specimen is then measured to the nearest 0.01 in. (0.25 mm). This thickness is determined by averaging three measurements taken equally spaced around the test specimen with a single center measurement.

The diameter of each test specimen is determined to the nearest 0.01 in. (0.25 mm) by averaging a minimum of two diametral measurements. The diameter of the axis parallel to the direction of traffic is measured first. Subsequently, the diameter of the axis perpendicular to this axis is measured.

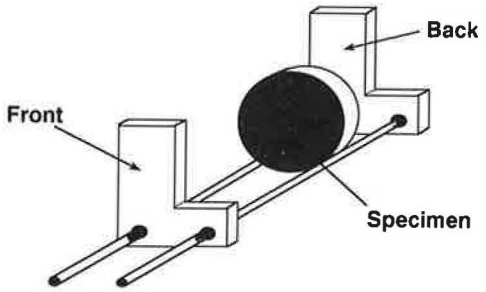

FIGURE 4 Specimen marking device.

These two measurements are averaged to determine the diameter of the test specimen. If the average diameter of the core is less than 3.85 in. or exceeds 4.15 in., the core is not to be tested. In this case, a replacement core is selected for the resilient modulus test.

TEST PROCEDURE

General

The asphalt cores are placed in a controlled temperature cabinet or chamber and brought to the specified test temperatures. Unless the core specimen temperature is monitored in some manner and the actual temperature known, the core samples remain in the cabinet for a minimum of 24 hr before testing.

The tensile strength of the designated test specimens are determined at 77 ± 2°F using the following procedure:

- The test specimen is marked, placed in the loading apparatus and positioned (this is a critical alignment and it is conducted with great care).
- A compressive load is applied at a controlled deformation rate along the axis marked parallel to traffic. A deformation rate of 2 in./min (50.8 mm/min) is used.
- The load is monitored during the entire loading time, or until the load sustained by the specimen begins to decrease. The indirect tensile strength is then calculated using the following equation:

$$S_t = \frac{(1.273 \times P_o)}{t} \times \left[\sin\left(\frac{57.2958}{D}\right) - \frac{1}{2 \times D}\right]$$

or

$$S_t = 0.156 \times P_o/t \text{ for a 4.00-in.-diameter core} \quad (1)$$

where

P_o = maximum load sustained by the specimen (lb),
t = specimen thickness (in.), and
D = specimen diameter (in.).

Alignment and Specimen Seating

At each temperature, the test specimen is placed in the loading apparatus and positioned so that the diametral markings are centered top to bottom within the loading strips on both the front and back face of the specimen along the axis parallel to the direction of traffic (Figure 2). A check is also made to ensure that the midpoint of the specimen in the lengthwise (or thickness) direction is located and coincident with a vertical line of action through the test machine actuator shaft and the shank of the load guide device. The alignment of the front face of the specimen can be checked by ensuring that the diametral marking is centered on the top and bottom loading strips. With the use of a mirror, the back face can be similarly aligned. The first axis to be tested is the axis parallel to the direction of traffic (i.e., the load is being applied along the axis parallel to traffic). The head of the arrow should always be located at the top (12 o'clock) position and the upper surface (i.e., the newer pavement surface facing to the front).

The second axis tested is the axis 45 degrees from the initial axis parallel to the direction of traffic. The core specimen is similarly aligned along this axis before resilient modulus testing. The electronic measuring system is adjusted and balanced as necessary. Before testing and after the horizontal deformation transducers are mounted in the holding device, adjustments are required in the relative position of the transducers in order to match the mechanical "null" position with the electrical null or a near-zero voltage position (a similar null position is required for the transducers used to measure the vertical deformations during testing). When starting from the null position, the "travel" of the transducer shaft should be sufficient to require no further adjustment in the transducer position for the duration of a test.

Preconditioning

Preconditioning and testing are conducted while the specimen is in the temperature-control cabinet. Selection of the applied loads for preconditioning and testing at the three test temperatures is based on the tensile strength at 77°F, determined as specified previously. Tensile stress levels of 30, 15, and 5 percent of the tensile strength, measured at 77°F (25°C), are used in conducting the resilient modulus determinations at the test temperatures of 41, 77, and 104 ± 2°F (5, 25, and 40°C ± 1°C), respectively. Minimum specimen contact loads of 3, 1.5, and 0.5 percent of the 77°F tensile strength value shall be maintained during resilient testing for test temperatures, respectively, of 41, 77, and 104 ± 2°F (5, 25, and 40 ± 1°C).

The sequence of resilient modulus testing consists of initial testing at 41°F, intermediate testing at 77°F, and final testing at 104°F. The test specimens are brought to the specified temperature before each test. The test specimen is preconditioned along the axis by the application of a repeated haversine-shaped load pulse of 0.1-sec duration with a rest period of 0.9 sec, until a minimum of 10 successive horizontal deformation readings agree within 10 percent. The number of load applications to be applied depends on the test temperature. The expected ranges in number of load applications for preconditioning are 50 to 150 for 41 ± 2°F, 50 to 100 for 77 ± 2°F, and 20 to 50 for 104 ± 2°F. The minimum number of load applications for a given situation must be such that the resilient deformations are stable. If adequate horizontal deformations (greater than 0.0001 in.) are not recorded using 5, 15, and 30 percent of the tensile strength measured at 77°F (25°C), then the loads can be increased in increments of 5 (i.e., 10, 15, 20, 25 percent). If load levels different from 5, 15, and 30 percent of the tensile strength measured at 77°F (25°C) are used, they are noted on the data sheet.

Both the horizontal and vertical deformations are monitored during preconditioning of the test specimen. If total cumulative vertical deformations greater than 0.025 in. (0.625 mm) for 41°F or 0.050 in. (1.25 mm) for 77 and 104°F occur, the applied load is reduced to the minimum value possible and still maintain adequate deformations for measurement

purposes. If use of smaller load levels does not yield adequate deformations for measurement purposes, the preconditioning is discontinued and an additional 10 load pulses are generated to use in the resilient modulus determination.

Testing

After preconditioning a specimen at a specific test temperature, the resilient modulus test is conducted as follows:

- A minimum of 30 load pulses (each 0.1-sec load pulse with a rest period of 0.9 sec) are applied and measured deformations are recorded. The application of load pulses continues beyond 30 until the range in deformation values of five successive horizontal deformation values (i.e. from lowest to highest value) is less than 10 percent of the average of the five deformation values. The rest period is then increased to 1.9 sec and a minimum of 30 load repetitions are applied. The rest period is then increased to 2.9 sec and a minimum of 30 load repetitions are applied.
- The recoverable horizontal and vertical deformations over the last five loading cycles are measured and recorded after the repeated resilient deformations have become stable. One loading cycle consists of one load pulse and a subsequent rest period. The vertical deformation measurements are also measured and reported. The resilient modulus will be calculated along each axis for each test period and temperature by averaging the deformations measured for the last five load cycles.
- After testing is completed for the first axis (load applied along the axis parallel to the direction of traffic), the specimen is rotated to the axis 45 degrees from the axis parallel to traffic and the preceding steps are repeated.
- When the specimen has been tested along both axes at a specific test temperature, it is raised to the next high temperature.
- After testing is completed at 104°F, the specimen is brought to a temperature of 77 ± 2°F and an indirect tensile strength test is conducted.

Calculations

The M_R equation used in ASTM D4123 is based to some extent on work by Hadley et al. (*4*) in which the equations for the indirect tensile test developed by Hondros (*5*) were used to develop a direct method of estimating modulus. These equations, however, are based on uniform contact pressure or a "flexible" loading condition. The resilient modulus equation used in SHRP's P07 Protocol was developed by Hadley to account for the use of the "rigid" curved steel applied loading strips used in applying the repeatedly applied load to the specimen (*6*). The P07 equation generally produces M_R values 20 to 25 percent greater than the ASTM equation.
The resilient modulus of elasticity, E, in pounds-force per square inch is calculated as follows:

$$E_{RI} = \frac{P \times D(0.080 + 0.297\nu + 0.0425\nu^2)}{H_I \times t} \quad (2)$$

$$E_{RT} = \frac{P \times D(0.080 + 0.297\nu + 0.0425\nu^2)}{H_T \times t} \quad (3)$$

where

E_{RI} = instantaneous resilient modulus of elasticity (psi),
E_{RT} = total resilient modulus of elasticity (psi),
P = repeated load (lbf) (P = applied load − minimum contact load),
t = thickness of test specimen (in.),
D = diameter of specimen (in.),
H_I = instantaneous recoverable horizontal deformation (in.),
H_T = total recoverable horizontal deformation (in.), and
ν = Poisson's ratio.

If calculated and not assumed, ν is as follows:

$$\nu_{RI} = \frac{0.859 - 0.08R_i}{0.285R_i - 0.040} \quad (4)$$

$$\nu_{RT} = \frac{0.859 - 0.08R_t}{0.285R_t - 0.040} \quad (5)$$

and

$$R_i = V_i/H_i \quad (6)$$

$$R_T = V_T/H_t \quad (7)$$

where V_i is instantaneous recoverable vertical deformation (in inches) and V_T is total recoverable vertical deformation (in inches).

QUALITY ASSURANCE AND QUALITY-CONTROL PROCEDURES

During the course of pilot study and production resilient modulus testing, the SHRP contract laboratories must follow very specific quality-assurance and quality-control (QA/QC) checks. These tests are meant to ensure consistent, repeatable results for the testing program.

Unscheduled Calibration Checks

The laboratories performing this testing have been issued a set of four synthetic reference samples. The moduli of these samples are known, and they are used for in-house quality assurance and quality control. To ensure that the test equipment is properly calibrated, these reference samples must be tested when

- The testing program is initiated;
- Start-up follows a 5-day delay;
- Equipment is replaced or repaired;
- Controller settings are adjusted; and
- Measurement problems are discovered.

Scheduled Calibration Checks

The following scheduled checks must be completed by each SHRP contract laboratory. Transducers must be calibrated

daily to ensure proper deformation measurements. This calibration process can be conducted by the operator or technician performing the modulus testing. The load cell must also be checked weekly by the use of a proving ring. The transducers and load cell shall be sent to the manufacturer for calibration and inspection every 6 months.

Ongoing Operator Quality-Control Checks

During the actual testing of the SHRP samples, the operators must be aware of many simple checks that may be performed to ensure reasonable test results (Figure 5). During testing, the output from the vertical and horizontal transducers should be checked to identify specimen misalignment or rocking. Additionally, the response should be checked to identify "noise" (electrical disturbances in the signal output) in the system. Response curves should be smooth and free of erratic peaks and valleys. If these peaks and valleys are present, it is a sure sign that electrical disturbance is present too. The minimization of this noise is essential in order to record accurate results.

Upon initiation of M_R testing, the deformation values between the two vertical transducers must be checked primarily to identify improper specimen placement within the load guide device. In completing this check the greater vertical deformation reading should not exceed the lesser vertical deformation reading by more than 50 percent (i.e., $Y_G \leq 1.5\ Y_L$). If this limitation is exceeded, the test should be stopped and the contributing problem identified and corrected. Misalignment of the midpoint of the asphalt core thickness (or centroid of specimen) with respect to the system actuator–load guide device line of action is the usual cause of observed differences in vertical deformation readouts from the two transducers.

Deformation values between the two horizontal transducers must be checked to determine if the specimen is rocking. The deformation values should be compared, and the greater output should not exceed the lesser value by more than 50 percent (i.e., $X_G \leq 1.5\ X_L$). If this is not so, the test should be stopped and the problem identified and corrected. The problem is usually indicative of improper alignment of the test specimen (i.e., diametral markings) between the loading strips.

Horizontal transducer output should be checked to make sure that negative values are not obtained. If negative values are obtained, this is a sure sign of specimen misalignment or placement in the diametral load guide device.

Load cell output must be monitored to ensure that a consistent and appropriate load is being applied to the specimen. Nonconsistent load outputs can indicate that the contact load is unstable or that no minimum contact load is being applied.

The operator is the key person involved with resilient modulus QA/QC procedures. It is imperative that the system operators are aware of the warning signs and that action be taken to alleviate any of these problems as they occur.

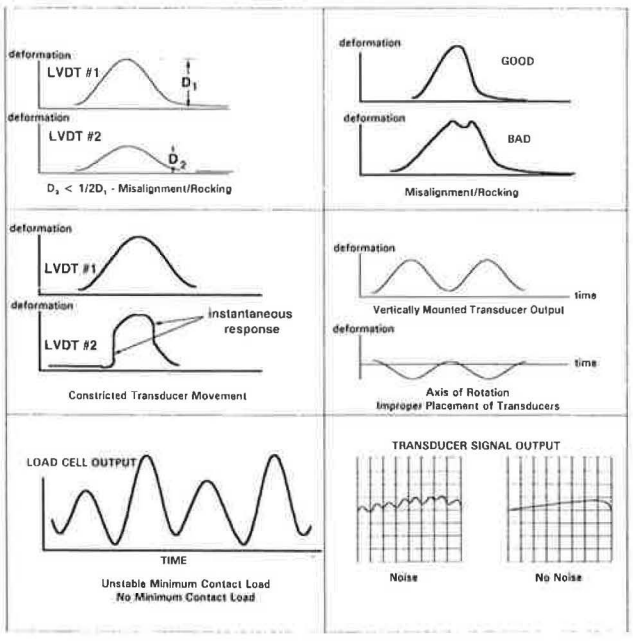

FIGURE 5 Ongoing QA/QC procedures.

CONCLUSION

Significant progress has been achieved in the development of the SHRP-LTPP asphalt concrete resilient modulus testing procedure. However, much must still be learned about actual production testing using this procedure. Testing to date has been accomplished on a limited basis on few samples. This project has the potential to bring the AC resilient modulus test procedures now being used out of the university laboratories and into the mainstream. This will be accomplished only by proceeding with production type testing for a long period of time. During this time, many factors will be evaluated and the procedure may be streamlined or modified to decrease the complexity of the test and its many processes.

Through the resilient modulus of asphalt concrete testing program, it is believed that many things will be learned about pavement performance due to various materials and procedures currently in use. This test has the potential to go a long way in reaching the objectives set for the SHRP-LTPP program in 1987.

ACKNOWLEDGMENTS

The research in this paper was sponsored by SHRP, National Research Council; appreciation is extended to the cooperative efforts of SHRP personnel. The contents reflect the views of the authors, who were responsible for the development of the modulus procedure outlined herein. The publication of this article does not necessarily indicate approval or endorsement by the National Academy of Sciences, by FHWA, or by any state highway or transportation department of the findings, opinions, conclusions or recommendations either inferred or specifically expressed herein.

REFERENCES

1. *SHRP-LTPP Interim Guide for Laboratory Material Handling and Testing*. SHRP-LTPP Operational Guide 004. Strategic Highway Research Program, Washington, D.C., Feb. 1991.

2. *SHRP-LTPP Analysis of Requirements for Field Sampling and Testing and Laboratory Testing Contracts*. Strategic Highway Research Program, Washington, D.C., Jan. 1988.
3. Steele, Garland. *Proficiency Sample Program Interim Report*. Strategic Highway Research Program, Washington, D.C., May 1991.
4. W. O. Hadley, W. R. Hudson, and T. W. Kennedy. *A Method of Estimating Tensile Properties of Materials Tested in Indirect Tension*. Research Report 98-2. Center for Highway Research, University of Texas, Austin, Sept. 1970.
5. G. Hondros. The Evaluation of Poisson's Ratio and the Modulus of Materials of a Low Tensile Resistance by the Brazilian (Indirect Tensile) Test with Particular Reference to Concrete. *Australian Journal of Applied Science*, Vol. 10, No. 3.
6. W. O. Hadley and H. Vahita. A Fundamental Comparison of the Flexural and Indirect Tensile Tests. In *Transporation Research Record 253*, TRB, National Research Council, Washington, D.C., 1983.

Evaluation of a New Indirect Tension Test Apparatus

LOUAY N. MOHAMMAD AND HAROLD R. PAUL

Engineering characterization of Louisiana's asphaltic concrete mixtures using the indirect tensile test has been the focus of a recent comprehensive research program sponsored by the Louisiana Transportation Research Center. Large variations in test results were observed between similar specimens. These variations were attributed to variable aggregate orientation, compaction procedure, and the test device. A new indirect tension test device was fabricated locally and used to reduce the test variability. The repeatability and performance of the new indirect tension device was evaluated. A statistically designed test factorial was used to examine the variation between the existing and the modified test devices. Mechanical tests were conducted for indirect tensile strength, diametral resilient modulus, and indirect tensile creep. The effects of the test devices, deformation measurement system, and operator error on the mechanical properties—as measured from the indirect tensile strength, resilient modulus, and creep modulus—of a specific asphalt concrete mixture are presented. The results of the test program indicated that both test devices provided repeatable results; mechanical properties were not significantly different due to operator error; mechanical properties measured with the modified test device were significantly different than those measured with the existing test device; and the modified test device can capture the temperature effect on the resilient modulus better than the existing test device.

Engineering characterization of Louisiana's asphaltic concrete mixtures using the indirect tensile test has been the focus of recent comprehensive research programs sponsored by the Louisiana Transportation Research Center (LTRC). In these studies, large variations between similar specimens were observed. Generally, this variation was attributed to variable aggregate orientation between the individual specimen and the Marshall compaction procedure.

Baladi, in an attempt to integrate material and structural design methods for asphalt concrete pavements, also found variation that he deemed to be unacceptable (*1–3*). He identified specimen placement in the testing apparatus and rotation of the upper loading strip as the principle causes. To minimize this error, Baladi designed and fabricated a new apparatus (*1–3*).

The objective of this study was to evaluate the cost-effectiveness, performance, and repeatability of the new indirect tension test device developed by Baladi. To assess the performance and repeatability of the Baladi test device, a statistically designed test factorial was used to examine the variation of several test parameters for a specific asphaltic concrete mixture between the Baladi and the LTRC test devices.

The effects of the test devices, deformation measurement system, and operator error on the mechanical properties of a specific asphaltic concrete mixture have been investigated. Mechanical tests conducted were the indirect tensile test, the diametral resilient modulus test, and the indirect tensile creep test.

Louisiana Transportation Research Center, P.O. Box 94245, Baton Rouge, La. 70804.

INDIRECT TENSION TEST DEVICE

Test Devices

LTRC Test Device

The current LTRC test device—essentially, the Schmidt device—is a modified shoe die with upper and lower platens constrained to remain parallel during testing. The vertical deformations of the specimen were measured with two linear variable differential transducers (LVDTs) mounted on opposite corners of the top platens. The horizontal deformations of the specimen were obtained through the use of two LVDTs mounted on an adjustable frame that is rigidly attached to the lower platen. Steel curved loading strips were used in the test device.

Louisiana Modified (LM) Test Device

The Baladi device was fabricated locally in the machine shop of Louisiana State University's civil engineering department. It was built according to the engineering drawings provided by FHWA, except for the extension of the support posts outward by 1.25 in. to provide easier access to the specimen and to allow for the placement of an extensometer (Figure 1). Fabricating the new device cost $2,200. During the initial testing program, inconsistencies in the resilient moduli and Poisson's ratio were discovered. The swivel base was causing the specimen to rock, thus distorting the horizontal deformation measurement. As a result, after consultation with FHWA, the Baladi device was further modified. The top loading strip was fixed instead of mounted on the swivel base that was provided in the initial drawing. Also, the vertical deformation was monitored using two LVDTs mounted 180 degrees apart on the top of the piston guided plate to ensure that the specimen was not rocking.

Measurement System

Displacement measurement of the specimen due to dynamic loading is a critical factor in determining resilient modulus. A typical range of the deformation along the horizontal di-

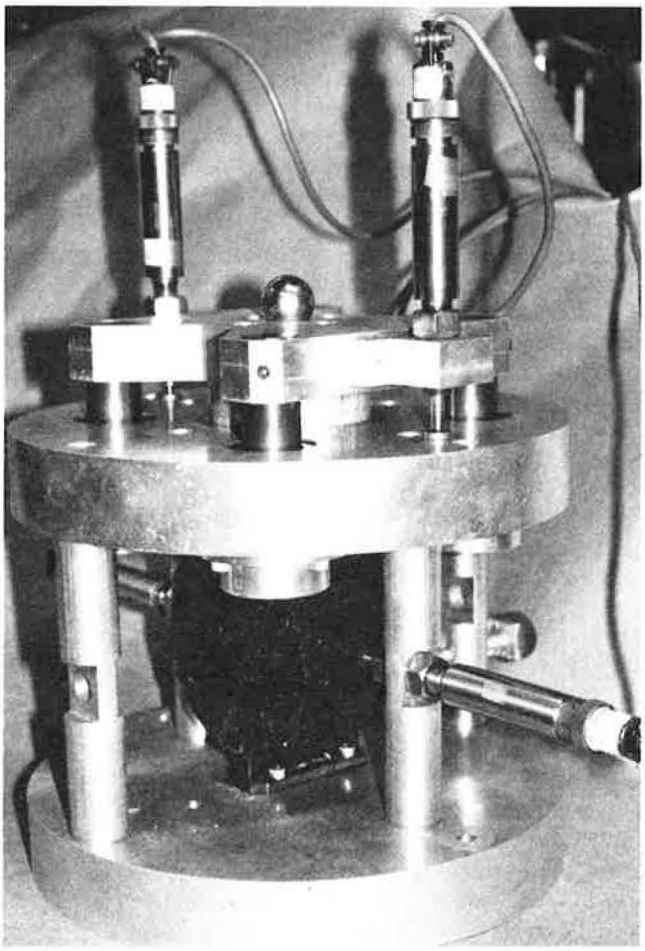

FIGURE 1 LM test device.

ameter is 40 to 100 μin. Thus, the measurement device must have this sensitivity range to respond to dynamic change of sample deformation.

Horizontal Deformation Measurement

Two LVDTs were used to measure the horizontal deformation, and the outputs from each LVDT were monitored independently and summed for analysis. This was accomplished through software developed for acquisition and control of the MTS test system in the concurrent parametric research study.

Two types of LVDT were used for each test device. The first type was an existing set manufactured by TransTek (Model 351-000), hereafter called old LVDT (LVDT-O). The second set of LVDTs was made by Schaevitz (Model GCD-121-050), hereafter called new LVDT (LVDT-N). The maximum strokes for LVDT-O and LVDT-N were ±0.31 in. (±7.9 mm) and ±0.05 in. (±1.3 mm) full scale, respectively. The LVDT-N was selected because of the higher resolution needed to capture the small amount of horizontal deformation during dynamic loadings.

In addition, a modified strain gauge clip-on extensometer system developed by MTS Systems Corp. was used with the LM device. The extensometers have a special bracket that attached to the specimen and provided positive spring loading.

The lateral constraint of the horizontal deformation of the specimen due to the tension in the springs used to hold the extensometer assembly in place was investigated. During the initial system calibration, the diametral resilient modulus test at 40°F (5°C) was used to test the possibility of lateral constraint in the same sample at 40°F. Both the spring assembly and adapter brackets glued to the specimen were examined. Because the results appear to be similar, the spring assembly was used for the test factorial.

Vertical Deformation Measurement

The vertical deformation was measured with two LVDTs mounted 180 degrees apart on the piston-guided plate. The output from each LVDT was monitored independently and simultaneously compared with the output of the other LVDT. If the difference between the peak value was not within 10 percent, the seating of the loading device was adjusted. The LVDTs used for both test devices were manufactured by Schaevitz (Model GCD-121-050).

EXPERIMENTAL DESIGN

A statistically designed laboratory experiment was used to examine the influences of the test device, measurement system, and operator error on the mechanical properties of a specific asphalt concrete mixture. Previous work on more than 550 samples of different mix types and materials had a standard deviation of 23 psi in the indirect tensile test. The mean range for any triplicate set of specimen was 12.9 psi. Assuming that the standard deviation of 23 psi of this sample was a fair estimate of the population standard deviation, the number of samples for each cell in the test factorial was determined to be 12 with 95 percent confidence. This cell size was further subdivided to six specimens to investigate operator error.

The results from the LTRC and the LM test devices were statistically analyzed using the analysis of variance procedure provided in the Statistical Analysis System (SAS) program from SAS Institute, Inc. A multiple comparison procedure with a risk level of 5 percent was performed on the means. A REGWF test was selected to control the experimentwise error. The REGWF test was selected because it can detect significant differences in the mean that might not be detected with other multiple comparison procedures. The independent variables (i.e., test device, measurement system, and operator error) had populations with normal distributions. In addition, the repeatability of the test results have been examined using the single-operator, one-sigma limit as described in ASTM C670.

EXPERIMENTAL SETUP

Loading System and Data Acquisition

The loading system was a 22,000-lb MTS Model 810 servo-hydraulic test system equipped with an environmental chamber. Specimens were thermally conditioned before being tested. A thermostatically controlled probe was inserted in a drilled hole in a dummy specimen of the same size and shape as the

test specimen to ensure an equilibrium test temperature for the samples tested. Fully automated test software for equipment control and data acquisition was developed to perform tests, acquire and analyze data, and calculate and print out the test results.

Specimen Preparation

A total of 168 specimens were fabricated and tested using the LTRC and the LM test devices. Each specimen was 4 in. in diameter and about 2.5 in. high. A typical Louisiana Type 1 mixture was used with 65 percent by weight crushed gravel, 25 percent coarse sand, and 10 percent fine sand. Southland AC-30 asphalt cement was used. Specimens were prepared using 75 blows per face of the Marshall hammer. Each cell in the test factorial of Figure 2 was statistically grouped. The average air void content was 4.3 percent, with a standard deviation of 0.22. The optimum binder content was determined from preliminary standard Marshall mix design. Each sextuplicate specimen was tested under the same conditions (temperature and load) for indirect tensile strength, diametral resilient modulus, and indirect tensile creep for each of the LTRC and the LM test devices.

TESTING PROCEDURE

Indirect Tensile Test

This test was conducted at 40 and 77°F (5 and 25°C) according to AASHTO T245-82. Test specimens were loaded to failure at a deformation rate of 2 in./min. The load to failure was then recorded.

Diametral Resilient Modulus Test

The tests were conducted at 40, 77, and 104°F (5, 25, and 40°C) according to ASTM D4123, with the following modifications:

1. Test samples were seated with a sustained load of 50 lb, and then a cyclic haversine load of 10 percent of the indirect tensile strength was applied. The two vertical deformations were monitored independently. If the two measurements were not within 10 percent, then further adjustment to the loading device was made in order to not exceed this tolerance. The average of the two measurements was used in the data analyses.
2. With the sustained load applied to the sample, the specimen was conditioned by monitoring the deformation continuously until the deformation rate of the specimen was essentially constant. The transducers were then rezeroed.
3. A repetitive haversine waveform load with a peak value equal to 10 percent of the indirect tensile strength was applied to the specimen. The load frequency was 2 Hz with a 0.1-sec loading time and a 0.4-sec relaxation period. All materials response parameters were measured with the data acquisition system at a rate of 500 Hz.
4. The response curves (load, vertical deformation, and horizontal deformation) over the 2 cycles were digitized. The data from these curves were then scanned to determine the instantaneous and total recoverable horizontal and vertical deformation. Data associated with the beginning of the relaxation period were used to compute instantaneous properties; values associated with the end of the relaxation period were used to compute total properties.

Each specimen was tested at each of the three temperatures starting with the lowest temperature to minimize permanent damage to the sample. At each temperature, the sample was tested twice; after the first test, the sample was rotated approximately 90 degrees and the test was repeated (Steps 1 through 4).

Indirect Tensile Creep Test

Creep tests were conducted at 77°F (25°C) using a ramp load of 250 lb (1112 N) applied as quickly as possible using the stress-controlled mode of the MTS servohydraulic system. The load and vertical and horizontal deformations were monitored continuously with the data acquisition system. The test was terminated either after 60 min of load duration or at failure. The mean horizontal deformations and mean vertical deformations were computed by summing the deformation at a particular time for each cell of the test factorial described in Figure 2 and dividing the sum by the number of specimen. The creep modulus, $S(t)$, is computed from the measured deformations as follows:

$$S(t) = \frac{P_o(\mu + 0.27)}{t\delta H(t)}$$

where

$S(t)$ = creep modulus at time t,
P_o = applied vertical load,
μ = Poisson's ratio,
t = sample thickness, and
$\delta H(t)$ = horizontal deformation at time t.

The mean creep modulus was computed similar to the mean creep deformations. Mean values of vertical deformation,

Test Device	LTRC		LM		
Deformation Measurement System	LVDT – O	LVDT – N	LVDT – O	LVDT – N	Extensometer
Operator 1	6	6	6	6	6
Operator 2	6	6	6	6	6

FIGURE 2 Test factorial.

horizontal deformation, and creep modulus were used in the statistical analyses.

DISCUSSION OF RESULTS

Indirect Tensile Strength Test

Table 1 presents a comparison of the test results for the indirect tensile strength test at 40°F (5°C) and 77°F (25°C) along with their means, standard deviations, coefficients of variation, and test repeatability. For any sextuplicate, the variation in the test results was between 2 and 9 percent. At low temperature, with increased stiffness, test results measured with the LTRC device have more variation that those tested with the LM device. The indirect tensile strength test was highly repeatable for a single operator. In the tables, columns having the same letter indicate there is no significant difference in the mean. Table 2 indicates that there is no significant difference in the mean indirect tensile strength due to operator error. Table 3 shows that the mean indirect tensile strength measured with the LTRC device at 40°F was significantly higher than the mean measured with the LM device; the means at 77°F were not significantly different between the two devices. Similar findings were obtain when test results were analyzed for each operator (Table 4).

Diametral Resilient Modulus Test

Tables 5, 6, and 7 present the results of the effects of operator error, test devices, and measurement system, respectively, on resilient modulus and Poisson's ratio. Table 5 indicates no significant difference in the means due to operator error except for the instantaneous moduli measured with the LTRC and LVDT-O, so the data from the two operators were combined for further analyses. Table 6 indicates that the mean of the mean instantaneous and total resilient moduli and instantaneous and total Poisson's ratios were significantly different between the two test devices. The diametral test results were repeatable for a single operator at the three temperature levels.

Table 7 indicates that the instantaneous and total moduli were not significantly different using the various measuring devices. This is because the resilient modulus is a function of the vertical deformation only when computed using a calculated Poisson's ratio. Both devices used the same vertical deformation system, that is, LVDT-N. In order to investigate the effect of the measurement devices on the mechanical properties, one needs to look at Poisson's ratio, which is function of the vertical and the horizontal deformations. Instantaneous and total Poisson's ratios were significantly different between the LVDT-O and the LVDT-N except for the total Poisson's ratio of samples tested with the LTRC device. The extensometer assembly was tested with the LM device only because the LTRC device did not have the requisite space. Instantaneous Poisson's ratio calculated with the extensometer was significantly different than the one computed using the LVDT-O; the total Poisson's ratio is significantly different computed from the LVDT-N and the extensometer.

The temperature influence on the mechanical properties of specimen tested with the LTRC and LM devices is shown in Table 8. Generally, the LM device–LVDT-N and the LM device–extensometer combinations seem to capture the temperature effect on the resilient modulus and Poisson's ratio better than the LM device–LVDT-O and LTRC device–LVDT-O combinations. The results of Tables 7 and 8 demonstrate that the LTRC–LVDT-O combination is not as sen-

TABLE 1 Indirect Tensile Strength, Present Serviceability Index

Test Device	LM		LTRC	
Temperature (°F)	40	77	40	77
Operator 1	265	78	328	77
	260	75	318	68
	276	77	311	76
	268	79	307	83
	260	78	314	74
	275	76	310	77
Mean	267	77	315	76
STD	6	1	7	4
(%) CV	2	2	2	6
Repeatability	Y	Y	Y	Y
Operator 2	291	72	374	57
	278	74	347	72
	249	75	321	72
	267	68	363	74
	271	76	313	77
	262	80	295	70
Mean	270	74	336	70
STD	13	4	28	6
(%)CV	5	5	8	9
Repeatability	Y	Y	Y	Y

STD : Standard Deviation

CV : Coefficient of Variation

Y : Indicates Test is Repeatable as per ASTM C670.

TABLE 2 Effect of Operator Error on Mean Indirect Tensile Strength

Test Device	LM		LTRC	
Temperature (°F)	40	77	40	77
Operator 1	A	A	A	A
Operator 2	A	A	A	A

TABLE 3 Effect of Test Device on Mean Indirect Tensile Strength by Temperature

Mechanical Property	Test Device	Temperature (°F) 40	77
Indirect Tensile Strength	LTRC	A	A
	LM	B	A

TABLE 4 Effect of Loading Device on Mean Indirect Tensile Strength

Operator	1		2	
Temperature (°F)	40	77	40	77
LM Device	A	A	A	A
LTRC Device	B	A	B	A

TABLE 5 Effect of Operator Error on Mean Diametral Resilient Modules Test Results

DEVICE	LM												LTRC							
Measurement Device	Extensometer				LVDT–N				LVDT–O				LVDT–N				LVDT–O			
Mechanical Properties	MRI	MRT	MUI	MUT	MRI	MRT	MUI	MUT	MRI	MRT	MUI	MUT	MRI	MRT	MUI	MUT	MRI	MRT	MUI	MUT
Operator 1	A	A	A	A	A	A	A	A	A	A	A	A	A	A	A	A	A	A	A	A
Operator 2	A	A	A	A	A	A	A	A	A	A	A	A	A	A	A	A	B	A	A	A

MRI = Instantaneous Resilient Modulus
MRT = Total Resilient Modulus
MUI = Instantaneous Poisson's Ratio
MUT = Total Poisson's Ratio

TABLE 6 Effect of Test Device on Mean Diametral Resilient Modulus Test Results

Measurement System	LVDT – N				LVDT – O			
Mechanical Properties	MRI	MRT	MUI	MUT	MRI	MRT	MUI	MUT
LM	A	A	A	A	A	A	A	A
LTRC	B	B	B	B	B	B	B	B

MRI = Instantaneous Resilient Modulus
MRT = Total Resilient Modulus
MUI = Instantaneous Poisson's Ratio
MUT = Total Poisson's Ratio

TABLE 7 Influence of Measurement System on Diametral Resilient Modulus Test Results

Test Device	LM				LTRC			
Mechanical Properties	MRI	MRT	MUI	MUT	MRI	MRT	MUI	MUT
LVDT – O	A	A	B	B	A	A	B	A
LVDT – N	A	A	A	A	A	A	A	A
Extensometer	A	A	A	B	N/A	N/A	N/A	N/A

MRI = Instantaneous Resilient Modulus
MRT = Total Resilient Modulus
MUI = Instantaneous Poisson's Ratio
MUT = Total Poisson's Ratio

sitive as the LM–LVDT-N or extensometer combination especially in the dynamic, instantaneous mode, thus not differentiating between properties at different temperatures.

A typical relationship of the effect of temperature on the resilient moduli between the LTRC and LM test devices for each operator is presented in Figure 3. Generally, a distinct cluster of lines is exhibited between the LTRC and LM device for each operator. However, the LM device seems to capture the temperature effect on the moduli better than the LTRC

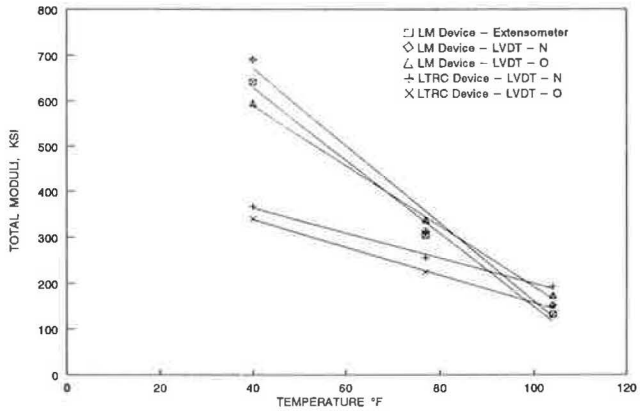

FIGURE 3 Total resilient modulus, temperature dependency (Operator 2).

device. This could be because of friction in the guiding post, weight of the loading mechanism, and the sensitivity of the measurement system.

Table 9 shows that there was no significant difference in the resilient moduli between samples tested at the 0-degree and 90-degree positions.

A typical variation of Poisson's ratio due to temperature, calculated from measured horizontal and vertical deformations during resilient modulus testing, is presented in Figure 4. Clusters similar to the resilient modulus are found with respect to the two test devices. The variation ranges from −0.2 to 0.93 depending on the combination of the loading device and measurement system used. Poisson's ratio should increase as testing temperature increases. Theoretically, Poisson's ratio ranges from 0 to 0.50. This increase was more

TABLE 8 Effect of Temperature on Diametral Resilient Modulus Test Results

Mechanical Properties	MRI			MRT			MUI			MUT		
Measurement System	LVDT – N	LVDT – O	EXTE	LVDT – N	LVDT – O	EXTE	LVDT – N	LVDT – O	EXTE	LVDT – N	LVDT – O	EXTE
LM	Y	Y	Y	Y	Y	Y	40 77 104	N	Y	Y	40 77 104	Y
LTRC	40 77 104	40 77 104	N/A	Y	Y	N/A	Y	Y	N/A	Y	Y	N/A

Y – Indicates Significant Difference in the Mean Between the 40, 77, and 104 °F Tests
N – Indicates No Significant Difference in the Mean Between the 40, 77, and 104 °F Tests
40 – Indicates Significant Difference in the Mean Between the 40 °F Test and the 77 and 104 °F Tests
40 –
77 – Indicates No Significant Difference in the Mean Between the 40 and 77 °F Tests
77
104 – Indicates No Significant Difference in the Mean Between the 77 and 104 °F Tests

TABLE 9 Effect of Sample Rotation on Diametral Resilient Modulus Test Results

DEVICE	LM												LTRC							
Measurement Devices	Extensometer				LVDT–N				LVDT–O				LVDT–N				LVDT–O			
Mechanical Properties	MRI	MRT	MUI	MUT	MRI	MRT	MUI	MUT	MRI	MRT	MUI	MUT	MRI	MRT	MUI	MUT	MRI	MRT	MUI	MUT
0° Position	A	A	A	A	A	A	A	A	A	A	A	A	A	A	A	A	A	A	A	A
90° Position	A	A	A	A	A	A	A	A	A	A	A	A	A	A	A	A	A	A	A	A

Note: Columns with similar letters indicate no significant difference in the mean.
MRI = Instantaneous Resilient Modulus; MRT = Total Resilient Modulus
MUI = Instantaneous Poisson's Ratio'; MUT = Total Poisson's Ratio

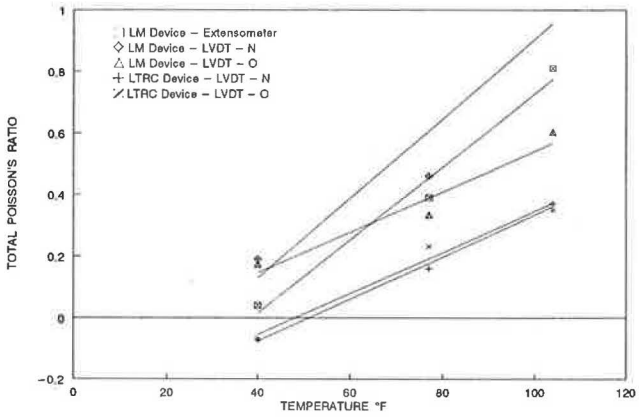

FIGURE 4 Total Poisson's ratio, temperature dependency (Operator 2).

TABLE 11 Effect of Test Device on Mean Creep Modulus By Time

Mechanical Properties	Test Device	Time (seconds)			
		5	10	100	500
Calculated Creep Modulus	LTRC	A	A	A	A
	LM	A	A	A	B
Creep Modulus with Assumed MU = 0.35	LTRC	A	A	A	A
	LM	B	B	B	B

TABLE 12 Overall Effect of Measurement System on Mean Creep Modulus

Creep Modulus	Calculated	Assumed MU = 0.35
LVDT – N	A	A
LVDT – O	A / B	B
Extensometer	B	A

pronounced with the LM device than the LTRC device. At high temperature the applied load was too high, which produces the higher-than-theoretical value of Poisson's ratio. This indicates that Poisson's ratio at high temperature should be calculated using deformations from a lower load magnitude than the load at 77°F (25°C).

Indirect Tension Creep Test

The creep modulus was calculated using either a computed Poisson's ratio from the measured horizontal and vertical deformations or an assumed Poisson's ratio of 0.35. The indirect tension creep modulus was statistically analyzed at time intervals of 5, 10, 100, and 500 sec. The test results were repeatable at those time intervals.

The influence of the operator error on the mean creep modulus is presented in Table 10. It indicates that operator error was not significant for creep modulus based on either a computed or an assumed Poisson's ratio at the different time intervals.

The effect of the test device on the mean creep modulus is presented in Table 11. The creep modulus with an assumed Poisson's ratio was significantly different between the two devices, whereas the modulus with a calculated Poisson's ratio was not significantly different except at 500 sec. The creep modulus with an assumed Poisson's ratio depended on the horizontal deformation of the sample where three types of horizontal measuring systems were used: LVDT-O, LVDT-N, and extensometer. The moduli based on computed Poisson's ratio depended on the vertical deformation only where the same LVDT-N was used in both devices. Therefore, for static loading it is anticipated that both test devices will render similar results when using a calculated Poisson's ratio.

The influence of the measurement system on the mean creep modulus is presented in Table 12. The overall effect of the measurement system indicated that there was a significant difference in mean creep modulus between LVDT-N and extensometer for a calculated Poisson's ratio, whereas no significant difference was apparent between LVDT-N and extensometer when using an assumed Poisson's ratio. Because the horizontal deformation influences the moduli when an assumed Poisson's ratio is used, these results indicate similar accuracy in measuring horizontal deformations between the LVDT-N and the extensometer assembly.

CONCLUSIONS

The effects of the test device, deformation measurement system, and operator error on the mechanical properties of a specific asphaltic concrete mixture have been investigated.

TABLE 10 Effect of Operator Error on Mean Creep Modulus By Time

Creep Modulus	Calculated Poisson's Ratio				Assumed Poisson's Ratio, MU = 0.35			
Time (secs)	5	10	100	500	5	10	100	500
Operator 1	A	A	A	A	A	A	A	A
Operator 2	A	A	A	A	A	A	A	A

Mechanical tests conducted were the indirect tensile, diametral resilient modulus, and indirect tensile creep tests. Generally, the LM test device provided less variation in test results than the LTRC test device. Specific conclusions can be drawn from analysis of the data as follows:

1. The use of two LVDTs to measure the vertical deformations has considerably reduced variation in the test results of dynamic mode due to rocking of the sample.
2. Mechanical properties (indirect tensile strength, resilient modulus, and creep modulus) were not significantly different due to operator error.
3. Mechanical properties measured with the LM device are significantly different than those measured with the LTRC device except for indirect tensile strength at 77°F.
4. The LM device captures the temperature effect on resilient moduli better than the LTRC device.
5. Resilient moduli for specimen tested in the LM device and calculated from deformations measured with extensometer did not significantly differ from those measured with the LVDT-N.

ACKNOWLEDGMENTS

The authors are grateful to FHWA and the Louisiana Department of Transportation and Development for their support and sponsorship of this research. The authors express their appreciation to Roland Doucet for the statistical analysis and to LTRC's lab technicians for their efforts in specimen preparation.

REFERENCES

1. G. Y. Baladi. *Integrated Material and Structural Design Method for Flexible Pavements, Volume I—Technical Report.* Report FHWA-RD-88-109. FHWA, U.S. Department of Transportation, Feb. 1988.
2. G. Y. Baladi. *Integrated Material and Structural Design Method for Flexible Pavements, Volume II—Appendices.* Report FHWA-RD-88-110. FHWA, U.S. Department of Transportation, Feb. 1988.
3. G. Y. Baladi. *Integrated Material and Structural Design Method for Flexible Pavements, Volume III—Laboratory Design Guide.* Report FHWA-RD-88-118. FHWA, U.S. Department of Transportation, Feb. 1988.

Abridgment

Influence of Construction-Induced Cracks on Asphalt Concrete Resistance to Moisture Damage

EL HUSSEIN H. MOHAMED, A. O. ABD EL HALIM, AND GERHARD J. KENNEPOHL

Present stripping mechanisms fail to specify the source of water necessary for stripping to start and progress with time. Finding the water source and route to the pavement interior is of great significance to efforts seeking a preventive measure against stripping. Investigation of the influence of contruction-induced cracks, referred to as checking, on pavement resistance to stripping is reported. A new field-compaction technique was used to produce a crack-free asphalt concrete surface that offered a much higher resistance to stripping than conventionally compacted surfaces. Cores recovered from field-compacted pavements were used throughout the investigation. The results of the experimental investigation indicated that compaction technique has a significant influence on the mix resistance to stripping. Vacuum saturation, used as part of the moisture-conditioning procedure, has in the past obscured the influence of construction-induced cracks on stripping susceptibility.

Virtually all investigators agree that stripping is caused by water displacing the asphalt from the aggregate surface (*1*,*2*). However, the existing stripping mechanisms cannot explain how water manages to reach locations close to the aggregate-asphalt interface. Air voids have been suggested as the cause of water penetration, circulation, and accumulation inside the asphalt concrete layer. As a result, many agencies, such as the Ministry of Transportation of Ontario (MTO), specified air void percentage as low as 2 percent. In Ontario, water still finds its way inside the pavement despite low air void percentage (*1*).

Surface cracks that exist at an early stage in the pavement life—that is, during and after construction—can constitute a path for surface water to penetrate the asphalt concrete layer where any of the suggested stripping mechanisms may start functioning. In the presence of such cracks, surface water is the source of water supply necessary for stripping to start and continue during the life of the pavement. Halim used a new analytical approach to prove that construction cracks are associated with the present compaction equipment (*3*). Laboratory investigations using models of the conventional and a new compactor, called the asphalt multi-integrated roller (AMIR), proved the outcome of the theoretical approach. The new compactor has a flat geometry coupled with a rubber mat at the interface of the asphalt surface and roller (*4*). The surface produced by the new compactor is crack-free as observed during the construction of field trials.

The concern of this study is to examine the role these cracks created by compaction play in the phenomenon of asphalt stripping. In the past when field tests were carried out to evaluate the effect of construction on a given problem related to pavements, the finished asphalt pavement always had the same cracking characteristic. Therefore, the influence of these cracks was common across most of the investigated projects and, as a result, masked the actual influence of such cracks. The presence of cracks also resulted in poor correlation between test results of laboratory-prepared samples and cores recovered from the field since such cracks were not always present in laboratory-prepared samples.

EXPERIMENTAL INVESTIGATION

The experimental program was designed and carried out to verify the hypothesized influence of construction-induced cracks on stripping. A field-compacted section was prepared on the campus of the National Research Council (NRC) of Canada in Ottawa. The conventional and the AMIR prototype rollers were used to compact a standard MTO HL-4 asphalt concrete mixture. Cores 3.7 in. in diameter were recovered from each section for laboratory conditioning and testing. No laboratory-prepared samples were used in this investigation to avoid the limitations imposed on compacted mixes by laboratory compaction procedures that influence their performance.

Simple Soaking

This type of conditioning included vacuum saturation of cores using 14 in. of mercury. Cores were then left in the water bath for 2 days at a specified temperature. The −20°F group was conditioned by storing in an environmental chamber in which the temperature remained controlled at −20°F. The

H. M. El Hussein, Institute for Research in Construction, National Research Council, Ottawa, Ontario, Canada K1A 0R6. A. O. Abd El Halim, Civil Engineering Department, Carleton University, Ottawa, Ontario, Canada K1S 5B6. G. J. Kennepohl, Pavement and Roadway Office, Research and Development Branch, Ontario Ministry of Transportation, 1201 Wilson Avenue, Downsview, Ontario, Canada M3M 1J8.

cores were wrapped in a plastic sheet immediately after vacuum saturation and before storage in the temperature-controlled chamber. Following the 2-day conditioning period, all cores were soaked in a water bath at room temperature (75°F) for 2 hr and then tested for indirect tensile strength. A loading rate of 2 in./min was used throughout the investigation.

Soaking After Sealing

Other groups from the steel roller– and AMIR-compacted sections were treated differently so that the effect of surface cracks by sealing the sides and bottom of the cores before soaking could be studied. No vacuum pressure was used. Water can enter the core only through the surface. Cores were left in the water bath for 7 days. Three water bath temperatures were investigated (35, 65, and 110°F). A higher temperature was not possible because it would cause the plastic sealing to melt. A temperature below freezing was also not possible because the water would freeze before saturation water penetrates the core. Cores were removed from the temperature-conditioning water bath to a water bath at room temperature for 2 hr before loading.

Test Results and Analysis

Simple Soaking

Test results of cores soaked in water for 2 days are presented in Table 1. Figure 1 shows the relationship between soaking temperature and indirect tensile strength for both compaction techniques. The average indirect tensile strength of AMIR compacted cores increased from 101 to 113 psi after exposure to −20°F. The strength of AMIR compacted cores soaked at 110°F decreased by 17 percent. Similarly, the strength of the 140°F group decreased by 23 percent.

From Figure 1, the soaking temperature–strength curve shows relatively no change in the strength of steel roller–compacted cores after their exposure to temperatures ranging from −20 to 65°F. Above 75°F, the relationship indicated a sharp decrease in strength caused by stripping observed at the failure surfaces of tested cores. The strength drop was 41.8 percent due to 140°F exposure and 19.7 percent due to 110°F exposure. AMIR-compacted cores offered higher resistance to stripping than conventionally compacted cores after being exposed to warm-water soaking above 75°F. Construction cracks must have allowed warm water to circulate, thereby reducing the resistance of steel-compacted cores to stripping damage.

Soaking After Sealing

This experiment was designed to confirm that construction cracks provide a path for surface water to penetrate the pavement freely. In the previous experiment, when vacuum saturation was used the amount of water entering cores was relatively the same for both compaction methods. The sides of cores are not coated and, therefore, during vacuum saturation a large amount of water penetrated through the sides

TABLE 1 Indirect Tensile Strength Results (Simple Soaking)

Conditioning Temperature (°F)	Type of Compaction	Bulk Specific Gravity	Permeable Voids %	Indirect Tensile Strength (psi)	Average Strength (psi)
-20	VSR/PR*	2.380	3-4	92	93
		2.401	2-3	85	
		2.414	2-3	104	
	AMIR	2.460	1-2	114	112
		2.366	3-4	96	
		2.421	2-3	127	
35	VSR/PR*	2.383	4-5	84	93
		2.399	4-5	101	
	AMIR	2.434	3-4	95	101
		2.450	2-3	109	
		2.366	4-5	100	
65	VSR/PR*	2.418	2-3	95	92
		2.381	3-4	89	
	AMIR	2.463	1-0	104	94
		2.413	1-2	96	
		2.377	3-4	82	
110	VSR/PR*	2.394	3-4	84	75
		2.395	2-3	66	
	AMIR	2.435	1-2	88	83
		2.438	1-2	70	
		2.376	3-4	82	
140	VSR/PR*	2.383	4-5	37	54
		2.412	2-3	71	
	AMIR	2.456	1-2	89	77
		2.358	-	-	
		2.429	2-3	66	
NA	Control Group – Tested Dry				
	VSR/PR*	2.389	4-5	85	93
		2.395	2-3	101	
	AMIR	2.351	4-5	102	101
		2.399	3-4	96	
		2.450	1-2	104	

* Vibratory Steel Roller and Pneumatic Roller

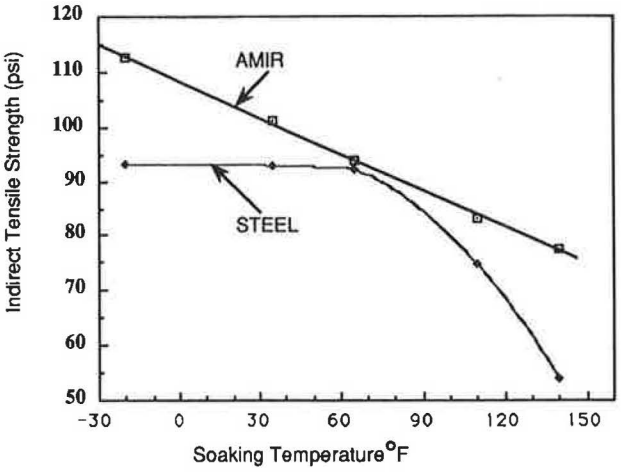

FIGURE 1 Relationship between soaking temperature and indirect tensile strength.

without regard to the surface condition. Measurements made immediately after removal of the plastic sheets and before loading the cores indicated that the AMIR-compacted core allowed 0.9 percent of its weight in water to enter the cores; the steel roller–compacted core allowed 1.3 percent to enter the cores. Test results are shown in Table 2. Figure 2 shows

TABLE 2 Indirect Tensile Strength Results (Soaking After Sealing)

Conditioning Temperature (°F)	Type of Compaction	Bulk Specific Gravity	%Water After Soaking	Indirect Tensile Strength (psi)	Average Strength (psi)
110	VSR/PR*	2.404	-	-	86
		2.380	1.3	86	
		2.378	1.4	86	
	AMIR	2.443	0.8	112	113
		2.439	0.9	120	
		2.436	1.0	107	
65	VSR/PR*	2.382	-	124	117
		2.364	-	108	
		2.410	-	120	
	AMIR	2.447	-	102	121
		2.438	-	129	
		2.436	-	134	
35	VSR/PR*	2.406	-	141	120
		2.383	-	120	
		2.371	-	100	
	AMIR	2.449	-	126	131
		2.436	-	141	
		2.432	-	126	
	Control Group – Tested Dry				
	VSR/PR*	2.406	-	121	120
		2.383	-	120	
	AMIR	2.460	-	128	122
		2.422	-	116	

- *data unavailable* *Vibratory Steel Roller and Pneumatic Roller

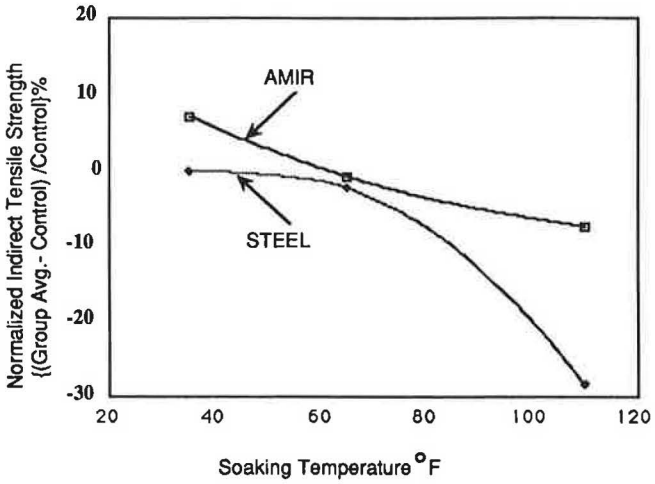

FIGURE 2 Relationship between soaking temperature and normalized indirect tensile strength.

the relationship between soaking temperature and normalized indirect tensile strength for protected (sealed) cores.

After soaking at 35°F for 7 days, the strength of protected crack-free cores (AMIR) increased by 7.2 percent. The increase in strength was more than that observed for similar unprotected cores following vacuum saturation and soaking for 2 days. This increase was the result of preventing water from entering the cores. No substantial change was observed to be due to the 65°F exposure. The 1 percent decrease in strength was much less than that observed following soaking after vacuum saturation (9.8 percent). This difference may be attributed to the fact that soaking after sealing allowed less water to enter the aggregate-asphalt matrix interface than vacuum saturation. After 7 days of exposure at 110°F, protected crack-free cores lost 7.4 percent of their strength. Unprotected crack-free cores soaked for only 2 days after vacuum saturation resulted in 17.3 percent decrease in strength.

Soaking protected steel roller–compacted cores at 35 and 65°F had no effect on indirect tensile strength as compared with the unsealed cores after vacuum saturation and soaking. Tests on protected steel-compacted cores soaked at 110°F indicated a decrease in strength of 28 percent. This decrease is substantially more than the 7.4 percent decrease observed for the crack-free cores under the same conditions. All cores were obtained from the same mix compacted to relatively the same density. The only major difference was the presence or lack of cracks after compaction. These cracks provided access for surface water to the interior of the cores, thereby enabling stripping to proceed.

An additional consideration is the influence of vacuum saturation on the test results. The vacuum-saturated crack-free cores after only 2 days of soaking indicated a decrease in strength of 17.3 percent. In contrast, the cores that were simply allowed to soak in the bath (i.e., not vacuum-saturated) showed a decrease of only 7 percent after 7 days of soaking. These data verify a common concept, that vacuum saturation forces water into the core. However, there was no substantial difference for the steel roller–compacted cores, that is, vacuum saturation had no effect. This observation is important because vacuum saturation has in the past obscured the potential benefits of relatively crack-free construction and has led to difficulties in accurately evaluating stripping susceptibility.

CONCLUSIONS

The results presented in this paper support the following:

1. Construction-induced cracks formed during compaction by conventional steel rollers allow excessive surface water penetration of the compacted mixture.
2. Cracks through the dense surface formed by migration of fines to the surface after steel vibratory rolling negate any possible benefit of the dense surface.
3. The crack-free cores offered better resistance to stripping damage when soaked in water without vacuum saturation. This indicates that a crack-free asphalt concrete surface can resist the free flow of surface water into the pavement. Vacuum pressure, used in the past for moisture conditioning, obscured the influence of surface cracks on the stripping problem.

ACKNOWLEDGMENTS

The authors would like to express their deep appreciation and many thanks for the financial support provided by the National Science and Engineering Research Council, MTO, and Carleton University. Acknowledgment is also due to O. Svec and L. Palmer of the Institute of Research in Construction, NRC, for providing the field test sections.

REFERENCES

1. R. Haas and P. Joseph. *Asphalt Stripping and Thermal Cracking at Canadian Airports: Phase 1*. Transport Canada, Canadian Air Transport Administration, Ottawa, Ontario, April 1984.
2. H. J. Fromm. The Mechanisms of Asphalt Stripping from Aggregate Surfaces. *Proc., Association of Asphalt Paving Technologists*, Vol. 43, 1974.
3. A. O. Abd El Halim. Influence of Relative Rigidity on the Problem of Reflection Cracking. In *Transportation Research Record 1007*, TRB, National Research Council, Washington, D.C., 1985, pp. 53–58.
4. A. O. Abd El Halim, G. E. Bauer, and W. A. Phang. Improvement of the Engineering Properties of Asphalt Pavements Using a Soft Compaction Technique, AMIR-Compaction. *Journal of Construction and Building Materials*, Vol. 1, No. 4, Dec. 1978, pp. 202–208.

Demonstration of Potential Benefits of Performance-Oriented Specifications

EMMANUEL G. FERNANDO AND ROBERT L. LYTTON

The implementation of performance-oriented specifications holds the promise of providing pavements that perform as they were designed to and of optimizing the use of tax dollars spent for highway construction. This will require the application of models relating materials, traffic, and environmental variables to expected pavement performance and life-cycle costs. To illustrate the potential benefits of performance-oriented specifications, hypothetical case studies were conducted in which the expected performance of pavements constructed using existing specifications was evaluated. The aim was to determine whether asphalts and mixtures considered to be acceptable under existing specifications may actually show significant differences in predicted performance and life-cycle costs under similar conditions, based on applications of the performance relationships selected for this particular exercise. The differences obtained would indicate the potential benefits of performance-oriented specification and the adequacy, or lack thereof, of existing specifications with respect to controlling asphalt and mixture properties that determine pavement performance.

Traditionally, state highway agencies have relied almost exclusively on recipe-type specifications for highway materials and construction. Under these specifications, the procedures to be followed in the construction of a pavement project are prescribed by the highway agency. A major drawback is that, by specifying materials, methods, and equipment, the highway agency obligates itself, to a great degree, to accept the end product, even though there is no assurance that it will meet the performance requirements.

More recently, many state highway agencies have adopted end-result specifications in which the contractor is given more latitude to choose construction methods and equipment and is responsible for controlling construction quality. Whereas these specifications are generally judged to be superior to traditional specifications, acceptance plans and price adjustment schedules are generally based on the historical ability of the producer or contractor to perform. Therefore, acceptance and payment tend to be based on current testing methods and construction practice rather than on test criteria and quality levels needed to achieve a certain level of performance.

Still another concept that has been introduced is that of performance-oriented specifications. The major difference between this type of specification and an end-result specification is that the acceptance plan and payment schedule are tied to the predicted loss in pavement performance due to contractor nonconformance and to the resulting increase in pavement cost that will be incurred by the highway agency over the life of the project.

Performance-oriented specifications are a research item in the ongoing Strategic Highway Research Program (SHRP), which is expected to lead to the development of performance-based binder specifications. In addition, the recently completed NCHRP 10-26A project led to the development and demonstration of a conceptual framework for performance-related specifications for hot-mix asphalt concrete mixtures and to an identification of research needs to develop fully functional and reliable performance-related specifications (*1*).

The implementation of performance-oriented specifications promises to provide pavements that perform as they were designed to and to optimize the use of tax dollars spent for highway construction. To illustrate the potential benefits of performance-oriented specifications, hypothetical case studies were conducted in which the expected performance of pavements constructed using existing specifications was evaluated. The aim was to determine whether asphalts and mixtures considered to be acceptable under existing specifications may actually show significant differences in predicted performance and life-cycle costs under similar conditions, based on applications of the performance relationships selected for this particular exercise. The differences obtained would indicate the potential benefits of performance-oriented specifications and the adequacy, or lack thereof, of existing specifications with respect to controlling asphalt and mixture properties that determine pavement performance.

CASE STUDIES

Three hypothetical case studies—designated as A, B, and C—were conducted to estimate the potential benefits of performance-oriented specifications

Case Study A involved the evaluation of the expected performance and life-cycle costs of two mixtures, prepared using the same asphalt, aggregates, and aggregate gradation but designed according to two different methods, referred to as Methods 1 and 2. Actual mix design data determined from laboratory tests were used.

Case Study B was conducted to estimate the effect of aggregate gradation on expected pavement performance and life-cycle costs. Two gradations were evaluated, as illustrated in Figure 1. In both cases, the gradations satisfy the ASTM grading specification for dense bituminous mixtures having a

E. G. Fernando, Texas Transportation Institute, Texas A&M University, College Station, Tex. 77843. R. L. Lytton, Department of Civil Engineering, Texas A&M University, College Station, Tex. 77843.

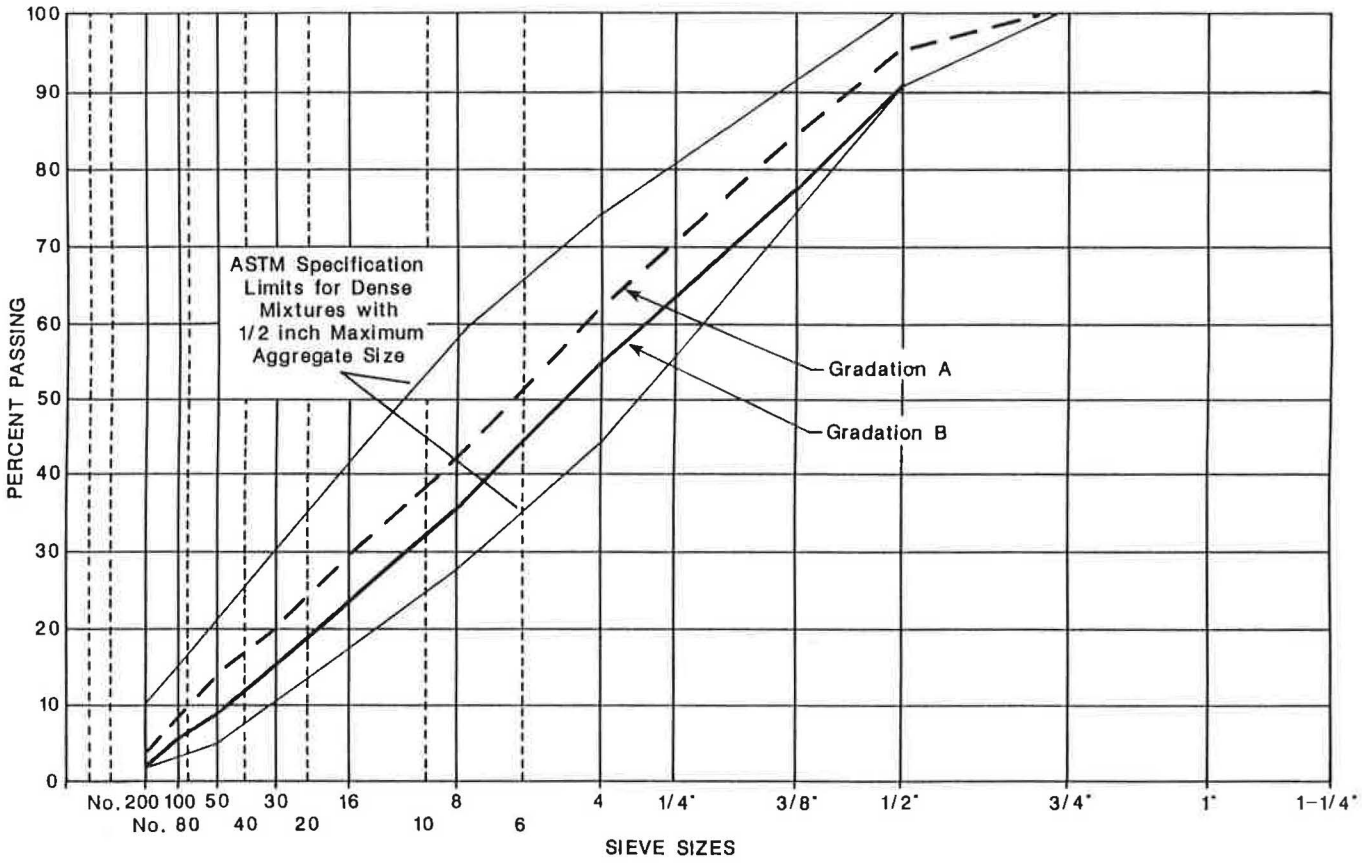

FIGURE 1 Aggregate gradations used for Case Study B.

nominal maximum aggregate size of ½ in. (ASTM D3515-89). For this case study, Jimenez's procedure (*2*) was used with the assumed gradations and assumed values of asphalt specific gravity, asphalt absorption, and effective specific gravity of the aggregate blend to predict theoretically the relationships between air voids, asphalt content, and film thickness for the two gradations evaluated.

Case Study C involved the evaluation of the expected performance and life-cycle costs of two mixtures, each prepared using a binder that meets the specifications for an AC-20 asphalt. The binders evaluated, designated as Binders 1 and 2, are included in the SHRP Materials Reference Library of asphalt cements. For this case study, bitumen stiffness data measured at different test temperatures and loading times were used in predicting pavement performance. Figures 2 and 3 illustrate the original bitumen stiffness data for the binders used in this case study.

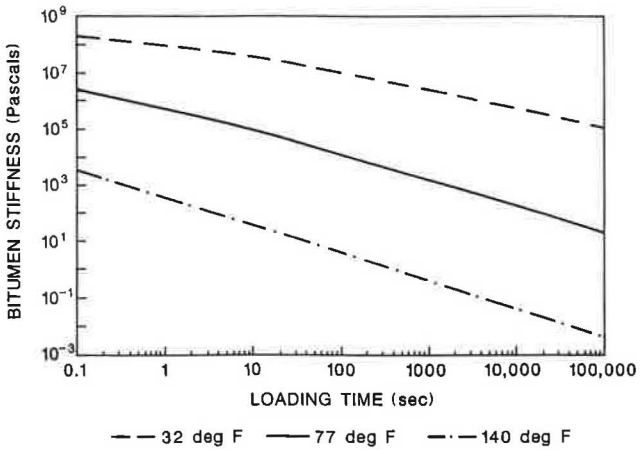

FIGURE 2 Original bitumen stiffness at various loading times and temperatures for Binder 1.

PERFORMANCE EVALUATION

The evaluation of expected pavement performance for the different case studies described generally followed a two-step procedure involving

1. The evaluation of fundamental material properties from basic mixture variables that are commonly used in existing specifications, such as asphalt content, air voids content, aggregate gradation, binder viscosity, and penetration; and

2. The application of existing performance models in conjunction with the fundamental material properties determined in Step 1 to predict fatigue cracking, rutting, and serviceability loss with time.

Two important fundamental material properties—the mixture stiffness and the slope of the creep compliance curve—were determined from the basic mixture data established for each case study. The relationship developed by Witczak was used to predict the dynamic modulus from data on volumetric

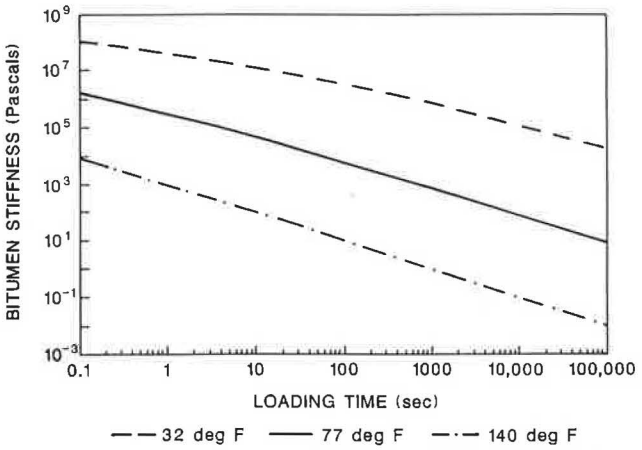

FIGURE 3 Original bitumen stiffness at various loading times and temperatures for Binder 2.

asphalt content, air voids content, aggregate gradation, and asphalt viscosity for each of the mixtures considered in Case Studies A and B (*3*). For Case Study C, McLeod's procedure was used with the available data on bitumen stiffness to estimate mixture stiffness. A computerized version of McLeod's nomograph was used for predicting the slope of the creep compliance curve for the three case studies (*4*).

The performance evaluation was made using a mechanistic finite element program called FLEXPASS developed at Texas A&M University. Because the results presented are dependent on the models used for predicting distress, the performance relationships in FLEXPASS are briefly described in the following. A detailed discussion of the development of FLEXPASS including efforts made to verify and calibrate the model is given by Tseng (*5*).

Fatigue Cracking

The following phenomenological equation is used in FLEXPASS to predict fatigue cracking:

$$N_f = K_1\left(\frac{1}{\varepsilon_t}\right)^{K_2} \tag{1}$$

where

N_f = number of load applications to failure,
ε_t = tensile strain at the bottom of the asphalt concrete layer, and
K_1 and K_2 = fatigue parameters.

The fatigue parameters K_1 and K_2 of Equation 1 are evaluated in the FLEXPASS program using the following relationships derived by Tseng and Lytton (*6*) from fracture mechanics theory:

$$K_1 = \frac{d^{1-n/2}\left[1 - \left(\frac{C_o}{d}\right)^{1-nq}\right]}{[A(1 - nq)(rE)^n]} \tag{2}$$

$$K_2 = n \tag{3}$$

where

d = depth of the asphalt concrete layer,
C_o = radius of the largest aggregate in the mix,
E = mix stiffness,
r and q = constants that relate the stress-intensity factor at the crack tip to the geometry of the sample, the loading, and the crack length, and
A and n = fracture parameters of the Paris and Erdogan equation (*7*) given by

$$\frac{dc}{dN} = A(\Delta K)^n \tag{4}$$

where $(dc)/(dN)$ is the rate of crack growth, and ΔK is the change in the stress-intensity factor with each load cycle N.

On the basis of theoretical work done by Schapery (*8*) and experimental studies conducted at the Texas Transportation Institute (TTI), the following relationship for predicting the fracture parameter n was established (*9*).

$$n = 2/m \tag{5}$$

where m is the slope of the creep compliance curve.

Equation 5 is used, in conjunction with a computerized version of McLeod's nomograph to predict the fracture parameter n, thus the fatigue parameters K_1 and K_2 in the FLEXPASS program. The slope, m, of the creep compliance curve is estimated using McLeod's nomograph given the asphalt viscosity at 140 or 275°F, the penetration at 77°F, the asphalt content and air voids content of the mixture, and the service temperature. The fracture parameter A is estimated using the following regression equation developed from beam fatigue data:

$$\log_{10}A = 7.0889 - 2.4755n - 2.1163\log_{10}E$$

$$R^2 = .86,\ N = 32 \text{ observations} \tag{6}$$

If the slope of the creep curve m and the fracture parameter n are known, the fatigue parameter K_2 is determined. In addition, if the stiffness (E) and the predicted value of n are known, the fracture parameter A can be estimated from Equation 6 and the fatigue parameter K_1 can subsequently be predicted from Equation 2.

The fatigue parameters determined using this methodology are further adjusted to account for the healing of the pavement between load applications and residual stress buildup in the asphalt concrete layer. For this purpose, the predicted fatigue constants are adjusted following a procedure proposed by Tseng and Lytton (*6*).

After the parameters of the phenomenological equation for fatigue are determined, Miner's law is applied stochastically for predicting the increase in cracked area with time.

Rutting Model

The increase in rut depth with time is predicted by accumulating the permanent vertical strains due to repetitive traffic loadings. In the procedure used, the permanent deformation

in each pavement layer is evaluated as the product of the total vertical resilient strain in a given layer and the fractional increase in total strain with cumulative load applications. The total vertical resilient strain is evaluated using the finite element method, whereas the fractional increase in total strain is predicted on the basis of an assumed model relating permanent strain to number of load repetitions. For the case studies conducted, the model used in the VESYS computer program (*10*) was adopted:

$$\varepsilon_a = IN^s \tag{7}$$

where

ε_a = permanent strain,
N = cumulative load repetitions, and
I and s = model parameters determined from laboratory data.

Assuming that the resilient strain, ε_r, is large in comparison to the increase of permanent strain with each load repetition, the fractional increase in permanent strain is approximately given by

$$F(N) \approx \Delta\varepsilon_a/\varepsilon_r \tag{8}$$

where $F(N)$ is the fractional increase in permanent strain with load repetition N.

The change in permanent strain, $\Delta\varepsilon_a$, is given by

$$\Delta\varepsilon_a = \frac{\partial\varepsilon_a}{\partial N} \tag{9}$$

Differentiating Equation 7 with respect to N and substituting the result into Equation 8 leads to the following expression for $F(N)$:

$$F(N) = \frac{ISN^{-(1-s)}}{\varepsilon_r} = \mu N^{-\alpha} \tag{10}$$

where μ and α are permanent deformation parameters. The rut depth, $\delta_i(N)$, for any given layer i is then determined by

$$\delta_i(N) = \int_0^N \int_0^{Z_{max}} \varepsilon_c(Z)F(N)\, dZ\, dN \tag{11}$$

where

$\delta_i(N)$ = rut depth at N load repetitions for a layer i,
Z_{max} = depth of the pavement layer, and
$\varepsilon_c(Z)$ = vertical compressive strain at depth Z.

Finally, the total rut depth is obtained by adding the individual rut depths for each layer:

$$\delta(N) = \sum_{i=1}^{n} \delta_i(N) = \sum_{i=1}^{n} \int_0^N \mu_i N^{-\alpha_i}\, dN \int_{d_{i-1}}^{d_i} \varepsilon_c(Z)\, dz$$

$$= \sum_{i=1}^{n} \left\{ \frac{\mu_i}{1 - \alpha_i} N^{1-\alpha_i} \int_{d_{i-1}}^{d_i} \varepsilon_c(Z)\, dz \right\} \tag{12}$$

where

$\delta_i(N)$ = total rut depth at N load repetitions,
n = number of pavement layers,
d_{i-1} = depth at bottom of a layer i, and
d_i = depth at top of a layer i.

Equation 12 was used to predict the increase in rutting with cumulative load applications for the different case studies. In the analyses, the vertical compressive strain at a given depth within the layer was evaluated using the finite element method; the permanent deformation parameters (α and μ) for the asphalt concrete layer were evaluated from the following relations:

$$\alpha = 1 - m \tag{13}$$

$$\mu = C_2(p)mt^m \tag{14}$$

where

$C_2(p)$ = a calibration constant dependent upon the rutting characteristics of the asphalt mix and the quality of the aggregate,
m = slope of the creep compliance curve, and
t = time of loading.

Equation 13 is based on work done by Lytton (*11*), whereas Equation 14 is from development work conducted at TTI on the Texas Flexible Pavement System (*12*). For the base and subgrade layers, typical values for α and μ were assumed in the analyses and were kept the same for the three case studies.

Serviceability Loss Model

With the FLEXPASS computer program, serviceability loss is evaluated using the AASHO present serviceability index (PSI) equation with the predicted values of rut depth, cracked area, and slope variance. The slope variance is predicted from the rut depth variance using the following equation based on VESYS (*10*):

$$E(SV) = \frac{2\beta}{c} \text{var}(\delta) \tag{15}$$

where

$E(SV)$ = expected value of slope variance,
var(δ) = variance of rut depth, and
β and c = constants that have typical values of 1.0 and 0.058, respectively, based on regression analysis of field roughness data.

The rut-depth variance is evaluated from a probabilistic analysis of the rut-depth equation.

Age-Hardening

In the analyses conducted, age-hardening of the different mixtures was also considered using relationships developed for

predicting the change in asphalt viscosity and penetration with time. These equations are based on data collected by Lee from eight different projects in Iowa, where observations of asphalt penetration and viscosity were made at 6-month intervals over 4 years (*13*). A hyperbolic model of the form given by Equation 16 was used to model the change in asphalt consistency with time.

$$\Delta y = t/(a + bt) \tag{16}$$

where Δy is the difference between the measured viscosity or penetration at time t and the value of the property at time of construction, and a and b are hyperbolic model parameters that are functions of basic mixture variables.

Relationships for predicting the hyperbolic model parameters of Equation 16 were developed and are summarized as follows:

- Viscosity at 70°F (megapoises):

$$a = 1.614494 \times 10^{-14} \cdot (V_{ref,70})^{3.1530} \cdot (FT)^{1.9937} \cdot (V_{140,TFOT})^{2.7830} \cdot (P_{air}/P_{200})^{-0.5283}$$

$R^2 = .9963$, $RMSE = 0.0368$, $N = 8$ obs.

$$b = 6.0399 \cdot p_{ac}^{0.3322} \cdot (P_{30}/P_4)^{1.2935} \cdot (P_{air})^{-0.2102} \cdot (V_{140,TFOT}/V_{140,0})^{-0.8081}$$

$R^2 = .9833$, $RMSE = 0.0186$, $N = 8$ obs.

- Viscosity at 140°F (poises):

$$a = 1.285740 \times 10^{-10} \cdot (V_{140,TFOT})^{2.1875} \cdot (P_{30}/P_4)^{-14.5233} \cdot (\text{pen}_{77,TFOT}/\text{FT})^{-3.1502}$$

$R^2 = .9619$, $RMSE = 0.1176$, $N = 8$ obs.

$$b = 0.2979 \cdot (P_8)^{-6.5466} \cdot (P_{30})^{11.8950} \cdot (P_{air})^{-2.2582} \cdot (\text{pen}_{77,TFOT}/\text{FT})^{-4.0697}$$

$R^2 = .9558$, $RMSE = 0.0746$, $N = 8$ obs.

- Penetration at 77°F (0.1 mm):

$$a = 3.287416 \times 10^{-5} \cdot (\text{pen}_{ref,77})^{-9.0932} \cdot (\text{pen}_{77,0})^{11.5555} \cdot (P_{200}/P_{30})^{4.2124}$$

$R^2 = .9723$, $RMSE = 0.1192$, $N = 8$ obs.

$$b = 190{,}387 \cdot (\text{FT})^{0.3245} \cdot (P_{air})^{-0.2860} \cdot (\text{pen}_{77,0})^{-4.0208} \cdot (P_{200}/P_{30})^{-1.2031} \cdot (\text{pen}_{77,TFOT}/\text{pen}_{77,0})^{-1.042}$$

$R^2 = .9708$, $RMSE = 0.0144$, $N = 8$ obs.

where

$V_{ref,70}$ = reference viscosity at 70°F, at time of construction (megapoises);
FT = film thickness (microns);
$V_{140,TFOT}$ = viscosity at 140°F after thin-film oven testing (TFOT) (poises);
$\text{pen}_{ref,77}$ = reference penetration at 77°F, at time of construction (0.1 mm);
$\text{pen}_{77,TFOT}$ = penetration at 77°F after TFOT (0.1 mm);
$\text{pen}_{77,O}$ = original penetration at 77°F (0.1 mm);
$V_{140,O}$ = original viscosity at 140°F (poises);
P_{air} = percentage air voids;
P_{ac} = percentage asphalt;
P_{200} = percentage passing No. 200 sieve;
P_{30} = percentage passing No. 30 sieve;
P_8 = percentage passing No. 8 sieve; and
P_4 = percentage passing No. 4 seive.

For viscosity, the dependent variable Δy in Equation 16 is $\log_{10}(V_t/V_{ref})$, where V_t is the predicted viscosity at time t and V_{ref} is the reference viscosity. For penetration, Δy is the predicted difference between the reference penetration, and the penetration at some time t. In both cases, the reference values should be the estimated properties at the time of construction.

The preceding equations were used to estimate the effects of aging on the predicted performance of the different mixtures evaluated in Case Studies A and B. The prediction equations for viscosity at 70°F were used in conjunction with the dynamic modulus equation developed by Witczak to predict the change in modulus with time (*3*). The equations for viscosity at 140°F and penetration at 77°F were used to predict the change in fatigue and permanent deformation properties as the mixture ages. Table 1 summarizes the data used in conjunction with the given equations to evaluate the age-hardening of the mixtures considered in Case Studies A and B. For Case Study C, estimates of bitumen stiffness with time, obtained from a SHRP A-002 subcontractor, were used in conjunction with McLeod's procedure (*4*) to predict the change in mixture stiffness with time.

The predicted age-hardening characteristics of the different mixtures were used in subdividing the analysis period into several time intervals, with each time interval characterized by mixture properties representative of the aging associated with the given interval. A 20-year analysis period was used

TABLE 1 Input Data Used to Characterize Age-Hardening for Case Studies A and B

Input Variable	Case Study A		Case Study B	
	Method 1	Method 2	Gradation A	Gradation B
1. $V_{ref,70}$ (megapoises)	17.55	17.55	17.55	17.55
2. FT (microns)	9.92	10.97	8.52	13.76
3. $V_{140,TFOT}$ (poises)	2637	2637	2637	2637
4. $V_{140,0}$ (poises)	1071	1071	1071	1071
5. $\text{Pen}_{ref,77}$ (0.1 mm)	38	38	38	38
6. $\text{Pen}_{77,TFOT}$ (0.1 mm)	51	51	51	51
7. $\text{Pen}_{77,0}$ (0.1 mm)	85	85	85	85
8. P_{air} (%)	4.9	3.9	4	4
9. P_{ac} (%)	5.4	5.9	4.73	5.18
10. P_{200} (%)	3.9	3.9	3.9	2.0
11. P_{30} (%)	20.2	20.2	20.2	15.2
12. P_8 (%)	41.8	41.8	41.8	35.8
13. P_4 (%)	61.6	61.6	61.6	54.6

for all case studies. The performance evaluation for each mixture was therefore conducted in stages, starting with the first time interval and proceeding in succession through the last time interval or period. At each time period, the associated mixture properties were used in conjunction with the selected performance models to predict the fatigue cracking, rutting, and serviceability loss for that particular period. The predicted levels of distress at the end of any given time period were then used as the starting levels of distress for the subsequent time period.

LIFE-CYCLE COST ANALYSIS

For all case studies, a hypothetical pavement section consisting of a 4 in. bituminous-bound surface layer and a 10 in. granular base course overlaying a clay subgrade was assumed. A 9,000-lb load acting on dual wheels spaced 13 in. apart and inflated to a pressure of 75 psi was used to represent the standard 18-kip equivalent single axle load (ESAL). In addition, an initial traffic rate of 353 ESALs a day and a traffic growth rate of 4 percent were used in the simulations. The cumulative traffic for the 20-year analysis period was approximately 4 million 18-kip ESALs.

Properties of the surface layer were varied depending on the particular bituminous mixture that was being evaluated. These properties varied with time and with the assumed seasonal temperatures. For all mixtures, the properties of the base and the subgrade layers were kept the same.

The performance predictions were used in evaluating the life-cycle costs for the different case studies considered. For this analysis, the following failure criteria were used to determine the timing of overlays:

1. Maximum allowable fatigue cracking—500 ft^2/1,000 ft^2.
2. Maximum allowable rut depth—0.50 in.
3. Terminal serviceability index—2.50.

An overlay was assumed to be necessary when one or more of these failure limits has been reached. For the life-cycle cost analysis, the thickness design of overlays was accomplished using the overlay design equations developed for FHWA (*14*). These equations assume that overlay life is governed by reflection cracking. For each case study, an overlay thickness was determined to last the remainder of the analysis period. The properties of the overlay material for determining the required overlay thicknesses were kept the same for all three case studies.

Life-cycle costs were calculated using a cost-analysis program known as FLAGCAP developed at TTI in a recent research project sponsored by the Florida Department of Transportation (*15*). Pavement costs associated with the predicted performance of each of the different mixtures were evaluated, and included costs due to initial construction, routine maintenance, overlays, and level-ups. In addition, user costs associated with vehicle depreciation, fuel consumption, oil consumption, tire wear, vehicle maintenance, and user travel time were estimated on the basis of assumed distribution of vehicles in the traffic stream and the predicted serviceability history for the given analysis period. The assumed vehicle distribution was compatible with the daily 18-kip ESALs used in the performance evaluation. In addition, user operating costs were adjusted for the effects of pavement roughness using relationships developed from data compiled by Zaniewski (*16*).

Future costs were converted to equivalent present worth costs using a discount rate of 5 percent. A summary of the pavement and user costs evaluated for the different case studies considered is presented in Table 2. The costs shown are for a 10-mi stretch of one-lane roadway; they are specific to the case studies considered herein.

As may be observed from Table 2, the percent difference in pavement costs associated with the different case studies considered varies from approximately 3.9 to 12.5 percent. Considering that the mixtures in each case study are, by existing specifications, "equally acceptable," the differences in pavement life-cycle costs obtained illustrate the need for specifications that are based on predicted pavement performance, and indicate the potential savings that may be realized if such specifications are implemented. Note that the predicted pavement costs shown in Table 2 are only for a 10-mi stretch of one-lane highway. If the predicted differences in pavement costs are applied over an entire highway network, the potential savings can easily be substantial and will be even more if the potential reductions in user costs are also considered. This is readily apparent from Table 2, in which it is observed that the predicted differences in user costs are significantly greater than the predicted differences in pavement costs. This indicates that not only will highway agencies realize savings from implementing performance-oriented specifications, but that road users will, as well, and at a potentially greater amount.

ILLUSTRATION OF ALTERNATIVE APPROACH TO SPECIFICATION DEVELOPMENT

The limited number of simulations conducted therefore demonstrate the importance of developing materials and construction specifications on the basis of predicted pavement performance. This will entail specifications on variables that significantly influence pavement service life. The choice of variables to be controlled will logically depend on the distress criteria and models used for pavement design, which in turn may vary with local conditions. Whatever materials and construction variables are selected for specification purposes, the choice should be guided by the following considerations: (a) the variables selected are significant predictors of pavement performance, and (b) the variables are properties that can be controlled by the producer or contractor during construction.

The first guideline can be addressed through a sensitivity analysis of the particular distress prediction models used in pavement design. By way of illustration, the slope m of the creep compliance curve is a material property input to the simulation program, FLEXPASS, used in different hypothetical case studies considered herein. How this material property relates to expected pavement performance is evident from the mechanics-based relationships presented earlier between the slope of the creep curve, the fatigue parameters, and the permanent deformation parameters. To illustrate the sensitivity of the performance predictions from FLEXPASS to variations in the slope of the creep curve, simulation runs were made wherein the slope was varied from 0.40 to 0.50

TABLE 2 Summary of Life-Cycle Costs for Three Case Studies

Speculative Case Study	Time to Failure (Years)	Failure Mode	Pavement Cost (x 1000$)	Difference in Pavement Costs (x 1000$)	Percent Difference in Pavement Cost	User Cost (x 1000$)	Difference in User Costs (x 1000$)	Total Cost (x 1000$)	Difference in Total Costs (x 1000$)
A. Mix Design Method									
1. Method 1	6.55	Fatigue Cracking	765			437,825		438,590	
2. Method 2	5.59	Rutting	796	31	3.89	438,325	500	439,121	531
B. Effect of Aggregate Gradation									
1. Gradation A	12.27	Fatigue Cracking	679			430,703		431,382	
2. Gradation B	7.34	Fatigue Cracking	740	61	8.24	436,525	5,822	437,265	5,883
C. Viscosity Grading									
1. Binder 1	12.24	Fatigue Cracking	765			425,901		426,666	
2. Binder 2	8.52	Fatigue Cracking	874	109	12.47	428,118	2,217	428,992	2,326

and all other variables were held constant. The layer thicknesses and base and subgrade properties from earlier runs were also used in these new simulations. Figures 4, 5, and 6 illustrate the performance predictions obtained.

Based on the distress models used, it is apparent from the figures that the slope (m) of the creep curve is a significant predictor of pavement performance. Life-cycle costs associated with the different levels of this material property are summarized in Table 3, which indicates substantial differences in predicted pavement life-cycle costs between the cases considered. These results further demonstrate the importance of the slope of the creep curve, and how, from a performance prediction standpoint, it is an appropriate variable to use for establishing target values for construction quality control. An example of how this may be done is illustrated in Figure 7 and Table 4. Assuming for instance a required minimum predicted service life of 20 years and a required maximum predicted pavement life-cycle cost of $10,000/lane-mi, a target value of 0.40 for the slope (m) of the creep curve is obtained based on the results of simulations. This target value is of course specific to the conditions analyzed and will undoubtedly vary depending on traffic and environmental conditions and with different pavement layer thicknesses and material properties. The effect of deviations from target on predicted pavement life-cycle costs will then be used as the basis for establishing payment schedules in a performance-based specification.

CONCLUSION

On the basis of the hypothetical case studies reported herein, it is apparent that existing asphalt and mixture specifications do not necessarily ensure that pavements constructed "within

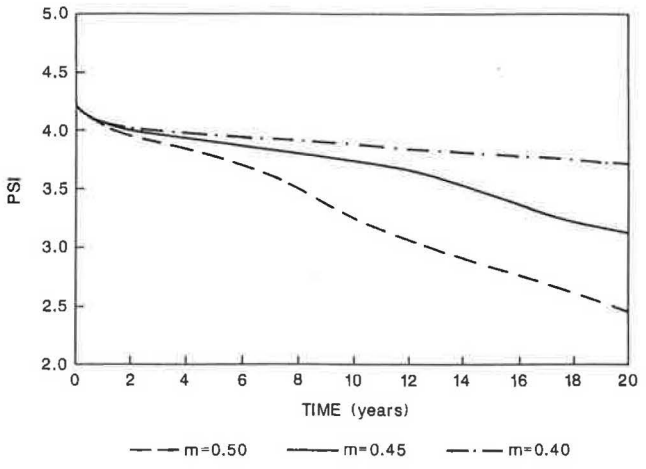

FIGURE 4 Predicted trends in serviceability loss with time for different levels of *m*.

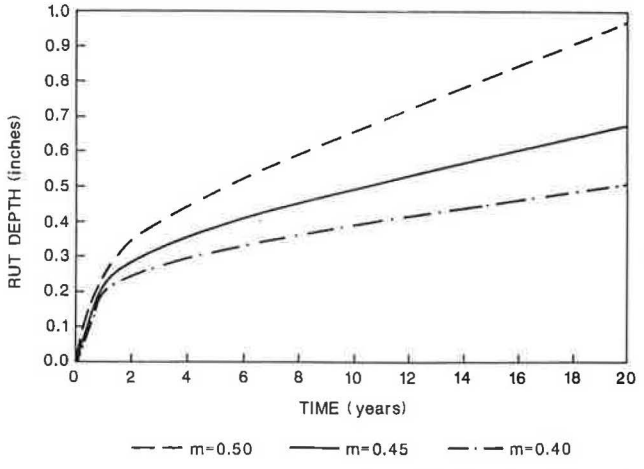

FIGURE 5 Predicted trends in rutting with time for different levels of *m*.

specs" will yield similar performance and life-cycle costs. Indeed, the simulations have shown that significant differences in pavement life-cycle costs may be predicted for asphalt mixtures that are within specification limits. Consequently, there is merit to implementing specifications that are tied to predicted pavement performance.

As part of developing performance-oriented specifications, materials and construction variables have to be identified which are significant predictors of pavement performance and are factors that can be controlled during construction. The choice of materials and construction variables for specification development will logically depend on the distress criteria and models used for pavement design. An example of a material property for which target values for construction quality control may be specified is the slope of the creep compliance curve. This material property has been shown, from theory, to be a predictor of fatigue cracking and rutting, and its significance as a performance-related variable was illustrated herein.

It is emphasized that the slope (m) was only used as an example of the kinds of materials and construction variables that need to be considered for specification development. Fundamental material properties such as the slope of the creep curve or mixture stiffness may be suitable variables to use from the standpoint of being performance-related, but implementing working specifications based on these variables is another issue. It is recognized that actual measurement of fundamental material properties for determining compliance to specifications may be beyond existing capabilities of some state highway agencies and contractors. For this reason, surrogate tests or relationships for these variables may have to be used that relate fundamental material properties, which are significant predictors of pavement performance, to materials and construction variables that have been traditionally used in materials and construction specifications. Alternatively, algorithms may be developed, or existing procedures implemented, for estimating fundamental material properties in situ. Already, there are a number of computer programs available for back calculation of layer stiffnesses from measured surface deflections, including a recent computer program called SCALPOT, developed by Magnuson and Lytton at Texas A&M University (*17*), that is capable of estimating creep compliance parameters of layered systems from falling weight deflection measurements. Developments like these should provide additional impetus for acceptance and implementation of performance-oriented specifications within the highway community.

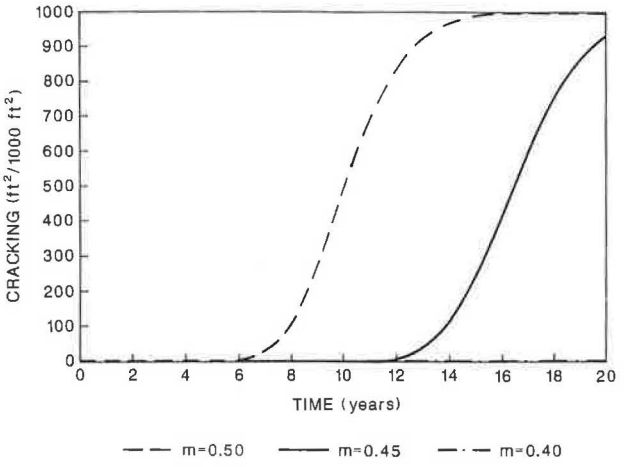

FIGURE 6 Predicted trends in fatigue cracking with time for different levels of m.

TABLE 3 Summary of Life-Cycle Costs for Different Values of m

SLOPE, m, OF CREEP CURVE	PAVEMENT COST[a] (x 1000 $)	DIFFERENCE IN PAVEMENT COSTS (x 1000)[b]	USER COST[a] (x 1000 $)	DIFFERENCE IN USER COST (x 1000)[b]
0.50	566	---	231,157	
0.45	387	-179	227,448	-3,709
0.40	87	-479	220,818	-10,339

[a] Present worth costs for a 10-mile, one lane stretch of highway; 20-yr analysis period at a 5% discount rate.

[b] Relative to costs for case where slope m = 0.50.

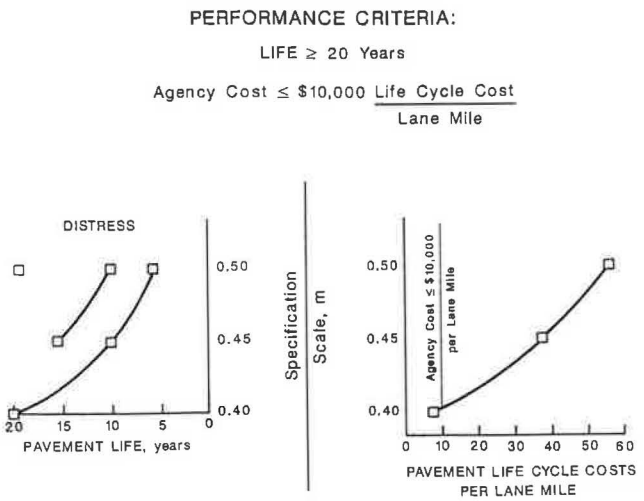

FIGURE 7 Determination of target value for m = 0.40 based on performance considerations.

TABLE 4 Failure Time (Years) for Figure 7

Slope, m	Distress			Agency Life Cycle Costs per Lane Mile (x $1000)
	PSI (2.5)*	Rutting (0.5 in)*	Fatigue (600ft²/1000ft²)*	
0.40	-	20	-	8.7
0.45	-	10	17	38.7
0.50	19	5.43	10	56.6

*Failure Criterion

REFERENCES

1. D. A. Anderson et al. *Performance-Related Specification for Hot-Mix Asphaltic Concrete*. Final Report, NCHRP 10-26A. Pennsylvania Transportation Institute, Pennsylvania State University, University Park, Aug. 1990.
2. R. A. Jimenez and D. A. Dadeppo. *Asphalt Concrete Mix Design*. Report ATTI-86-2. Arizona Transportation and Traffic Institute, University of Arizona, Tucson, June 1986.
3. M. W. Witczak. *The Universal Airport Pavement Design System—Report II: Asphaltic Mixture Material Characterization*. University of Maryland, College Park, May 1989.
4. N. W. McLeod. Asphalt Cements: Pen-Vis Number and Its Application to Moduli Stiffness. *Journal of Testing and Evaluation*, Vol. 4, No. 4, 1976.

5. K. Tseng. *A Finite Element Method for the Performance Analysis of Flexible Pavements*. Ph.D. dissertation. Texas A&M University, College Station, 1988.
6. K. Tseng and R. L. Lytton. Fatigue Damage Properties of Asphaltic Concrete Pavements. In *Transportation Research Record 1286*, TRB, National Research Council, Washington, D.C., 1990.
7. P. C. Paris and F. Erdogan. A Critical Analysis of Crack Propagation Laws. *Journal of Basic Engineering* (Transactions of the ASME, Series D), Vol. 85, No. 3, 1963.
8. R. A. Schapery. A Theory of Crack Growth in Viscoelastic Media. Technical Report MM 2764-73-1. Mechanics and Materials Research Center, Texas A&M University, College Station, 1973.
9. F. P. Germann and R. L. Lytton. *Methodology for Predicting the Reflection Cracking Life of an Overlay*. Report TTI-2-8-75-207-5. Texas Transportation Institute, Texas A&M University, College Station, March 1979.
10. W. J. Kenis. Predictive Design Procedures—A Design Method for Flexible Pavements Using the VESYS Structural Subsystem. *Proc., 4th International Conference on the Structural Design of Asphalt Pavements*, Vol. 1, University of Michigan, Ann Arbor, 1977, pp. 101–138.
11. R. L. Lytton. Materials Property Relationships for Modeling the Behavior of Asphalt-Aggregate Mixtures in Pavements. Technical Memorandum SHRP A-005. Strategic Highway Research Program, Washington, D.C., June 1990.
12. J. Uzan, D. G. Zollinger, and R. L. Lytton. *The Texas Flexible Pavement System (TFPS), Volume II—Mechanistic/Empirical Model*. Research Report 455-1. Texas Transportation Institute, Texas A&M University, College Station, Nov. 1990.
13. D. Lee. Asphalt Durability Correlation in Iowa. In *Highway Research Record 468*, HRB, National Research Council, Washington, D.C., 1973, pp. 43–60.
14. P. W. Jayawickrama, R. E. Smith, R. L. Lytton, and M. R. Tirado. *Development of Asphalt Concrete Overlay Design Equations: Volume I—Development of Design Procedures*. Final Report DTFH61-84-C-00053. FHWA, McLean Va., 1987.
15. E. G. Fernando, R. L. Lytton, W. L. McFarland, J. L. Memmott, F. Helin, and A. N. Jamy. *The Florida Comprehensive Pavement Analysis System (COMPAS)—Volume I: Development of Analytical Models*. Texas Transportation Institute, Texas A&M University, College Station, April 1991.
16. J. P. Zaniewski, B. C. Butler, G. Cunningham, G. E. Elkins, M. S. Paggi, and R. Machemehl. *Vehicle Operating Costs, Fuel Consumption, and Pavement Type and Condition Factors*. Report DOT-FH-11-9678. U.S. Department of Transportation, June 1982.
17. A. H. Magnuson, R. L. Lytton, and R. C. Briggs. A Comparison Study of Computer Predictions and Field Data for Dynamic Analysis of Falling Weight Deflectometer Data. Presented at the 70th Annual Meeting of the Transportation Research Board, Washington, D.C., Jan. 1991.

The contents of this paper reflect the views of the authors, who are responsible for the facts and accuracy of the evaluation presented herein. The contents do not necessarily reflect the official views or policies of TRB or FHWA.

Influence of Test Parameters in SHRP P07 Procedure on Resilient Moduli of Asphalt Concrete Field Cores

Y. R. KIM, K. A. SHAH, AND N. P. KHOSLA

The results of resilient modulus (M_R) testing at North Carolina State University as a part of the Strategic Highway Research Program (SHRP) asphalt concrete core proficiency testing program are presented. As a requirement of participating in this proficiency testing, thorough calibration was conducted on the M_R testing system at NCSU before the commencement of any testing. Then four synthetic specimens were tested within the framework of ASTM D4123-82. After the M_R values of the synthetic specimens were verified to be within the acceptable range, the M_R testing was performed on field cores supplied by the proficiency testing program. The MTS Systems Corp. M_R testing fixture was used with the MTS servohydraulic closed-loop loading system. The mountable measurement device consisting of two extensometers with springs was used in measuring the horizontal deformation. Load and deformation data were acquired by a 12-bit data acquisition board and the LabWindows data acquisition program. A computer program that automatically calculates the instantaneous and total deformation values from the raw data was developed on the basis of regression analysis. The M_R testing of field cores was performed in accordance with the SHRP P07 protocol (September 1990 version). The test results indicated that the effects of testing axis and rest period are relatively small compared with the influence of Poisson's ratio. The M_R values from the assumed Poisson's ratio were as much as five times larger than those calculated by using Poisson's ratio calculated from the vertical and horizontal deformations.

A characterization of various highway materials is one of the most influencing steps involved in pavement design schemes. Material properties are usually obtained from laboratory testing by simulating the field conditions as close as possible. These material properties are input to constitutive models of different design analyses to predict stresses, strains, and deflections induced in a layered pavement structure under moving wheel loads.

As a major constituent of the flexible pavement, the resilient properties of asphalt concrete have been continuously studied using various types of test methods. All of these efforts have led ASTM to standardize the resilient modulus testing method of asphalt concrete (ASTM D4123-82). However, as demonstrated in the Workshop on Resilient Modulus Testing held in Oregon State University in March 1989, there was strong consensus among pavement engineers that ASTM D4123 in unnecessarily time-consuming and that the test results are difficult to reproduce. Furthermore, although the resilient modulus is considered to be a material property, the value of resilient modulus seems to depend on the load history applied.

Department of Civil Engineering, North Carolina State University, P.O. Box 7908, Raleigh, N.C. 27695.

In recognition of the importance and existing problems of resilient modulus testing of asphalt concrete, the Strategic Highway Research Program's (SHRP) material testing program is developing a resilient modulus test procedure for asphalt concrete (SHRP Protocol P07). This procedure incorporates recent findings on resilient modulus testing into the existing ASTM D4123-82.

Another effort by SHRP in the evaluation of the resilient moduli values of field cores is being undertaken as a part of SHRP's Long-Term Pavement Performance program (LTPP). This project is entitled *SHRP Asphalt Concrete Core Proficiency Sample Program for Resilient Modulus Testing*. More than 50 laboratories in the United States are voluntarily ticipating in this project, including North Carolina State University (NCSU).

The objectives of this paper are first to describe the SHRP asphalt concrete core proficiency testing activities at NCSU (hereafter called proficiency testing); second, to introduce the data acquisition and analysis program developed for the resilient modulus testing; and third, to summarize findings from the resilient modulus testing of LTPP field cores.

RESILIENT MODULUS TESTING FIXTURE

The testing apparatus used in this study was provided by MTS Systems Corp. The schematic presentation of this fixture is shown in Figure 1. The fixture was installed inside an environmental chamber in which temperature could be maintained within ±1°F for extended periods.

Horizontal displacements were measured by extensometers designed by MTS Systems with full-scale travels of 0.15 in. (0.381 cm). Ranging the transducers to 10 percent of full scale calibrates the output to a finer-scale travel and allows higher-resolution measurements of small deformations. Vertical deformations were measured directly from the actuator movement using the stroke reading in the MTS microconsole.

The diametral device consists of two extensometers with gauge length extenders and two specimen adapter brackets as shown in Figure 1. The brackets are machined to the same radius as the specimen and remain in contact with the specimen all along the thickness. This design allows each bracket to measure the maximum deformation instead of measuring local deformation due to point contact with a linear variable differential transducer (LVDT) that is used in some diametral tensile test fixtures. The mounting method of these extensometers can be found elsewhere (*1*,*2*).

Some advantages of the device are as follows:

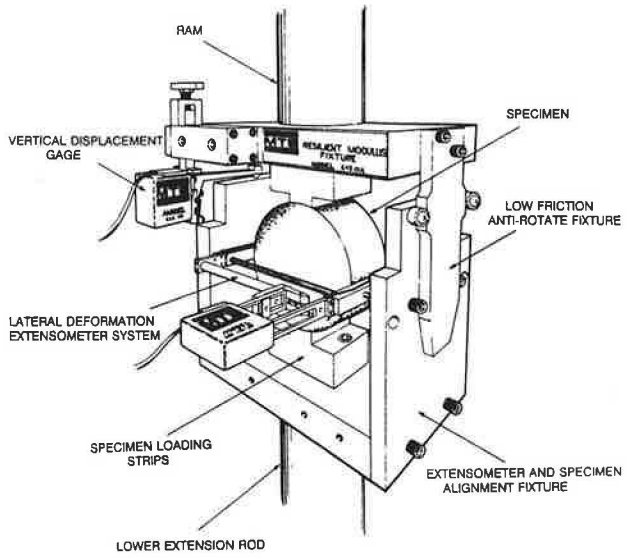

FIGURE 1 Resilient modulus testing fixture and extensometers.

1. Because the brackets are placed at the sides of the specimen guided by pin screws through the holes in fixed side walls, this fixture gives more precise control over the vertical locations of the brackets.
2. Once the test starts, the low-friction antirotate bar in the upper fixture (Figure 1) prevents rotation of the actuator due to repetitive loading.
3. Another advantage of this fixture is that the improper measurements due to "rocking" of the specimen can be minimized. Because the extensometers are attached to the specimen by springs, extraneous deformation due to rigid-body rotation cannot affect the deformation measurements.

TESTING PROTOCOL

Calibration with Synthetic Specimens

Participation in the SHRP proficiency testing required calibration of the resilient modulus testing system before the commencement of any testing. The calibration procedure included alignment of the top and bottom loading rams, calibration of extensometers and load cell, and adjustment of gain settings in the MTS console to check the shape and timing of wave form.

Then four types of synthetic specimens were tested to verify the calibration of the system. The synthetic specimens were made from polyacrylate (Lucite), polyethylene, Teflon, and cast synthetic rubber used for Hveem stabilometer calibration. The testing protocol that was required to determine the resilient modulus, within the framework of ASTM D4123, called for

- Test temperature—77 ± 0.9°F (25 ± 0.5°C);
- Applied load—50 lb;
- Record deflection—after 15 conditioning cycles; and
- Determination of resilient modulus—twice for each sample, second replication done after rotating the sample through 90 degrees.

Results were then submitted to the researchers of the proficiency testing program for analysis.

Resilient Modulus Testing of Field Cores

After the M_R values of the synthetic specimens were found to be within the acceptable range of known M_R values, testing was conducted on the asphalt concrete cores obtained from the test sections at the Pennsylvania State University and sent by the SHRP proficiency testing project. Two sets of cores, consisting of five samples each, were supplied with the labels "O" or "N" followed by a two-digit number. The samples labeled N and O are the cores from a new and a 5-year old pavement, respectively. Two mutually perpendicular diametral lines were drawn on the sample and marked either "A" or "B". The cores were not trafficked; consequently, traffic direction was not marked on the cores. Indirect tensile strength at 77°F was 223 psi for cores marked "N" and 61 psi for cores marked "O".

All the samples were tested in accordance with the SHRP P07 procedure (September 1990 version) along both axes. Each time a core was tested, Direction A or B was chosen randomly for the first set of readings. The differences and modifications between this procedure and ASTM D4123 are listed in Table 1.

DATA ACQUISITION AND ANALYSIS PROGRAM

Noise in Data Acquisition

At NCSU, LabWindows (Version 1.2) is being used to acquire the data from the MTS. The programs used for data acquisition have been written in Quick Basic within the LabWindows. To acquire the data, an AT-MIO-16 board has been set up. The AT-MIO-16 is a high-performance multifunction analog, digital, and timing input and output board. The input voltage range for the AT-MIO-16 has been set up to remain between −10 and 10 V. Therefore, the precision of the input signal measured by the AT-MIO-16 twelve-bit analog-to-digital converter can be calculated by dividing the total voltage range (20 V) by 2^{12}, which results in 4.88 mV. Thus, when displacement cartridges of 0.5 in. (for vertical deformation) and 0.015 in. (for horizontal deformation) maximum capacity were used, the minimum values of deformation measured were $(0.5/10) \times (4.88/1{,}000) = 2.44 \times 10^{-3}$ in. and $(0.015/10) \times (4.88/1{,}000) = 7.32 \times 10^{-6}$ in., respectively. Similarly, for a 2,000-lb. load cartridge, the minimum value of load that could be read was 0.976 lb. This accounts for most of the fluctuation in the output deformation curves. As can be seen from Figures 2 and 3, the values of the deformations are seen to fluctuate between two precision levels. The "noise" in the data can be easily accounted for from the minimum precision values as explained. It is not claimed here that there is no fluctuation at all in the actual data, but it is believed that the small fluctuations can be amplified because of the limitation of the acquisition board.

Resilient Modulus Analysis Program

An effort has also been made at NCSU to develop a program that automatically calculates the M_R values from the data file obtained using the data acquisition program. This program

TABLE 1 Comparison of ASTM D4123 and SHRP P07 Protocol

Criteria	ASTM D 4123	SHRP P07
Testing machine	It should have the capability of applying a load pulse over a range of frequencies, load duration and load levels. Note 2 suggests use of electrohydraulic m/c's or other m/c's such as those using pneumatic devices.	It shall be a top-loading, closed loop electrohydraulic testing m/c with a function generator capable of applying a haversine shaped load pulse over a range of load durations, load levels and rest period.
Deformation measurements	* By LVDT's or other suitable devices. * Positive contact between the specimen and measuring device by spring loading or gluing attachments. * Gauges wired to preclude the effects of eccentric loading so as to give algebraic sum of movement of each side of the specimen. Alternatively, each gauge can be read independently and results summed independently.	By LVDT's. Positive contact by using a spring loaded LVDT and attaching a flat head (3/8" x 1/4") as a contact point. The two LVDT's shall be wired so that each transducer can be read independently and the results summed during the test program.
Temperatures recommended	41,77 (or ambient laboratory temperature) & 104°F.	41,77 & 104°F
Measurement of indirect tensile strength	Destructive test on a specimen and the use of equation 8.3 in ASTM D 4123.	According to the procedure in attachment A to protocol P07 at 77 ± 2°F.
Recommended load for testing and preconditioning	10 to 50% of indirect tensile strength.	30, 15 & 5% of indirect tensile strength for test temperatures of 41±2, 77±2 & 104±2°F respectively.
Seating load	ASTM remains silent.	3, 1.5 & 0.5% of indirect tensile strength for test temperatures of 41±2, 77±2 & 104±2°F respectively.
Axes of loading	Sample to be rotated 90° each time a test with a different variable is done on the same specimen.	Testing is to be performed along two mutually perpendicular diametral axis (latest version, July 1991, requires testing along two axes 45° apart).
Wave form Loading pattern & preconditioning	Haversine or suitable waveform; Load duration 0.1 to 0.4 sec, Frequency of load: 0.33, 0.5 & 1 Hz. suggested.	Haversine; Load duration 0.1 sec; Rest periods 0.9, 1.9 & 2.9 secs.
Period of preconditioning	Until the deformations are stable.	Until a minimum of 10 successive readings of horizontal deformation agree within 10%.
Expected load repetitions	A minimum of 50 to 200 load repetitions is typical.	Expected ranges are 50-150, 50-100, & 20-50 for 41±2, 77±2, 104±2°F resp.
If cumulative vertical deformation exceeds (x)"	**here x = 0.001"** Reduce the test temperature, the applied load, or both.	**here x = 0.025" for 41° F** **= 0.050" for 77 & 104°F** Reduce applied load to min. possible retaining adequate deformation. If not possible to retain adequate deformation for measurements, stop the preconditioning and generate 10 load pulses for M_R determination and so indicate on test report.

(*continued on next page*)

TABLE 1 (*continued*)

Criteria	ASTM D 4123	SHRP P07
Number of load pulses to be applied for M_R	Measure the avg. recoverable horizontal and vertical deformations over at least 3 loading cycles after the repeated resilient deformations are stable.	Minimum of 30 load pulses to be applied. Continued beyond 30 until the range in deformation values of five successive horiz. deformation values is less than 10% of the avg. Then M_R is the avg. of the M_R values measured individually from 5 load cycles after deformations are stable.
Poisson's ratio	0.35 suggested to be reasonable at 77°F.	0.2, 0.35 & 0.5 to be assumed for temperatures of 41±2, 77±2, and 104±2°F respectively.
Specimens	Lab-molded: prepare as per 6.1 core specimens: as per 6.2.	Lab molded specimens: no suggestions Core specimens: as per ASTM.
Test sequence	Testing to begin at the lowest temperature, shortest load duration and smallest load. Subsequent testing on the same specimen should be so as to provide progressively lower moduli.	The sequence shall consist of initial testing at 41°F, followed by intermediate testing at 77°F and final testing at 104°F.

Additions in SHRP P07:

Section 6 gives a description about specimen requirements and measurements.
Section 7.2 describes the procedures related to alignment and specimen seating.

determines the peak values of load applied at each consecutive load cycle after compensating for the level of precision (which has been discussed earlier) of load measured. The program also calculates instantaneous and total values of horizontal and vertical deformations.

The program first picks up the peak values of load and deformations at each cycle and compensates for repeated peaks (which result because of the limitation of the level of precision, as discussed earlier) using the following equation:

$$\delta_A = \delta_O + (R - 1) \times PL/C$$

where

δ_A = adjusted peak value,
δ_O = peak value obtained from the raw data,
R = number of times the same peak value appeared,
PL = half of the precision level (0.488 lb, 3.66 μin., and 122 μin. for 2,000-lb load cell, 0.015-in. maximum capacity horizontal deformation cartridge, and 0.5-in. maximum capacity vertical deformation cartridge, respectively), and
C = weighting factor (1, 2, and 7 for load, horizontal deformation, and vertical deformation, respectively).

This equation was developed from the comparison of peak values obtained from the data acquisition program and a Hewlett-Packard Model 7090A plotter. Average seating load was then calculated and subtracted from peak values of load.

To get the instantaneous and total deformation values, regression is done in three portions of the deformation curve:

1. Linear regression in the straight portion of the unloading path.
2. Regression in the curved portion that connects the unloading path and the recovery portion to yield the following hyperbolic equation:

$$Y = a + (b/X)$$

where

Y = deformation value,
X = time, and
a, b = regression constants.

3. Regression in the recovery portion between 40 and 90 percent of rest period to yield a hyperbolic equation. A tangent was drawn to this hyperbola at the point corresponding to 55 percent of rest period. The portion used for regression and the point for calculating a tangent were selected after examining deformation-versus-time curves from various test conditions.

Two linear equations, one from the unloading path and the other from the tangent of the hyperbola in the recovery period, are solved to determine the intersection. Then the point on the hyperbolic curve corresponding to the time coordinate of the intersection (for convenience, say Point A) is selected

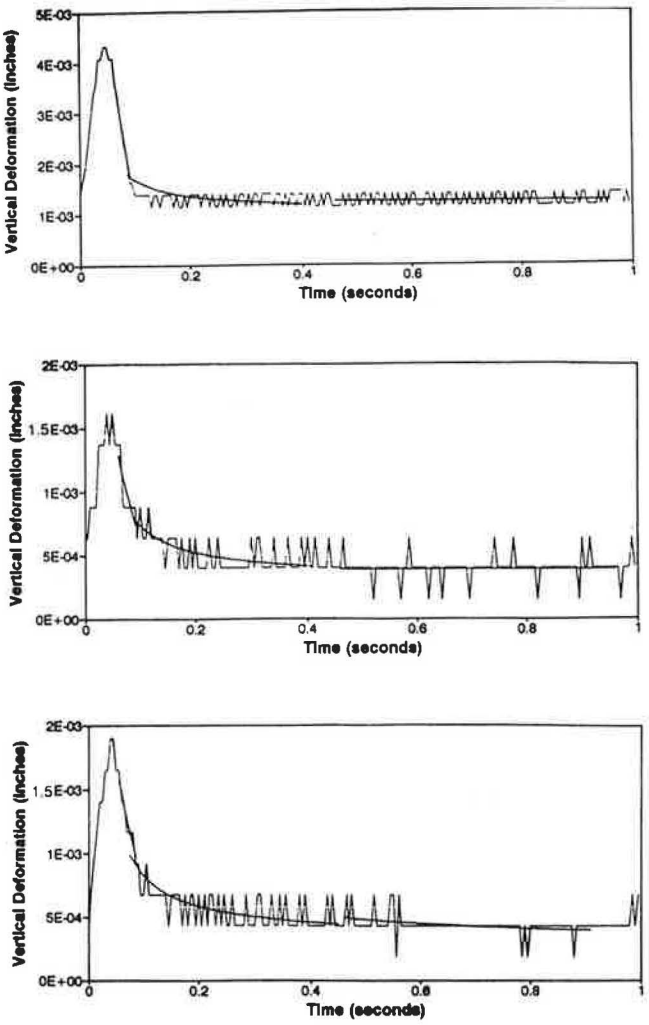

FIGURE 2 Actual vertical deformations and prediction from regression: *top*, N-core at 41°F; *middle*, O-core at 77°F; *bottom*, N-core at 104°F.

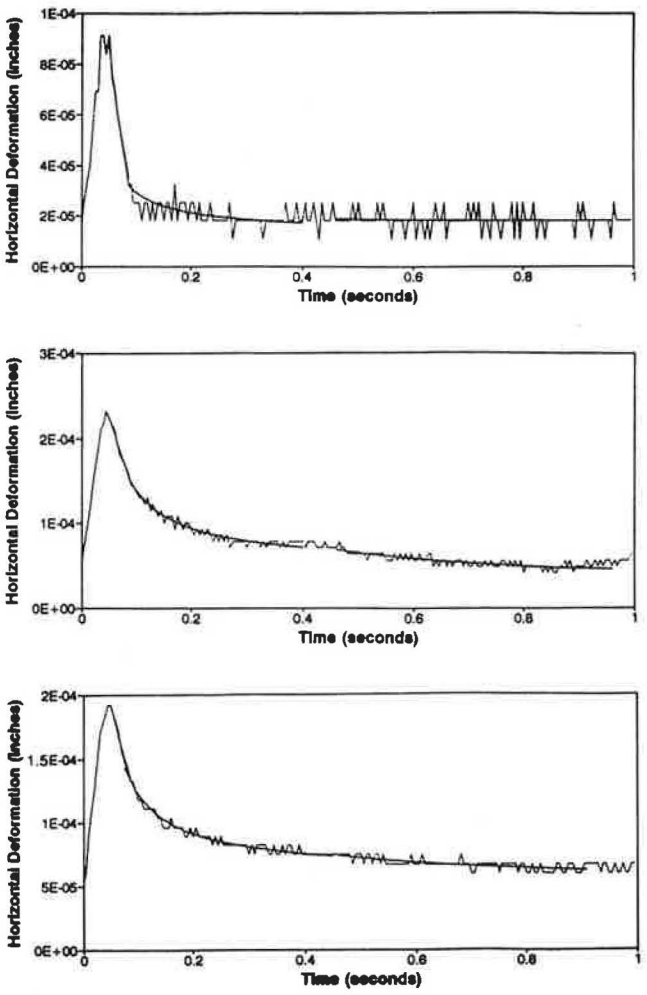

FIGURE 3 Actual horizontal deformations and prediction from regression: *top*, N-core at 41°F; *middle*, O-core at 77°F; *bottom*, N-core at 104°F.

to determine the instantaneous deformation by subtracting the deformation at Point A from the peak deformation. Subtracting the deformation value at the end of the rest period (calculated from the regressed hyperbolic equation) from the peak deformation yields the total deformation value.

The program was checked for random cases to see how accurately the regression equations fit the actual data. The comparison was very satisfactory in the region where the accuracy of the curves and lines was most significant. Some of the results at different testing conditions are shown in Figures 2 and 3. The equations in ASTM D4123 were used to calculate the resilient modulus and Poisson's ratio from the deformation measurements.

TEST RESULTS AND DISCUSSION OF RESULTS

Effect of Testing Axis

Results from the proficiency testing indicated that the M_R values were slightly higher along the diametral axis that was tested first as shown in Figures 4 and 5. Figures 4 and 5 present the total M_R values calculated from assumed and calculated Poisson's ratios, respectively. Comparison of Figures 4 and 5 revealed that the axis dependency became more significant when M_R values were determined from Poisson's ratios calculated from vertical and horizontal deformations than from assumed Poisson's ratios.

Fairhurst et al. (*2*) studied the change in M_R values based on calculated Poisson's ratios at different specimen rotations using laboratory-compacted specimens. It was reported that M_R values at a 0-degree specimen position were larger than those at 90 degrees. Since the 90-degree position was always tested after the initial 0-degree position, they suggested that the decrease in the M_R values at the 90-degree position could be due to internal damage done to the specimen during testing in the initial position.

The same data used in Fairhurst's paper were plotted in Figure 5 under the legend of "lab.specimens" with the M_R values from the field cores. The axis dependency from the field cores was not as prominent as that obtained by Fairhurst et al. (*2*). This might be a direct consequence of the load level applied. If higher load levels were used, damage would be more and hence the difference in M_R values would be larger.

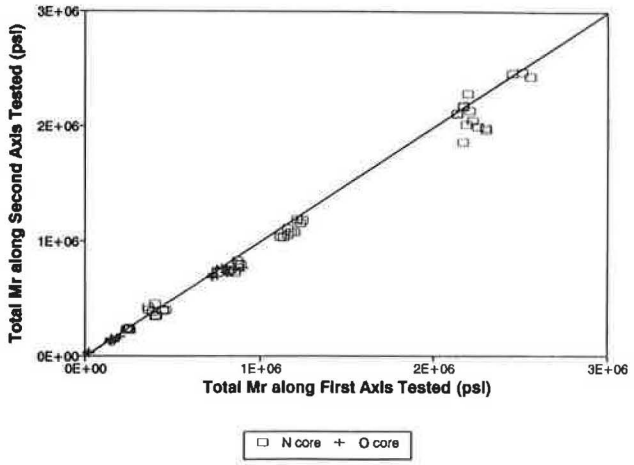

FIGURE 4 Axis dependency of M_R values from assumed Poisson's ratio.

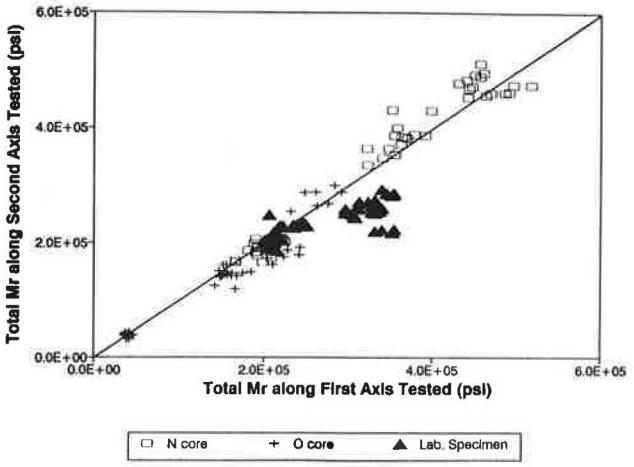

FIGURE 5 Axis dependency of M_R values from calculated Poisson's ratio.

It should be noted that SHRP P07 limits the load to 30, 15, and 5 percent of the indirect tensile strength at 77°F for testing temperatures of 41, 77, and 104°F, respectively, whereas the load level used in Fairhurst's paper was 20 percent of the indirect tensile strength at 73°F that was allowed in ASTM D4123. The load levels required by SHRP P07 probably yield less damage, hence causing less axis dependency. A sensitivity analysis must be done to determine whether these differences are significant in pavement design.

Effect of Rest Period

Several researchers have studied the effect of rest period on the resilient modulus of asphalt concrete (*3–5*). Terrel et al. suggested that the computed value of resilient modulus would depend on the rest period between the individual stress pulses as the asphalt mixes exhibit viscoelastic behavior (*4*). At low temperatures and short stress durations the dependency is not significant, but that is not the case with warm temperatures and long stress durations. For that case, the viscoelastic response should be included as a factor in the material characterization.

Monismith also stated that the rest period has a great influence on the value of resilient modulus because of the viscoelastic behavior of the asphalt concrete (*5*). However, it was suggested to be important to consider the ratio of the rest period (time OFF) to the time of loading (time ON), because it would directly affect the amount of recoverable strain and hence the resilient modulus. The smaller the ratio, the smaller will be the recoverable strain and hence larger the values of resilient modulus (Figure 6). This dependence is also temperature-dependent: dependence decreases with decrease in temperature.

Fairhurst et al. investigated the effect of cycle frequency which is directly related to the rest period duration on the magnitude of resilient modulus (*2*). The results indicated that M_R increased slightly with the shorter rest periods. This was not surprising, because shorter rest periods for the specimen between loading pulses resulted in less time for rebound strain and thus higher M_R values.

The results from the proficiency testing on cores indicated that there was very little effect of rest period on the values of resilient modulus as shown in Figure 7. In some cases the M_R values even increased slightly with increasing rest periods. The increase was seen more often in O-specimens than in N-specimens.

The apparent contradiction in the obtained results to the expectations can be easily explained. First, as is clear from Figure 6, the beneficial effect of rest period is not very significant after a certain time-OFF/time-On ratio (close to 8 in Figure 6). The time-OFF/time-ON ratios in the proficiency testing were 9, 19, and 29; therefore, we can expect very little effect of rest period. Second, the order of testing the specimens at different rest periods was in the direction of causing lesser damage; that is, the case in which the worst damage was expected (0.9-sec rest period) was tested before the case with minimum damage (2.9-sec rest period). This order of testing might have increased the fatigue damage as the test progressed, resulting in lesser recoverable deformation and a slight increase in the M_R values. All the observations made

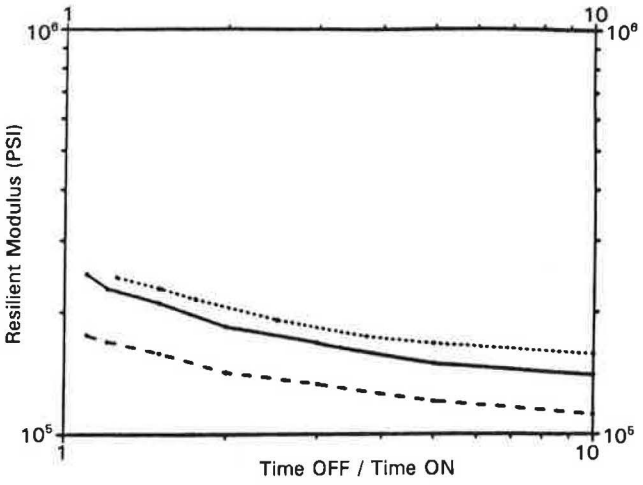

FIGURE 6 Influence of time interval between load applications on M_R determined in repeated loading in compression at 25°C: solid line = Specimen R7, Time ON = 1.0 sec; dashed line = Specimen R6, Time ON = 1.0 sec; dotted line = Specimen R6, Time ON = 0.4 sec (*5*).

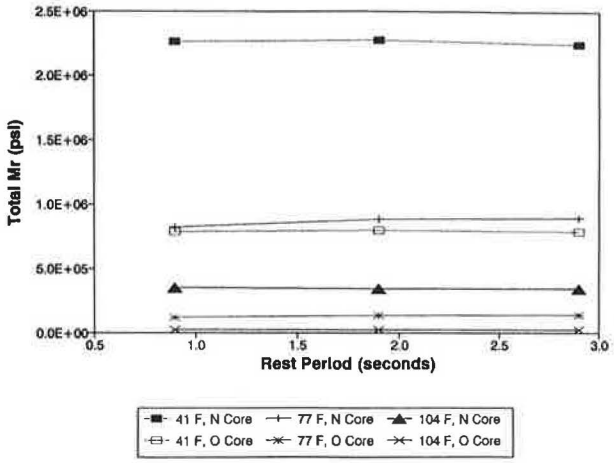

FIGURE 7 Effect of rest period on total M_R using assumed Poisson's ratio.

can explain the lack of a definite pattern in the effect of rest period on the M_R values.

Effect of Temperature

The role that the temperature plays in material response for pavements built with viscoelastic binders is the most significant variable affecting the choice of test and condition of test as well as the ultimate performance of the pavement. Kennedy et al. stated that the effect of temperature on pavement materials should be thought of not only in terms of high and low temperature but also in terms of the complete temperature range the pavement will experience (*6*). This may vary from −22 to 140°F. However, as far as resilient modulus is concerned, testing below the glass transition temperature, which ranges from −10 to 0°F, is not necessary.

Actual test data indicated that the resilient modulus depends a great deal on the temperature at which the specimen is tested (Figure 8). It was also observed by Cochran (*7*) and Furber (*8*) that with increase in temperature the resilient modulus decreases notably.

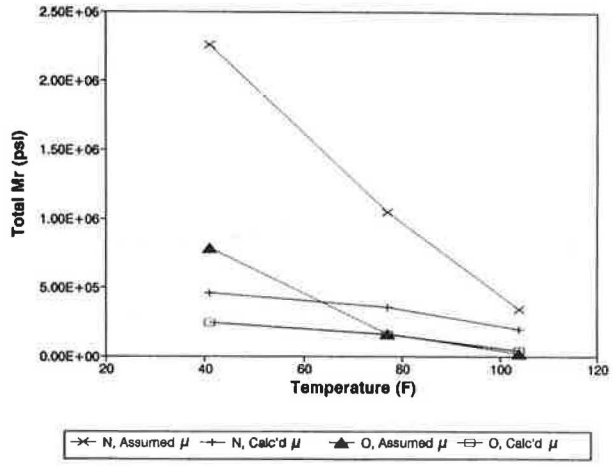

FIGURE 8 Effect of temperature on total M_R.

Effect of Poisson's Ratio

Figure 8 clearly demonstrates the magnitude of difference in the M_R values depending on whether assumed or calculated Poisson's ratio has been used in calculating the M_R values. The largest discrepancy occurred with N-cores at 41°F, the M_R from assumed Poisson's ratio being about five times the size of the M_R from calculated Poisson's ratio. Also the temperature susceptibility (tangential slope of M_R-versus-temperature curve) was lessened by using the calculated Poisson's ratio. Actual Poisson's ratio as determined from the total vertical and horizontal deformations was found to vary between negative values and 1.5 (Figure 9), which is definitely out of the theoretical range of 0 to 0.5 for elastic materials.

The significance of Poisson's ratio on M_R values has been reported by several researchers. From the experience of the Minnesota Department of Transportation (*7*), it was found that using the assumed value of 0.35 for Poisson's ratio resulted in 1.5 to 2 times higher values of resilient modulus than those obtained by using the "actual" Poisson's ratio calculated from measured horizontal and vertical deformations. Similar observation was made by Baladi and Harichandran, that the resilient moduli values with Poisson's ratio of 0.35 were different by as much as a factor of two or more than those with calculated Poisson's ratio (*9*).

Fairhurst et al. investigated the influence of temperature on Poisson's ratio and concluded that Poisson's ratio increased with increase in the temperature, which resulted in a decrease in M_R values (*2*). These results appear reasonable because the plastic portion of the asphalt binder increases with temperature. They concluded that Poisson's ratio near 0.5, the theoretical maximum for elastic materials, suggested that the applied load might be too high. Another interesting finding was that Poisson's ratio at the 90-degree position is slightly higher than that at 0 degrees. This could be due to a redistribution of the applied load into the region outside the center (as a result of the "weakened" central zone), causing greater overall horizontal deformation, hence a higher Poisson's ratio. These observations drew a conclusion that Poisson's ratio could serve as an indicator for excessive damage in the specimen during the resilient modulus testing.

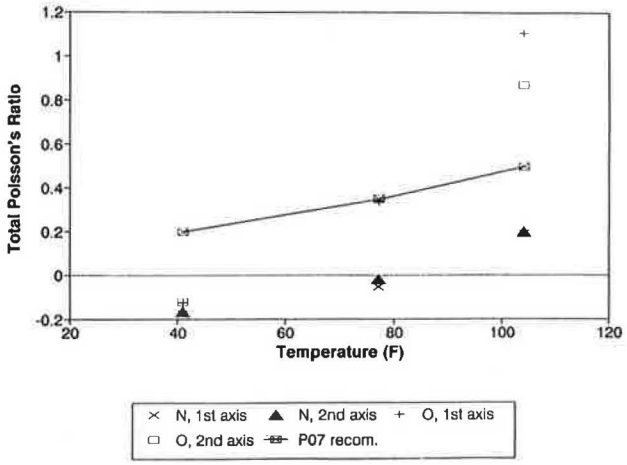

FIGURE 9 Poisson's ratio as function of temperature.

Vinson (*10*) concluded from a theoretical study using a finite element program that the increase in Poisson's ratio from 0.15 to 0.45 did not affect the results very much. It was also concluded that for a resilient modulus test performed under typical loading conditions (i.e., a steel–asphalt concrete interface) the resilient modulus with an assumed Poisson's ratio is more accurate because of induced shear stresses in the specimen. However, better results were obtained with calculated values of Poisson's ratio when a soft modulus material is placed between the steel platen and asphalt concrete.

McGee, however, concluded from the experimental study that resilient modulus values calculated with an assumed value of 0.35 have shown more scattering than those calculated by using calculated values (*11*). It has also been found that Poisson's ratio increases with increase in loading level, temperature, and asphalt content.

CONCLUSIONS

On the basis of the resilient modulus testing of field cores in accordance with the SHRP P07 procedure, the following conclusions were made:

1. The M_R values from the second axis testing were slightly smaller than those from the first axis testing. The load levels recommended by SHRP P07 seemed to reduce the testing axis dependency significantly by minimizing the damage from the first axis testing.
2. The effect of rest period was not significant for the loading history required by SHRP P07 (0.1-sec loading with 0.9-, 1.9-, and 2.9-sec rest periods).
3. The resilient modulus decreased as temperature increased. The temperature dependency of the M_R values were reduced when the M_R values were calculated from the calculated Poisson's ratios.
4. The most influencing parameter on the M_R values was Poisson's ratio. The discrepancies in M_R values due to the testing axis dependency and different lengths of rest periods were almost negligible compared to the magnitude of difference in the M_R values from assumed and calculated Poisson's ratios.

ACKNOWLEDGMENTS

The authors are grateful to NCHRP for its support and sponsorship of this research. Special thanks are due to G. Steele for his most constructive information.

REFERENCES

1. Y. R. Kim, N. P. Khosla, and N. Kim. Effect of Temperature and Mixture Variables an Fatigue Life Predicted by Diametral Fatigue Testing. In *Transportation Research Record 1317*, TRB, National Research Council, Washington, D.C., 1991.
2. C. E. Fairhurst, Y. R. Kim, and N. P. Khosla. Resilient Modulus Testing of Asphalt Specimens in Accordance with ASTM D4123-82. *Proc. 4th International RILEM Symposium*, Budapest, Hungary, Oct. 1990.
3. F. P. Bonnaure, A. H. J. J. Huibers, and A. Boonders. A Laboratory Investigation of the Influence of Rest Periods on the Fatigue Characteristics of Bituminous Mixes. *Proc., Association of Asphalt Paving Technologists*, Vol. 51, Kansas City, Mo., 1982.
4. R. L. Terrel, I. S. Awad, and L. R. Foss. *Techniques for Characterizing Bituminous Materials Using a Versatile Triaxial Testing System*. ASTM Special Technical Publication 561. ASTM, Philadelphia, Pa., 1974.
5. C. L. Monismith. Resilient Modulus Testing: Interpretation of Laboratory Results for Design Purposes. *Proc., Workshop on Resilient Modulus Testing*, Oregon State University, Corvallis, 1989.
6. T. W. Kennedy, T. D. White, and J. A. Epps. Use of Material Tests and Pavement Design Procedures to Evaluate New Paving Binders. In *Properties of Flexible Pavement Materials*. ASTM Special Technical Publication 807 (J. J. Emery, ed.). ASTM. Philadelphia, Pa., 1983.
7. G. R. Cochran. Minnesota Department of Transportation Experience with Laboratory MR Testing. *Proc., Workshop on Resilient Modulus Testing*, Oregon State University, Corvallis, 1989.
8. A. B. Furber. Strain and Temperature Effects on Resilient Moduli. *Proc., Workshop on Resilient Modulus Testing*, Oregon State University, Corvallis, 1989.
9. G. Y. Baladi and R. S. Harichandran. Asphalt Mix Design and the Indirect Test: A New Horizon. In *Asphalt Concrete Mix Design: Development of More Rational Approaches*. ASTM Special Technical Publication 1041 (W. Gartner, Jr., ed.). ASTM, Philadelphia, Pa., 1989.
10. T. S. Vinson. Fundamentals of Resilient Modulus Testing. *Proc., Workshop on Resilient Modulus Testing*, Oregon State University, Corvallis, 1989.
11. N. McGee. Laboratory MR Investigation of 2331 Mix. *Proc., Workshop on Resilient Modulus Testing*, Oregon State University, Corvallis, 1989.

NCHRP Asphalt-Aggregate Mixture Analysis System

HAROLD L. VON QUINTUS, CHUCK S. HUGHES, AND JAMES A. SCHEROCMAN

A summary of the procedures for an asphalt-aggregate mixture analysis system (AAMAS) developed under NCHRP Project 9-6(1) is provided. Most of the information is documented and reported in *NCHRP Report 338*. The implementation process of the AAMAS procedure is reviewed, and some of the problems that can be incurred regarding the field control of asphalt concrete mixtures being designed by the AAMAS process are discussed.

The asphalt-aggregate mixture analysis system (AAMAS) research project, NCHRP Project 9-6(1), was initiated because AASHTO realized the importance of tying mixture design to structural design and pavement performance variables (*1*). Project 9-6(1) was completed in three phases. The first phase (completed in October 1986) was concerned with evaluating the feasibility for the development of an AAMAS. Phase I identified the primary forms of pavement distress (associated with both load and environment), evaluated current testing and mixture design procedures, and identified new or modified laboratory procedures to be considered in the development of the AAMAS. Items that the Phase I concept emphasized included mixture preparation, conditioning, testing, and analyzing asphalt concrete specimens to duplicate field conditions. Tests to measure the engineering properties of asphalt concrete mixtures for estimating pavement performance were also included and discussed.

Phases II and III were concerned with developing procedures for the AAMAS concepts and tying structural design to mixture design. This project emphasized compatibility between mixture design and structural design, including the AASHTO design manual. Phase II (completed in February 1989) included the initial development work, and Phase III included follow-up field studies and conversion of the AAMAS into a mixture design procedure. Phase III was completed in May 1990, and the final report for this project was published in March 1991. In summary, Project 9-6(1) resulted in the development of an AAMAS for evaluating dense-graded asphalt concrete mixtures proposed for use primarily on high-volume roadways and in a mixture design procedure based on performance-related criteria. These criteria are compatible with the recommendations from NCHRP Project 1-26 (*2*).

H. L. Von Quintus, Brent Rauhut Engineering, Inc., 8240 MoPac, Suite 220, Austin, Tex. 78759. C. S. Hughes, Virginia Transportation Research Council, P. O. Box 3817, University Station, Charlottesville, Va. 22903. J. A. Scherocman, 11205 Brookbridge Drive, Cincinnati, Ohio 45249.

The fourth phase of this evolutionary process was initiated through a series of four 2-day workshops sponsored by FHWA. The purpose of these workshops was to review the current procedures and obtain input and information from state highway agencies (SHAs) on problems with the use of AAMAS to design and evaluate asphalt concrete mixtures in their specific laboratories (*3*). These workshops have been completed.

AAMAS OVERVIEW

Mixture Design and Evaluation

AAMAS consists of three basic laboratory steps. The first step is simply the initial mixture design phase, which is accomplished with current mixture design procedures or with the procedure based on the AAMAS concept (i.e., performance-related criteria). The mixture design procedure using the AAMAS concept is included in Part I of *NCHRP Report 338* (*1*). An agency can use either the AAMAS approach or its own current procedure to determine the design asphalt content and job mix formula. The performance-related mixture design procedure using the AAMAS approach is a scaled-down version of AAMAS; it was formulated considering implementation and production factors in SHA laboratories.

Once an initial mixture design has been completed, these materials are mixed, compacted, and conditioned in the second step. This step includes age-hardening simulations (both for production and for the environment), moisture conditioning, and traffic densification. This second step is the mixture compaction and conditioning phase.

After the materials have been mixed, compacted, and conditioned, the specimens are tested in the third step to measure critical mixture properties. This third step provides the data that can be integrated into pavement design and analysis models to predict pavement performance. This third step is the mixture evaluation phase; it is compatible with results from NCHRP Project 1-26 (*2*). The mixture evaluation phase includes the laboratory testing and performance evaluations.

Procedural Manual

These three steps are integrated in the procedural manual for mixture design and evaluation. The procedural manual (*1*, Part I) is divided into four sections. Figure 1 shows the current AAMAS procedure in flow-chart form, identifying

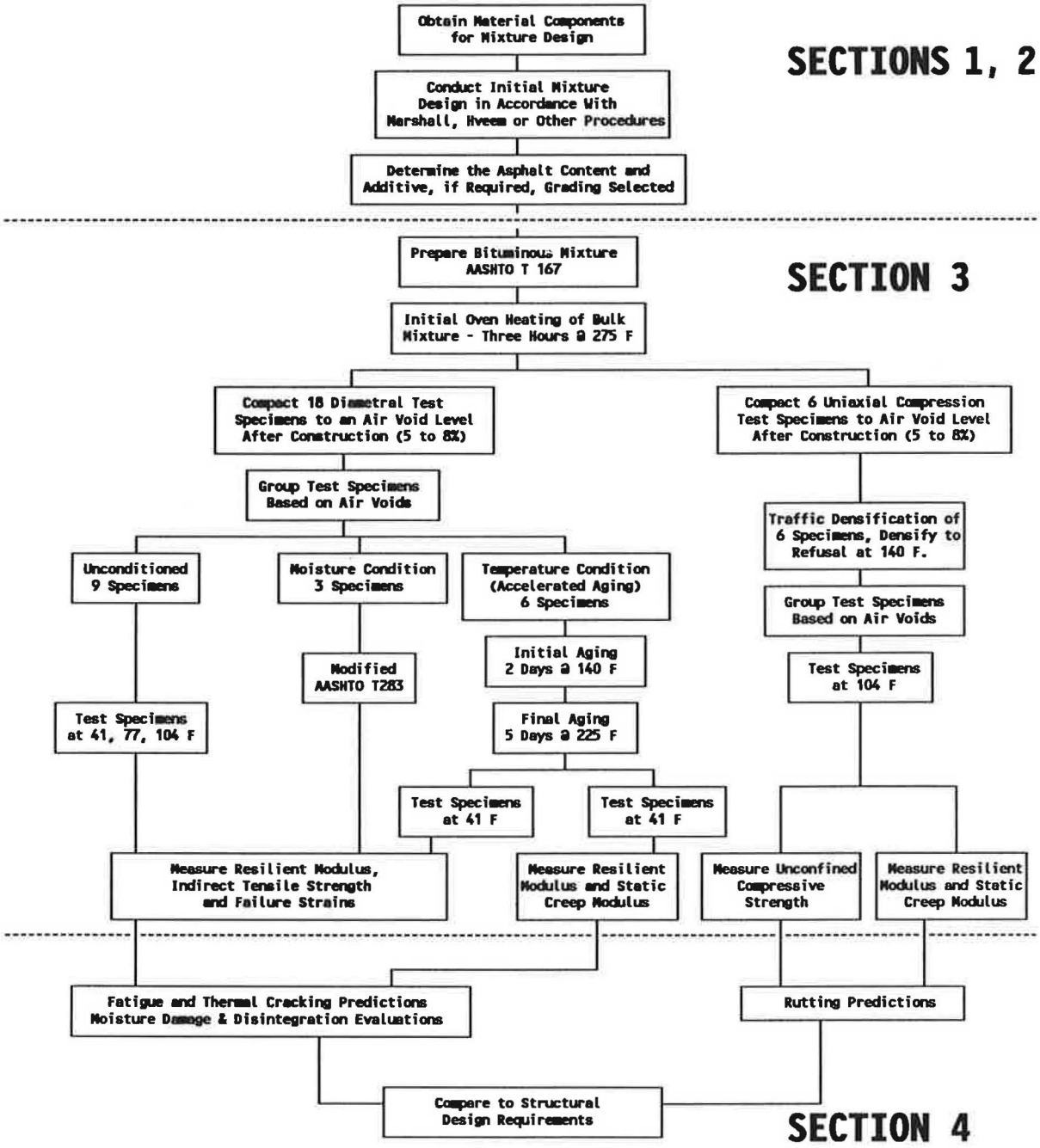

FIGURE 1 Flow Chart for AAMAS.

the four sections; Table 1 summarizes the approximate time required for the laboratory compaction, conditioning, and testing of asphalt concrete mixtures. Section I provides criteria and values recommended for selecting the mixture components, and Section II presents the procedures used to design dense-graded asphalt concrete mixtures. Figure 2 shows the mixture design procedure (including Sections I and II) in flowchart form. Section III, the mixture analysis section, includes procedures for preparing, conditioning, and testing specimens for measuring properties required for structural design and evaluation. Section IV, the mixture performance evaluation, discusses mechanistic-empirical models used to evaluate asphalt concrete pavements.

PARAMETERS AND TESTS INCLUDED IN AAMAS

Pavement Distress

Distresses selected for incorporation into AAMAS include rutting, fatigue cracking, low-temperature cracking, and

TABLE 1 Summary of Approximate Time Required for Laboratory Compaction, Conditioning, and Testing of Asphalt Concrete Mixtures Using AAMAS

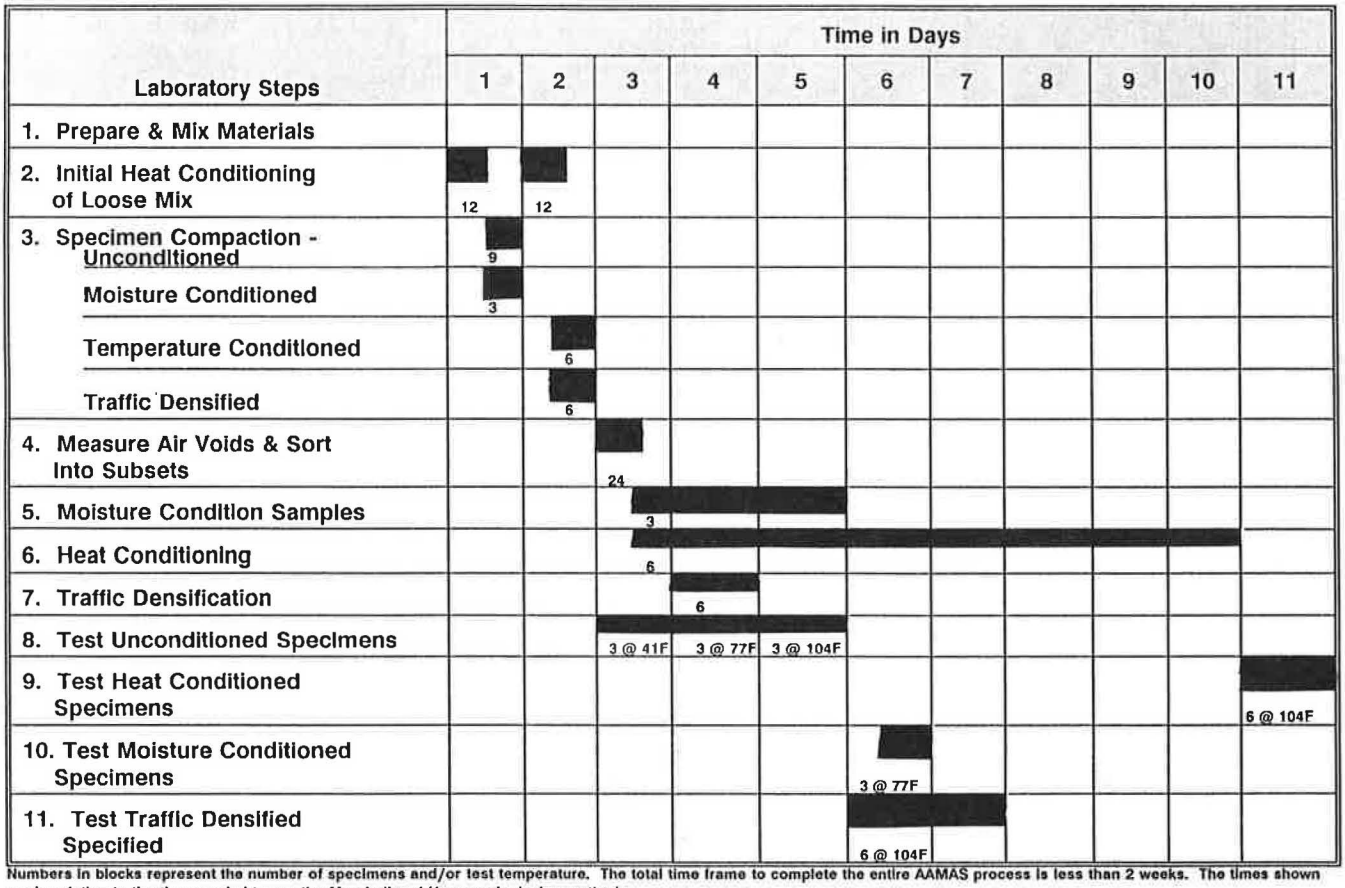

Numbers in blocks represent the number of specimens and/or test temperature. The total time frame to complete the entire AAMAS process is less than 2 weeks. The times shown are in relation to the time needed to run the Marshall and Hveem mix design methods.

moisture damage. Secondary consideration is given to raveling or disintegration and loss of skid resistance.

Mixture Tests

To evaluate in the laboratory how asphalt concrete mixtures will perform under traffic and the environment, a review and a study of various test procedures were conducted. To design mixes for preventing the aforementioned distresses, it is necessary to use a test that measures the engineering properties and characteristics of the asphalt concrete mixture that are related to the distress or performance measure. Tests were selected on the basis of simplicity, efficiency, reliability, reproducibility, and sensitivity of mixture variables. Special consideration was given to sample size. For AAMAS to be useful and applicable for a range of mixtures, the test procedures and equipment must be capable of preparing and testing different size specimens that are compatible with the aggregates used in the mix.

Five tests are used as tools for mixture evaluation in AAMAS. These tests are the static cylindrical (unconfined compression) creep and recovery test, the diametral resilient modulus test, the indirect tensile strength test, the indirect tensile creep and recovery test, and the gyratory shear test. The compressive strength of the mix is also measured in accordance with the creep and recovery compressive test.

The AAMAS program requires a combination of laboratory tests and conditioning procedures to evaluate the behavior and performance characteristics of asphalt concrete mixtures. All factors considered, tensile strain at failure, gyratory shear strength, and creep are the properties most useful for evaluating and comparing different mixtures. Resilient modulus is required, but only because of its incorporation into the AASHTO design guide. Thus, tensile strain at failure, creep, resilient modulus, and gyratory shear strength are used to ensure that the mixture, as placed, will satisfy the structural design requirements.

Initial Mixture Design Optimization Guidelines

Guidelines are provided for selecting an aggregate blend and selection of an initial asphalt content for optimizing the mixture's performance on the basis of predictions of fatigue cracking, rutting, and thermal cracking. The program ASPHALT (*4*) was found to be a good tool for selecting the "seed" asphalt content in mixture design and theoretically determining the relationship between asphalt content and air void. In addition, correlations were performed between the engineering prop-

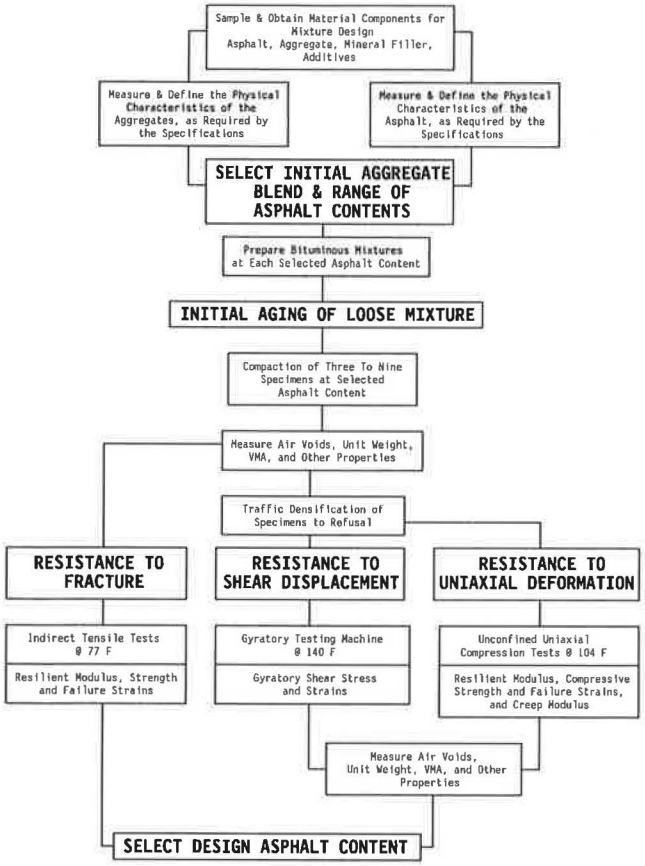

FIGURE 2 Flow chart for design of dense-graded asphalt concrete mixtures.

erties and factors normally considered during mixture design. From these analyses, it was found that the product of voids filled with asphalt (VFA) and aggregate diameter were related to work, VFA was related to tensile strain at failure, and voids in mineral aggregate (VMA) was related to indirect tensile strength. Through these correlations, an initial asphalt content and aggregate gradation are selected before any mechanical tests are performed. Using the distress functions suggested in NCHRP Project 1-26, criteria for mixture optimization and adequacy have been presented for a range of traffic and environmental conditions in the procedural manual.

Mixture Performance Evaluation

No consensus exists on the proper mathematical models to use for predicting the behavior and performance of asphalt concrete mixes. Such models are being developed by other researchers under additional NCHRP contracts. Further, the Strategic Highway Research Program (SHRP) is to conduct research work in this same area under Contracts A-005 (Performance Models and Validation of Test Results) and A-001 (Development of Performance-Based Specifications for Asphalt-Aggregate Mixtures). These research efforts, however, will not be completed until 1993. Thus, the types of performance relationship recommended by NCHRP Project 1-26 were used to evaluate the mixture's response to loads. Models are included to predict fatigue cracking, rutting, moisture damage, and low-temperature cracking.

LABORATORY PREPARATION AND CONDITIONING PROCEDURES

Plant-Hardening Simulation

To determine the plant-hardening simulation, the penetration and viscosity values of plant-produced material were compared to those conditioned (or aged) in the laboratory. The thin-film oven test (TFOT) at 285°F appeared to do a reasonable job of matching the asphalt cement characteristics (penetration and viscosity value) after mix production. Thus, the TFOT is used to predict the physical characteristics of the asphalt after mix production, when there is no historical data on binder aging through a mix plant.

The virgin asphalt cement is mixed with the aggregate blend and the loose mix placed in a forced-draft oven set at 275°F (or the expected mix discharge temperature from the plant) for 3 hr. After the first 1.5 hr, the mixture is removed from the oven and remixed by hand and replaced in the oven for the final 1.5 hr. The exact time the mixture is in the forced-draft oven can be determined from extraction tests of different samples aged at different times (2, 4, 8, 12, and 24 hr). The time selected is that which will age or harden the liquid asphalt to the penetration and viscosity values measured from the TFOT at 285°F or to the actual binder properties after mix production.

Mixture Compaction

Compaction was one of the critical factors studied in preparing samples for laboratory evaluation. From an evaluation and comparison of field cores and laboratory-compacted specimens, it was found that specimens compacted with the gyratory shear compactor more consistently matched the engineering properties measured on field cores. Thus, the gyratory shear compactor was the device included in the procedural manual.

Two methods of compaction are written into the procedure. One uses the U.S. Army Corps of Engineers' gyratory testing machine (GTM; ASTM D3387), and the other method uses the Texas gyratory shear compactor (ASTM D4013). The GTM is the preferred device, because angle of gyration, specimen height (an estimate of the decrease in air voids), and the mixture's resistance to compaction can be monitored with each revolution.

Moisture Conditioning

Another critical item was moisture conditioning or moisture damage evaluation. Two procedures were used to evaluate the moisture susceptibility of asphalt concrete mixtures. These were the modified Lottman procedure, or AASHTO T283, and the procedure documented in *NCHRP Report 246*, or the Lottman procedure. The Lottman procedure recommended in *NCHRP Report 246* consistently showed a more severe

conditioning and testing technique. However, a version of the modified Lottman procedure was used in AAMAS, because of the concern that the procedure in *NCHRP Report 246* is too severe and unduly damages the specimens before testing. In summary, a vacuum of 26 in. of mercury is applied to the specimen for 15 min, the sample is frozen for 16 hr and placed in a 140°F water bath for 24 hr, and then it is tested. The test temperature of the procedure is 77°F, and a loading rate of 2.0 in./min is used, which are consistent with the other tests used in AAMAS. The moisture-conditioned test specimens are compacted to the air void level immediately after construction.

Environmental Aging Simulation

A long-term age-hardening simulation procedure was also developed. However, the change in physical properties of the asphalt and mixture were available for the AAMAS test sections only over a short time period. The pavements were cored twice: immediately after placement and 2 years after placement. The recommended procedure is to place compacted specimens in a forced-draft oven set at 140°F for 2 days. The specimens are then rotated, the oven's temperature is increased to 225°F, and the specimens are left in the oven for additional 5 days.

These heat-conditioned specimens are then used for measuring the resilient modulus, indirect tensile strength, strain at failure, and indirect tensile creep at 41°F. These test specimens are also compacted to the air void level immediately after construction.

Traffic Densification

Asphalt concrete mixtures densify under traffic. To simulate that densification process and its effect on the mixture's properties, specimens that had been compacted in the laboratory to an air void content similar to that of the field specimens were further compacted to a refusal density. This additional densification was accomplished using the Corps of Engineers' GTM. The initially compacted specimens are cooled to 140°F (60°C) and then compacted further in the GTM gyratory device. Initial sample height readings were obtained before the refusal densification and again after each 25 to 50 revolutions of the machine. The compaction process is stopped when the mixture's resistance reduces excessively or when there is an excessive increase in the angle of gyration.

If the Corps of Engineers' GTM is unavailable, the procedure manual suggests that the Texas gyratory shear compactor be used. With the use of this device, however, the traffic densification process continues immediately after initial compaction (i.e., the temperature is not reduced and the mold stays in the compaction machine).

LABORATORY TEST PROCEDURES

Resilient Modulus Test

One of the primary test methods considered in the AAMAS study was the repeated-load resilient modulus test, because of its tie to the AASHTO design guide. ASTM D4123 (Indirect Tension Test for Resilient Modulus of Bituminous Mixtures) was the primary test procedure used. Three test temperatures are used: 41, 77, and 104°F (5, 25, and 40°C). The secondary test method for resilient modulus is a modification of ASTM D3497 (Dynamic Modulus of Asphalt Mixtures); it is used as the conditioning procedure for all uniaxial compressive type tests. The differences or modifications are that a rest period of 0.9 sec was used with a 0.1-sec load pulse and that both the instantaneous and total resilient moduli were calculated.

Indirect Tensile Strength and Failure Strain Test

The indirect tensile strength and failure strain are determined using a test method derived from ASTM D4123 (Indirect Tension Test for Resilient Modulus of Bituminous Mixtures). The actual test procedure used is published in the AAMAS final report (*1*). The test is conducted at the same three temperatures as the resilient modulus test: 41, 77, and 104°F (5, 25, and 40°C). The loading rate used at 41°F is 0.05 and 2.0 in./min (1.27 and 50.8 mm/min); a rate of 2 in./min (50.8 mm/min) is used only at 77 and 104°F (25 and 40°C). These data are used in the fatigue cracking evaluation.

Indirect Tensile Creep and Recovery Test

The indirect tensile creep and recovery test is conducted on field cores and on laboratory-compacted specimens. This test is conducted in accordance with a procedure published in the AAMAS final report. In summary, a static load of fixed magnitude is applied along the diametral axis and the horizontal displacement measured over a 60-min loading duration. After the fixed load is removed, the resilient strain is also measured over 60 min. The indirect tensile creep and recovery test is performed at a test temperature of 41°F for use in the low-temperature cracking evaluation.

Uniaxial Unconfined Compression Creep and Recovery Test

Laboratory-compacted test specimens, which are a minimum of 4 in. in diameter and 4 in. high, are tested in uniaxial compression. A static load of fixed magnitude is applied along the cylindrical axis of an asphalt concrete specimen for a set amount of time. The total axial (compressive) deformation response of the specimen is measured and used to calculate the creep compliance at particular durations of time. After the fixed load is released, the resilient deformation is also measured over a set amount of time. Although the test can be conducted with confining pressure on the specimens, all testing for the AAMAS project was completed without the use of confining pressures. For the AAMAS testing, the loading and unloading times are both 60 min and the data are used in the rutting evaluation.

The unconfined compressive strength test is also performed on a few specimens at 104°F to calculate the compressive strain

at failure. This failure strain is used to set a limiting value for the allowable permanent deformation in the rutting evaluation for the mix being tested.

AAMAS MIXTURE DESIGN PROCEDURE

Selection of Mixture Components

The program ASPHALT (*4*) is used as a starting point to select a gradation and the seed asphalt content for that gradation. ASPHALT provides a theoretical relationship between asphalt content, VMA, air voids, and film thickness for a specific aggregate blend or gradation. Mixture is prepared in the laboratory at the seed asphalt content, as well as two asphalt contents above and two below this seed value.

Initial Heat Conditioning of Loose Mix

Mixture at each of the asphalt contents is aged in a forced-draft oven using the procedure previously discussed (i.e., placing a mix in the oven at 275°F for 3 hr).

Compaction

Specimens are compacted at each asphalt content using ASTM D3387, if the Corps of Engineers' GTM is available, or ASTM D4013 at a specified compactive effort. Three indirect tensile specimens per asphalt content are compacted at an air void level anticipated after construction (i.e., 6 to 8 percent), and a minimum of three uniaxial compression test specimens per asphalt content are used in the traffic densification procedure or compacted to the refusal density (i.e., no increase in density with additional compactive effort). The design air void level for the refusal density is 3 percent or greater.

Mixture Testing

Three specimens at each asphalt content are initially tested for resistance to fracture (Figure 2). Indirect tensile resilient moduli and strength tests are performed on the same sample to define the initial allowable range of asphalt contents to meet the design criteria for resistance to fracture.

Gyratory shear tests are run with the GTM during the traffic densification procedure to ensure that minimum design requirements for shear are met (i.e., resistance to shear). For mix design, a minimum shear value of 54 is used in the procedure.

Uniaxial compression creep and recovery tests are performed on specimens compacted to the refusal density. The uniaxial compression creep and recovery test is used to ensure that the design value will satisfy the deformation criteria (i.e., resistance to deformation). The minimum creep modulus value used for design is dependent on the pavement structure. Figures 3 and 4 are included in the procedural manual for presenting the mixture design data.

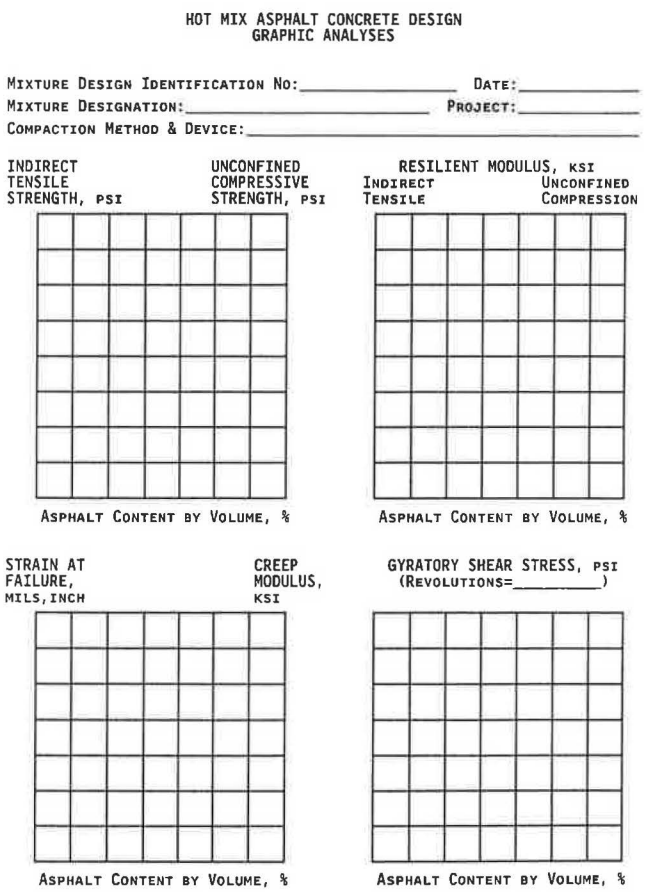

FIGURE 3 AAMAS graphical presentation of mixture design data for engineering properties.

Allowable Range of Asphalt Contents

The allowable range of asphalt contents for the specific aggregate gradation is defined as being those values that are within the minimum and maximum limits as established by the fatigue, shear, and deformation criteria. Figure 5 is a graphical summary of the mixture design test for selecting the design asphalt content and an allowable tolerance. These criteria include a minimum creep modulus for different structures, minimum gyratory shear strength, and minimum tensile strain at failure for fatigue. Figure 6 illustrates the minimum fatigue criteria.

AAMAS MIXTURE EVALUATION

Initial Heat Conditioning of Loose Mix

The mixture is aged in a forced-draft oven using the procedure previously discussed (i.e., placing the mixture in the oven at 275°F for 3 hr).

Compaction

After initial heat conditioning, eight sets of three specimens are compacted. Eighteen specimens are compacted to be used

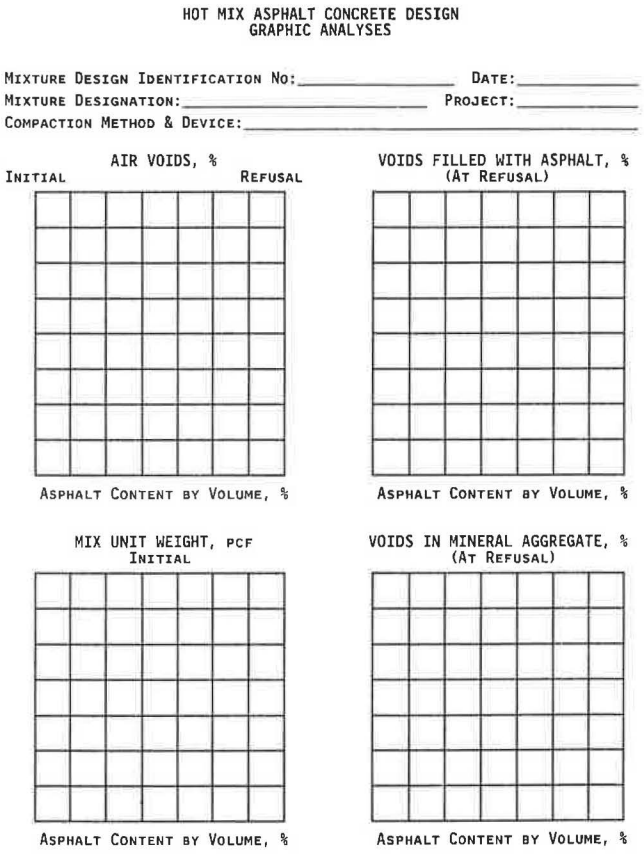

FIGURE 4 AAMAS graphical presentation of mixture design data for compaction properties.

for indirect tensile testing and six specimens to be used for uniaxial compression type testing. All specimens are compacted using the GTM because of its ability to monitor changes in mixture behavior with a reduction in air voids. If the GTM is unavailable, the specimens can be compacted using the Texas gyratory shear compactor.

All specimens are initially compacted to the air void level specified immediately after construction. Of the 18 specimens compacted for indirect tensile testing, 9 are unconditioned, 6 are conditioned by the accelerated aging technique, and 3 are moisture-conditioned. The six uniaxial compression specimens are all unconditioned and used in the traffic densification procedure.

Grouping by Air Voids

Before conditioning and testing, all specimens are grouped in sets of three by air voids. The intent is to have both the average air voids and standard deviation of air voids between the different sample sets as close as possible.

Moisture Conditioning

Three specimens are moisture-conditioned in accordance with a modification of AASHTO T283, with the exception that the test procedure is at 77°F and a loading rate of 2 in./min is used.

Accelerated Aging

Six indirect tensile specimens are used for accelerated aging for the low-temperature cracking evaluation. These specimens

	ASPHALT CONTENT BY TOTAL VOLUME, %						
ENGINEERING PROPERTIES							
Total Resilient Modulus (Layer Coefficients)							
Tensile Strain at Failure and Total Resilient Modulus							
Gyratory Shear Stress and Shear Index							
Creep Modulus							
COMPACTION PROPERTIES							
Aggregate Unit Weight							
Final Air Voids, %							
VMA (Porosity), %							
VFA (Degree of Saturation), %							
Allowable Range of the Design Asphalt Content							
	ASPHALT CONTENT BY TOTAL WEIGHT, %						

FIGURE 5 Worksheet for summarizing test results and selecting design asphalt content and tolerance.

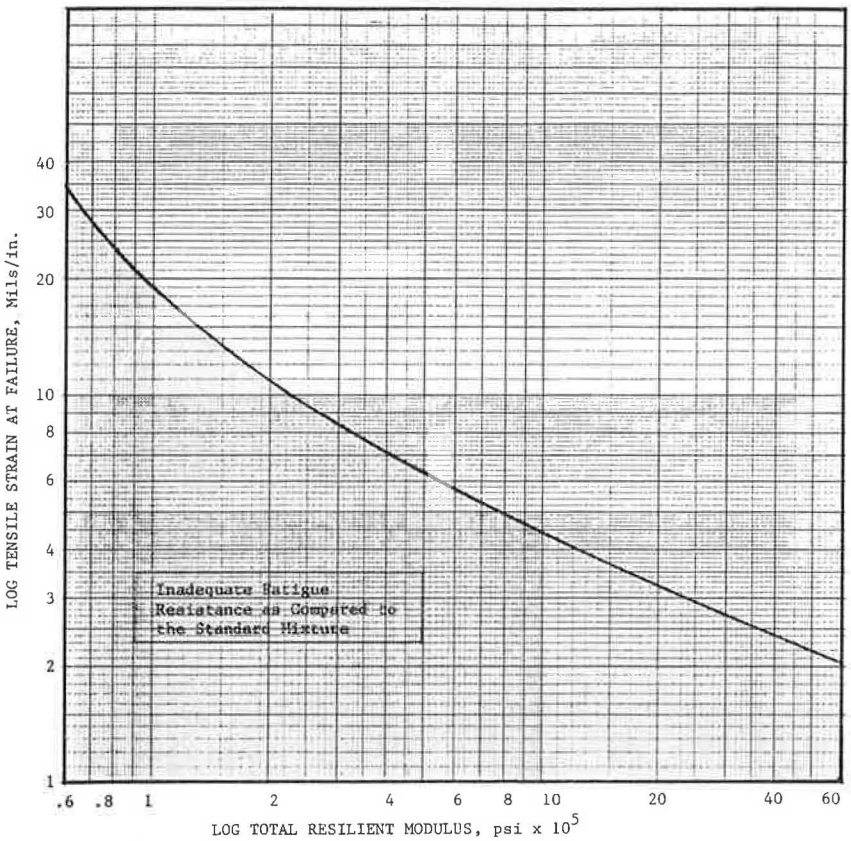

FIGURE 6 Minimum tensile strains at failure required for mixture as function of total resilient modulus as measured by indirect tensile testing techniques.

are aged using the procedure previously discussed (i.e., placing the specimens in a forced-draft oven at 140°F for 2 days, then elevating the oven's temperature to 225°F for an additional 5 days of aging).

Traffic Densification

The six uniaxial compression specimens previously compacted are all used in the traffic densification process. The temperature of these specimens is reduced to 140°F. The specimens are then placed in the GTM, and additional compactive effort is applied to achieve the refusal density of the mix. The gyratory shear stress and sample height are monitored with a number of gyrations during this densification process.

If the GTM is unavailable, specimens are compacted using the Texas gyratory shear compactor to the refusal density or air void content during initial compaction. In other words, the six specimens are compacted to the refusal density for uniaxial compression testing at the initial compaction temperature.

Mixture Testing

The repeated-load indirect tensile resilient modulus test is performed on all unconditioned and conditioned specimens (18 specimens). The indirect tensile strength and failure strains are measured on all unconditioned and moisture-conditioned specimens, and one set of accelerated age specimens (15 specimens). The indirect tensile creep and recovery test is performed on the second set of accelerated age specimens (three specimens). These tests are performed on the specimens as previously discussed and used to predict fatigue and low-temperature cracking.

The uniaxial compression specimens are used to predict rutting and distortion type failures from the uniaxial compressive resilient modulus, unconfined compressive strength and failure strain, and compression creep and recovery tests. The repeated-load uniaxial compression resilient modulus is measured on all traffic-densified specimens at 104°F (six specimens). The unconfined compressive strength is measured on one set of traffic-densified specimens and the compressive creep and recovery measured on the other set of specimens.

Mixture Performance Evaluation

For the fatigue cracking evaluation, the total resilient modulus and tensile strain at failure are used for mixture evaluation. These two values are measured on the unconditioned specimens are 41, 77, and 104°F. These values can be used to generate a fatigue cracking curve or can be compared to the results for a "standard" mixture, as graphically illustrated in Figure 6.

For thermal cracking, the test results from the indirect tensile strength and creep and recovery tests on the accelerated age specimens are used to define the critical temperature

change at which cracking can be expected to occur. The creep and recovery tests results are used to evaluate and determine the creep modulus at the lower testing temperature.

For the moisture damage evaluation of the mixture, the tensile strength ratio, the resilient modulus ratio, and the tensile strain at failure ratio are used to evaluate the mixes' susceptibility to moisture damage.

For rutting evaluation, three tests are performed on the traffic-densified specimens. These are the repeated-load resilient modulus, the unconfined compressive strength, and the compressive creep and recovery tests. The uniaxial compression creep and recovery test is used to evaluate the rutting potential of each mixture, as shown by an example in Figure 7. It can also be used to estimate the expected level of rutting to occur in the pavement for each of the asphalt concrete layers. The unconfined compressive strength and resilient moduli are used to set limiting criteria for the mix under specific loading conditions for the pavement and environment.

IMPLEMENTATION

It should be recognized and understood that implementing the AAMAS concepts and methodology will not be a quick process because most of these tests and evaluation procedures are unfamiliar to some SHA personnel. Therefore, it becomes very important that each agency take a systematic approach in reviewing the AAMAS concept when considering its implementation.

It is obvious that many of those tests previously discussed are not adaptable or practical for the use of field control of mixtures. However, other fundamental properties of the mixture are adaptable to field control. These are the indirect tensile strength and unconfined compressive strength. There are relationships, which are mixture-dependent, between strength properties and those used in AAMAS to evaluate mixture performance.

The evaluation and implementation of the AAMAS concepts for the design and control of asphalt concrete mixtures

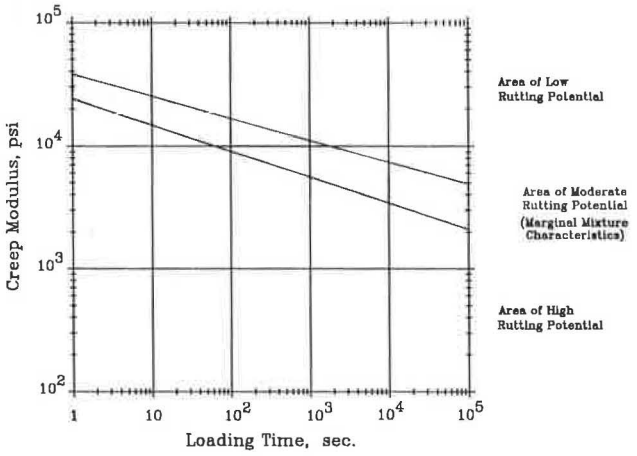

FIGURE 7 Asphalt concrete mixture rutting potential for surface layers of asphalt concrete pavements.

still requires that many questions be answered about the policies of different agencies. A few of these are listed as follows:

- Are the AAMAS tests practical or adaptable for field control variables? For example, what length of time is required to run the test and analyze the results? Many contractors can place 2,000 to 3,000 tons of asphalt concrete a day. It would be highly advantageous that the results of quality control and acceptance tests be obtained within a short time period. Additionally, some of the more sophisticated tests may require that the expertise of field and laboratory personnel be upgraded from present levels, both for the contractor and for SHA personnel.
- Can the AAMAS concepts be readily implemented where different organizations are responsible for mix design? For example, some SHAs require that contractors or consultants conduct the mixture designs; others are responsible for mix design themselves. In some cases, this may prevent smaller contractors from competing on smaller projects, because they do not have the financial backing to purchase the equipment.
- Is the AAMAS compaction, conditioning, and testing equipment practical for the field control of mixtures? If one device is used in the laboratory for mixture design and another device used in the field, equivalency factors become extremely important. Most equivalency factors are mixture-dependent, which can result in confusion between the field and laboratory, similar to what exists to date with the empirical-based methods.
- Will AAMAS be cost-effective for those SHAs that control and accept mixtures based on specifications geared toward method as opposed to end product?

With these few questions, implementation and acceptance of the AAMAS concepts will not be simple. There should be at least four steps in the implementation process: (a) familiarization with AAMAS, (b) training, (c) education, and (d) field pilot studies. The familiarization with AAMAS is simply an understanding of the concepts and methodology employed by AAMAS. This is a relatively short part of the implementation process.

The second step of the implementation process is training. It is the more detailed in terms of how to run the tests and interpret the test results. Training is important to ensure that the tests are performed in accordance with the procedure and that the output of the tests is being interpreted properly.

The third part of the implementation is education. This is probably the most important step toward full-scale implementation of AAMAS. Basically, the education part is to evaluate, on a trial basis, mixes for high-volume roadways. The objective is to allow the user to become confident in using AAMAS, understanding the properties measured and sensitivity of those properties to pavement performance, and establishing typical properties for their local materials. This part of the implementation process is also the more time-intensive, because it involves most of the learning curve.

The final step of the implementation is conducting mix designs and analyzing those mixes for actual projects. This step is the one that leads to defining the time requirements that are required to perform the tests on a routine basis and to establish day-to-day operational procedures in a working laboratory.

SUMMARY

In conclusion, the development of an AAMAS, as initiated through NCHRP Project 9-6(1), is a very important element of a multimillion-dollar research effort involving SHRP, FHWA, and the asphalt pavement industry, an effort that will ultimately result in improved performance of asphalt concrete pavements. Premature and costly pavement failures can be drastically reduced by (a) designing structures that more realistically consider traffic loadings, climate, and material conditions; (b) selecting asphalt, aggregates, and additives or modifiers consistent with the structural design; (c) producing new or modified asphalt binders that provide the desired characteristics for minimizing distress; and (d) developing and using performance-related specifications for control of construction.

ACKNOWLEDGMENTS

The research work summarized in this paper was performed under NCHRP Project 9-6(1) by Brent Rauhut Engineering and is reported in *NCHRP Report 338*. This project was sponsored by NCHRP. The primary consultants involved in the work were Dallas N. Little of Texas A&M University, Robert P. Lottman of University of Idaho, Byron E. Ruth of University of Florida, James L. Burati of Clemson University, and Thomas W. Kennedy of University of Texas. Harry Smith and Daniel Dearasaugh were the NCHRP contract technical managers for this project.

REFERENCES

1. H. L. Von Quintus, J. A. Scherocman, C. S. Hughes, and T. W. Kennedy. *NCHRP Report 338: Asphalt-Aggregate Mixture Analysis System: AAMAS*. TRB, National Research Council, Washington, D.C., March 1991.
2. M. R. Thompson, and E. Barenberg. *Calibrated Mechanistic Structural Analysis Procedures for Pavements*. Preliminary Draft Final Report, NCHRP Project 1-26. TRB, National Research Council, Washington, D.C., March 1990.
3. *A Two-Day Workshop on an Asphalt-Aggregate Mixture Analysis System: AAMAS*. Workshop outline and notes. FHWA, U.S. Department of Transportation, March 1991.
4. R. A. Jimenez and D. A. Dadeppo. *Asphalt Concrete Mix Design*. Report FHWA/AZ-86/189. Arizona Department of Transportation, Phoenix, June 1986.

Arizona Experience with Asphalt-Aggregate Mixture Analysis System Procedure

MICHAEL S. MAMLOUK, PUNYA P. KHANAL, DOUGLAS A. FORSTIE, AND DONALD K. CORUM

An asphalt concrete mixture used by the Arizona Department of Transportation (ADOT) is evaluated on the basis of a asphalt-aggregate mixture analysis system (AAMAS) procedure. Two sets of ADOT asphalt concrete specimens were prepared using the California kneading compactor and the Marshall hammer. All tests recommended by the AAMAS procedure were performed. The test results were analyzed using the AAMAS guidelines. It was found that the diametral resilient moduli of the ADOT mixture are within the acceptable range. The ADOT structural layer coefficient is close to the value recommended by the AAMAS study. The rutting potential is low in some cases and moderate in other cases. The ADOT mixture has slightly higher fatigue resistance at low temperatures than the asphalt concrete placed at the AASHO Road Test. Recommendations for the evaluation of thermal cracking are provided. The potential for moisture damage is high, whereas the potential for disintegration is marginal. The AAMAS prediction generally matches the historical experience of the asphalt mixture. The current version of the AAMAS procedure is quite comprehensive and seems to provide good performance predictions.

The asphalt concrete mix design in Arizona is based on the Marshall procedure. The Marshall method of mix design is basically empirical, so it results in index-type values such as Marshall stability and flow. In general, empirical characterization parameters are useful for comparing materials under specific conditions. However, empirical correlations are valid only for conditions similar to those under which they were originally developed. Further, empirical methods of characterization do not provide material properties needed for fundamental or theory-based structural analysis of pavements. With the continuous increase in truck weight, tire pressure, and traffic volume, and with the fast deterioration of the nation's highway system, more rational philosophy for asphalt concrete characterization is needed so that the pavement design can be based on a more optimal manner.

NCHRP Project 9-6, *Asphalt-Aggregate Mixture Analysis System: AAMAS*, has been recently completed (*1*). One of the objectives of that project was to develop a more rational mixture characterization procedure based on performance-related criteria. The AAMAS method provides rational evaluation procedure that is directly related to the mixture performance in the field. Because the project was completed only recently, the AAMAS procedure has not been implemented by most states. However, various highway agencies are planning to implement it soon. The implementation of the AAMAS procedure by the Arizona Department of Transportation (ADOT) could be a major step forward toward rationalizing the asphalt concrete mix design process.

According to the AAMAS procedure, six test types should be performed. Some of these tests are nondestructive, so each specimen could be tested using different test types and at different test temperatures. Some specimens are to be tested without conditioning; others should be conditioned, by being subjected to some treatments before testing. The detailed test and analysis procedure are reported by Von Quintus et al. (*1*). A summary of the test procedure is presented in the next section for completeness.

The objectives of this study are to evaluate typical ADOT hot-mixed asphalt concretes using the AAMAS recommendations (*1*), to expand the ADOT data base by providing typical lab test values for ADOT asphalt concrete, and to evaluate the amount of effort and equipment cost required for the AAMAS procedure and discuss its potential use by ADOT engineers.

SUMMARY OF AAMAS PROCEDURE

Specific items addressed in the AAMAS report include compaction of laboratory mixtures to simulate the characteristics of mixtures placed in the field, preparation and mixing of materials in the laboratory to simulate the asphalt concrete plant production process, simulation of the long-term effects of traffic and the environment (this includes accelerated aging and densification of the mixes caused by traffic), and conditioning of laboratory samples to simulate the effects of moisture-induced damage and hardening of the asphalt. Specific laboratory tests are recommended as well as methods of evaluating the expected performance of dense-graded asphalt concrete mixtures. Suggested recommendations for incorporating results of the AAMAS program into a final mixture design procedure are also provided.

Laboratory Tests

The NCHRP report (*1*) includes a detailed laboratory program to simulate the characteristics of mixtures placed in the

M. S. Mamlouk and P. P. Khanal, Department of Civil Engineering, Arizona State University, Tempe, Ariz. 85287. D. A. Forstie and D. K. Corum, Materials Section, Arizona Department of Transportation, Phoenix, Ariz. 85007.

field. The complete AAMAS procedure requires six types of test, as shown in Table 1. The diametral resilient modulus test is performed according to ASTM D4123. The indirect tensile strength test is summarized in applying a compressive load with a constant rate of deformation along a diametrical plane of a Marshall-size specimen until failure. The load at failure is recorded, from which the indirect tensile strength is computed. The horizontal deformation at failure can be used to compute the indirect tensile strain at failure. The AAMAS procedure requires that the diametral resilient modulus test be performed before the indirect tensile strength test. It is also required to use a deformation rate of 0.05 in./min at 41°F and 2 in./min at 77 and 104°F.

In the indirect tensile creep test, a constant-magnitude compression load is continuously applied along the vertical diametral plane of a Marshall-size specimen. The horizontal deformation is then used to calculate the tensile creep modulus at a particular duration. After the load is released, the rebound vertical and horizontal deformations are recorded over a fixed duration, and the recovery efficiency is determined. A loading time of 60 min and an unloading time of 60 min are required.

The concept of the uniaxial compression resilient modulus test is similar to the diametral indirect tensile resilient modulus test except that an axial load is applied. Unlike the diametral resilient modulus test, the uniaxial test results in a uniform axial compressive stress in the specimen. In this test, a pulsating uniaxial load is applied on a cylindrical specimen every 1 sec with a 0.1-sec duration, and the corresponding axial deformation is recorded. The total resilient modulus is determined by dividing the repeated axial compressive stress by the total recoverable axial strain. A specimen 4 in. in diameter and 4 in. high is recommended by the AAMAS study.

The unconfined compressive strength test is performed on a specimen 4 in. in diameter and 4 in. high, according to ASTM D1074. In the AAMAS report, however, a rate of strain of 0.15 in./in./min and a test temperature of 104°F are required. At failure, the compressive strength is calculated by dividing the load at failure by the cross-sectional area.

In the uniaxial creep test, a constant-magnitude uniaxial compression load is applied on a 4- × 4-in. cylindrical specimen, and the axial deformation is continuously recorded. The compressive creep modulus can be computed at any loading time by dividing the axial compressive stress by the axial compressive creep strain. The AAMAS procedure requires a test temperature of 104°F. A loading time of 60 min and an unloading time of 60 min are required. The slope and intercept of the creep curve as well as the recovery efficiency are computed.

TABLE 1 Laboratory Tests Recommended by AAMAS Study

Test No.	Test Name	Loading Pattern	Specimen Loading
1	Diametral resilient modulus	Pulses with 0.1 sec duration and 0.9 sec rest period (ASTM D 4123)	Diametral
2	Indirect tensile strength	Loading at a rate of deformation of 0.05 or 2 in/min until failure	Diametral
3	Indirect tensile creep	Static load with a specified magnitude for 60 min and unloading for 60 min	Diametral
4	Uniaxial compression resilient modulus	Pulses with 0.1 sec duration and 0.9 sec rest period	Axial
5	Unconfined compressive strength	Loading at a rate of deformation of 0.6 in/min until failure	Axial
6	Uniaxial creep	Static load with a specified magnitude for 60 min and unloading for 60 min	Axial

Specimen Conditioning

The AAMAS study recommends three types of specimen conditioning in the lab to simulate field conditions. A summary of the procedure is as follows:

1. Moisture conditioning—Specimens are vacuum-saturated until the water absorption is greater than 55 percent. Specimens are then frozen for 16 hr and thawed at 140°F for 24 hr and at 77°F for 2 hr.
2. Environmental aging (temperature conditioning)—Specimens are heated at 140°F for 2 days and at 225°F for 5 days. Specimens are then cooled at 41°F for 12 hr.
3. Traffic densification—Specimens are heated and further compacted to simulate traffic densification until refusal or until the final air void level is reached.

Table 2 shows a summary of specimen-conditioning types and procedures.

Grouping and Test Sequence

The complete AAMAS procedure requires 24 specimens: eighteen 4- by 2.5 in. specimens and six 4- by 4-in. specimens. Specimens are grouped into eight sets of three specimens each. The first six sets have 4- by 2.5-in. specimens; the last two sets have 4- by 4-in. specimens. The specimens are grouped so that the average unit weight (and air voids) of the different sets are approximately equal. Table 3 shows the conditioning as well as test type, sequence, temperature, and measurements for each specimen set.

EVALUATION OF ADOT MIXTURE PROPERTIES

Specimen Preparation and Testing

The AAMAS study recommends the use of the gyratory compactor (ASTM D3387 or D4013) because it closely simulates the mix compaction in the field. The report further concludes that the California kneading compactor (ASTM D1561) is the next preferred device, and the Marshall hammer (ASTM D1559) is the least desirable compactor. Because the Marshall hammer is the most commonly used compactor and it is the compactor currently used by ADOT, there is a need to compare the responses of Marshall-compacted specimens and of specimens compacted by other devices. Also, because the

TABLE 2 Specimen Conditioning

Conditioning No.	Name	Procedure
a	Moisture conditioning	Vacuum saturation + freeze and thaw
b	Environmental aging	Heating for 7 days + cooling for 12 hours
c	Traffic densification	Heating and further compaction

TABLE 3 Conditioning, Test Sequence, and Measurements

Set No.	No. of Specimens	Size (in.)	Conditioning*	Test No., ** Sequence & Temperature	Measurement
1	3	4 x 2.5	None	1, 2 (41°F)	Diametral resilient modulus, indirect tensile strength, tensile strain at failure
2	3	4 x 2.5	None	1, 2 (77°F)	Same as set 1
3	3	4 x 2.5	None	1, 2 (104°F)	Same as set 1
4	3	4 x 2.5	a	1, 2 (77°F)	Same as set 1
5	3	4 x 2.5	b	1, 2 (41°F)	Same as set 1
6	3	4 x 2.5	b	3 (41°F)	Tensile creep modulus, recovery efficiency
7	3	4 x 4	c	4, 5 (104°F)	Axial resilient modulus, unconfined compressive strength, compressive strain at failure
8	3	4 x 4	c	6 (104°F)	Slope and intercept of creep curve, compressive creep modulus, recovery efficiency

* *See Table 2*
** *See Table 1*

gyratory compactor was not available to the authors at that time, it was decided to evaluate two sets of 24 specimens: one set compacted by the kneading compactor, and the other set compacted by the Marshall hammer. It was also decided that the bulk specific gravities and air voids of all specimens should be similar to those of typical ADOT mixes. The aggregate was prepared following the midpoint of the typical ADOT dense gradation with a maximum size of ¾ in. An AC-30 asphalt cement was used in the mix preparation with a penetration of 40 and a kinematic viscosity of 320 cSt at 275°F.

The mix was designed according to the ARIZ 815c procedure (*2*), which is a modified version of ASTM D1559. The design asphalt content was 4.7 percent by total weight of mix. The bulk density was 145.2 pcf. The maximum theoretical density of the loose mixture was 152.4 pcf, and the air void of the compacted specimens was 4.7 percent. This mix is typically used in areas with desert climate and low to moderate traffic volume.

The first set of specimens was compacted using the California kneading compactor according to ASTM D1561. The compacting effort was adjusted on a trial-and-error basis to achieve a bulk specific gravity and air voids similar to those of typical ADOT mixtures. After several trials it was found that 20 blows at 250 psi followed by 100 blows at 500 psi provided the required density for the 4- by 2.5-in. specimens. The 4- by 4-in. specimens were compacted using the same procedure except for 20 blows at 250 psi and 120 blows at 500 psi. The second set of specimens was compacted using the manual Marshall hammer according to ASTM D1559. Seventy-five blows on each side of the specimen were applied on the 4- by 2.5-in. specimens; 100 blows on each side were applied on the 4- by 4-in. specimens.

All of the kneading-compacted and Marshall-compacted specimens were grouped into eight sets so that the average unit weights of all sets were similar, as recommended by the AAMAS study (*1*).

Both kneading-compacted and Marshall-compacted specimens were conditioned according to the AAMAS procedure. Three types of conditioning were used: moisture conditioning, environmental aging, and traffic densification. The California kneading compactor was used for the traffic densification of the kneading-compacted and the Marshall-compacted specimens. Five hundred kneading blows were applied to each specimen to ensure that refusal was reached. Table 4 shows the bulk unit weights and air voids before and after traffic densification. The results show that traffic densification of kneading-compacted specimens resulted in slightly larger unit weights and slightly less air voids than those of Marshall-compacted specimens.

Test Results

Testing was performed as specified in the AAMAS report. An electrohydraulic testing machine was used for all tests. Table 5 shows the average test results of unconditioned, moisture-conditioned, environmental-conditioned, and traffic-densified specimens. Comparison of the kneading- and the Marshall-compacted specimens indicates that the test results are close in most cases.

TABLE 4 Average Unit Weights and Air Voids Before and After Traffic Densification

Property	Set No.	Kneading Compacted	Marshall Compacted	Average
Unit weight before (pcf)	7	145.3	145.2	145.3
Unit weight after (pcf)	7	148.4	147.1	147.8
Unit weight before (pcf)	8	145.3	145.2	145.3
Unit weight after (pcf)	8	148.8	147.4	148.1
Air voids before (%)	7	4.7	4.8	4.8
Air void after (%)	7	2.6	3.4	3.0
Air voids before (%)	8	4.7	4.8	4.8
Air void after (%)	8	2.4	3.3	2.9

TABLE 5 Average Test Results of Unconditioned and Conditioned Specimens

Property	Set No.	Temp. (F)	Kneading Compacted	Marshall Compacted	Average
Diametral E_r (ksi)	1	41	2,414	2,371	2,393
Tensile strength (psi)	1	41	374	357	366
Tensile strain at failure (mils/in)	1	41	3.0	4.0	3.5
Diametral E_r (ksi)	2	77	785	943	864
Tensile strength (psi)	2	77	283	322	303
Tensile strain at failure (mils/in)	2	77	6.7	6.5	6.6
Diametral E_r (ksi)	3	104	192	179	186
Tensile strength (psi	3	104	93	107	100
Tensile strain at failure (mils/in)	3	104	8.2	6.0	7.1
Diametral E_r (ksi)	4	77	399	296	348
Tensile strength (psi)	4	77	87	81	84
Tensile strain at failure (mils/in)	4	77	6.4	4.0	5.2
Diametral E_r (ksi)	5	41	3,086	3,912	3,499
Tensile strength (psi)	5	41	392	443	418
Tensile strain at failure (mils/in)	5	41	2.6	2.7	2.7
Tensile creep modulus at 3,600 sec.(ksi)	6	41	92	475	284
Recovery efficiency	6	41	0.17	0.37	0.27
Axial E_r (ksi)	7	104	30	31	31
Compressive strength (psi)	7	104	715	705	710
Compressive strain at failure (mils/in)	7	104	24.0	18.5	21.3
Slope of creep curve	8	104	.051	.050	.050
Intercept of creep curve (10^{-3})	8	104	3.26	3.62	3.44
Compressive creep modulus (ksi)					
at 10 sec	8	104	15.5	15.2	15.4
100 sec	8	104	11.1	10.4	10.8
1,000 sec	8	104	9.8	8.0	8.9
3,600 sec	8	104	9.2	8.1	8.7
Recovery efficiency	8	104	0.55	0.45	0.50

PREDICTION OF ADOT MIXTURE PERFORMANCE

The concept of relating the mixture properties to the pavement performance is logical and appropriate in order to optimize mixture and structural designs. Many models have been developed for this purpose. However, these models are limited in use to some degree, mainly because they are not comprehensive enough to cover all variables involved in pavement performance. The AAMAS study presents some guidelines to provide a recommended practice for evaluating asphalt concrete mixtures on the basis of performance-related criteria.

The AAMAS procedure consists of a series of steps using results from the test program, discussed earlier, as well as interactions with various models predicting the types of distress more common with asphalt concrete pavements. The final products of the AAMAS are the structural and material combinations needed to meet the design requirements or assumptions used by the pavement design engineer. In this section, the properties of typical ADOT mixtures presented earlier are compared with the performance-related criteria reported in the AAMAS study.

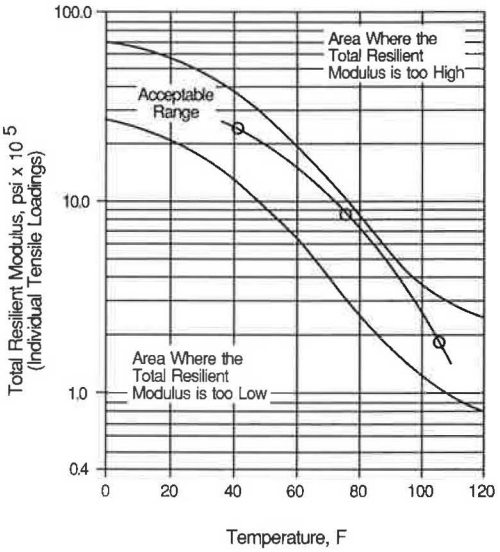

FIGURE 1 Acceptable range of diametral total resilient moduli at various temperatures and typical ADOT moduli.

AASHTO Structural Layer Coefficient

The 1986 AASHTO guide (*3*) recommends the estimation of the structural layer coefficient from the resilient modulus measured at 68°F in accordance with ASTM D4123. The AAMAS study, however, recommends the consideration of the environmental effects on the structural design by considering the seasonal fatigue damage. In other words, use seasonal resilient moduli to calculate seasonal fatigue damage and add the seasonal damages to determine an annual damage. From the annual damage, an effective asphalt concrete resilient modulus can be calculated, which can be used to estimate the structural layer coefficient.

The following is a step-by-step procedure that can be used to ensure that the asphalt concrete mixture meets or exceeds the layer coefficient assumed during structural design (*1*).

1. Obtain the seasonal average pavement temperature for each season.
2. Determine the total resilient modulus at each seasonal temperature. Figure 1 shows the acceptable range of moduli (unconditioned) at various temperatures. Figure 1 also shows that the ADOT moduli (average of results using the two compaction methods) are within the acceptable range at all three test temperatures; 41, 77, and 104°F for unconditioned specimens.
3. Obtain the fatigue factor for each seasonal resilient modulus from Figure 2 (*1*).
4. Calculate the effective resilient modulus using Equation 1.

$$E_{RE} = \frac{\sum[E_{RT}^{(i)} \times FF^{(i)}]}{\sum FF} \quad (1)$$

where

E_{RE} = effective resilient modulus based on a fatigue damage approach,

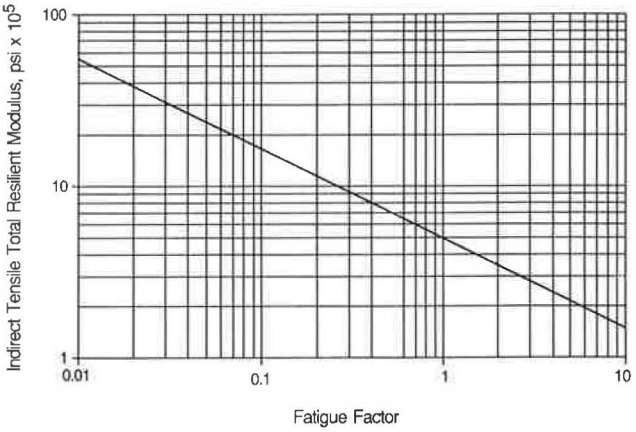

FIGURE 2 Estimation of fatigue factor to determine equivalent annual modulus (*1*).

$E_{RT}^{(i)}$ = total resilient modulus as measured by ASTM D4123 at the average pavement temperature for season i, and

FF = fatigue factors obtained from Figure 2.

This effective resilient modulus should equal or exceed the modulus value used to estimate the AASHTO structural layer coefficient used for design [Figure 3 (*3*)].

As an example for determining the structural layer coefficient, use AC-30 for asphalt concrete, an aggregate type and gradation as used in this study, and an asphalt content of 4.7 percent by total weight of mix. The seasonal average pavement temperatures are 80°F for fall, 70°F for winter, 85°F for spring, and 100°F for summer.

From Figure 1 the moduli at 80, 70, 85, and 100°F are 700, 1050, 560, and 260 ksi. From Figure 2 the corresponding fatigue factors are 0.50, 0.22, 0.80, and 3.6. Using Equation 1, the effective resilient modulus is 384 ksi. Figure 3 shows that the structural coefficient (a_1) for this material should be

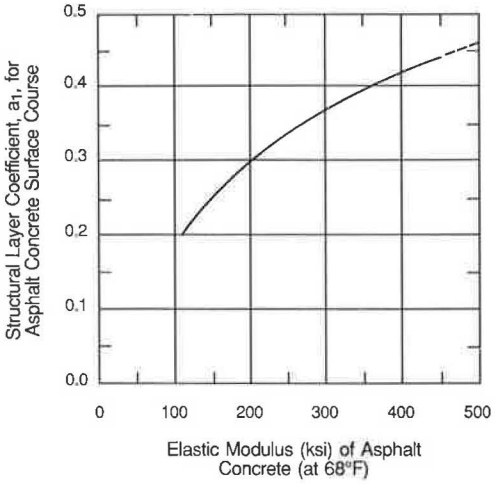

FIGURE 3 Chart for estimating structural layer coefficient of dense-graded asphalt concrete based on elastic (resilient) moduli (*3*).

0.42. The ADOT design manual (*2*) recommends a value of 0.44 for this mixture. This indicates that the structural layer coefficient used by ADOT is close to the value recommended by the AAMAS study. Note, however, that the seasonal average pavement temperatures used in this sample are approximate.

Rutting

Two types of rutting are considered: (a) densification or one-dimensional consolidation, and (b) the lateral movement or plastic flow of asphalt from wheel loads. The more severe premature rutting failures and distortion of asphalt concrete materials are related to lateral flow or loss of shear strength of the mix, rather than to densification. Currently, there is no mechanistic or empirical model that adequately considers the lateral flow problem (*1*).

Rutting from one-dimensional consolidation can be estimated using the traffic densification procedure recommended in the AAMAS report (*1*). Limiting the air voids at mixture refusal limits the amount of additional densification caused by traffic, assuming that the mixture is properly compacted on the roadway to an air void level between 5 to 7 percent. The air voids at mixture refusal should be greater than 2 percent when compacted with the gyratory devices (*1*). Table 4 indicates that the air voids after densification of specimens tested in this study are greater than 2 percent. Therefore, the possibility of rutting due to one-dimensional consolidation is small.

A few mathematical models are reported in the AAMAS report to estimate the rutting rate of asphalt concrete layers in the field. Figures 4 through 7 illustrate graphical solutions of the range of data that can be generated for different pavements, climates, and loading conditions. The figures can be used as gross guidelines for mixture evaluation on high-volume roadways.

The compressive creep moduli (average of results using the two compaction methods) reported in Table 5 (Set 8) for

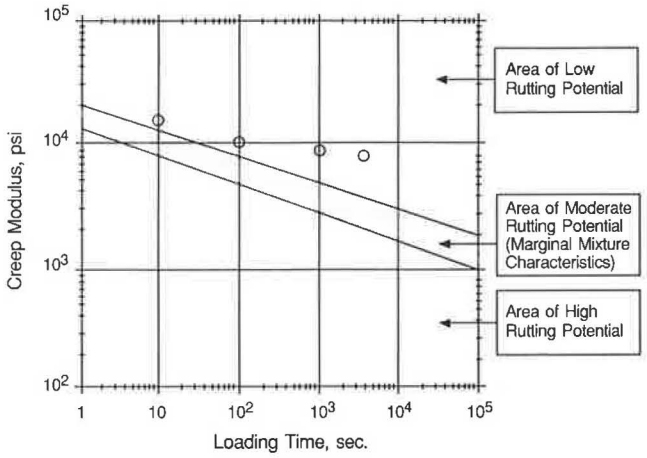

FIGURE 4 ADOT mixture rutting potential for lower layers of full-depth asphalt pavements.

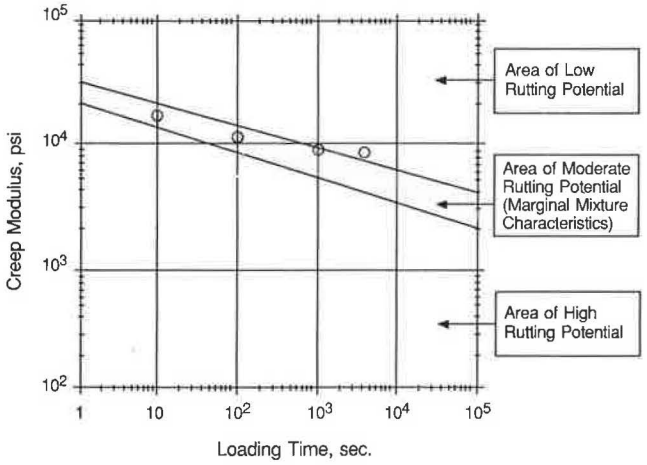

FIGURE 5 ADOT mixture rutting potential for intermediate layers in thick or full-depth asphalt pavements.

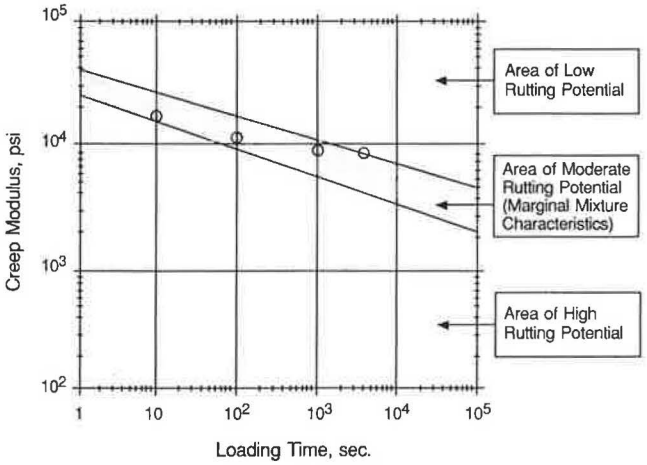

FIGURE 6 ADOT mixture rutting potential for surface layers of asphalt pavements.

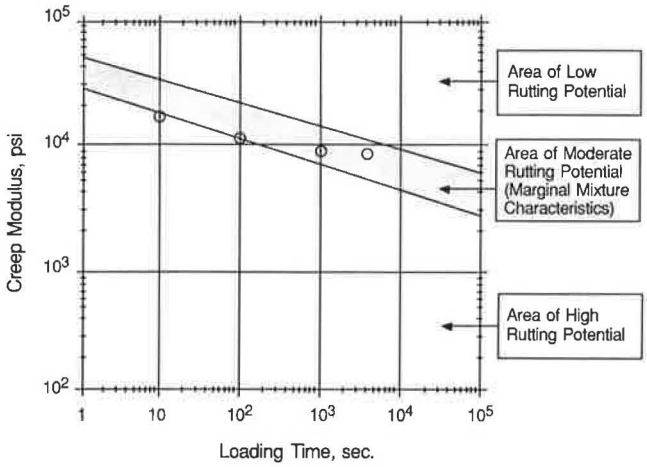

FIGURE 7 ADOT mixture rutting potential for layers placed over rigid pavements or rigid base materials.

typical ADOT mixtures are plotted in Figures 4 through 7. It can be concluded that the ADOT mixture has a low rutting potential for the lower layers of full-depth asphalt pavements (Figure 4). On the other hand, it has a moderate rutting potential (marginal) for the intermediate layers in thick or full-depth asphalt pavements (Figure 5), for surface layers (Figure 6), and for layers placed over rigid pavements or rigid base materials (Figure 7).

Fatigue Cracking

According to the AAMAS procedure, two methods can be used for evaluating asphaltic concrete mixtures for fatigue cracking. The first is to ensure that the mixture meets or exceeds the fatigue resistance of a "standard" material (which is assumed in structural design), and the second is to ensure that the mixture has the required fatigue resistance for the specific environment and pavement cross section. The first method is recommended because it is simpler.

For purposes of AAMAS, the standard mixture will be the dense-graded asphaltic concrete placed at the AASHO Road Test. The fatigue curves from NCHRP 1-10B (*4*) were developed from these data, which have been used in other research and design studies (*5,6*). Figure 8 shows two relationships between the total resilient modulus and indirect tensile strain at failure for the standard mixture.

If the total resilient modulus and indirect tensile strains at failure for a particular mixture plot above the standard mixture (FHWA fatigue curve is recommended), it is assumed that the mixture has better fatigue resistance than the standard mixture.

The test results of unconditioned ADOT specimens (average between the two compaction methods) (Table 5, Sets 1, 2, and 3) are plotted in Figure 8. It can be seen that two of the points are above the FHWA fatigue curve and one point is below the curve. Thus, the ADOT mixture has higher fatigue resistance at low temperatures and lower fatigue resistance at high temperatures when compared with the "standard" mix.

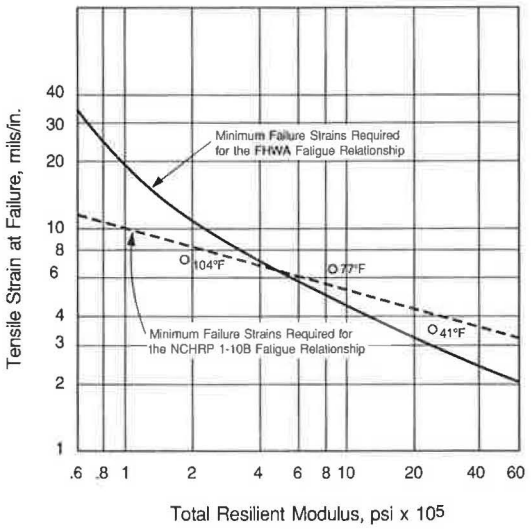

FIGURE 8 Fatigue cracking potential of ADOT mixture.

Thermal Cracking

To evaluate thermal cracking, certain critical mixture properties as well as project-specific environmental conditions must be determined. The mixture properties include indirect tensile strength, low-temperature creep modulus, failure strains, and the thermal coefficient of contraction. These parameters can be used to calculate the occurrence of thermal cracking with time.

The critical temperature change (°F) at which cracking is expected to occur can be calculated as follows (*1*):

$$\Delta T = \left[\frac{E_{ct}(T_i)}{E_o}\right]^{1/n_t} \frac{t_r^{n_c}}{\alpha A^{E_o(T_i)}}$$

where

$E_{ct}(T_i)$ = indirect tensile creep modulus measured at temperature T_i;
E_o = regression constant developed from laboratory test data;
n_t = slope of relationship between indirect tensile strength and total resilient modulus of the mixture measured at temperatures of 41, 77, and 104°F (unconditioned);
$E_o(T_i)$ = intercept of indirect tensile creep curve at temperature T_i (psi);
t_r = relaxation time (3,600 sec);
n_c = slope of the indirect tensile creep curve at temperature T_i; and
αA = thermal coefficient of contraction of the asphalt concrete (typical values range from 1.0×10^{-5} to 1.8×10^{-5} in./in./°F).

From these criteria, the cracking potential of ADOT mixture can be evaluated. The available data, however, are not enough to provide complete evaluation.

Moisture Damage

Currently, the moisture damage evaluation—tensile strength ratio (TSR) and resilient modulus ratio (MRR) after and before moisture conditioning—of AAMAS is simply used as a means of accepting or rejecting a mixture. Both of these ratios should exceed a value of 0.80 for dense-graded asphalt concrete. If values less than 0.80 are measured, an asphalt additive or antistripping agent may be required or the aggregate blend may need modification. If these ratios are less than 0.70, an antistripping agent will be required for the aggregate blend (*1*).

For the ADOT mixture, the tensile strength ratio and the resilient modulus ratio at 77°F can be obtained from Table 5 by dividing the results of moisture-conditioned specimens (Set 4) by the results of the unconditioned specimens (Set 2) as follows:

$$\text{TSR} = \frac{84}{303} = 0.28$$

$$\text{MRR} = \frac{348}{864} 0.40$$

It can be seen that both ratios are less than 0.70, which indicates high potential for moisture damage. Therefore, an antistripping agent is required for the aggregate blend, according to the AAMAS recommendations. It should be noted, however, that this mixture is typically used in the Phoenix area where the amount of rainfall is very limited. In other areas within the state where the rainfall is higher, the aggregate would require treatment with either lime or portland cement to increase the stripping resistance. The applicability of the 0.70 ratio recommended by the AAMAS study to desert climate is questioned.

Disintegration

The following summarizes the AAMAS criteria that can be used as guidelines to evaluate the acceptability of surface mixtures as related to disintegration:

- Air voids at refusal > 3 percent;
- Indirect tensile strength ratio, TSR > 0.80;
- Bonding loss < 50;
- Tensile strain at failure (77°F) > 10 mils/in.;
- Tensile strain at failure (41°F after accelerated aging) > 2.0 mils/in.; and
- Bonding loss = $(1 - \varepsilon_{ht}/\varepsilon_{ho}) \times 100$, where ε_{ht} is the indirect tensile strain at failure measured on specimens that have been temperature-conditioned (accelerated aging), and ε_{ho} is the indirect tensile strain at failure measured on unconditioned specimens

The following information is obtained from the ADOT mixture:

- Air voids at refusal (Table 4) = 3 percent (OK);
- Indirect tensile strength ratio, TSR (from Table 5, Sets 4 and 2) = 0.28;
- Bonding loss at 41°F (from Table 5, Sets 5 and 1) = 23 (OK);
- Tensile strain at failure (77°F) (Table 5, Set 2) = 6.6 mils/in.; and
- Tensile strain at failure (41°F) (Table 5, Set 5) = 2.7 mils/in. (OK).

It can be seen that three of the conditions are satisfied and the other two are not. This indicates that the potential for disintegration is marginal.

COMPARING AAMAS PREDICTION WITH HISTORICAL EXPERIENCE

The AASHTO structural layer coefficient predicted by the AAMAS procedure for the typical ADOT mixture conditions is similar to that recommended by the AASHTO procedure. It should be noted, however, that the AAMAS procedure considers the seasonal average pavement temperatures, whereas the AASHTO procedure does not explicitly consider the pavement temperature.

The AAMAS procedure indicates that the ADOT mixture has a moderate rutting potential for surface layers. The ADOT experience, however, shows that rutting is very limited despite the hot climate of the Phoenix area. On the other hand, the AAMAS procedure shows low to moderate resistance to fatigue cracking. The historical experience with the mixture is similar to the AAMAS prediction in that respect.

The potential for thermal cracking of the ADOT mixture was not completely evaluated in this study. Moreover, the AAMAS procedure indicates that the ADOT mixture has a high potential for moisture damage. This condition, however, is not applicable to the asphalt mixture evaluated in this study, because the amount of rainfall is very limited in the Phoenix area, where the mixture is used. Finally, the AAMAS procedure shows that the disintegration potential of the ADOT mixture is marginal. The ADOT experience shows that raveling sometimes occurs when the mixture is placed during cold weather. However, raveling usually heals during the hot weather. Also, the routine maintenance used by ADOT usually solves disintegration problems when they arise.

SUMMARY AND CONCLUSIONS

In this study an ADOT asphalt concrete mixture typically used in areas with desert climate was evaluated on the basis of the AAMAS procedure (*1*). Two sets of ADOT asphalt concrete specimens were prepared using the California kneading compactor and the manual Marshall hammer. All tests recommended by the AAMAS study were performed. The test results were analyzed using the AAMAS guidelines.

It was found that the diametral resilient moduli of the ADOT mixture are within the acceptable range. The ADOT structural layer coefficient is close to the value recommended by the AAMAS study. The rutting potential is low in some cases and moderate in others. The ADOT mixture has higher fatigue resistance at low temperatures than the asphalt concrete placed at the AASHO Road Test. Recommendations for the evaluation of thermal cracking are provided. The potential

for moisture damage is high, but the potential for disintegration is marginal. The AAMAS prediction generally matches the historical experience of the asphalt mixture, although the moisture-damage evaluation may not apply to the mixture used in desert climates.

The current version of the AAMAS procedure is quite comprehensive and seems to provide good performance prediction. Further research is currently being conducted by the Strategic Highway Research Program. Thus, the results obtained in this study should not be considered final. More studies are needed for comprehensive evaluations of ADOT asphalt concrete performance.

REFERENCES

1. H. L. Von Quintus et al. *NCHRP Report 338: Asphalt-Aggregate Mixture Analysis System: AAMAS*. TRB, National Research Council, Washington, D.C., March 1991.
2. *Preliminary Engineering and Design Manual*. Arizona Department of Transportation, Phoenix, March 1989.
3. *Guide for Design of Pavement Structures*. AASHTO, Washington, D.C., 1986.
4. F. N. Finn et al. *Development of Pavement Structural Subsystems*. Final Report, Project 1-10B. NCHRP, TRB, National Research Council, Washington, D.C., Feb. 1977.
5. J. B. Rauhut et al. *Pavement Damage Functions for Cost Allocation, Volume 1—Damage Functions and Load Equivalence Factors*. Report FHWA-RD-84-018. FHWA, U.S. Department of Transportation, June 1984.
6. Austin Research Engineers, Inc. *Asphalt Concrete Overlays of Flexible Pavements, Volume 1—Development of New Design Criteria*. Report FHWA-RD-75-75. FHWA, U.S. Department of Transportation, June 1975.